



# UNIVERSIDAD DE ALMERÍA

Departamento de Informática

## TESIS DOCTORAL

MODELADO Y OPTIMIZACIÓN PARA UNA  
GESTIÓN EFICIENTE DE RECURSOS EN  
TECNOLOGÍA TERMOSOLAR

**Jose Antonio Carballo López**

Programa de doctorado Informática (RD99/11)

Directores:

Dr. Javier Bonilla Cruz

Dr. Manuel Berenguel Soria

Tesis presentada para la obtención del título de Doctor  
Universidad de Almería, noviembre de 2019



# MODELADO Y OPTIMIZACIÓN PARA UNA GESTIÓN EFICIENTE DE RECURSOS EN TECNOLOGÍA TERMOSOLAR

MODELING AND OPTIMIZATION FOR EFFICIENT  
RESOURCE MANAGEMENT IN SOLAR THERMAL  
TECHNOLOGY

Autor:

Jose Antonio Carballo López

Directores:

Dr. Javier Bonilla Cruz  
Dr. Manuel Berenguel Soria

Programa de doctorado:

Informática (RD/99)  
Automática, Informática Industrial, Robótica y Mecatrónica

Escuela Superior de Ingeniería  
Universidad de Almería

Noviembre 2019



*A mi familia,  
Andrea Ibáñez  
y  
amigos.*



*Para algunos,  
la vida es galopar un camino  
empedrado de horas,  
minutos y segundos.  
Yo, más humilde soy,  
y solo quiero que la ola  
que surge del último suspiro  
de un segundo me transporte  
mecido hasta el siguiente.*

**Robe Iniesta**



# Agradecimientos

*Cuando bebas agua,  
recuerda la fuente.*

**Proverbio chino**



# Contribuciones científicas derivadas de la tesis

De acuerdo con la normativa de estudios oficiales de doctorado de la Universidad de Almería en su artículo 24, que establece los requerimientos mínimos de calidad de una tesis doctoral, se permitirá presentar una tesis por la modalidad de compendio de publicaciones cuando esta esté avalada por un mínimo de 3 contribuciones científicas que cumplan las siguientes condiciones mínimas:

1. Que dos contribuciones se incluyan en la categoría A de la escala de valoración de los resultados de investigación contenida en el Plan Propio de Investigación y Transferencia de la Universidad de Almería aprobado en el correspondiente año.
2. Que una tercera contribución, distinta de las anteriores y que no consista en comunicación a congreso, se incluya en la categoría B de la escala de valoración de los resultados de investigación contenida en el Plan Propio de Investigación y Transferencia de la Universidad de Almería aprobado en el correspondiente año.

De acuerdo con el Plan Propio de Investigación y Transferencia de la Universidad de Almería las categorías A y B quedan definidas de la siguiente manera:

1. *Categoría A:* Artículos en revistas de carácter científico (Q1 de InCites Journal Citation Reports (IJCR) de Clarivate Analytics, categoría A de CARHUS+, categoría A+ de CIRC), capítulos de libro de la lista de editoriales de la categoría A o autor de patente, software u otra modalidad de propiedad industrial en explotación.

2. *Categoría B*: Artículos en revistas de carácter científico (Q2 y Q3 de IJCR de Clarivate Analytics, Q1 y Q2 de Scimago Journal and Country Rank (SJR) de Elsevier B.V, categoría B de CARHUS +, categoría A de CIRC), capítulos de libro de la lista de editoriales de la categoría B, aportaciones a congresos indexados en Web of Science, aportaciones a congresos indexados en SCOPUS, aportaciones a congresos publicadas por editoriales y revistas de las categorías A y B (con ISBN o ISSN).

Esta tesis está respaldada por 8 artículos de revistas científicas internacionales, 4 de ellos en revistas categoría A, 2 categoría B y 2 artículos bajo revisión en revistas categoría A.

De los trabajos realizados se derivan 7 contribuciones en congresos científicos internacionales y la participación en dos proyectos de investigación nacionales. También se derivan otras aportaciones como una solicitud de patente y 4 contribuciones divulgativas en el marco del proyecto europeo Marie Skłodowska Curie Actions. Todo estos hitos se detallan a continuación.

## Artículos en revistas internacionales

- [R1]. J. A. Carballo, J. Bonilla, L. Roca, A. De la Calle, P. Palenzuela, M. Berenguel. “Optimal operating conditions analysis of a multi-effect distillation plant”. *Desalination and Water Treatment*, 69 229-235, 2017. DOI: <https://doi.org/10.5004/dwt.2017.0703> . (**F.I 1.397, Q3, Cat B**).[Ap A.1]
- [R2]. J. A. Carballo, J. Bonilla, L. Roca, A. De la Calle, P. Palenzuela, D. C. Alarcón-Padilla. “Optimal operating conditions analysis for a multi- effect distillation plant according to energetic and exergetic criteria”. *Desalination*, 435 70–76, 2018. DOI: <https://doi.org/10.1016/j.desal.2017.12.013> . (**F.I 6.603, Q1, Cat A**). [Ap A.2]
- [R3]. J. A. Carballo, J. Bonilla, L. Roca, M. Berenguel. “New low-cost solar tracking system based on open source hardware for educational purposes”. *Solar Energy*, 174 826–836, 2018. DOI: <https://doi.org/10.1016/j.solener.2018.09.064> . (**F.I 4.374, Q1, Cat A**). [Ap A.3]

- [R4]. J. A. Carballo, J. Bonilla, M. Berenguel, J. Fernández-Reche, G. García. “New approach for solar tracking systems based on computer vision, low cost hardware and deep learning”. *Renewable energy*, 133, 1158-1166, 2018. DOI: <https://doi.org/10.1016/j.renene.2018.08.101>. (**F.I 4.9, Q1, Cat A**). [Ap A.4]
- [R5]. J. A. Carballo, J. Bonilla, M. Berenguel, P. Palenzuela. “Parabolic trough collector field dynamic model: Validation, energetic and exergetic analyses”. *Applied Thermal Engineering*, 148 777–786, 2019. DOI: <https://doi.org/10.1016/j.applthermaleng.2018.11.093>. (**F.I 3.771, Q1, Cat A**). [Ap A.5]
- [R6]. J. A. Carballo, J. Bonilla, M. Berenguel, J. Fernández-Reche, G. García. “Machine learning for solar trackers”. *AIP Conference Proceedings*, 21-26, 2019. DOI: [\(Q2, Cat B\)](https://doi.org/10.1063/1.5117524). [Ap A.6]
- [R7]. J. A. Carballo, J. Bonilla, M. Berenguel, J. Fernández-Reche, G. García. “Solar tower power mockup for the assessment of advanced control techniques”. *Renewable Energy*, (**Under Review**). [Ap A.7]
- [R8]. J. A. Carballo, J. Bonilla, L. Roca, A. De la Calle, D. C. Alarcón-Padilla, M. Berenguel. “Optimal operation of solar thermal desalination systems coupled to double-effect absorption heat pumps”. *Energy Conversion and Management*, (**Under Review**). [Ap A.8]

## Congresos Internacionales

- [C1]. J. A. Carballo, J. Bonilla, L. Roca, A. De la Calle, P. Palenzuela, M. Berenguel. “Optimal operating conditions analysis of a multi-effect distillation plant”. In: *Proceedings of the EDS conference on Desalination for the Environment: Clean Water and Energy*, Rome, Italy, 22–26 May 2016. Number 69. ISSN Print 1944-3994, ISSN Online 1944-3986.
- [C2]. J. A. Carballo, J. Bonilla, M. Berenguel. “Modeling, optimization and control for efficient management of resources in solar desalina-
-

- tion processes”. *12<sup>th</sup> SOLLAB Doctoral Colloquium on Solar Concentrating Technologies*, Almeria, Spain, 6-8 June 2016.
- [C3]. J. A. Carballo, J. Bonilla, L. Roca, A. De la Calle, P. Palenzuela, M. Berenguel. “Optimal operating conditions analysis for a double-effect absorption heat pump coupled to a multi effect distillation plant”. In: *Proceedings of the EuroMed 2017 Desalination for Clean Water and Energy: Cooperation around the World*, Tel Aviv, Israel, 09-1 May 2017. Number 67, European Desalination Society 46–47 2017.
- [C4]. J. Bonilla, J. A. Carballo, L. Roca, M. Berenguel. “Development of an open source multi-platform software tool for parameter estimation studies in fmi models”. In: *Proceedings of the 12th International Modelica Conference*, Prague, Czech Republic, 15-17 May 2017. Number 132, Linköping University Electronic Press 683–692 2017.
- [C5]. J. A. Carballo, J. Bonilla, M. Berenguel. “Modeling, optimization and control for efficient management of resources in solar desalination processes”. *13<sup>th</sup> SOLLAB Doctoral Colloquium on Solar Concentrating Technologies*, Berlin, Germany, 15-17 May 2017.
- [C6]. J. A. Carballo, J. Bonilla, M. Berenguel, J. Fernández-Reche, G. Garcia. “Machine learning for solar trackers”. In: *Proceedings of SolarPACES 2018 Concentrating Solar Power and Chemical Energy Systems*, Casablanca, Morocco, 2-5 October 2018.
- [C7]. J. Bonilla, J. A. Carballo, M. Berenguel, J. Fernández-Reche, L. Valenzuela. “Machine learning in solar thermal energy: state of the art and perspectives”. In: *Proceedings of Eurosime 2019*, La Rioja, España, 1-5 Julio 2019.

## Colaboraciones en proyectos de investigación

- [P1]. Efficient energy control and management of solar thermal desalination systems (**EFFERDESAL**).
-

- Ref: DPI2014-56364-C2
  - Organismo de financiación: Fondo Europeo de Desarrollo Regional y Ministerio de Economía y competitividad
- [P2]. Soluciones termosolares para integración en procesos industriales (**SOLTERMIN**).
  - Ref: ENE2017-83973-R
  - Organismo de financiación: Fondo Europeo de Desarrollo Regional y Ministerio de Economía, Industria y Competitividad

## Otras aportaciones derivadas

- [O1]. J. A. Carballo, J. Bonilla, J. Fernández-Reche, G. García. Solicitud de patente en España No. 201830073. Sistema de captación solar mediante técnicas de visión artificial.
- [O2]. J. A. Carballo. Modelado, simulación y control de sistemas solares. Open researchers, Marie Skłodowska Curie Actions, Comision Europea. Almería, España, 30 Septiembre 2016.
- [O3]. J. A. Carballo. Destilación solar por membranas para desalación de aguas. Open researchers, Marie Skłodowska Curie Actions, Comision Europea. Almería, España, 29 Septiembre 2017.
- [O4]. J. A. Carballo. Modelado y Optmización para una gestión eficiente de recursos en tecnología termosolar. I Jornadas Universidad de Almería JSIDI 2018. Almería, España, 15 Febrero 2018.
- [O5]. J. A. Carballo. Modelado y control de sistemas de concentración de energía solar. Open researchers, Marie Skłodowska Curie Actions, Comision Europea. Almería, España, 28 Septiembre 2018.
- [O6]. J. A. Carballo, J. Bonilla, M. Berenguel. Modelado y optimización para una gestión eficiente de recursos en desalación Solar. XVI Simposio CEA de Ingeniería de Control. Almería, España, 7-9 Marzo 2018.
-

- [O7]. J. A. Carballo. Modelado y optimización para una gestión eficiente de recursos en tecnología termosolar. II Jornadas Universidad de Almería JSIDI 2019. Almería, España, 4 Marzo 2019.
  - [O8]. J. A. Carballo. Heliostato inteligente. Open researchers, Marie Skłodowska Curie Actions, Comision Europea. Almería, España, 27 Septiembre 2019.
-

# Resumen

La humanidad se enfrenta a uno de los mayores retos de su historia debido al uso inadecuado de los recursos naturales del planeta. Por un lado, el cambio climático derivado de la quema de combustibles fósiles para la obtención de energía y las emisiones de gases de efecto invernadero asociadas están provocando un calentamiento del planeta. Esta alteración del clima provoca que cada vez sean más frecuentes fenómenos meteorológicos extremos, muchos de ellos relacionados con la alteración del ciclo del agua como son las grandes sequías o las inundaciones.

Por otro lado, el uso irracional de los recursos naturales como el agua dulce está provocando que acuíferos de todo el mundo estén en una situación de estrés y hayan comenzado a agotarse, salinizarse o contaminarse. Por todo esto, parece razonable que debemos modificar nuestro modelo energético y el uso de los recursos naturales, en especial el del agua dulce.

Actualmente numerosos países han comenzado a instalar sistemas de desalinización, incluso algunos basan su suministro de agua dulce en estas plantas. A pesar del gran desarrollo sufrido por la mayoría de las tecnologías de desalinización, estas siguen siendo energéticamente inefficientes, lo que provoca que la mayor parte del coste del agua desalinizada se deba al consumo energético. Algunas tecnologías renovables, solar y eólica sobre todo, son capaces de proveer energía a un coste inferior que las tecnologías tradicionales basadas en la quema de combustibles fósiles, aunque la integración de sistemas de desalinización y energías renovables representa un gran desafío tecnológico.

Una de las tecnología de desalinización más empleada es la técnica de desalinización térmica, que aprovecha los cambios físicos del agua provocados por la transferencia de energía térmica para destilar agua dulce. Esta tecnología consume principalmente energía térmica, por lo que la tecnología solar térmica se erige como la mejor candidata para proveer energía a este tipo de procesos. El principal problema de la integración

desalinización-energía solar es que los actuales sistemas de desalinización no están diseñados para operar a cargas parciales o con interrupciones, condición básica para la hibridación con fuentes renovables debido a la no gestionabilidad del recurso. Afortunadamente, los sistemas de almacenamiento térmico están sufriendo un desarrollo muy veloz y una reducción de costes similar a la de las energías renovables, por lo que se espera que este tipo de almacenamiento de energía sea una opción factible que facilite la integración.

Debido al cambio del modelo energético promovido por las irrupción de las renovables y la eliminación de centrales contaminantes, ha surgido un nuevo paradigma en el modelo energético europeo en el que se espera que grandes plantas de generación centralizadas se combinen con sistemas de generación distribuida, ambos renovables. Este nuevo modelo podría estar integrado por micro-redes con producción inteligente y dependencia temporal en donde la gestión de energía y agua estén íntimamente relacionadas. Estos nuevos conceptos, unidos a los problemas de operación que presentan las plantas de desalinización y las energías renovables, demandan nuevas estrategias de operación.

Para el desarrollo de estos nuevos conceptos y sus estrategias de operación es necesario el uso de técnicas de modelado que nos permitan simular el comportamiento de los sistemas, ahorrando tiempo, dinero y evitando situaciones peligrosas para los sistemas y las personas. La irrupción de la industrial 4.0 nos brinda una serie de nuevas herramientas muy potentes que pueden revolucionar el desarrollo y la hibridación de las tecnologías renovables y desalinización, al igual que ha hecho en otros campos, mejorando su eficiencia y reduciendo costes. La inteligencia artificial es elemento central de esta revolución. Por este motivo en esta tesis se han empleado técnicas tradicionales de modelado como puede ser el modelado basado en primeros principios y técnicas de inteligencia artificial como son técnicas optimización basadas en algoritmos genéticos y modelado basado en redes neuronales.

En esta tesis doctoral se trata la aplicación de estas técnicas para lograr una gestión eficiente de energía y agua mediante el uso de energía solar. De manera general se pretende estudiar la viabilidad técnica de un sistema de destilación térmica acoplada a una bomba de calor de doble efecto cuya fuente de energía térmica es un campo solar y una caldera de gas, así como desarrollar nuevas estrategias de control y operación que solventen los problemas anteriormente expuestos.

---

En primer lugar se ha llevado a cabo un estudio bibliográfico de la temática. Posteriormente se ha desarrollado un conjunto de modelos de los subsistemas presentes en al instalación experimental empleada, basados en primeros principios, altamente configurables y capaces de ser interconectados entre sí. Permiten el análisis exergético necesario para calcular nuevos índices de rendimiento que han sido propuestos en estos trabajos. El conjunto de modelos ha resultado ser una herramienta muy potente para el análisis y la detección de ineficiencias en los sistemas.

Las estrategias de operación de los subsistemas más importantes han sido optimizadas haciendo uso del conjunto de modelos y aplicando optimizadores basados en inteligencia artificial (algoritmos genéticos). Finalmente, se ha propuesto una configuración para una planta de desalinización híbrida gas-solar, con el objeto de probar el conjunto de modelos y metodología para generar parámetros de operación óptimos. Esta metodología ha generado estrategias de operación óptimas que aseguren el funcionamiento óptimo de la planta, a pesar de las limitaciones en la operación introducidas por los subsistemas solar y desalinización. Uno de los principales problemas para la hibridación de estas tecnologías, como se comenta anteriormente.

También se han desarrollado modelos basados en redes neuronales que ayudan a mejorar las estrategias de control automático de plantas de energía solar debido al gran potencial que presentan. De todos los problemas analizados con potencial para ser resueltos por este tipo de modelado, se ha optado por desarrollar un modelo que hace posible un nuevo control basado en visión artificial para los sistemas de seguimiento solar. Este nuevo enfoque emplea un modelo basado en redes neuronales capaz de calcular el error de seguimiento y generar la señal de control para el sistema de seguimiento solar, a partir de una imagen. Con este nuevo enfoque no solamente se resuelven problemas tradicionales de los sistemas de seguimiento (errores debidos al desplazamiento del centro de gravedad, cargas de viento, encoders, referencias), además el modelo basado en redes neuronales podría proporcionar información muy relevante para el control óptimo de este tipo de sistemas como la predicción de transitorios debido al paso de nubes, distribución de flujos solar concentrado sobre el receptor, sombras y bloqueos debido a otros sistemas,

Además de estas ventajas, el nuevo enfoque ha sido implementado con software libre en hardware abierto, con lo que se ha conseguido abaratar en gran parte los costes asociados al hardware de estos sistemas. Otras

---

reducciones de costes aplicables a todo este tipo de instalaciones que se derivan del uso de esta nueva técnica, son reducción de costes en la comunicación gracias a las capacidades de comunicación inalámbricas del hardware y reducción de costes de los procesos de instalación y puesta en marcha de los sistemas al eliminar casi por completo las altas demandas de los sistemas tradicionales (estricto procedimiento de instalación para garantizar la precisión requerida y calibración periódica).

# **Abstract**



# Índice general

Agradecimientos	v
Contribuciones científicas derivadas de la tesis	vii
Resumen	xiii
Abstract	xvii
Índice general	xviii
Índice de figuras	xxi
Índice de tablas	xxiii
Acrónimos	xxvi
Nomenclatura	xxviii
<b>1. Introducción</b>	<b>1</b>
1.1. Cambio climático . . . . .	1
1.1.1. Luchar contra el calentamiento global . . . . .	2
1.2. Agua . . . . .	4
1.2.1. Desalinización . . . . .	5
1.2.2. Desalinización térmica . . . . .	8
1.2.3. Perspectivas de la desalinización . . . . .	10
1.2.4. Desalinización con energías renovables . . . . .	11
1.2.5. Desalinización con energía solar . . . . .	13
1.2.6. Sistema Aquasol . . . . .	14
1.3. Energías renovables . . . . .	17
1.3.1. Almacenamiento . . . . .	21

1.3.2. Tecnología de concentración solar . . . . .	22
1.3.3. Seguimiento solar . . . . .	24
1.3.4. Industria 4.0 y SMARTCSP . . . . .	26
1.4. Modelado basado en primeros principios y Modelica . . . . .	27
1.5. Inteligencia artificial . . . . .	29
1.5.1. Optimización . . . . .	29
1.5.2. Modelado basado en redes neuronales artificiales . .	31
<b>2. Hipótesis y objetivos</b>	<b>33</b>
2.1. Hipótesis . . . . .	33
2.2. Objetivos generales y específicos . . . . .	34
<b>3. Resultados</b>	<b>37</b>
3.1. Optimal operating conditions analysis of a multi-effect distillation plant [R1] . . . . .	37
3.2. Optimal operating conditions analysis for a MED according to energetic and exergetic criteria [R2] . . . . .	38
3.3. New low-cost solar tracking system based on open source hardware for educational purpose [R3] . . . . .	40
3.4. New approach for solar tracking systems based on computer vision, low cost hardware and deep learning [R4] . . . .	40
3.5. Parabolic trough collector field dynamic model: Validation, energetic and exergetic analyses [R5] . . . . .	41
3.6. Machine Learning for Solar Trackers [R6] . . . . .	43
3.7. Solar tower power mockup for the assessment of advanced control techniques [R7] . . . . .	44
3.8. Optimal Operation of Solar Thermal Desalination Systems coupled to DEAHP [R8] . . . . .	44
<b>4. Conclusiones y trabajos futuros</b>	<b>47</b>
4.1. Conclusiones generales . . . . .	47
4.2. Conclusiones específicas . . . . .	48
4.2.1. Optimal operating conditions analysis of a multi-effect distillation plant [R1] . . . . .	48
4.2.2. Optimal operating conditions analysis for a MED according to energetic and exergetic criteria [R2] . .	49
4.2.3. New low-cost solar tracking system based on open source hardware for educational purpose [R3] . .	50
4.2.4. New approach for solar tracking systems [R4] . .	51

---

4.2.5. Parabolic trough collector field dynamic model: Validation, energetic and exergetic analyses [R5] . . . . .	51
4.2.6. Machine Learning for Solar Trackers [R6] . . . . .	52
4.2.7. Solar tower power mockup for the assessment of advanced control techniques [R7] . . . . .	52
4.2.8. Optimal Operation of Solar Thermal Desalination Systems coupled to DEAHP [R8] . . . . .	52
4.3. Futuras líneas de investigación . . . . .	53
4.3.1. Modelado basado en primero principios . . . . .	53
4.3.2. Modelado basado en redes neuronales . . . . .	54
<b>Bibliografía</b>	<b>58</b>
<b>A. Artículos en revistas internacionales</b>	<b>69</b>
A.1. Optimal operating conditions analysis for a multi-effect distillation plant . . . . .	71
A.2. Optimal operating conditions analysis for a multi-effect distillation plant according to energetic and exergetic criteria	79
A.3. New low-cost solar tracking system based on open source hardware for educational purposes . . . . .	87
A.4. New approach for solar tracking systems based on computer vision, low cost hardware and deep learning . . . . .	99
A.5. Parabolic trough collector field dynamic model: Validation, energetic and exergetic analyses . . . . .	109
A.6. Machine learning for solar trackers . . . . .	120
A.7. Solar tower power mockup for the assessment of advanced control techniques . . . . .	129
A.8. Optimal Operation of solar thermal desalination systems coupled to double-effect absorption heat pumps . . . . .	142



# Índice de figuras

1.1.	Previsión del incremento de la temperatura media del planeta [1] . . . . .	2
1.2.	Tecnologías de desalinización . . . . .	6
1.3.	Celda MED . . . . .	9
1.4.	Principales combinaciones energías renovables-técnicas de desalinización . . . . .	12
1.5.	Sistema Aquasol . . . . .	15
1.6.	MED . . . . .	16
1.7.	Subsistemas Aquasol . . . . .	17
1.8.	Evolución del coste de las principales tecnologías de producción de energía renovable 2010-2018 [2]. . . . .	18
1.9.	LCOE y pujas de las principales tecnologías de generación de energía renovable en diferentes proyectos y subastas para nuevas instalaciones [2]. . . . .	19
1.10.	Tecnologías de concentración solar . . . . .	23
1.11.	Sistema de torre . . . . .	24
1.12.	Seguimiento solar . . . . .	25
1.13.	Neurona biológica y artificial . . . . .	31



# Índice de tablas

1.1.	Consumo específico energético de las principales tecnologías de desalinización [3]. . . . .	7
1.2.	Coste agua desalada mediante diferentes combinaciones de sistemas de desalinización y energía solar [4]. . . . .	14
1.3.	Coste actual [2] y previsión de coste de las principales fuentes renovables de producción de energía para 2030 [5] . . . .	20
1.4.	Evolución mix energético español 2017-2030 (Comision de Expertos (CE) [6], Protermosolar [5] y Plan Nacional Integrado de Energía y Clima 2021-2030 (PNIEC) [7] . . . .	21



# Acrónimos y abreviaturas

<b>AI</b>	<i>Artificial Intelligence.</i>
<b>ANNs</b>	<i>Artificial Neural Networks.</i>
<b>CPV</b>	<i>Concentrating Photovoltaic.</i>
<b>CPVT</b>	<i>Concentrating Photo Voltaic Thermal.</i>
<b>CSP</b>	<i>Concentrated Solar Power.</i>
<b>CST</b>	<i>Concentrating Solar Technology.</i>
<b>DEAHP</b>	<i>Double-Effect Absorption Heat Pump.</i>
<b>DNI</b>	<i>Direct Normal Irradiance.</i>
<b>ED</b>	<i>Electro Dialysis.</i>
<b>EDR</b>	<i>Electro Dialysis Reversal.</i>
<b>FO</b>	<i>Forward Osmosis.</i>
<b>GA</b>	<i>Genetic Algorithm.</i>
<b>GOR</b>	<i>Gained Output Ratio.</i>
<b>H2020</b>	Programa marco Horizonte 2020.
<b>HTF</b>	<i>Heat Tranfer Fluid.</i>
<b>I+D</b>	Investigación y Desarrollo.
<b>IEA</b>	<i>International Energy Agency.</i>
<b>LF</b>	<i>Linear Fresnel.</i>
<b>MD</b>	<i>Membrane Distillation.</i>
<b>MEB</b>	<i>Multi-Effect Boiling.</i>
<b>MED</b>	<i>Multiple Effect Distillation.</i>
<b>ML</b>	<i>Machine Learning.</i>
<b>MSF</b>	<i>Multi-Stage Flash.</i>

---

<b>MVC</b>	<i>Mechanical Vapor Compression.</i>
<b>ONU</b>	Organización de las Naciones Unidas.
<b>PD</b>	<i>Parabolic Dish.</i>
<b>PNIEC</b>	Plan Nacional Integrado de Energía y Clima 2021-2030.
<b>PR</b>	<i>Performance Ratio.</i>
<b>PSA</b>	Plataforma Solar de Almería.
<b>PTC</b>	<i>Parabolic Trough Collector.</i>
<b>PV</b>	<i>Photovoltaic.</i>
<b>RO</b>	<i>Reverse Osmosis.</i>
<b>SFWC</b>	<i>Specific Water Consumption.</i>
<b>STE</b>	<i>Solar Thermal Electricity.</i>
<b>STP</b>	<i>Solar Tower Power.</i>
<b>UE</b>	Unión Europea.

# Nomenclatura

## Unidades físicas

$C$  Grado Celsius

$GW$  Gigavatio

$kg$  Kilogramo

$kJ$  Kilojulio

$kWh$  Kilovatio hora

$kt$  Kilotonelada

$m$  metro

$MW$  Megavatio

$mrad$  Miliradianes

## Símbolos matemáticos

$\%$  Tanto por ciento

## Otros

$CO_2$  Dióxido de carbono

$dis$  Destilado

$\epsilon$  Euro

$h$  Entalpía  $kJ/kg$

$\bar{E}_{Thermal}$  Consumo térmico específico  $kJ/kg$

*feed* Alimentación

$\dot{m}$  Caudal másico  $kg/s$

*steam* Vapor

# Capítulo 1

## Introducción

*Cada día sabemos más  
y entendemos menos.*

**Albert Einstein**

**Resumen:** En este capítulo se da una descripción de los principales problemas que motivan la realización del presente trabajo y se expone una revisión del estado de la técnica en las tecnologías empleadas.

---

### 1.1. Cambio climático

Recientemente, la Organización de las Naciones Unidas (ONU) ha publicado un informe en el que se estima que las acciones humanas han causado un incremento aproximado de 1 °C de la temperatura media del planeta respecto de los niveles preindustriales (calentamiento global de origen antropogénico). Dicho informe advierte que de continuar con la tendencia actual (Fig. 1.1), sin combatir las causas que lo provocan, se incrementará la temperatura media del planeta más de 1.5 °C entre 2030 y 2050 [1].

Sobrepasar un incremento de 1.5 °C de la temperatura media del planeta provocará: temperaturas extremadamente altas, alteración del ciclo

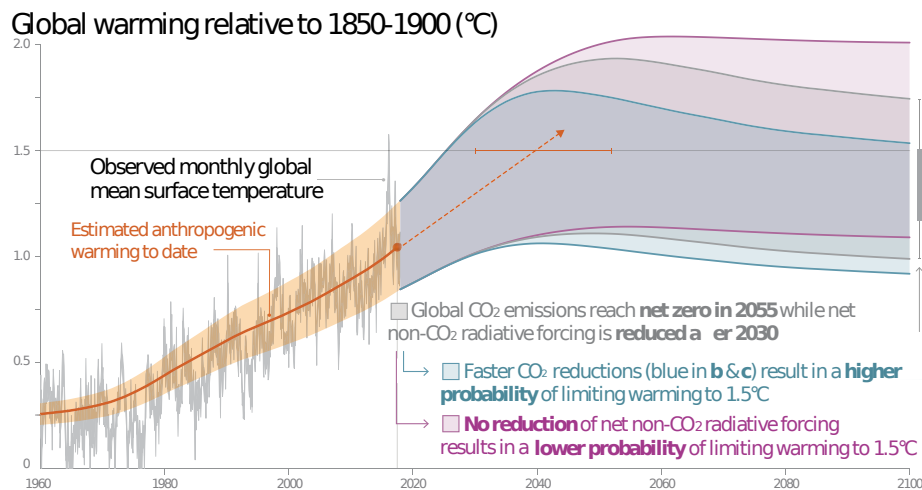


Figura 1.1: Previsión del incremento de la temperatura media del planeta [1]

del agua que dará lugar a precipitaciones torrenciales en determinadas regiones y escasez de estas en otras, aumento de la frecuencia de eventos climatológicos extremos, aumento del nivel del mar que tendrá especial repercusión en los ecosistemas y recursos hídricos de zonas costeras, consecuencias negativas directas sobre ganadería, agricultura y economía, aumento de la pobreza y desigualdad [1].

El calentamiento global de origen antropogénico está provocado principalmente por las emisiones de gases de efecto invernadero por la acción humana, derivadas en su mayoría del uso de combustibles fósiles. En Europa por ejemplo, la producción de energía eléctrica y transporte, cuya fuente principal de energía son los combustibles fósiles, son responsables del 78 % de las emisiones de gases de efecto invernadero. La agricultura contribuye con un 10.1 %, los procesos industriales con un 8.7 % y la gestión de residuos con un 3.7 % [8].

### 1.1.1. Luchar contra el calentamiento global

Limitar el incremento de la temperatura media del planeta requerirá cambios sin precedentes en el modelo energético global y en el uso de los recursos naturales. Se estima que para limitar el calentamiento global a 1.5 °C, las emisiones netas de gases de efecto invernadero deben ser nulas

antes de 2050 [8] y cuanto más rápida sea la reducción de emisiones más probabilidades existen de limitar el calentamiento.

Para poder acometer estos cambios son necesarias acciones inmediatas por parte de organizaciones y gobiernos que promuevan y financien acciones para esta transición sin precedentes en cuanto a escala. La Unión Europea ya dedica esfuerzos contra el cambio climático en gran parte de sus actividades en el Programa marco Horizonte 2020 (H2020). Además, recientemente Europa ha actualizado su hoja de ruta hacia una descarbonización sistemática de la economía y ha adoptado una visión estratégica a largo plazo para conseguir una economía próspera, moderna, competitiva y climáticamente neutra de aquí a 2050 que haga líder a Europa en este proceso de transición global.

España por su parte, acaba de publicar el Plan Nacional Integrado de Energía y Clima 2021-2030 (PNIEC) [7], donde fija un marco estratégico para la transición ecológica de la economía española que pretende reducir a corto plazo un 21 % las emisiones de gases de efecto invernadero y aumentar hasta un 74 % sobre el total de consumo el aporte de energía eléctrica renovable. Este plan también prevé reducir más de un 90 % las emisiones de gases de efecto invernadero y alcanzar el 100 % renovable del mix energético para 2050. Con todo esto, se pretende que España gane en prosperidad, seguridad energética, generación de empleo industrial, innovación, salud, desarrollo tecnológico y justicia social, acompañando a los colectivos más vulnerables.

Además de mitigar los problemas derivados del calentamiento global anteriormente citados, actualmente numerosos organismos [1,5–8] advierten de las ventajas ambientales, estratégicas y socioeconómicas que tiene la lucha contra el calentamiento global, la gestión eficiente de los recursos y el uso de energía de origen renovable.

Estos organismos prevén que la transición ecológica tenga un gran impacto positivo sobre el empleo y la economía, puesto que las energías renovables y la industria sostenible ayudan a un mejor reparto de riqueza. El uso de energías renovables podría reducir las importaciones de combustibles fósiles en países energéticamente dependientes. Según las previsiones del PNIEC, España podrá ahorrar más de 75 000 millones de euros en importaciones de combustibles fósiles respecto del escenario actual. Además, en España el PNIEC estima que se generarán entre 250 000 y 364 000 empleos netos hasta 2030 debido a la transición a un modelo energético renovable [7]. Si nos fijamos solamente en la demanda de

---

tecnología termosolar propuesta por el PNIEC, en la fase de construcción de las centrales termosolares se crearían 88 500 puestos de trabajo al año y en la fase de operación se generaría 1770 empleos directos adicionales al año. Se estima que las inversiones en termosolar contribuirían a un incremento del producto interior bruto de 62 000 millones de euros en su fase de construcción y de 5000 millones de euros en la fase de operación [5].

Finalmente, la lucha contra el cambio climático también tendrá efectos positivos en cuanto a la salud. En España se espera reducir el número de muertes prematuras debidas a la contaminación atmosférica, pasando de 8951 a 6729 muertes anuales debido a la reducción de gases contaminantes [7]. Por todo esto, parece razonable poner en marcha una transición hacia un modelo sostenible de aprovechamiento de recursos naturales como el agua dulce y generación de energía de forma limpia que ayude a mitigar y revertir los cambios a los que estaremos sometidos debido al calentamiento global.

## 1.2. Agua

El agua es un recurso fundamental para el desarrollo de la sociedad, actualmente las políticas incorrectas e insostenibles de desarrollo junto con los problemas derivados del calentamiento global anteriormente citados, han aumentado la presión sobre los recursos hídricos del planeta. El calentamiento global y el cambio climático asociado provocarán la alteración del ciclo del agua y un uso más intenso de este recurso, por lo tanto una extracción más intensiva de los recursos hídricos [9] que aumentará aún más la presión sobre los ya sobreexplotados acuíferos [10]. El problema será más grave en acuíferos costeros en los que junto con el aumento del nivel del mar se incrementarán los fenómenos de intrusión de agua salada.

Por otro lado, la población mundial sigue creciendo, aunque a menor ritmo desde 1950. Con esta tendencia se espera que la población mundial pase de 7.7 a 8.5 billones de habitantes en 2030, 9.7 billones en 2050 y 10.9 billones en 2100. También cabe destacar que el consumo de agua ha aumentado alrededor de 5, 18 y 10 veces para uso agrícola, industrial y energético, respectivamente [11]. Esta previsión de aumento en la población mundial y sus niveles de vida, junto con prácticas insostenibles, pondrán a los recursos hídricos bajo una presión cada vez mayor a nivel

---

mundial. Todo esto se traducirá en una disminución de los recursos de agua dulce disponibles de al menos un 15 %, aumentando el número de personas que no tendrán acceso a este recurso [12].

Con este escenario, la ONU pronostica que entre 2000 y 7000 millones de personas sufrirán problemas relacionados con la escasez de agua en 2050, incluso en regiones que actualmente disponen de suficientes reservas de este recurso natural. Si tenemos en cuenta que la mayor parte de la población mundial vive en regiones costeras, la obtención de agua dulce a partir de agua de mar se presenta como una buena herramienta contra los problemas anteriormente descritos. Actualmente, algunos países de Oriente Medio ya están usando el agua de mar desalinizada como principal o única fuente para cubrir sus demandas de agua dulce [13].

### 1.2.1. Desalinización

Durante las últimas décadas, la desalinización de agua salobre y agua de mar ha crecido rápidamente por todo el mundo. El riesgo de falta de suministro de agua dulce debido a los efectos del cambio climático y el incremento de la temperatura media del planeta, no sólo ha obligado a países de Oriente Medio a adoptar estas tecnologías, otros países como los Estados Unidos, España y Japón también han desplegado de forma masiva plantas de desalinización. En 2013, había más de 17 000 plantas desalinizadoras activas que suministraban 80 millones de  $m^3$  al día a 300 millones de personas en 150 países. En 2015, la capacidad de producción aumentó a casi 97.5 millones de  $m^3$  al día y se espera que esta cifra de producción de agua desalada se duplique en 2050 [14].

Actualmente las técnicas de desalinización más extendidas pertenecen a dos grupos (Fig. 1.2): técnicas de desalinización por evaporación y condensación (*Mechanical Vapor Compression* (MVC), *Multi-Stage Flash* (MSF), *Multiple Effect Distillation* (MED) y *Multi-Effect Boiling* (MEB)) y técnicas de desalinización por filtración (*Reverse Osmosis* (RO), *Forward Osmosis* (FO), *Membrane Distillation* (MD), *Electro Dialysis* (ED) y *Electro Dialysis Reversal* (EDR)).

Aunque inicialmente la mayor parte de la capacidad instalada pertenecía a la categoría de procesos de desalinización térmica, en la actualidad se estima que del total de la capacidad de producción instalada, dos tercios pertenecen a procesos de desalinización por filtración y un tercio a desalinización térmica [15]. A pesar de este cambio de tendencia, los pro-

---

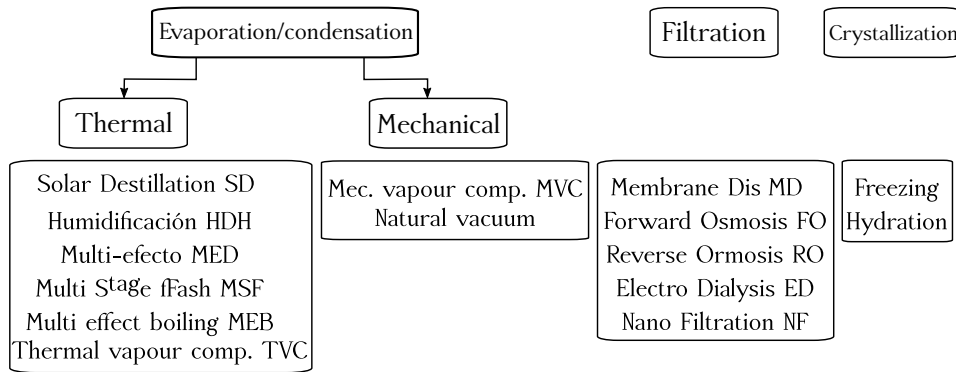


Figura 1.2: Tecnologías de desalinización

cesos basados en principios térmicos seguirán ocupando una buena parte de la nueva capacidad instalada, más aún cuando se abarate la energía térmica debido a la incorporación de fuentes de energía renovable o en plantas de cogeneración agua-energía eléctrica [15].

Los avances tecnológicos han provocado que las técnicas de extracción de sales y otras sustancias químicas disueltas en agua sean cada vez mas eficientes y económicas, además la incorporación energías renovables para satisfacer las demandas energéticas de estos procesos, están garantizando su sostenibilidad. A pesar de estos avances, aún existe un largo camino por recorrer [14], como muestra la gran diferencia que existe entre el consumo actual de energía de cualquier tecnología (Tab. 1.1) para desalinizar agua de mar y el mínimo teórico de 0.7 kWh/m<sup>3</sup> [16]. La Tab. 1.1 muestra el consumo eléctrico, térmico y eléctrico equivalente, calculado este último como la suma del consumo térmico y eléctrico aplicando un coeficiente de eficiencia de conversión térmico-electrico del 45 %, para cada una de las principales tecnologías de desalinización.

## Índices de rendimiento

Existen varios parámetros de rendimiento que caracterizan la eficiencia de un sistema de desalinización. El índice más extendido es el *Gained Output Ratio* (GOR), este muestra la relación entre la masa de destilado producido por unidad de masa de vapor suministrado a la planta de destilación térmica (Eq. 1.1).

	Elec. (kWh/m <sup>3</sup> )	Term. (kWh/m <sup>3</sup> )	Total elec. eq. (kWh/m <sup>3</sup> )
RO	3-6	-	3-6
ED	1-3.5	-	1-3.5
EDR	1-2	-	1-2
FO	0.2-0.5	20-150	10-68
MD	1.5-4	4-40	3-22
MVC	7-15	-	7-15
MSF	2.5-5	40-120	21-59
MED	2-2.5	30-120	15-57
MEB	2	60	30

Tabla 1.1: Consumo específico energético de las principales tecnologías de desalinización [3].

$$GOR = \frac{\dot{m}_{dis}}{\dot{m}_{steam}}. \quad (1.1)$$

El segundo parámetro es el *Performance Ratio* (PR), que se define como la relación entre la cantidad de energía térmica en forma de calor latente de vaporización del agua a 73 °C (2326 kJ/kg) y el consumo específico de energía térmica del proceso, medido este último como la diferencia de entalpías específicas entre el fluido que realiza el aporte de calor al proceso a la entrada ( $h_1$ ) y la salida ( $h_2$ ) del sistema (Eq. 1.2). El PR presenta un carácter más general que el GOR, puesto que también puede ser utilizado en procesos que emplean el calor sensible de un fluido. Aunque el PR y el GOR no son iguales, las diferencias entre ambos son muy pequeñas.

$$PR = \frac{\dot{m}_{dis} \cdot 2326}{(h_1 - h_2) \cdot \dot{m}_1}. \quad (1.2)$$

El consumo específico de energía térmica ( $\bar{E}_{Thermal}$ ) se define como la relación entre el consumo de energía térmica medida como en el PR y la producción de agua desalinizada (Eq. 1.3).

$$\bar{E}_{Thermal} = \frac{(h_1 - h_2) \cdot \dot{m}_1}{\dot{m}_{dis}}. \quad (1.3)$$

En procesos de desalinización en los que no se consume energía térmica, se emplea el consumo específico eléctrico (Eq. 1.4).

$$\overline{E}_{elec} = \frac{E_{elec}}{\dot{m}_{dis}}. \quad (1.4)$$

El consumo específico de agua o *Specific Water Consumption* (SFWC) muestra la relación entre el caudal de agua desalinizada producida y el agua de alimentación empleada en el proceso (Eq. 1.5).

$$SFWC = \frac{\dot{m}_{dis}}{\dot{m}_{feed}}. \quad (1.5)$$

Todos estos índices basados en balances energéticos consideran un único tipo de energía (térmica o eléctrica), a pesar de que numerosas técnicas de desalinización emplean tanto energía eléctrica como térmica en su operación (Tab. 1.1). En el caso de los índices basados en energía térmica, tampoco se considera la calidad (temperatura) de la energía térmica consumida. Estos hechos provocan que sea complicado comparar rendimientos entre diferentes tecnologías e incluso entre instalaciones del mismo tipo de tecnología que operan a diferentes temperaturas.

### 1.2.2. Desalinización térmica

La desalinización térmica se basa en los cambios de estado producidos por las variaciones de la temperatura del agua. Entre las principales ventajas que posee la desalinización térmica podemos destacar que emplea energía térmica de baja temperatura, son instalaciones fiables fáciles de operar en condiciones nominales y fáciles de mantener incluso con aguas de alimentación muy duras, muy contaminadas o muy salobres, además el agua dulce obtenida mediante estas técnicas es de gran pureza. A pesar de todas estas ventajas, las técnicas de desalinización térmicas son energéticamente ineficientes lo que hace que el coste energético represente al menos la mitad del coste total del agua desalada.

Como se puede apreciar en Tab. 1.1 los procesos de desalinización térmica demandan dos formas diferentes de energía que puede provenir de diferentes fuentes (combustibles fósiles, energía residual [17], energía solar [18, 19]). Por un lado energía térmica que representa la mayor parte de la energía consumida y por otro lado energía eléctrica consumida principalmente por los actuadores y sistemas de bombeo.

Actualmente la mayor parte de las instalaciones de desalinización térmica que existen son desalinizadoras tipo MED [20]. Las plantas MED

están formadas por una serie de elementos herméticos, llamados celdas (Fig. 1.3), conectados entre sí. Cada una de ellas compuestas por un efecto y un precalentador en los que se da lugar a una serie de procesos de evaporación y condensación simultáneos respectivamente. Las celdas se suelen asociar en serie en una secuencia decreciente de presiones y temperaturas. Cuando el agua de mar o la salmuera de un efecto anterior entra en el efecto se produce una evaporación súbita y parte de esta reduce la temperatura del agua hasta igualarla con la temperatura de saturación a esa presión, si la presión de saturación del agua de mar es mayor que la presión de la celda al entrar en ella [21].

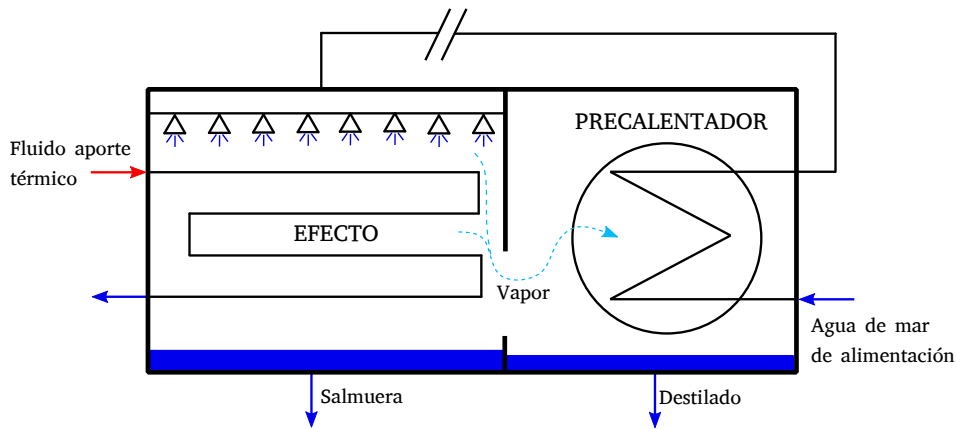


Figura 1.3: Celda MED

La parte del agua de mar que entra en el efecto y que no puede evaporarse súbitamente recibirá el calor cedido por el vapor del efecto anterior o la fuente de calor externa si es el primer efecto, que circula por el interior de los tubos del efecto. A medida que el agua adquiere calor se evaporará aumentando así la concentración de sales del agua de mar (salmuera), que pasa al siguiente efecto.

Todo el vapor producido alcanza el precalentador de la celda y condensa, debido a que el agua de mar de alimentación que circula por el interior de los tubos del precalentador se encuentra a menor temperatura que la de saturación del vapor. Un captador recoge el destilado y lo mezcla con el destilado que viene del interior del efecto. El destilado y parte del vapor pasan al efecto de la siguiente celda, donde al estar la superficie de los tubos a menor temperatura que la de saturación, se

forma una película delgada de agua en la parte interior superior del tubo, a medida que avanza el fluido esta película se hace más gruesa debido a que el vapor va condensando y cediendo calor. Solo el destilado consigue atravesar el efecto [21].

Aunque la operación en condiciones nominales de este tipo de plantas es sencilla, la operación a cargas parciales o transitorios es compleja, pudiendo fácilmente alcanzar puntos de operación muy inefficientes o peligrosos para la integridad de la planta.

### 1.2.3. Perspectivas de la desalinización

En la actualidad, la desalinización es una técnica madura y viable para la obtención de agua dulce, aunque como se comenta anteriormente, es considerada inefficiente energéticamente. Por esto, la clave del desarrollo de las técnicas de desalinización pasa por reducir el consumo o el coste energético, tratando de desarrollar sistemas respetuosos con el medio ambiente que no contribuyan al problema del calentamiento global. Este objetivo no ha sido siempre el mismo, puesto que anteriormente el foco estuvo puesto mayoritariamente en reducir el coste de inversión de las instalaciones, dando lugar a reducciones en el coste de membranas, nuevos intercambiadores de calor de bajo coste, etc [22].

Actualmente, ya se están dedicando gran parte de los esfuerzos de investigación en reducir el consumo energético, desarrollando nuevos sistemas híbridos que combinan dos o más sistemas de desalinización y también sistemas de cogeneración agua-energía principalmente [15, 22, 23]. Cabe destacar que el futuro de la red eléctrica probablemente incluirá conceptos tales como las micro-redes inteligentes, producción inteligente con dependencia temporal [24], integración de energías renovables y entornos inteligentes en los que la gestión de energía y agua están íntimamente relacionadas [25].

Por todo esto, los nuevos desarrollos en desalinización deberán tener en cuenta en primer lugar la operación variable del sistema. Las condiciones de operación del proceso de desalinización que históricamente se han fijado en condiciones de operación nominales, deberán optimizarse para uno o varios objetivos, por ejemplo, los ingresos máximos o el consumo mínimo de energía durante los precios pico de la electricidad, considerando de este modo una operación variable en el tiempo. El concepto de operación variable en el tiempo en la desalinización es también un avance

---

necesario para la integración con fuentes de energía renovables [22].

La interconexión de equipos debida a la hibridación o cogeneración, demanda también nuevas técnicas de optimización de los parámetros de diseño y operación de las plantas, diferentes de las técnicas heurísticas tradicionales basadas en la búsqueda de condiciones nominales en estado estacionario [22].

El desarrollo y la optimización de los nuevos sistemas mediante técnicas empíricas no es práctico, sin embargo las técnicas de simulación y optimización basadas en las nuevas posibilidades computacionales y técnicas numéricas proporcionan nuevas posibilidades. La simulación permite predecir el comportamiento de los sistemas de manera rápida, económica y evitando los posibles riesgos que conlleva someter a una planta real a situaciones límites.

De entre todas las perspectivas relacionadas con la desalinización, la integración con energías renovables es la de mayor proyección, siempre y cuando se puedan resolver los retos que plantea esta integración.

#### 1.2.4. Desalinización con energías renovables

Aunque en Sec. 1.3 se trata más en detalle el uso de las energías renovables, en este apartado se hace referencia a ellas desde el punto de vista de su acoplamiento a procesos de desalinización. Debido a los problemas relacionados con el cambio climático y al alto consumo energético de los procesos de desalinización, los sistemas integrados de desalinización con energías renovables ofrecen una solución beneficiosa para satisfacer la creciente demanda de agua desalada. Este tipo de sistemas están experimentando un interés creciente en todo el mundo, como muestra el gran número de contribuciones científicas recientes [26] y la construcción de más de 130 plantas en los últimos años [27]. La mayor parte de estas plantas son de mediana escala, emplean energías renovables pero están conectadas a la red eléctrica para garantizar un suministro continuo de energía y mantener de este modo un funcionamiento estable [4].

Se están realizando grandes esfuerzos por aumentar la escala de las plantas, pero este proceso se ve obstaculizado por varios desafíos tecnoeconómicos. El acoplamiento de los sistemas de desalinización con energías renovables requiere aún de un importante esfuerzo en investigación y desarrollo para que sean eficientes, fiables y económicamente competitivos con los sistemas de desalinización convencionales [4,27]. Los principa-

---

les retos técnicos que presenta el uso de energías renovables con sistemas de desalinización son debidos a la fluctuación en el suministro de energía, esto provoca que la eficiencia del sistema sea baja cuando se opera con carga variable y en condiciones de operación variables. La operación a cargas parciales y variable afecta la vida de las plantas, por lo tanto se requiere un sistema de almacenamiento de energía o una fuente alternativa de energía de respaldo para que la planta de desalinización basada en energía solar pueda mejorar su operación [28]. Como se ha comentado anteriormente, los principales retos económicos de este tipo de plantas son debidos a la ineficiencia energética del proceso y los elevados costes energéticos.

La energía solar, eólica, geotérmica, undimotriz y maremotriz son las principales fuentes de energía renovable, además de la energía hidroeléctrica, la biomasa y el biogas. La energía hidroeléctrica y la biomasa no son adecuadas para unirse a la tecnología de desalinización porque requieren recursos hídricos que pueden no estar disponibles en los países con escasez de agua (Tab. 1.4).

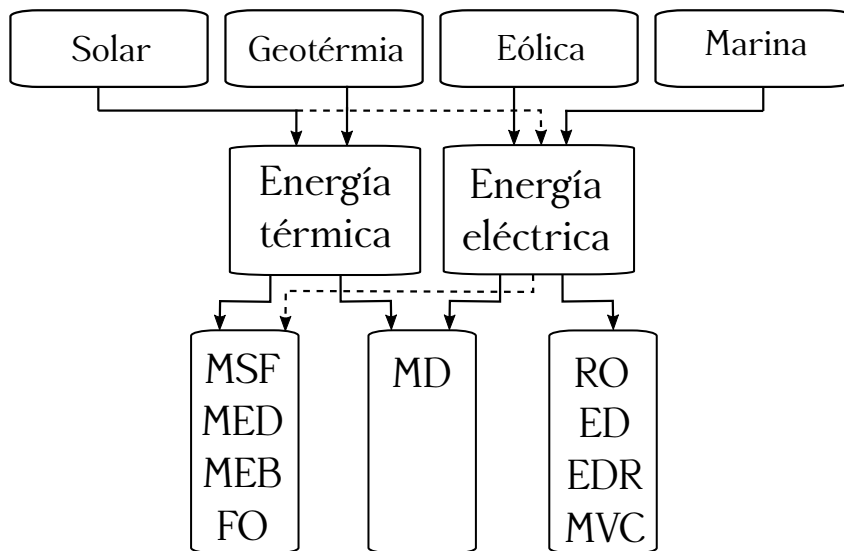


Figura 1.4: Principales combinaciones energías renovables-técnicas de desalinización

La energía eólica y marítima son más adecuadas para las áreas cos-

teras donde el viento y el agua están disponibles. Este tipo de energías se combina principalmente con los sistemas de desalinización RO y ED porque requieren electricidad en lugar de calor. La energía geotérmica, que utiliza la alta temperatura del subsuelo de la tierra para producir vapor o almacenar la energía térmica, requiere perforaciones subterráneas de hasta 5000 m y se puede combinar con sistemas de desalinización que demanden energía térmica.

Finalmente, la energía solar es la fuente más aplicable de energía renovable para integrarse con la tecnología de desalinización porque puede producir el calor y la electricidad que requieren todos los procesos de desalinización (Fig. 1.4). Además, la energía solar es más abundante y predecible que el resto de fuentes renovables. Actualmente, alrededor del 70 % de las plantas de desalinización renovables funcionan con energía solar.

Por lo tanto, la desalinización impulsada por energías renovables es una tecnología sólida para la producción de agua dulce a pequeña o mediana escala, sin embargo es necesario mejorar el rendimiento de estos sistemas si se quiere llevar a escalas más grandes. También es necesario realizar modificaciones a los procesos de desalinización convencionales para hacerlos más adecuados a sistemas integrados con energías renovables, debido al bajo rendimiento a cargas parciales y los problemas ante interrupciones de la mayoría de los sistemas de desalinización [4].

### 1.2.5. Desalinización con energía solar

Actualmente la desalinización solar a gran escala se enfrenta a problemas técnicos y económicos que plantean que los procesos de desalinización convencionales disponibles no sean técnica y económicamente adecuados para hibridarlos con energía solar [4]. Los costes económicos derivados de las grandes áreas de captadores solares necesarias por la baja eficiencia energética, convierten la desalinización solar en una tecnología más costosa que las tecnologías convencionales que utilizan combustibles fósiles [28], (Tab. 1.2).

Aun así, el 43 % de la capacidad de desalinización con energías renovables se apoya en energía solar [27]. Además, las posibilidades de almacenamiento de energía térmica que brinda la energía solar y sus perspectivas de abaratamiento pueden convertirla en una gran herramienta para solucionar la necesidad de suministro energético continuo que presentan

---

Tecnología	Capacidad media (m <sup>3</sup> /día)	Coste (\$/m <sup>3</sup> )
SD	<0.1	1.3-6.5
Solar MSF	1	1.-5
STP MSF	1	-
CCP MED	>5000	2.3-2.8
STP MED	1	-
STP VC	1	-
PV RO	<100	3-27
STP RO	1	-
PV EDS	<100	10.4-11.7
Solar MD	0.15-10	10.4-19.5
Solar AD	8	13-18

Tabla 1.2: Coste agua desalada mediante diferentes combinaciones de sistemas de desalinización y energía solar [4].

los sistemas de desalinización. Por lo tanto, para lograr un sistema de dealinización basado en energía solar se deben mejorar los procesos de desalinización y abaratar los costes de la energía solar [4].

Cabe destacar un creciente interés en sistemas de desalinización integrados en centrales solares para la producción de energía eléctrica, debido a que las demandas de agua dulce y electricidad generalmente están vinculadas [26]. El problema principal de este tipo de sistemas es la disponibilidad de modelos válidos para simular el subsistema de desalinización a carga parcial, o simular el efecto de la planta de desalinización en la eficiencia del ciclo de potencia [26].

### 1.2.6. Sistema Aquasol

El sistema Aquasol ha sido empleado para la realización del presente trabajo. La planta Aquasol data de 1987, cuando un sistema de desalinización tipo MED fué instalado en la Plataforma Solar de Almería (PSA). En lo sucesivo este sistema ha sido modificado numerosas veces, una de las modificaciones más importantes en el marco del proyecto Aquasol, que finalmente le ha dado su nombre a la instalación experimental. El proyecto Aquasol (*Enhanced Zero Discharge Seawater Desalination using Hybrid Solar Technology*), tenía como objetivo desarrollar el proceso de destilación acoplado con energía solar térmica, reducir sus costes, reducir

vertidos de salmuera y operar 24 horas al día. Actualmente, el sistema Aquasol está compuesto por una planta desalinizadora tipo MED, una bomba de absorción de doble efecto, tanques de almacenamiento, una caldera de gas, un generador de vapor y un campo solar de canal parabólico o *Parabolic Trough Collector* (PTC) de pequeña apertura (Fig. 1.5). Esta composición y un diseño flexible en cuanto a conexiones entre subsistemas, convierte al sistema Aquasol en una notable instalación experimental.

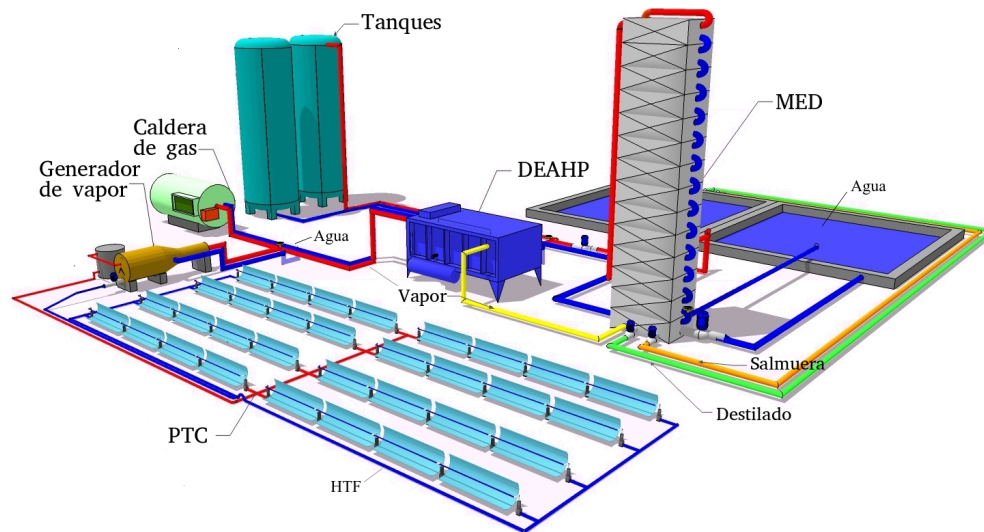
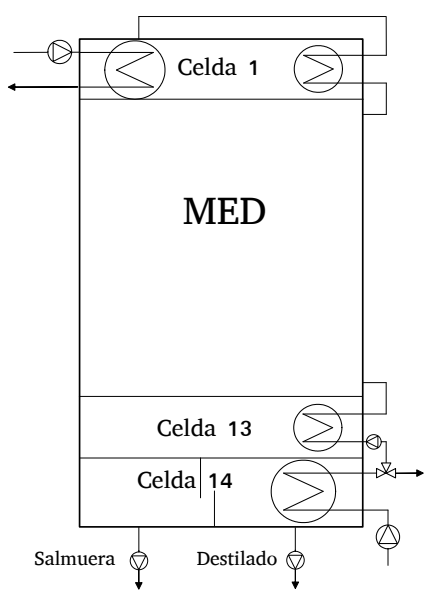


Figura 1.5: Sistema Aquasol

La unidad central del sistema Aquasol es un sistema de desalinización tipo MED compuesto por 14 celdas con precalentadores y alimentación frontal. El sistema tiene una disposición vertical en la que el agua de mar desciende por gravedad desde la primera hasta la última celda, en orden decreciente de presiones reguladas por un sistema de vacío (Fig. 1.6). Cada celda está compuesta por un efecto y un precalentador, todas son identicas excepto la primera y la última celda. La primera celda original, permitía trabajar con vapor saturado a baja presión [29], fue reemplazada para permitir trabajar directamente con agua caliente [30]. La última celda difiere de una celda normal porque su precalentador (condensador) tiene 4 veces el tamaño del resto, por el interior circula una gran cantidad de agua de mar con el fin de condensar todo el vapor acumulado en el último efecto. A la salida del condensador, parte de este agua de mar

es rechazada y vuelve a las piscinas, el agua no rechazada se envía a los precalentadores de las celdas y posteriormente se rocía sobre el primer efecto de la planta.



(a) Esquema MED



(b) Imagen real MED

Figura 1.6: MED

El sistema Aquasol tambien está compuesto por una bomba de calor por absorción de doble efecto o *Double-Effect Absorption Heat Pump* (DEAHP) que emplea agua-bromuro de litio como fluido de trabajo [31] (Fig. 1.7). La DEAHP se encarga de recuperar parte del calor del vapor saturado de baja presión del último efecto de la MED (Fig. 1.5). La planta MED consume aproximadamente 200 kW a 65 °C, de los cuales son recuperables por la DEAHP unos 100 kW a 35 °C. Una caldera de gas aporta el resto, esta vez a 180 °C, para que sea la DEAHP la encargada de proporcionar toda la energía a la planta MED.

Aquasol dispone de un campo de PTC de pequeña apertura para suministrar calor solar al proceso, compuesto por un total de 8 PTC dispuestos en 4 lazos en paralelo con 2 PTC en serie por lazo. Los PTC tienen una eficiencia del 55 % trabajando entre 120-220 °C y 1000 W/m<sup>2</sup> de radiación solar directa o *Direct Normal Irradiance* (DNI). Emplean



Figura 1.7: Subsistemas Aquasol

como fluido aceite térmico Therminol 55. El campo de PTC está conectado con un generador de vapor carcasa-tubo (Fig. 1.5), cuya función es suministrar parte de la demanda de vapor de la DEAHP a partir de la energía térmica recolectada por el campo PTC (Fig. 1.7).

### 1.3. Energías renovables

Existen diferentes tecnologías capaces de aprovechar fuentes renovables de energía, en función de la fuente se pueden clasificar en: eólica, solar, geotérmica, oceánica, hidráulica, biomasa y residuos. Realmente, la mayor parte de estas fuentes son una forma de energía solar transformada por procesos naturales [32]. Cada fuente puede ser aprovechada por sistemas basados en diferentes principios físicos como por ejemplo la energía solar, que puede ser aprovechada por un sistema fotovoltaico o *Photovoltaic* (PV) o por un sistema de radiación solar concentrada o *Concentrated Solar Power* (CSP).

Como se comenta en Sec. 1.1.1, numerosos organismos advierten de

las ventajas ambientales, estratégicas y socioeconómicas del uso de las energías renovables frente a las energías fósiles y la gestión eficiente de los recursos, en especial el agua dulce [1, 5–8]. En la actualidad, en la mayor parte del mundo las tecnologías renovables son la fuente más económica de producción de energía eléctrica (Fig. 1.8). El 77 % de la capacidad de los proyectos eólicos en tierra y el 83 % de la capacidad de los proyectos basados en tecnología PV ofertada en subastas públicas para 2020, pujan por debajo de la opción más barata de generación con combustibles fósiles (Fig. 1.9).

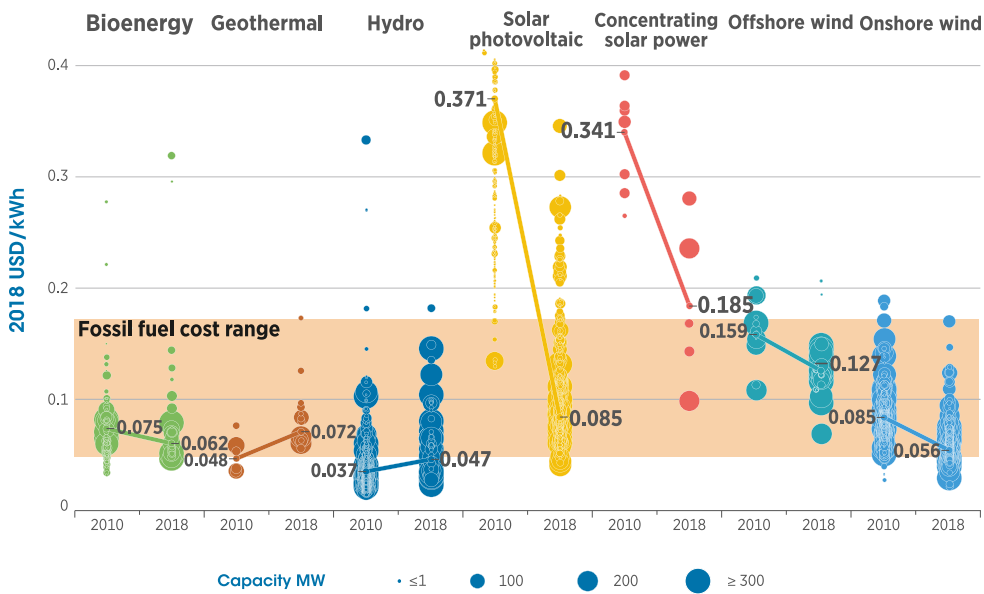


Figura 1.8: Evolución del coste de las principales tecnologías de producción de energía renovable 2010-2018 [2].

Por estos motivos, la mayoría de los países más democráticos están aumentando la inversión en energías renovables, tanto en nuevas instalaciones como en Investigación y Desarrollo (I+D) sobre las mismas [33]. En Europa por ejemplo, durante el periodo 2007-2017, se aumentó de 258 a 512 GW la capacidad de generación de origen renovable, se incrementó exponencialmente el número de publicaciones científicas relacionadas y se publicaron nuevos trabajos que muestran la viabilidad técnica y económica de un sistema 100 % renovable apoyado con una mejora de las interconexiones entre países [34]. Cabe destacar un estudio que indica que

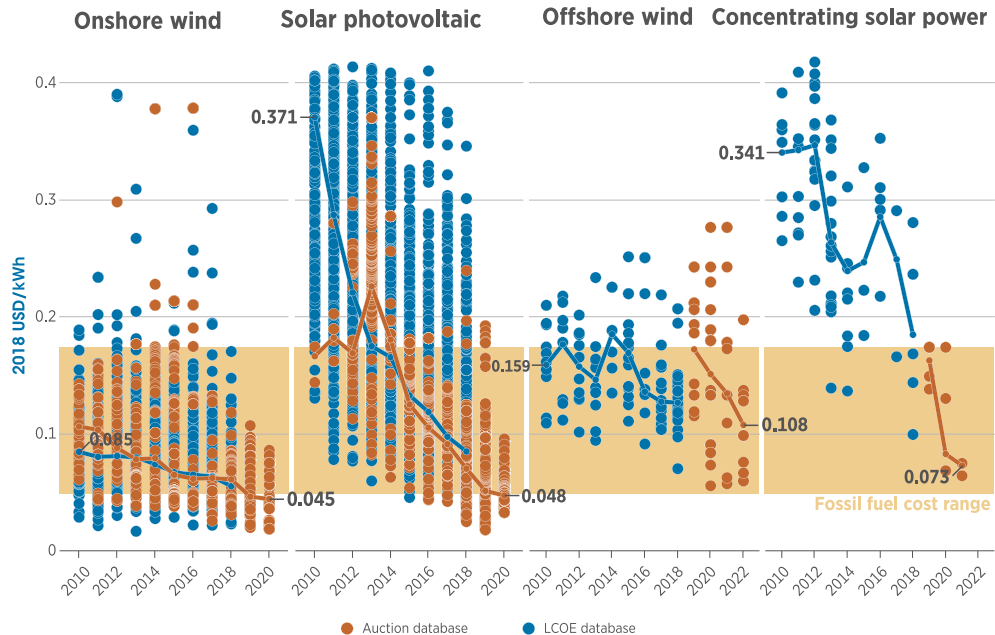


Figura 1.9: LCOE y pujas de las principales tecnologías de generación de energía renovable en diferentes proyectos y subastas para nuevas instalaciones [2].

lejos de las visiones de sistemas centralizados o descentralizados de producción de energía eléctrica para Europa, el enfoque Super Smart Grid hybrid [35] que contempla un mix de plantas de generación centralizada y generación distribuida, ambas basadas en tecnologías renovables y altamente interconectadas, puede ser el esquema que más ventajas presente para sustituir al sistema actual [36].

Las previsiones auguran que los costes de producción de energía con tecnología PV y eólica en tierra, así como las CSP y la energía eólica marina reduzcan su coste significativamente, convirtiéndolas en la columna vertebral de la transformación global del sector energético (Tab. 1.3).

De las tecnologías más baratas según las proyecciones a 2030, se debe tener en cuenta que tanto la tecnología PV como eólica no son gestionables. En lo referente a hidráulica y biomasa, serán esenciales debido a su capacidad de ser gestionadas, aunque presentan un menor potencial de desarrollo y de reducción de costes por diferentes motivos [5]. En cuanto a CSP, presenta el mayor potencial de reducción de coste y la solución a

Tecnología	Coste 2018 (€/kWh)	Coste 2030 (€/kWh)
Ciclo combinado	—	0.074
Biomasa	0.062	0.060
Hidráulica	0.047	0.020
PV	0.055	0.035
CSP	0.185	0.055
Eólica	0.056	0.040

Tabla 1.3: Coste actual [2] y previsión de coste de las principales fuentes renovables de producción de energía para 2030 [5]

la gestión eficiente de la producción gracias a su capacidad de almacenamiento de energía térmica. El pronóstico de la agencia internacional de la energía o *International Energy Agency* (IEA) para 2023 sobre energías renovables predice un crecimiento a nivel mundial de la CSP de un 87% respecto de la capacidad en 2018 [37].

Por lo tanto todo parece indicar que que los futuros sistemas energéticos estarán basados en un mix de varias tecnologías renovables y el incremento de las interconexiones entre países, haciendo posible garantizar el suministro, reducir costes y un aprovechamiento óptimo de estas tecnologías [34, 38, 39].

En España, donde el recurso solar es muy abundante, además de considerar nuevas interconexiones con los países vecinos, se debe considerar un mix energético basado en energía hidráulica, eólica y solar, donde las tecnologías PV y CSP se operen de forma complementaria como pilar del sistema energético [5]. Diferentes propuestas de mix energético para España en 2030 se han realizado por parte de diferentes organismos (Tab. 1.4). De todas estas propuestas, la más equilibrada en lo referente a potencia total entre diferentes tecnologías es el mix propuesto por Protermosolar [5]. Este mix energético, además de alcanzar los objetivos propuestos por la Unión Europea (UE) en cuanto a la contribución de renovables y reducción de emisiones, permitiría bajar el coste de la producción de energía en el mix español por debajo de 0.05 €/kWh.

Adoptar un mix energético basado en renovables tambien abaratará el precio de la energía eléctrica aumentando la competitividad de las empresas. Protermosolar estima que los precios de generación eléctrica para las tecnologías renovables como hidráulica, eólica, fotovoltaica y termosolar serán 0.02, 0.04, 0.035 y 0.055 €/kWh respectivamente; mientras que

	Mix 2017	CE	Protermosolar	PNIEC
Demanda (GW)	104.5	147	130	157
Potencia eólica (GW)	23	31	33	50
Potencia fotovoltaica (GW)	4.7	47	25	37
Potencia termosolar (GW)	2.3	2.3	20	7
Potencia hidráulica (GW)	14	23	23	14
Emisiones (kt CO <sub>2</sub> )	66 000	12 593	4991	—

Tabla 1.4: Evolución mix energético español 2017-2030 (Comision de Expertos (CE) [6], Protermosolar [5] y Plan Nacional Integrado de Energía y Clima 2021-2030 (PNIEC) [7]

para cogeneración y ciclo combinado 0.07 y 0.074 €/kWh (ver Tab. 1.3) . Estas últimas más caras incluso que las importaciones directas de energía eléctrica, con un coste estimado de 0.06 €/ kWh [5].

### 1.3.1. Almacenamiento

En un sistema energético la variación entre la generación y la demanda de energía debido a las fluctuaciones de ambas a corto y largo plazo debe ser cero. Por lo tanto, en sistemas energéticos basados en diversas fuentes renovables, algunas no gestionables, los sistemas de almacenamiento de energía juegan un papel fundamental para garantizar la continuidad del suministro y mejorar la capacidad de respuesta del sistema debido a su fácil manejo, control y previsibilidad. Los sistemas de almacenamiento energético además de aumentar la fiabilidad y estabilidad del sistema, pueden ser una parte crucial de las redes de energía inteligentes en el futuro [32, 40].

Las principales técnicas de almacenamiento de energía se basan en principios físicos relacionados con magnetismo, superconductores, electroquímica, pilas de combustible, supercondensadores, hidroeléctricos, neumáticos, mecánicos y térmicos. Para grandes capacidades cobran mayor importancia sistemas de almacenamiento hidráulico por bombeo mecánico y sistemas de almacenamiento de energía térmica basados en calor latente o materiales de cambio de fase [32].

Recientemente parte de las tecnologías de almacenamiento han mostrado reducciones de costes similares a la evolución de las energías renovables, por lo tanto cabe esperar que la combinación de energías renovables

y almacenamiento puedan ofrecer soluciones a menor coste en el futuro [34]. Reducir costes en sistemas de almacenamiento térmico requiere desarrollos adicionales que mejoren la eficiencia y materiales más estables y económicos [40].

Los sistemas de generación hidroeléctrica están limitados por una serie de factores [5] que también limitan el desarrollo del almacenamiento hidráulico por bombeo. Por otro lado, el almacenamiento térmico, además de poder suministrar energía térmica directamente a aplicaciones que la demanden, permite a las plantas CSP que transformen la radiación solar en energía térmica a alta temperatura, funcionando como una planta de energía convencional y suministrando energía de manera totalmente gestionable. Este hecho unido a la previsión de gran reducción de costes de la tecnología CSP, hacen que el almacenamiento térmico tome especial relevancia. Un sistema completo de almacenamiento térmico basado en calor sensible cuesta de 0,1 a 10 €/kWh, dependiendo del tamaño y la tecnología de aislamiento [40].

### 1.3.2. Tecnología de concentración solar

Las tecnologías basadas en energía solar son aquellas que emplean directamente la radiación solar. Existen tres mecanismos distintos de aprovechamiento: térmico, químico (fotosíntesis) y físico (fotovoltaica), para producir calor, energía química y electricidad respectivamente en un elemento receptor. Para aumentar el rendimiento de estos sistemas, es habitual concentrar previamente el flujo solar que llega al receptor, logrando temperaturas más elevadas y densidades de flujo solar más altas, mejorando la eficiencia termodinámica y reduciendo el área de pérdida en relación con el área del receptor. Esta fase previa se lleva a cabo mediante concentradores ópticos principalmente, que redirigen y concentran el flujo de radiación solar. Esta tecnología se conoce como *Concentrating Solar Technology* (CST) o tecnología de concentración solar. Cuando la CST se emplea con receptores térmicos para producir calor y posteriormente transformarlo en electricidad se conoce con el nombre de CSP o *Solar Thermal Electricity* (STE), mientras que si se emplean receptores tipo PV se conoce como *Concentrating Photovoltaic* (CPV). Recientemente, los avances en investigación han conseguido combinar CSP y CPV dando lugar a *Concentrating PhotoVoltaic Thermal* (CPVT), esta nueva tecnología muestra un gran potencial y características únicas [41, 42]. Los

---

concentradores ópticos más empleados en CST son: *Parabolic Dish* (PD), PTC, *Solar Tower Power* (STP) y *Linear Fresnel* (LF), Fig. 1.10.

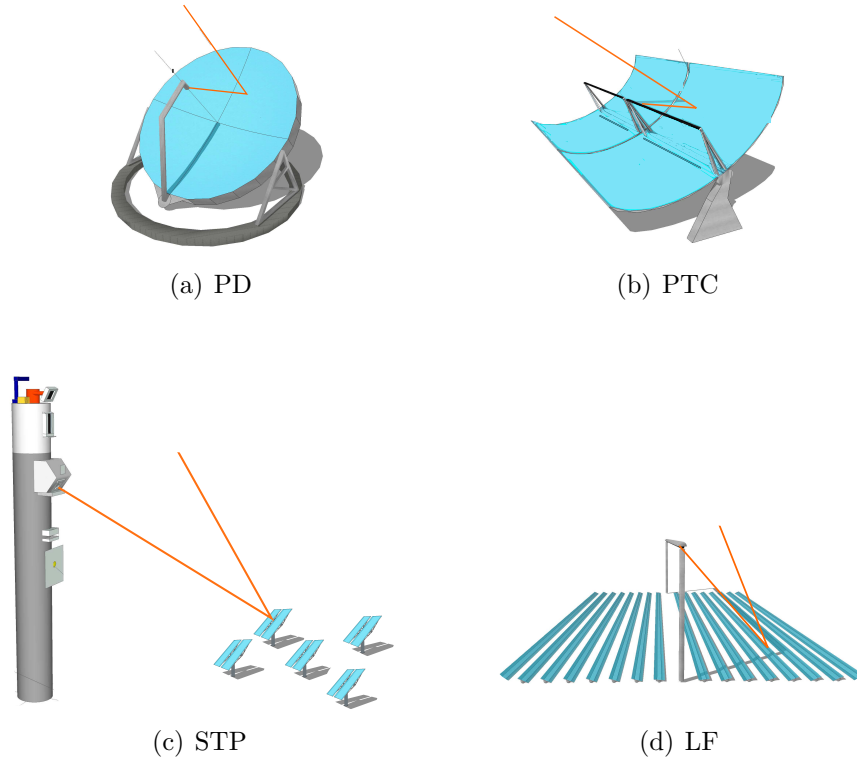


Figura 1.10: Tecnologías de concentración solar

Todas las plantas tipo CSP poseen un principio de funcionamiento similar, por ejemplo en una planta del tipo STP, el flujo de radiación solar que alcanza el campo de captadores solares, en este caso llamados heliostatos, es reflejado y concentrado sobre un receptor. El receptor se encarga de absorber y transformar el flujo solar concentrado en energía térmica y transferirla a un fluido (*Heat Tranfer Fluid* (HTF)) que refrigerara el receptor. La energía térmica es transportada por el HTF hacia el sistema de intercambio, de almacenamiento o el sistema de generación de energía eléctrica Fig. 1.11.

Como se comenta en la Sec. 1.3, se espera que para 2023 casi se duplique la capacidad CSP instalada a nivel mundial, donde el 70 % de esta nueva capacidad se estima que será del tipo STP [37, 43]. Un estudio basado en los resultados de las subastas públicas de energía indica que

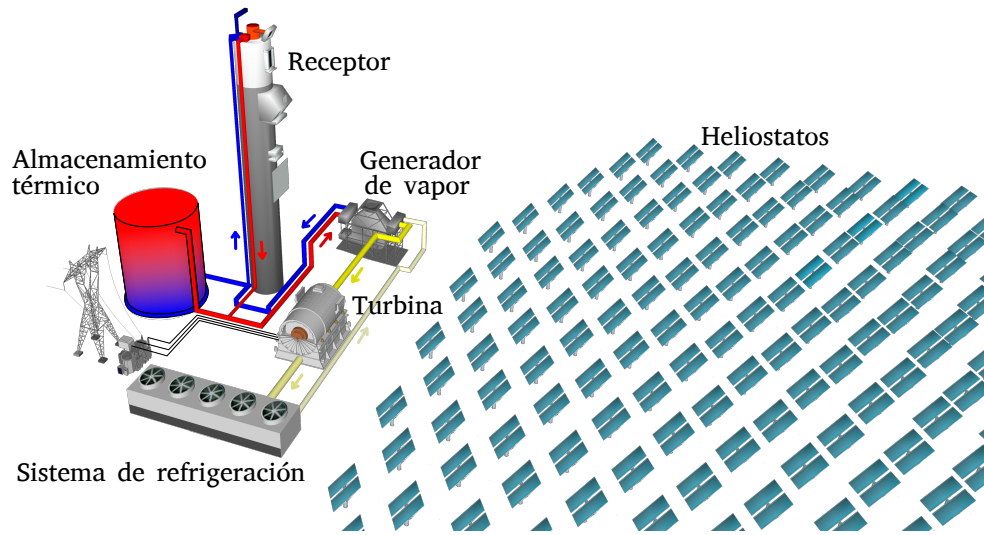


Figura 1.11: Sistema de torre

la CSP experimentará una reducción de costes del 61 % entre 2018 y 2021, o un 27 % por año [2], sin embargo, estos datos deben tratarse con cautela ya que esto se basa en solo cinco puntos de datos recogidos desde 2020 hasta 2021. Esto situará el precio de la CSP cerca del límite inferior del rango de 0.055-0.09 €/kWh para generación con combustibles fósiles, que junto a su capacidad para proporcionar energía renovable gestionable, podría desempeñar un papel fundamental para permitir altas cuotas de energía solar fotovoltaica y eólica en áreas con buenos recursos solares directos, incluso una gran cuota de capacidad CSP en el mix energético [2].

### 1.3.3. Seguimiento solar

Un sistema clave para la tecnología CSP es el sistema de seguimiento solar que se encarga de alinear correctamente el concentrador durante el continuo movimiento del sol. Por ejemplo en un sistema tipo STP, el sistema de seguimiento solar es el encargado de reorientar la superficie reflectante de cada heliostato de manera que el eje óptico del heliostato ( $\vec{V}_A$ ) coincida con la bisectriz del ángulo formado por el vector solar ( $\vec{V}_S$ ) y el vector receptor ( $\vec{V}_T$ ) (Fig. 1.12).

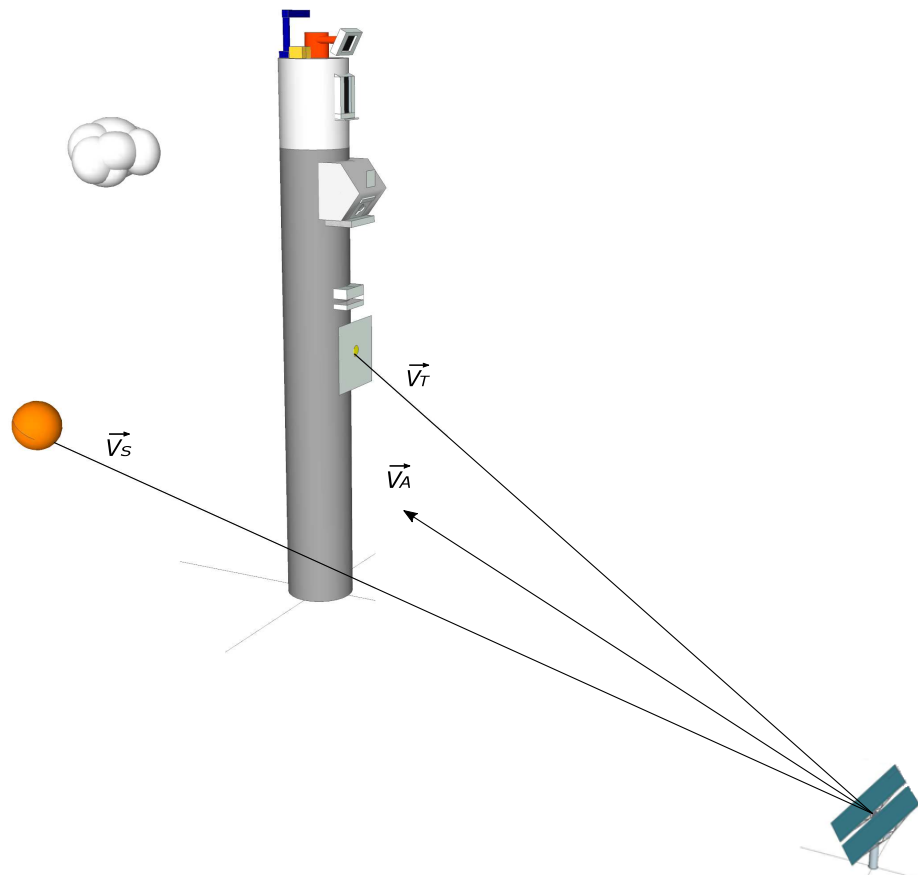


Figura 1.12: Seguimiento solar

Los sistemas de seguimiento solar pueden clasificarse según diferentes criterios, uno de ellos es el número de ejes de rotación del sistema de seguimiento que viene determinado por los requerimientos del concentrador. Los sistemas lineales tipo PTC o LF necesitan un sistema de seguimiento con un eje de rotación, mientras que sistemas puntuales tipo disco PD o STP emplean sistemas de seguimiento con dos ejes de rotación.

Otro criterio de clasificación puede ser según el tipo de esquema de control automático que posee el seguidor solar. Se emplean controladores en bucle abierto que utilizan solamente su estado actual y un algoritmo para determinar sus acciones de control sin realimentación, por lo tanto no puede determinar si las acciones tomadas han logrado el resultado deseado. Por otro lado, un esquema de control en bucle cerrado utili-

za realimentación para mitigar errores y perturbaciones. Finalmente, los sistemas de seguimiento solar también pueden clasificarse según sean sistemas pasivos o activos, que emplean la expansión térmica de materiales o utilizan sensores y actuadores respectivamente.

Los seguidores solares más empleados actualmente son del tipo bucle abierto que emplean algoritmos de posicionamiento solar para calcular la señal de control de los actuadores. El algoritmo de posicionamiento del sol más preciso tiene un error de 0.005 mrad [44] y un gran coste computacional, en cambio existen algoritmos menos precisos pero más eficientes computacionalmente [45, 46].

Este tipo de seguidores solares en lazo abierto requieren un costoso procedimiento de instalación que garantice una precisa medida de los parámetros geométricos del sistema y un perfecto alineamiento. Debido a las condiciones durante la instalación y el gran número de concentradores que se emplean normalmente en los sistemas CSP, es complicado garantizar la precisión requerida. Además, los seguidores solares en lazo abierto requieren estimar un modelo de error para cada concentrador que minimice los errores de apunte. Estos modelos individuales de error deben calibrarse periódicamente puesto que los concentradores pueden desalinearse debido a condiciones meteorológicas y otras perturbaciones. Existen numerosos trabajos sobre seguidores solares, pero la gran mayoría hace referencia a sistemas de seguimiento solar para sistemas PV, que tienen por lo general requerimientos diferentes a los de la CSP [47].

#### 1.3.4. Industria 4.0 y SMARTCSP

La industria 4.0 es una revolución digital que tiene el potencial de alterar todos los enfoques convencionales de la industria. Los principios básicos de la industria 4.0 son: interoperabilidad, virtualización, descentralización, capacidad en tiempo real, orientación del servicio y modularidad [48]. Se espera que tenga un impacto en áreas clave, incluida la energía [49, 50], y que guíe a los países europeos hacia una nueva era de fabricación moderna [51]. La agenda de investigación estratégica de la plataforma tecnológica europea sobre la integración de sistemas inteligentes establece que los dispositivos basados en sistemas inteligentes desempeñarán un papel clave para lograr mayores eficiencias energéticas y un uso inteligente de la energía.

La tecnología CSP aún no ha incorporado estas innovaciones que han

---

empezado a ser incluidas de manera exitosa en otros sectores industriales. En realidad la CSP incorpora un bajo grado de inteligencia y autonomía. Este es uno de los principales motivos por los que se espera una reducción significativa de los costes de la CSP. Por ejemplo, una planta STP como la de Ivanpah en el desierto de Mojave en los Estados Unidos, está compuesta por 173 500 heliostatos y tres torres con una potencia total de 392 MW y un coste total de 2200 millones de dólares. Se estima que entre el 30 % y el 50 % del coste total de la planta se debe al coste del campo de heliostatos [52], por lo que cualquier reducción del coste de los heliostatos tiene una gran repercusión sobre el coste total de los sistemas STP.

Por ejemplo, la mayor parte de los heliostatos poseen un esquema de control en lazo abierto, lo que encarece en gran medida el coste de instalación y operación debido a los requerimientos de precisión durante la instalación y la periódica calibración del heliostato durante la operación. El esquema de control en lazo abierto además reduce la eficiencia del sistema por la ausencia de realimentación. Nuevos esquemas de control en lazo cerrado basados en nuevas técnicas inteligentes pueden resolver estos problemas. Por otro lado, el coste del hardware de control empleado habitualmente en los heliostatos es elevado en relación a los nuevos sistemas de bajo coste, que además ofrecen nuevas posibilidades.

Por todo esto, recientemente ha surgido un nuevo concepto llamado SMARTCSP [53] que consiste en aplicar las innovaciones derivadas de la Industria 4.0 sobre la tecnología CSP. Se espera que la adopción de estas innovaciones revolucione el desarrollo de la tecnología CSP, reduciendo costes y mejorando su eficiencia.

## 1.4. Modelado basado en primeros principios y Modelica

El modelado y la simulación es una herramienta indispensable que nos permite ahorrar tiempo, dinero y evitar situaciones peligrosas durante el análisis o el diseño de sistemas. Actualmente existe una gran demanda de modelos capaces de simular el comportamiento complejo de los sistemas de desalinización y energía frente a transitorios y cargas parciales, más aún cuando este tipo de sistemas se combinan [26]. Modelica [54] es un lenguaje de modelado que permite la formulación acausal de problemas,

convirtiéndose en una excelente herramienta para describir sistemas ciber físicos. El principal inconveniente de este tipo de modelado es su coste computacional.

En primer lugar, Modelica es un lenguaje de modelado basado en ecuaciones y primeros principios que permite representar convenientemente sistemas físicos complejos de diversos campos en el mismo modelo, por ejemplo, control, mecánica, electricidad, electrónica, hidráulica y térmica. Modelica es un lenguaje de modelado modular, que permite dividir el problema de modelado en submodelos más fácilmente abordables para componer posteriormente el modelo total. De esta forma se facilita la depuración, actualización y reutilización de modelos. Es también un lenguaje jerarquizado, donde los submodelos van de menor a mayor grado de descripción. Modelica se basa en la programación orientada a objetos que logra la abstracción y ocultación de la información. Esta técnica permite encapsular datos, estructuras y comportamientos en un modelo del mismo modo que se encapsulan atributos y métodos en un objeto. La abstracción permite usar cada parte del modelo sin conocer sus detalles internos, la ocultación de la información permite el acceso solo a determinadas variables para la comunicación entre modelos y la modularidad permite tratar cada una de las partes de manera independiente.

La causalidad computacional es un impedimento para la modularidad por no poder decidirse localmente en un subsistema sin considerar el resto de partes, sus conexiones y las condiciones de contorno del sistema. Para evitar esto, Modelica se diseñó como un lenguaje acausal de programación, que se encarga de asignar automáticamente la causalidad computacional del modelo a partir de las relaciones matemáticas de las partes del modelo. Este proceso de asignación automática de la causalidad consiste en una ordenación según una serie de reglas de las ecuaciones que componen el modelo. El siguiente paso en la simulación del modelo dinámico es la integración numérica del mismo y obtener las soluciones. DASSL (Differential / Algebraic System Solver) es el algoritmo empleado principalmente para tal efecto, es uno de los integradores numéricos para simulación más exitosos del mercado. Tras la implementación del modelo es imprescindible el calibrado y la validación del mismo, para ello se debe realizar una campaña experimental que compruebe la bondad del ajuste entre el modelo y el sistema real.

---

## 1.5. Inteligencia artificial

Las herramientas basadas en técnicas de inteligencia artificial o *Artificial Intelligence* (AI) pueden ayudar a eliminar ciertas limitaciones que presenta el modelado basado en primeros principios, como puede ser el alto coste de computación para modelos complejos o incluso solventar problemas que no se pueden modelar mediante esta técnica de modelado tradicional.

La idea de la AI es antigua, introducida en el campo de la informática a mediados de los años cincuenta [55, 56], pero en los últimos años el aumento de las capacidades computacionales ha provocado una enorme evolución de las técnicas de AI. La investigación sobre AI relacionada con procesos y en especial procesos de desalinización y energía se ha intensificado recientemente, sobre todo para los campos de predicción, automatización y mejora del rendimiento [57]. Además, el desarrollo de las técnicas de AI ha sido fundamental para la creación del concepto Industria 4.0 y los beneficios derivados de esta sobre numerosos procesos industriales [48].

Las principales herramientas derivadas de las técnicas de AI empleadas en este trabajo son las técnicas de optimización basadas en algoritmos genéticos o *Genetic Algorithm* (GA) y las técnicas de modelado basadas en redes neuronales artificiales o *Artificial Neural Networks* (ANNs). La hibridación de ANNs y GA con otros enfoques de modelado clásicos o herramientas AI tiene un gran potencial que puede ser empleado para obtener estrategias óptimas de operación, especialmente en circunstancias operativas complejas [57].

### 1.5.1. Optimización

El proceso de optimización puede ser muy complejo en función de la naturaleza del problema a optimizar, podemos encontrar problemas con varios puntos óptimos, puntos óptimos locales que dificulten encontrar el óptimo global, es posible que el problema sea tan complicado que no haya forma de saber si un óptimo dado es global o solo local, pueden existir varios criterios de optimización (optimización multi-objetivo), etc.

Actualmente es difícil crear una clasificación general de métodos de optimización debido a la evolución sufrida en los últimos años citerats-chek1988,torn1989global,neumaier2004 por la que la mayoría de los algo-

---

ritmos combinan diferentes estrategias. En cualquier caso, la clasificación fundamental mas aceptadas distingue entre métodos heurísticos y métodos deterministas. Los métodos deterministas garantizan una solución óptima, actualmente existen problemas que pueden ser resueltos mediante estrategias deterministas aunque en muchos otros casos no se puede o todavía no existe un método determinista para ello. Los métodos heurísticos generalmente no garantizan encontrar una solución óptima, en cambio proporcionan soluciones válidas reduciendo el coste de cómputo, incluso en problemas que no se pueden resolver de manera exacta.

La heurística se basa en estrategias lógicas que pueden contener algunas componentes aleatorias o estocásticas que atenúan su limitado alcance de decisión para buscar soluciones al problema. Existen tres tipos principalmente: heurística constructiva, métodos de búsqueda local y metaheurística. Este último, que es el tipo empleado para la realización de esta tesis, se basa en la aplicación de un principio de optimización genérico que funciona con una amplia variedad de problemas independientemente de sus particularidades. Además son algoritmos robustos y eficientes que obtienen soluciones de alta calidad en un tiempo razonable [58]. Estos están especialmente diseñados para analizar el espacio de búsqueda con componentes especiales para escapar de los óptimos locales [59].

Entre todos los métodos metaheurísticos, el más interesante según las características de los problemas presentados en la realización de este trabajo son los métodos basados en población. Estos métodos se basan en la creación de un conjunto de soluciones candidatas diferentes que se manejan simultáneamente e interactúan entre sí. La principal característica de estos métodos es que están diseñados para realizar exploraciones amplias de espacios de búsqueda complicados. Es posible distinguir dos grupos principales en la categoría de métodos basados en la población: algoritmos de enjambre y evolutivos. Estos últimos son métodos que adaptan el principio de la evolución natural para resolver problemas. Se interpreta cada solución como un individuo que forma parte de un conjunto de soluciones o población que además interactúan entre ellos. Este tipo de métodos promueve la mejora progresiva o la adaptación de los individuos. En la realización de esta tesis se han empleado concretamente GA. Las ventajas principales que presentan los GA son su capacidad para explorar todo el espacio de búsqueda y encontrar soluciones aunque el problema sea muy complejo y multidimensional. Por el contrario son muy costo-

---

sos computacionalmente y muy dependientes de hiperparámetros. Las técnicas de optimización basadas en GA han sido aplicadas con éxito en numerosas ocasiones en desalinización [57].

### 1.5.2. Modelado basado en redes neuronales artificiales

Las ANNs son modelos matemáticos inspirados en la sinapsis de las redes neuronales biológicas. Estas redes son capaces de aprender ciertas tareas sin ser programadas específicamente para tal efecto. La unidad básica de una red es un nodo o neurona artificial (Fig. 1.13). Una neurona artificial puede recibir una o varias señales a través de sus entradas (dendritas) que suelen estar ponderadas. La neurona artificial envía una salida a cada neurona que hay conectada a ella (terminales), que se calcula mediante la suma de las entradas (núcleo) y alguna función de activación (axón), generalmente no lineal. Al igual que en el cerebro biológico, las neuronas artificiales se agrupan en estructuras, normalmente en capas por las que va avanzando la información a la vez que se modifica. Actualmente se emplean para tareas específicas incluyendo visión por computador, reconocimiento de voz, traducción automática, diagnóstico médico e incluso en actividades que tradicionalmente se han considerado reservadas para los humanos, como el arte.

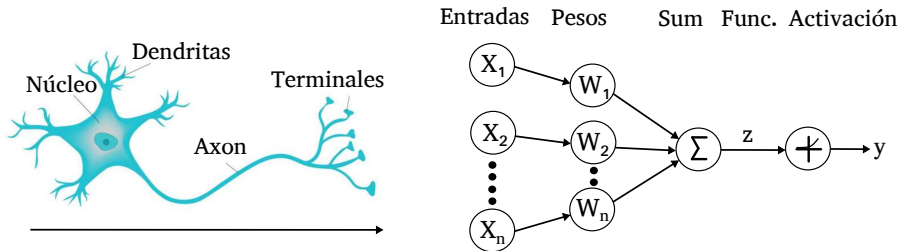


Figura 1.13: Neurona biológica y artificial

El modelado con ANNs es una técnica de modelado especial para generar modelos de caja negra en donde los modelos están entrenados con datos experimentales (aprendizaje automático o *Machine Learning* (ML)), en lugar de diseñar un modelo detallado para un problema específico. Por lo tanto, el modelado con ANNs no requiere diseñar y re-

solver modelos matemáticos complejos basados en primeros principios y permite desarrollar modelos flexibles y robustos cuando el conocimiento físico del proceso es insuficiente o difícil de expresar con programación convencional [60, 61].

El aprendizaje automático de estas redes intenta minimizar una función de coste que evalúa el rendimiento de la red, mediante la actualización de los de los parámetros que definen cada neurona. Existen tres paradigmas de aprendizaje: supervisado, no supervisado y por refuerzo.

En literatura científica se pueden encontrar numerosos modelos relacionados con energía solar [61–63], la mayoría de ellos para el pronóstico de la radiación solar [63, 64], rendimiento o producción de energía en sistemas de captadores solares PV o planos [65]. También han comenzado a ser empleados para el diseño y optimización de sistemas térmicos solares [66], control automático [67], detección de fallos [68] y mantenimiento predictivo [69]. A pesar de los buenos resultados y el gran potencial de este tipo de modelado, no está muy extendido el uso de modelos basados en ANNs para CSP.

# Capítulo 2

## Hipótesis y objetivos

*La gran tragedia de la ciencia,  
el asesinato de una bella hipótesis  
por un hecho feo*

Thomas Henry Huxley

**Resumen:** En este capítulo se expone la hipótesis principal y los objetivos que se plantearon alcanzar en la fase previa a la realización del presente trabajo. También se justifica la consecución de los mismos haciendo referencia a las contribuciones científicas derivadas.

---

### 2.1. Hipótesis

Como se ha visto en el capítulo anterior, el cambio del actual modelo energético y problemas derivados del cambio climático como la escasez de agua dulce, la salinización y la contaminación de las fuentes son algunos de los principales problemas que debe afrontar la humanidad en las próximas décadas.

Es por esto por lo que la gestión racional de los recursos naturales y la promoción de las energías limpias y renovables en sustitución de

las energías fósiles que contaminan y esquilman a su vez los recursos naturales ha pasado a ser un tema principal para numerosos organismos que advierten de las ventajas ambientales, estratégicas y socioeconómicas del uso de las energías renovables frente a las energías fósiles y la gestión eficiente de los recursos.

Se pone de manifiesto, en multitud de trabajos realizados en la propia instalación Aquasol, en otras instalaciones e incluso estudios teóricos, el gran potencial que muestra la tecnología de desalación por destilación térmica combinada con bombas de calor y energía solar. La mayoría de estos trabajos apuntan a que el rendimiento de estos sistemas puede ser mejorado en gran medida de manera individual y colectiva, debiendo profundizar más en el estudio de nuevos esquemas de control, condiciones óptimas de funcionamiento, la relación entre los subsistemas y la respuesta del sistema general para crear así estrategias de operación eficientes que hagan viables técnica y económicamente el sistema.

Por esto en esta tesis doctoral se trata la aplicación de técnicas de modelado, control y optimización para lograr una gestión eficiente de energía y agua mediante el uso de energía solar. El uso de técnicas de modelado y simulación permite predecir el comportamiento de los diferentes sistemas frente a nuevos escenarios, ahorrando costes y tiempo, evitando además los posibles riesgos que supondría realizar los experimentos en el sistema real bajo determinadas condiciones. Además, el uso de técnicas de optimización junto con técnicas de modelado y simulación permite encontrar los parámetros de funcionamiento óptimos. Finalmente, técnicas de modelados basadas en AI hacen posible el desarrollo de nuevas técnicas de control automático que pueden mejorar el rendimiento de los sistemas.

## **2.2. Objetivos generales y específicos**

### **Objetivos generales**

Esta tesis doctoral pretende realizar contribuciones en el campo del modelado, control y optimización de sistemas termosolares con aplicaciones industriales. De manera general se pretende estudiar, modelar y optimizar, a partir de los estudios previos que muestran el gran potencial, la viabilidad técnica de un sistema de destilación térmica acoplado a una bomba de calor de doble efecto cuya fuente de energía térmica es un campo solar y una caldera de gas. Para ello, se pretende con ayu-

da de técnicas de modelado, desarrollar nuevas estrategias de operación y control que nos permitan una operación óptima y control avanzado, aumentando de este modo la eficiencia del sistema.

### Objetivos específicos

Dentro de los objetivos de la presente tesis se encuentran, en primer lugar, realizar un análisis bibliográfico completo de toda la temática involucrada [R1-R9, C1-C7].

Para el modelado de la MED se pretende emplea un modelo dinámico desarrollado previamente, aunque dicho modelo mostró un grado de ajuste de sus predicciones frente a los valores reales muy elevado durante su validación, es necesario realizar algunas modificaciones y mejoras sobre este. Mediante el empleo del modelo modificado se debe estudiar el comportamiento individual de la planta y analizar los puntos óptimos de funcionamiento ([R1], [R2], [C1], [C2], [C5]). Para la optimización se deben analizar diferentes técnicas, entre ellas técnicas basadas en inteligencia artificial como son los GA.

En el caso de la DEAHP, se parte de otro modelo dinámico desarrollado previamente al que se deben implementar mejoras y ajustes que permitan, al igual que en el caso de la MED, estudiar el comportamiento individual de la bomba de calor en todo su espacio de decisión respecto a unos determinados criterios y se puedan analizar los puntos de funcionamiento óptimos. Debido a que la bomba de calor puede operarse a carga parcial, se pretende estudiar los puntos de funcionamiento óptimos a carga parcial y estrategias de control para poder obtener de ella un flujo de calor bajo demanda ([R8], [C3]).

Ampliados y validados los modelos de la MED y DEAHP, el siguiente objetivo es desarrollar un modelo conjunto y estudiar las condiciones más favorables de funcionamiento respecto a los criterios anteriormente mencionados para el sistema integrado por ambos subsistemas ([R8], [C5]).

El desarrollo y la validación de un modelo de la caldera de gas, generador de vapor y campo PTC, hacen posible el estudio del comportamiento de ambos sistemas y la obtención de los parámetros óptimos de funcionamiento. El siguiente objetivo es entender mejor el acoplamiento con la DEAHP y la MED. Este acoplamiento requiere previsiblemente del diseño de lazos de control de bajo nivel y el modelado de subsistemas

---

como válvulas, bombas, etc. Acoplados todos los sistemas, el siguiente objetivo es optimizar el sistema completo mediante la técnica de optimización más idónea, incluyendo las técnicas basadas en inteligencia artificial ([R5], [R8], [C4], [C5]).

Entre los objetivos de la tesis también se encuentra estudiar la eficacia de técnicas de modelado basadas inteligencia artificial, concretamente basadas en redes neuronales, con el objetivo de solventar los problemas que presentan las técnicas tradicionales de modelado, así como su uso para el control de los subsistemas que conforman a instalación Aquasol. El objetivo final es mejorar la eficiencia y facilitar el control de estos sistemas. Se hace especial hincapié en el uso de modelos basados en redes neuronales para los subsistemas más relacionados con la parte solar, como el sistema de seguimiento solar que poseen todos los sistemas de concentración solar ([R3], [R4], [R6], [R7], [C6], [C7]). Para ello, se debe determinar qué problemas y necesidades pueden ser susceptibles de ser modeladas con técnicas basadas en ANNs.

A continuación en función de las necesidades que planteen estos problemas se debe determinar el entorno para el desarrollo y la implementación más idónea que permita resolver de manera eficaz los problemas planteados. Seguidamente se debe analizar entre las técnicas disponibles de calibración de modelos cuál es la que mejor se ajusta a las necesidades planteadas ([R4], [R6], [R7], [C6], [C7]). Al igual que con modelos basados en primeros principios, los modelos basados en ANNs deben ser validados con datos experimentales obtenidos en las instalaciones reales en campañas de ensayos diseñadas para tal efecto ([R4]).

También se encuentra entre los objetivos, desarrollar nuevos esquemas de control a partir de estos modelos basados en redes neuronales que se prevé que aporten más información instantánea e incluso predicciones de algunas de las principales perturbaciones que afectan en gran medida a los sistemas basados en energía solar. Por último, se debe determinar el rendimiento de estos nuevos esquemas de control comparados con los sistemas tradicionales, primero en simulación y posteriormente en las instalaciones reales ([R4], [R6], [R7], [C6], [C7]).

---

# Capítulo 3

## Resultados

*Si buscas resultados distintos,  
no hagas siempre lo mismo*

Albert Einstein

**Resumen:** En este capítulo se enumeran y resumen los principales resultados obtenidos que han sido plasmados en las diferentes contribuciones científicas. La exposición de los resultados se organiza de acuerdo con las diferentes publicaciones, siguiendo un orden natural de avance y complejidad en las investigaciones.

---

### 3.1. Optimal operating conditions analysis of a multi-effect distillation plant [R1]

El primer artículo que forma el compendio del presente trabajo es un estudio sobre las condiciones óptimas de operación de la planta MED, debido al cambio de algunos elementos de la misma era necesario encontrar nuevos puntos de operación óptimos. Para ello se empleó un modelo

basado en primeros principios implementado en Modelica y herramientas de optimización basadas en algoritmos genéticos. Varios índices de rendimientos típicos de esta tecnología, basados principalmente en balances de energía térmica han sido empleados como criterios de optimización. También, se ha analizado el espacio de decisión delimitado por los límites de operación del sistema y el efecto de los parámetros de operación sobre la producción de destilado.

Este trabajo revela que el caudal de producción de destilado puede aumentarse un 16 % respecto del nominal sin un aumento significativo en el consumo de energía térmica, para ello se debe aumentar al máximo la temperatura de entrada de agua al evaporador. La producción de destilado también puede aumentarse un 22 % y reducir el consumo térmico un 1.2 % respecto del nominal, aumentando al máximo el caudal de agua de refrigeración del último efecto. Por último, reducir la temperatura del agua de alimentación aumenta la producción un 19 % y permite reducir el consumo térmico un 1.5 %.

El punto de operación que maximiza la producción de destilado consigue un aumento de este del 79 % y una disminución de un 1 % del consumo térmico. El punto de operación que minimiza el consumo térmico disminuye el consumo un 3 % mientras que aumenta la producción de destilado un 36 %. La principal diferencia entre el punto de operación que maximiza la producción y el que minimiza el consumo térmico es que mientras que el primero necesita aumentar la temperatura en el evaporador y aumentar el caudal de refrigeración a valores cercanos a sus máximos, el segundo necesita reducir el caudal en el condensador y aumentar la temperatura en el evaporador a valores no tan lejanos al nominal.

El resto de optimizaciones multicriterio muestran otros puntos de operación en el espacio de criterios que son un compromiso entre dos o más criterios.

### **3.2. Optimal operating conditions analysis for a MED according to energetic and exergetic criteria [R2]**

Continuando con el trabajo desarrollado en el artículo previo [R1], se ha desarrollado un nuevo estudio con el fin de reducir el coste

---

energético y mejorar la operación del proceso de producción de agua desalada mediante técnicas de destilación térmica. El estudio tiene como objetivo analizar la influencia de las variaciones de los parámetros operativos y determinar las condiciones óptimas de operación de la planta MED, esta vez empleando nuevos criterios basados en exergía. El modelo dinámico usado en el trabajo anterior ha sido modificado y se le ha añadido todo el desarrollo que permite realizar análisis exergéticos.

En este trabajo se ha llevado a cabo un análisis energético y exergético del proceso en condiciones nominales, que revela las principales fuentes de pérdidas de energía y exergía. Por un lado, la mayor fuente de pérdidas de energía térmica se encuentra en los caudales salientes del condensador, la salmuera y el destilado, que son responsables del alto consumo energético. Por otro lado, el análisis exergético revela que las principales fuentes reales de pérdidas de exergía son diferentes a las principales fuentes de pérdidas de energía térmica. En el caso de la planta MED, la generación de entropía en procesos disipativos y las pérdidas térmicas a través de las paredes de la MED son las principales fuentes de pérdidas exergéticas. Estas diferencias revelan que los flujos con un mayor contenido de energía presentan la menor calidad de energía térmica (exergía).

El trabajo también presenta un estudio sobre la influencia de los parámetros operativos que muestra que la producción real de la planta en condiciones nominales está lejos de los valores máximos simulados y que algunos parámetros de operación no tienen una gran influencia en el proceso con respecto al resto.

Usando un algoritmo de optimización genética implementado en la herramienta de modelado, se llevó a cabo un proceso de optimización teniendo en cuenta criterios tradicionales basados en energía térmica ( $\bar{E}_{Thermal}$ ) y nuevos criterios desarrollados basados en balances de exergía (consumo exergético específico). Se ha obtenido el espacio de criterios simulando 6000 combinaciones diferentes de parámetros de operación distribuidos a lo largo del espacio de decisión.

Desde el punto de vista energético, el consumo térmico específico de los puntos obtenidos en el espacio de criterios oscila entre 243 y 207 kJ/kg<sub>dis</sub>, aunque la mayoría de los puntos están en el rango entre 220 y 207 kJ/kg<sub>dis</sub>. Desde el punto de vista de la exergía, los puntos optimizados de acuerdo con los criterios de exergía logran un bajo consumo específico de exergía y baja producción de destilado, la optimización con criterios exergéticos conduce a una reducción en el consumo de exergía de 53.9 a

19.9 kJ/kg<sub>dis</sub>.

Finalmente, este trabajo muestra una optimización multicriterio llevada a cabo que proporciona el frente óptimo de Pareto, el cual muestra un compromiso entre los diferentes criterios. Cambiar el peso de cada criterio en la optimización conduce a una solución óptima diferente que se mueve a lo largo del frente óptimo de Pareto.

### **3.3. New low-cost solar tracking system based on open source hardware for educational purpose [R3]**

Debido al gran auge de las renovables es necesario proporcionar herramientas que puedan emplearse para desarrollar mejores competencias profesionales en energía solar ya que no hay suficientes recursos con este enfoque. Entre todos los campos de las renovables, el trabajo se centra en el subsistema de control de seguimiento solar empleado en colectores solares, debido a las deficiencias detectadas en el mismo. Por esto, se ha planteado el desarrollo de un pequeño prototipo basado en hardware abierto de bajo costo y visión por computador. Este prototipo está diseñado para probar nuevos algoritmos de control en el ámbito educativo y profesional.

La gran conectividad que ofrece el hardware de código abierto, el bajo coste, y la capacidad de implementar entornos de laboratorios virtuales y remotos o emplear diferentes lenguajes y software de código abierto lo convierte en una herramienta muy potente para el desarrollo y aprendizaje.

### **3.4. New approach for solar tracking systems based on computer vision, low cost hardware and deep learning [R4]**

Continuando con el trabajo anterior [R3], este trabajo presenta un nuevo enfoque para los sistemas de seguimiento solar basado en hardware abierto, visión por computador y modelos derivados de técnicas de inteligencia artificial. Las pruebas preliminares realizadas con éxito en

---

PSA, revelan el gran potencial y presentaron el nuevo enfoque como una buena alternativa a los sistemas tradicionales. Además de resolver problemas típicos que presentan los sistemas tradicionales, el nuevo enfoque propuesto puede proporcionar información clave para el control del sistema de seguimiento solar, como la predicción de movimientos de nubes, detección de bloqueos y sombras, attenuación atmosférica o medidas de radiación solar concentrada, de la que hasta ahora no se disponían en el sistema de seguimiento. Esta nueva información pueden emplearse para mejorar las estrategias de control del sistema y, por lo tanto, el rendimiento del mismo.

En este trabajo se realiza una comparativa entre el error de seguimiento obtenido simultáneamente mediante el sistema tradicional y el nuevo sistema durante un ensayo sobre el mismo heliostato. Los resultados muestran que ambos sistemas estiman el error de manera similar, las diferencias más amplias (15 mrad) se ven en grandes transiciones cuando el heliostato entra o sale del modo seguimiento y se está moviendo a máxima velocidad. Por lo tanto, aunque son importantes, estas diferencias no son las más relevantes para el rendimiento del helióstato.

Las diferencias se mantienen por debajo de 3 mrad para movimientos a baja velocidad durante la mayor parte del ensayo excepto en dos instantes cuando el error aumenta hasta 4 mrad debido a una detección inexacta del sol causada por una configuración incorrecta de la cámara.

Se determina que la interacción de otros heliostatos sobre el receptor no perturba el funcionamiento del sistema. Además, el sistema resulta independiente de la tecnología solar, el tamaño del sistema, la ubicación y el tiempo. El sistema no se ve afectado por perturbaciones debidas a la deformación de la estructura del colector debidas a las cargas de viento o el desplazamiento del centro de masas ni a la posición aparente del Sol.

### **3.5. Parabolic trough collector field dynamic model: Validation, energetic and exergetic analyses [R5]**

Este trabajo presenta un modelo dinámico, flexible y altamente personalizable que simula el comportamiento térmico transitorio de un campo solar de colectores de canal parabólico, con fines de optimización, evaluación del rendimiento y tareas de control. El modelo se basa en principios

físicos descritos en trabajos previos que han sido ampliados con el desarrollo matemático necesario para realizar análisis exergéticos. Para el desarrollo del modelo se utilizó la librería ThermoCycle y se implementó en el lenguaje de modelado orientado a objetos basado en ecuaciones Modelica. En primer lugar se determinó la relación entre el coste computacional y la precisión del modelo debido al número de volúmenes de control empleados, posteriormente se validó con datos experimentales y finalmente se analizó el comportamiento térmico y exergético de la instalación gracias al modelo.

Durante la primera tarea se realizaron numerosas simulaciones atendiendo al tiempo empleado en la simulación, la precisión del modelo comparando datos reales y simulados y la definición espacial del receptor (número de volúmenes de control). Los resultados mas relevantes son en primer lugar que el tiempo de simulación aumenta linealmente con respecto al número de volúmenes de control para el rango estudiado. En segundo lugar que los niveles de discretización superiores a 20 volúmenes de control no reducen significativamente el error entre las medidas experimentales y las simuladas, por lo que el número de volúmenes de control debe seleccionarse entre 2 y 20 para simulaciones diarias del modelo, según los requisitos de tiempo de cálculo, 10-60 s. El comportamiento del modelo durante transitorios es el más afectado por las variaciones en el número de volúmenes de control.

La validación del modelo respecto a los datos experimentales conseguidos en una campaña experimental con tal propósito revela que el modelo mantiene su precisión incluso con cambios repentinos en la temperatura de entrada del HTF. El modelo sobreestima ligeramente la temperatura de salida cuando se producen cambios repentinos en la DNI, lo que parece indicar que las pérdidas térmicas se subestiman. El error cuadrático medio máximo y el error absoluto máximo obtenidos en las simulaciones anteriores son 1.5 °C y 4.5 °C respectivamente.

Finalmente, para el análisis del comportamiento dinámico térmico y exergético del campo solar, se emplea el modelo validado. El análisis térmico revela que la principal ineficiencia térmica es debida a las pérdidas térmicas con el ambiente, mientras que el análisis exergético revela que la principales ineficiencias exergéticas son debidas al rendimiento óptico y la absorción en la superficie del tubo absorbedor (al menos el 50 % de la exergía que llega a la superficie del tubo se destruye), especialmente cuando hay variaciones grandes en la DNI.

### 3.6. Machine Learning for Solar Trackers [R6]

A continuación, se publicó un nuevo trabajo sobre el empleo de una nueva librería de machine learnirng para crear modelos de redes neuronales y emplearlos en tareas de seguimiento solar. Esta nueva librería de código abierto se ha mostrado más flexible y aumenta las capacidades de desarrollo respecto de la empleada en los trabajos anteriores.

Diferentes tipos de redes se entrenaron, optimizaron y validaron, obteniendo como resultado que la red SSD MobileNet V1 0.75 es el modelo más rápido, mientras que SSD MobileNet V1 quant es el modelo más preciso de los evaluados. SSD MobileNet V1 opt también muestra un buen comportamiento. El resto de los modelos muestran resultados similares, aunque han sido un poco más lentos o menos precisos. Cabe señalar que el modelo Mask R-CNN Inception V2 no es solo un detector de objetos, también es un segmentador semántico, es decir, proporciona máscaras de objetos, no solo cuadros delimitadores. Esto podría ofrecer nuevas capacidades al enfoque del seguimiento solar inteligente.

En este trabajo también se introduce el término seguimiento solar inteligente (*smart tracking*) y heliostato inteligente (*smart heliostat*). Este enfoque inteligente se consigue implementar en dos tipos de dispositivos gracias a la nueva librería: dispositivos embebidos y dispositivos móviles (telefonos, tablets, etc), aunque también funciona en computadoras convencionales.

Para la implementación en dispositivos embebidos se emplea hardware de la plataforma de hardware de bajo coste RaspberryPi. El software se implementa utilizando el lenguaje de programación de código abierto Python. Esta implementación resulta ser la implementación ideal para probar y evaluar el nuevo enfoque en instalaciones reales, ya que este tipo de dispositivos pueden controlar y comunicarse con facilidad con los actuadores y sensores de los colectores actuales.

También se llevó a cabo la implementación del sistema para dispositivos móviles iOS y Android. Esta aplicación está destinada a ser utilizada para demostrar fácilmente el concepto y como recurso educativo, también puede usarse para otros fines que deben estudiarse, por ejemplo, para pruebas y calibración.

---

### **3.7. Solar tower power mockup for the assessment of advanced control techniques [R7]**

Posteriormente se publicó un trabajo sobre el desarrollo de banco de ensayos para sistemas de seguimiento solar empleados en sistema de torre central compuesto por un heliostato y una torre donde se encuentra el receptor. El trabajo tiene como objetivo desarrollar un banco de pruebas para evaluar nuevas técnicas de control avanzadas incluido técnicas de machine learning, continuando con los trabajos desarrollados sobre modelos para seguimiento solar basados en redes neuronales. El prototipo emplea hardware de bajo coste y software de código abierto.

Este nuevo prototipo es más barato, mas fácil de montar y replicar que el desarrollado en trabajos anteriores debido al uso de impresoras 3D y hardware de bajo coste. El sistema de seguimiento solar del heliostato posee una resolución de 1.8 mrad. Los resultados obtenidos del entrenamiento e implementación de un modelo basado en redes neuronales para realizar las tareas de seguimiento solar son satisfactorios, lo que motiva la implementación del sistema de control probado en el banco de ensayos en el campo real.

### **3.8. Optimal Operation of Solar Thermal Desalination Systems coupled to DEAHP [R8]**

Por último se presentó un artículo basado en el conjunto de modelos dinámicos desarrollados en los trabajos previos para el diseño, control y optimización de sistemas de desalinización solar térmica. Este trabajo también describe una metodología para la generación de puntos de operación óptimos del sistema mediante algoritmos basados en inteligencia artificial, concretamente en algoritmos genéticos. Esta técnica permite encontrar puntos de operación óptimos de acuerdo a una o varias variables manipulables que pueden depender de otras variables externas. La metodología ha sido probada en una configuración híbrida gas-solar modelada en este trabajo considerando los modelos previos (MED, DEAHP, caldera de gas, campo PTC, generador de vapor, etc). Los resultados

de las pruebas demuestran que la metodología puede encontrar puntos de operación óptimos de acuerdo con uno o varios criterios, incluso en condiciones muy adversas.

El trabajo expone dos optimizaciones, la primera trata de encontrar los valores de las variables manipulables que conforman el punto de operación del sistema de manera que se maximice la producción de destilado y mantiene la planta en funcionamiento a pesar de las condiciones adversas. La optimización del algoritmo genético se limitó a 1000 generaciones con 10 individuos por generación. Durante la optimización, la mejora de los resultados de la simulación del individuo 1200 al 1700 fue inferior al 0,5 %, por lo que se consideró 1700 evaluaciones suficientes para que el optimizador converja en una solución óptimas. Más del 70 % de las simulaciones no terminaron satisfactoriamente, debido a las restricciones de los subsistemas que componen el sistema general o debido a problemas en la inicialización del modelo. Este hecho muestra lo difícil que es encontrar un punto de ajuste para que el sistema propuesto mantenga las condiciones de operación en los rangos permitidos y encontrar el punto de operación óptimo.

Los resultados de esta optimización determinan que la producción máxima total de destilados es de  $7.1 \text{ m}^3$  con un consumo térmico de la caldera de 240 kWh, un 20 % de producción más con respecto a las condiciones iniciales determinadas manualmente. El sistema pudo funcionar de manera óptima durante la serie de tiempo optimizada, a pesar de las condiciones adversas de cargas parciales y estados transitorios.

La segunda optimización trata de encontrar el punto de máximo de producción de destilado minimizando el aporte de energía térmica de la caldera de gas (optimización multicriterio). En este caso, el algoritmo genético convergió en menos de 2000 simulaciones. Una solución óptima en el frente de Pareto determina una producción total de destilado de  $6.7 \text{ m}^3$ , consumiendo toda la energía solar recolectada en el campo PTC y 193 kWh de energía térmica de la caldera.

El frente óptimo de Pareto sugiere que la demanda de energía térmica para aumentar la producción de destilado crece exponencialmente. La optimización multiobjetivo proporciona un conjunto de soluciones que son un compromiso entre el consumo de energía térmica y la producción de agua dulce. Estas optimizaciones se pueden utilizar para seleccionar la solución óptima que garantice el máximo de producción de destilado a un costo mínimo al establecer pesos para cada criterio, por ejemplo, el

---

costo de la energía térmica y el precio del agua dulce.

---

# Capítulo 4

## Conclusiones y trabajos futuros

*En dos palabras puedo resumir  
cuanto he aprendido acerca de la vida:  
Sigue adelante.*

**Robert Frost**

**Resumen:** Este capítulo enumera las principales conclusiones extraídas durante la realización de la tesis, así como las conclusiones específicas de cada uno de los trabajos publicados. Finalmente, se enumeran una serie de trabajos futuros que dan continuidad al trabajo desarrollado en esta tesis.

---

### 4.1. Conclusiones generales

A partir de los resultados obtenidos y la experiencia adquirida por los trabajos desarrollados durante esta tesis se puede concluir que existe un gran margen de mejora tanto en el campo de la desalinización como en el de CSP, mas aún si se combinan ambos tratando de reducir el impacto ambiental que deriva de la obtención de agua y energía.

Las técnicas de modelado, simulación y optimización han demostrado ser herramientas muy potentes que nos ayudan en el desarrollo y mejora de estos sistemas, además reducen el gasto de tiempo, recursos y evitan situaciones peligrosas. Las contribuciones realizadas a lo largo del presente trabajo han sido facilitadas por el uso de estas técnicas, sin las que no se hubiera podido llegar de manera experimental. Entre todos los campos de mejora posibles de las tecnologías de desalinización y CSP, ha quedado demostrado que uno de los más limitantes es la integración de dichos sistemas y la operación óptima de los mismos.

Dos técnicas de modelado diferentes se han empleado, la principal ha sido el modelado basado en ecuaciones y primeros principios que ha resultado ser una técnica capaz de proveer modelos muy precisos siempre y cuando se conozcan muy bien los fenómenos físicos que se pretenden modelar y puedan ser descritos en un lenguaje de modelado. Por otro lado, se han empleado técnicas de modelado basadas en redes neuronales artificiales capaces de crear un modelo en base a datos experimentales cuando el fenómeno es muy complejo, se desconoce o es muy difícil de describir. Es muy importante a la hora de modelar un problema analizar el objetivo del modelo y definir sus requerimientos, esto determinará la técnica de modelado a aplicar.

Finalmente, el uso de algoritmos de optimización y mas concretamente algoritmos genéticos ha permitido el desarrollo de una metodología para determinar estrategias y parámetros de operación, tanto de los subsistemas individualmente como del sistema fruto del acoplamiento de varios de ellos. Esta metodología ha demostrado ser eficiente y capaz de optimizar la operación incluso en condiciones muy adversas debido a las limitaciones impuestas por los subsistemas.

## 4.2. Conclusiones específicas

### 4.2.1. Optimal operating conditions analysis of a multi-effect distillation plant [R1]

Del primer trabajo podemos extraer como conclusión que las variaciones de caudal en el agua de aporte térmico tienen escaso efecto sobre los índices de rendimiento, en comparación con las variaciones de la temperatura del mismo. Por otro lado, incrementos en el flujo de agua de alimentación conducen a una disminución de la energía térmica consu-

---

mida y a un aumento en la producción de destilado. Similares resultados se obtienen cuando se reduce la temperatura de refrigeración del condensador. Estos hechos sugieren que el calentador del primer efecto ha sido sido sobredimensionado o el flujo de alimentación podría haber sido subestimado en condiciones nominales. Para poder aumentar el rendimiento de la planta de acuerdo con los tres criterios seleccionados para la realización de este trabajo, es necesario disminuir la temperatura del agua de refrigeración y/o aumentar el caudal de refrigeración que pasa por el condensador.

Los resultados de la optimización multicriterio basada en algoritmos genéticos muestran que la planta MED puede alcanzar mejores resultados de acuerdo con los criterios seleccionados, especialmente maximizar la producción de destilado.

Los criterios tradicionales, basados en balances de energía térmica, han demostrado no ser buenos criterios de optimización para mejorar la operación del proceso desde el punto de vista de la calidad de la energía empleada o la calidad del proceso. Estos índices proporcionan información en términos cuantitativos independientemente de la naturaleza, la temperatura o el estado en el que la energía se ha suministrado o descargado al medio ambiente. Estos últimos puntos son solo algunas de las principales ventajas de la destilación térmica, por lo que es desfavorecida en cualquier comparativa con otra tecnología que emplee estos índices. Además, los índices de rendimiento tradicionales sólo consideran el consumo de energía térmica sin tener en cuenta que el consumo eléctrico, que en la destilación térmica puede representar un 10 % del consumo total de energía.

#### **4.2.2. Optimal operating conditions analysis for a MED according to energetic and exergetic criteria [R2]**

En primer lugar el análisis energético y exergético demostró ser una gran herramienta que hizo posible determinar nuevas estrategias de operación y encontrar fuentes de ineficiencias que no podían ser detectadas con los métodos tradicionales. Por ejemplo, el análisis energético y exergético revela que aunque la mayor parte de la energía térmica abandona el sistema por el agua de rechazo del condensador, la mayor parte de la exergía de entrada es degradada en entropía y otra cantidad signifi-

---

ficativa sale del sistema por el flujo de calor que el sistema intercambia con el ambiente.

Por otro lado, la optimización multicriterio basada en algoritmos genéticos empleando nuevos criterios exergéticos, ha hecho posible determinar nuevas condiciones de operación y concluir que las condiciones nominales de la planta MED están lejos de cualquier punto optimizado considerado en este trabajo. Este hecho puede estar ocasionado por la modificación de la primera y la última celda de la planta.

Las optimizaciones respecto de los nuevos índices de rendimiento basados en exergía conducen a una baja generación de entropía y a un bajo consumo específico de exergía. Estos índices propuestos pueden ser útiles para comparar diferentes plantas y tecnologías, ya que tienen en cuenta todos los tipos de energía empleada, su calidad y las condiciones ambientales, en contraste con los criterios basados en análisis de energía que solo tienen en cuenta la energía térmica.

Finalmente la baja influencia de la variación de los caudales de refrigeración del condensador y aporte de calor en el calentador del primer efecto sugiere que el tamaño del intercambiador en el primer y el último efecto no están optimizados. De hecho, la producción de destilado se puede aumentar aumentando el caudal de agua de alimentación.

#### **4.2.3. New low-cost solar tracking system based on open source hardware for educational purpose [R3]**

El prototipo nos permite trabajar principalmente con conceptos de concentración de energía solar, control de seguimiento solar y visión por computador a diferentes niveles. Además de las grandes posibilidades que ofrece el código abierto, la plataforma de hardware y la capacidad de implementar entornos de laboratorios virtuales y remotos o emplear diferentes lenguajes, lo que convierte al prototipo en una herramienta extremadamente útil.

La solución de bajo coste propuesta se presenta como una buena alternativa para laboratorios con fines educativos y científicos cuyos problemas principales suelen ser sus grandes necesidades de espacio y fondos para su establecimiento, asistencia para el mantenimiento y operación.

---

#### 4.2.4. New approach for solar tracking systems [R4]

Según los resultados obtenidos en las pruebas, se concluye que el nuevo enfoque basado en AI y visión por computador para los sistemas de seguimiento solar es válido, totalmente funcional y muestra un amplio margen de mejora. El nuevo enfoque es independiente de la tecnología solar, el tamaño del sistema, la ubicación y la hora. No se ve afectado por errores de apunte como la inclinación del pedestal, las cargas de viento o la posición aparente del Sol. Además, el enfoque propuesto ofrece ventajas tales como la capacidad de detección de nubes, bloqueos y sombras, atenuación atmosférica o medición concentrada de radiación solar, que pueden mejorar las estrategias de control del sistema.

El nuevo enfoque combinado con técnicas de control tradicionales hace posible esquemas de control de lazo cerrado, además es versátil y barato, permite reducir costes relacionados con el hardware del sistema de seguimiento solar y otros aspectos como la comunicación o la puesta en marcha, brinda mayor autonomía y flexibilidad.

#### 4.2.5. Parabolic trough collector field dynamic model: Validation, energetic and exergetic analyses [R5]

El modelo desarrollado para la elaboración de este trabajo es muy preciso. Se aprecia una pequeña pérdida de precisión al estimar la temperatura del fluido de salida en su valor límite más alto, que es causado por una subestimación de las pérdidas térmicas.

La resolución espacial es un parámetro determinante para este modelo. El estudio de la influencia de este parámetro estableció en 20 volúmenes de control por tubo absorbente el valor óptimo para con un costo de tiempo de simulación de 60 s por simulación diaria. El tiempo de simulación puede reducirse significativamente (a menos de 10 s) al reducir la resolución espacial lo que conlleva una disminución de la precisión del modelo.

Los análisis energéticos y exergéticos demuestran que los niveles más altos de DNI mejoran los índices de rendimiento térmico y exergético. Por el contrario, los cambios rápidos en los valores de DNI causan una reducción en el rendimiento. Los índices de rendimiento térmico muestran valores más altos que los índices de rendimiento de exergía. El análisis

---

térmico revela que las mayores pérdidas se producen en la reflexión y concentración de DNI, mientras que el análisis exergético señala que la destrucción de exergía en la superficie del tubo absorbedor debida a la baja temperatura de la superficie del tubo absorbedor que es una fuente importante de ineficiencias exergéticas.

#### **4.2.6. Machine Learning for Solar Trackers [R6]**

De este estudio se puede concluir que la librería de aprendizaje automático (*Tensorflow*) empleada es más rápida y más precisa que la empleada en la implementación original [R4]. El rápido crecimiento de Tensorflow y la gran cantidad de contribuciones de la comunidad abierta auguran una mejora sustancial de la misma. La nueva librería es abierta y más flexible, permite implementar el sistema de seguimiento solar inteligente en casi cualquier tipo de dispositivo.

Por otro lado, los buenos resultados obtenidos en términos de velocidad y precisión permiten utilizar este enfoque para diseñar nuevas estrategias de control basadas en la AI y la visión por computadora.

#### **4.2.7. Solar tower power mockup for the assessment of advanced control techniques [R7]**

El sistema mecatrónico desarrollado permite a los investigadores evaluar técnicas de control en la etapa inicial de desarrollo, antes de la evaluación en una instalación real. El sistema está diseñado para ser fácilmente construido y ensamblado.

Este sistema se basa en componentes de hardware abierto de bajo coste y bajo consumo, software de código abierto y piezas impresas en 3D. Es el primer prototipo para la evaluación de técnicas de control inteligentes o avanzadas. El prototipo es un recurso útil para fines educativos, investigación y demostración.

#### **4.2.8. Optimal Operation of Solar Thermal Desalination Systems coupled to DEAHP [R8]**

El conjunto de modelos dinámicos presentados en este trabajo, ha demostrado ser una herramienta poderosa y altamente configurable para

---

tareas de modelado, control y optimización para sistemas de desalinización mediante energía solar, ya que permite replicar sistemas reales o diseñar nuevas configuraciones. El conjunto de modelos simula el comportamiento térmico del sistema teniendo en cuenta las limitaciones de operación de los subsistemas, lo que permite simular solamente las configuraciones y las estrategias de operación reales.

El método para la generación de condiciones óptimas de operación del sistema ha demostrado ser capaz de encontrar valores óptimos de variables manipulables con respecto a algunos criterios, incluso para configuraciones con esquemas de operación complejos mientras se mantiene el sistema en funcionamiento a pesar de las limitaciones impuestas por los subsistemas, la operación a carga parcial o transitorios.

Las trayectorias optimizadas para maximizar la producción de destilado a lo largo del día aumentan la producción y las trayectorias optimizadas para minimizar el consumo térmico y maximizar la producción.

## 4.3. Futuras líneas de investigación

A continuación se recopilan las futuras líneas de investigación detalladas en cada uno de los artículo publicados. Se dividen en dos grandes grupos de acuerdo a al tipo de técnica de modelado, aunque ambas pueden ser empleadas juntas, lo que origina por sí mismo otra línea de trabajo.

### 4.3.1. Modelado basado en primero principios

En relación a los trabajos de modelado basado en primeros principios, en primer lugar una línea de trabajo interesante es aumentar el conjunto de modelos dinámicos con otros subsistemas adicionales (tanques, colectores solares de placa plana, etc), incluso incluir modelos de otro tipo de sistemas de desalinización. Además, el conjunto de modelos puede ser mejorado añadiendo el desarrollo matemático necesario para obtener información económica y desarrollar nuevos índices que permitan optimizaciones basadas en términos económicos. Se pueden incluir varios factores adicionales para optimizaciones económicas más precisas, como costes de inversión, costes fijos y consumo de dispositivos eléctricos (bombas, válvulas, etc.).

---

En modelado suelen existir 3 líneas de mejora de cualquier modelo: aumento de la precisión, aumento del rango de validez y disminución del esfuerzo computacional. Normalmente estas líneas de mejora son antagonicas y la mejora en uno de estos campos puede influir negativamente en otros. Por esto es necesario determinar muy bien cual es el objetivo del modelo y los requerimientos de este. Según las conclusiones y los trabajos desarrollados, se debe estudiar la posibilidad de diseñar modelos más sencillos que hagan posible simular varios días de operación con el objeto de realizar optimizaciones de largas series temporales para generalizar la estrategia de operación óptima a lo largo del año. Estos modelos más sencillos deben requerir un esfuerzo menor de computación y ser más rápidos, sin penalizar en exceso la precisión. Se debe tener en cuenta que los algoritmos genéticos de optimización aún demostrando ser una excelente herramienta para este tipo de problemas tan complejos, consumen una gran cantidad de tiempo.

Otro aspecto a mejorar del conjunto de modelos es la inicialización de los modelos. Durante la realización de esta tesis, la inicialización de los modelos dinámicos ha sido un problema constante que se ha ido solucionando aplicando medidas particulares. Estas medidas han consumido demasiado tiempo y esfuerzo. Desarrollar nuevas estrategias o medidas para determinar los parámetros de inicialización de los modelos son necesarias para una mejora significativa del conjunto de modelos desarrollados.

#### **4.3.2. Modelado basado en redes neuronales**

En lo referente al modelado basado en redes neuronales con CSP y desalación, se abren infinidad de líneas puesto que este tipo de modelado no ha muy sido empleado en estos campos. De manera general, este tipo de modelado tiene un gran potencial para contribuir al desarrollo de dispositivos inteligentes y autónomos. Los dos recursos principales necesarios para el desarrollo de estas aplicaciones son la potencia computacional y la disponibilidad de datos experimentales. Los recursos computacionales pueden ser de bajo coste y están disponibles de forma masiva en clústeres y servicios de computación en la nube. Los datos se pueden recopilar de instalaciones experimentales o plantas comerciales. Los desarrollos recientes en otros campos se centran en dispositivos integrados, lo que fomenta el diseño de aplicaciones en el dispositivo que preservan la privacidad, reducen el consumo de energía y limitan el uso

de canales de transmisión y computación central. Todas estas mejoras probadas en otros campos pueden ser implementadas, beneficiándose de este modo de sus ventajas, como se ha demostrado en esta tesis en la implementación de estas técnicas para desarrollar el sistema de seguimiento solar inteligente.

En lo referente al sistema de seguimiento inteligente basado en redes neuronales, se debe desarrollar un conjunto de imágenes de entrenamiento y validación mucho mayor y mas general que permita desarrollar modelos más robustos y precisos. Para esta labor es imprescindible nuevas herramientas de etiquetado de imágenes que reduzcan el trabajo de etiquetado. El nuevo sistema puede ser mejorado implementando modelos que soparten técnicas de segmentación semántica. Estos modelos detectan objetos mientras generan simultáneamente una máscara de segmentación de alta calidad a nivel de píxel para cada instancia.

El sistema de seguimiento debe ser ensayado en condiciones reales (polvo, nubes parciales, etc...) durante un largo periodo de tiempo para demostrar su fiabilidad y poder ser caracterizado correctamente para avanzar a una fase industrial. Los ensayos deben estar diseñado para determinar el error del sistema. También se deben realizar experimentos adicionales para evaluar el error medio cometido por el colector solar mediante la evaluación de los valores de *Intersect over Union* (IoU) dados por el modelo basado en redes neuronales. IoU es una medida de evaluación utilizada para medir la precisión de un detector de objetos, representa la relación entre la intersección y la unión de la región predicha y real. Este nuevo sistema puede ser empleado para diseñar lazos cerrados de control en combinación con sistemas tradicionales.

La nueva información obtenida por el sistema de control basado en redes neuronales y visión por computador abre nuevas posibilidades de investigación, sobre todo para el desarrollo de estrategias de control más eficientes al hacer disponible nueva información relevante como posición, velocidad de nubes, bloqueos y sombras, junto con estimación futura de la potencia sobre el receptor. Predecir transitorios debidos al paso de nubes es uno de los problemas de control mas importantes que está consumiendo muchos esfuerzos y recursos. También, el desarrollo estrategias óptimas de apunte que minimicen los efectos de las sombras y los bloqueos aumentaría el rendimiento de los sistemas CSP.

Finalmente, las nuevas herramientas que nos brinda el nuevo paradigma denominado industria 4.0 deben ser analizadas con objeto de ver

---

su aplicabilidad en los campos de la desalación y CSP. Algunas de estas han sido probadas de manera inicial en esta tesis con buenos resultados como son la filosofía del uso de hardware y software libre de bajo coste y el empleo de técnicas de fabricación aditiva como impresión 3D.

# Bibliografía

*\*Este capítulo solamente recoge las fuentes bibliográficas más relevantes que se han empleado en el presente trabajo, en la sección bibliografía de los correspondientes artículos adjuntos hay referencias adicionales.*

# Bibliografía

- [1] V. Masson-Delmotte, H. Zhai, R. Pörtner, P. Skea, A. Shukla, W. Pirani, C. Moufouma-Okia, R. Péan, S. Pidcock, J. Connors, Y. Matthews, M. Chen, X. Zhou, E. Gomis, T. Lonnoy, M. Maycock, and T. Waterfiel, “Ipcc, 2018: Summary for policymakers. in: Global warming of 1.5 °C. an special report on the impacts of global warming of 1.5 °C above pre-industrial levels and related global greenhouse gas emission pathways, in the context of strengthening the global,” 2018. <http://cort.as/-SUrJ>.
- [2] IRENA, “Renewable Power Generation Costs in 2018, The International Renewable Energy Agency,” tech. rep., 2018. DOI: <http://cort.as/-SUrg>.
- [3] A. S. Stillwell and M. E. Webber, “Predicting the specific energy consumption of reverse osmosis desalination,” *Water*, vol. 8, no. 12, pp. 1–18, 2016. DOI: <https://doi.org/10.3390/w8120601>.
- [4] N. Ghaffour, J. Bundschuh, H. Mahmoudi, and M. F. Goosen, “Renewable energy-driven desalination technologies: A comprehensive review on challenges and potential applications of integrated systems,” *Desalination*, vol. 356, pp. 94–114, 2015. DOI: <http://dx.doi.org/10.1016/j.desal.2014.10.024>.
- [5] PROTERMOSOLAR, “Informe de transición del sector eléctrico Horizonte 2030. Otro mix de generación es posible y deseable,” 2018. <http://cort.as/-SUXq>.
- [6] T. y. A. D. Comisión de Expertos de Transición Energética, Ministerio de Energía, “Comisión de expertos de transición energética, análisis y propuestas para la descarbonización,” 2017. <http://cort.as/-SUxy>.

- [7] Instituto para la Diversificación y Ahorro de la Energía (IDAE). Ministerio para la transición ecológica. Gobierno de España, “Plan Nacional Integrado de Energía y Clima 2021-2030,” 2018. <http://cort.as/-SUxt>.
  - [8] R. Pachauri, L. Meyer, S. Hallegatte, G. Hegerl, S. Brinkman, L. van Kesteren, N. Leprince-Ringuet, and F. van Boxmeer, “IPCC, 2014: Climate Change 2014: Synthesis Report. Contribution of Working Groups I, II and III to the Fifth Assessment Report of the Intergovernmental Panel on Climate Change,” 2015. <http://cort.as/-SUu7>.
  - [9] A. Makarigakis and B. Elena Jimenez-Cisneros, “Unesco’s contribution to face global water challenges,” *Water*, vol. 11, no. 2, p. 388, 2019. DOI: <https://doi.org/10.3390/w11020388>.
  - [10] H. Treidel, J. L. Martin-Bordes, and J. J. Gurdak, *Climate change effects on groundwater resources. International association of hydrogeologist*. Taylor & Francis Group: London, unesco, in ed., 2012.
  - [11] United Nations, Department of Economic and Social Affairs, “World population prospects,” 2019. <https://population.un.org/wpp/>.
  - [12] Q. Schiermeier, “IPCC report under fire,” *Nature*, vol. 508, no. 7496, p. 298, 2014. DOI: <https://doi.org/10.1038/508298a>.
  - [13] H. Mehdizadeh, “Membrane desalination plants from an energy-exergy viewpoint,” *Desalination*, vol. 191, no. 1-3, pp. 200–209, 2006. DOI: <https://doi.org/10.1016/j.desal.2005.06.037>.
  - [14] N. C. Darre and G. S. Toor, “Desalination of Water: a Review,” *Current Pollution Reports*, vol. 4, no. 2, pp. 104–111, 2018. DOI: <https://doi.org/10.1007/s40726-018-0085-9>.
  - [15] N. Ghaffour, T. M. Missimer, and G. L. Amy, “Technical review and evaluation of the economics of water desalination: Current and future challenges for better water supply sustainability,” *Desalination*, vol. 309, no. 2013, pp. 197–207, 2013. DOI: <https://doi.org/10.1016/j.desal.2012.10.015>.
-

- [16] K. S. Spiegler and Y. M. El-Sayed, “The energetics of desalination processes,” *Desalination*, vol. 134, no. 1-3, pp. 109–128, 2001. DOI: [https://doi.org/10.1016/S0011-9164\(01\)00121-7](https://doi.org/10.1016/S0011-9164(01)00121-7).
  - [17] P. Palenzuela, G. Zaragoza, D. C. Alarcón-Padilla, and J. Blanco, “Evaluation of cooling technologies of concentrated solar power plants and their combination with desalination in the mediterranean area,” *Applied Thermal Engineering*, vol. 50, no. 2, pp. 1514–1521, 2013. DOI: <https://doi.org/10.1016/j.aplthermaleng.2011.11.005>.
  - [18] E. Zarza, J. Ajona, J. León, A. Gregorzewski, and K. Gentner, “Solar thermal desalination project at the plataforma solar de almería,” *Solar energy materials*, vol. 24, no. 1-4, pp. 608–622, 1991. DOI: [https://doi.org/10.1016/0165-1633\(91\)90094-2](https://doi.org/10.1016/0165-1633(91)90094-2).
  - [19] A. Al-Karaghouli and L. L. Kazmerski, “Energy consumption and water production cost of conventional and renewable-energy-powered desalination processes,” *Renewable and Sustainable Energy Reviews*, vol. 24, pp. 343–356, 2013. DOI: <https://doi.org/10.1016/j.rser.2012.12.064>.
  - [20] M. T. Ali, H. E. S. Fath, and P. R. Armstrong, “A comprehensive techno-economical review of indirect solar desalination,” *Renewable and Sustainable Energy Reviews*, vol. 15, no. 8, pp. 4187–4199, 2011. DOI: <https://doi.org/10.1016/j.rser.2011.05.012>.
  - [21] A. de la Calle, J. Bonilla, L. Roca, and P. Palenzuela, “Dynamic modeling and simulation of a solar-assisted multi-effect distillation plant,” *Desalination*, vol. 357, pp. 65–76, 2015. DOI: <https://doi.org/10.1016/j.desal.2014.11.008>.
  - [22] A. Ghobeity and A. Mitsos, “Optimal design and operation of desalination systems: new challenges and recent advances,” *Current Opinion in Chemical Engineering*, vol. 6, pp. 61–68, 2014. DOI: <https://doi.org/10.1016/j.coche.2014.09.008>.
  - [23] P. Palenzuela, D.-C. Alarcon, G. Zaragoza, and J. Blanco, *Evaluación del acoplamiento de plantas de destilación multiefecto a plantas termosolares*. Madrid: Centro de Investigaciones Energéticas, Medio Ambientales y Tecnológicas CIEMAT, 2012.
-

- [24] J. Y. Moon and J. Park, “Smart production scheduling with time-dependent and machine-dependent electricity cost by considering distributed energy resources and energy storage,” *International Journal of Production Research*, vol. 52, no. 13, pp. 3922–3939, 2014. DOI: <https://doi.org/10.1080/00207543.2013.860251>.
  - [25] H. Liu, H. Ning, Q. Mu, Y. Zheng, J. Zeng, L. T. Yang, R. Huang, and J. Ma, “A review of the smart world,” *Future Generation Computer Systems*, vol. 96, no. 2017, pp. 678–691, 2019. DOI: <https://doi.org/10.1016/j.future.2017.09.010>.
  - [26] A. B. Pouyfaucon and L. García-Rodríguez, “Solar thermal-powered desalination: A viable solution for a potential market,” *Desalination*, vol. 435, no. November 2017, pp. 60–69, 2018. DOI: <http://dx.doi.org/10.1016/j.desal.2017.12.025>.
  - [27] A. Alkaisi, R. Mossad, and A. Sharifian-Barforoush, “A review of the water desalination systems integrated with renewable energy,” *Energy Procedia*, vol. 110, pp. 268–274, 2017. DOI: <http://dx.doi.org/10.1016/j.egypro.2017.03.138>.
  - [28] N. Ghaffour, J. Bundschuh, H. Mahmoudi, and M. F. Goosen, “Renewable energy-driven desalination technologies: A comprehensive review on challenges and potential applications of integrated systems,” *Desalination*, vol. 356, 2015. DOI: <http://dx.doi.org/10.1016/j.desal.2014.10.024>.
  - [29] D. C. Alarcón-Padilla, L. García-Rodríguez, and J. Blanco-Gálvez, “Assessment of an absorption heat pump coupled to a multi-effect distillation unit within Aquasol project,” *Desalination*, vol. 212, no. 1-3, pp. 303–310, 2007. DOI: <http://dx.doi.org/10.1016/j.desal.2006.10.015>.
  - [30] P. Fernández-Izquierdo, L. García-Rodríguez, D. C. Alarcón-Padilla, P. Palenzuela, and I. Martín-Mateos, “Experimental analysis of a multi-effect distillation unit operated out of nominal conditions,” *Desalination*, vol. 284, pp. 233–237, 2012. DOI: <http://dx.doi.org/10.1016/j.desal.2011.09.004>.
  - [31] A. de la Calle, L. Roca, J. Bonilla, and P. Palenzuela, “Dynamic modeling and simulation of a double-effect absorption heat pump,”
-

- International Journal of Refrigeration*, vol. 72, pp. 171–191, 2016.  
DOI: <http://dx.doi.org/10.1016/j.ijrefrig.2016.07.018>.
- [32] M. S. Guney and Y. Tepe, “Classification and assessment of energy storage systems,” *Renewable and Sustainable Energy Reviews*, vol. 75, pp. 1187–1197, 2017. DOI: <https://doi.org/10.1016/j.rser.2016.11.102>.
  - [33] T. N. Sequeira and M. S. Santos, “Renewable energy and politics: A systematic review and new evidence,” *Journal of Cleaner Production*, vol. 192, pp. 553–568, 2018. DOI: <https://doi.org/10.1016/j.jclepro.2018.04.190>.
  - [34] M. Child, C. Kemfert, D. Bogdanov, and C. Breyer, “Flexible electricity generation, grid exchange and storage for the transition to a 100 % renewable energy system in Europe,” *Renewable Energy*, vol. 139, pp. 80–101, 2019. DOI: <https://doi.org/10.1016/j.renene.2019.02.077>.
  - [35] A. Battaglini, J. Lilliestam, A. Haas, and A. Patt, “Development of super smart grids for a more efficient utilisation of electricity from renewable sources,” *Journal of Cleaner Production*, vol. 17, no. 10, pp. 911–918, 2009. DOI: <https://doi.org/10.1016/j.jclepro.2009.02.006>.
  - [36] J. Lilliestam and S. Hanger, “Shades of green: Centralisation, decentralisation and controversy among European renewable electricity visions,” *Energy Research and Social Science*, vol. 17, pp. 20–29, 2016. DOI: <https://doi.org/10.1016/j.erss.2016.03.011>.
  - [37] International Energy Agency, “Market report series: Renewables 2018. Analysis and forecasts to 2023,” 2018. <http://cort.as/-SUrz>.
  - [38] D. Zhang, P. You, F. Liu, Y. Zhang, Y. Zhang, and C. Feng, “Regulating cost for renewable energy integration in power grids,” *Global Energy Interconnection*, vol. 1, no. 5, pp. 544–551, 2018. DOI: <https://doi.org/10.14171/J.2096-5117.GEI.2018.05.003>.
  - [39] S. Guo, Q. Liu, J. Sun, and H. Jin, “A review on the utilization of hybrid renewable energy,” *Renewable and Sustainable Energy*
-

- Reviews*, vol. 91, no. December 2017, pp. 1121–1147, 2018. DOI: <https://doi.org/10.1016/j.rser.2018.04.105>.
- [40] S. Ould Amrouche, D. Rekioua, T. Rekioua, and S. Bacha, “Overview of energy storage in renewable energy systems,” *International Journal of Hydrogen Energy*, vol. 41, no. 45, pp. 20914–20927, 2016. DOI: <https://doi.org/10.1016/j.ijhydene.2016.06.243>.
- [41] O. Z. Sharaf and M. F. Orhan, “Concentrated photovoltaic thermal (CPVT) solar collector systems: Part I - Fundamentals, design considerations and current technologies,” *Renewable and Sustainable Energy Reviews*, vol. 50, pp. 1500–1565, 2015. DOI: <https://doi.org/10.1016/j.rser.2015.05.036>.
- [42] O. Z. Sharaf and M. F. Orhann, “Concentrated photovoltaic thermal (CPVT) solar collector systems: Part II - Implemented systems, performance assessment, and future directions,” *Renewable and Sustainable Energy Reviews*, vol. 50, pp. 1566–1633, 2015. DOI: <https://doi.org/10.1016/j.rser.2014.07.215>.
- [43] CSP Today Global Tracker, “New energy update,” 2018. <http://cort.as/-SUs4>.
- [44] I. Reda and A. Andreas, “Solar position algorithm for solar radiation applications,” *Solar Energy*, vol. 76, no. 5, pp. 577–589, 2004. DOI: <http://dx.doi.org/10.1016/j.solener.2003.12.003>.
- [45] M. Blanco-Muriel, D. C. Alarcón-Padilla, T. López-Moratalla, and M. Lara-Coira, “Computing the solar vector,” *Solar Energy*, vol. 70, no. 5, pp. 431–441, 2001. DOI: [http://dx.doi.org/10.1016/S0038-092X\(00\)00156-0](http://dx.doi.org/10.1016/S0038-092X(00)00156-0).
- [46] R. Grená, “An algorithm for the computation of the solar position,” *Solar Energy*, vol. 82, no. 5, pp. 462–470, 2008. DOI: <http://dx.doi.org/10.1016/j.solener.2007.10.001>.
- [47] W. Nsengiyumva, S. G. Chen, L. Hu, and X. Chen, “Recent advancements and challenges in Solar Tracking Systems (STS): A review,” *Renewable and Sustainable Energy Reviews*, vol. 81, no. April 2017, pp. 250–279, 2018. DOI: <http://dx.doi.org/10.1016/j.rser.2017.06.085>.

- [48] M. Hermann, T. Pentek, and B. Otto, “Design principles for industry 4.0 scenarios,” *International Conference on System Sciences*, pp. 3928–3937, 2016. DOI: <http://dx.doi.org/10.13140/RG.2.29269.22248>.
  - [49] B. Schätz, M. Törngreen, S. Bensalem, M. Cengarle, H. Pfeifer, J. McDermid, R. Passerone, and A. Sangiovanni-Vincentelli, “Cyber-physical european roadmap and strategy: research agenda and recommendations for action,” *CyPhERS, Tech. Rep.*, 2015. <http://cort.as/-SUvi>.
  - [50] C. Santos, A. Mehrsai, A. C. Barros, M. Araújo, and E. Ares, “Towards Industry 4.0: an overview of European strategic roadmaps,” *Procedia Manufacturing*, vol. 13, pp. 972–979, 2017. DOI: <https://doi.org/10.1016/j.promfg.2017.09.093>.
  - [51] M. Kotynkova, “Re-Industrialization of Europe: Industry4.0 and the future of work,” *European Scientific Journal*, vol. 7881, pp. 249–256, 2017. <http://cort.as/-SUw2>.
  - [52] J. I. Ortega, J. I. Burgaleta, and F. M. Téllez, “Central Receiver System Solar Power Plant Using Molten Salt as Heat Transfer Fluid,” *Journal of Solar Energy Engineering*, vol. 130, no. 2, p. 024501, 2008. DOI: <https://doi.org/10.1115/1.2807210>.
  - [53] C. Villasante, “SMARTCSP: The Industry 4.0 approach for an effective CSP cost reduction,” *25th SolarPACES Annual Conference*, 2018.
  - [54] P. Fritzson, *Principles of object-oriented modeling and simulation with Modelica 3.3: a cyber-physical approach*. John Wiley & Sons, 2014.
  - [55] W. S. McCulloch and W. Pitts, “A logical calculus of the ideas immanent in nervous activity,” *The Bulletin of Mathematical Biophysics*, vol. 5, no. 4, pp. 115–133, 1943. DOI: <http://dx.doi.org/10.1007/BF02478259>.
  - [56] J. McCarthy, M. Minsky, N. Rochester, and C. E. Shannon, “A Proposal for the Dartmouth Summer Research Project on Artificial
-

- Intelligence,” vol. 27, pp. 12–14, 1955. DOI: <http://dx.doi.org/10.1609/aimag.v27i4.1904>.
- [57] S. Al Aani, T. Bonny, S. W. Hasan, and N. Hilal, “Can machine language and artificial intelligence revolutionize process automation for water treatment and desalination,” *Desalination*, vol. 458, pp. 84–96, 2019. DOI: <http://dx.doi.org/10.1016/j.desal.2019.02.005>.
- [58] T. Ibaraki, K. Nonobe, and M. Yagiura, *Metaheuristics: Progress as Real Problem Solvers*, vol. 32. Springer Science & Business Media, 2006.
- [59] S. Salhi, *Heuristic search: The emerging science of problem solving*. Springer, 2017.
- [60] G. Bloch and T. Denoeux, “Neural networks for process control and optimization: Two industrial applications,” *ISA Transactions*, vol. 42, no. 1, pp. 39–51, 2003. DOI: [http://dx.doi.org/10.1016/S0019-0578\(07\)60112-8](http://dx.doi.org/10.1016/S0019-0578(07)60112-8).
- [61] A. H. Elsheikh, S. W. Sharshir, M. Abd Elaziz, A. E. Kabeel, W. Guilan, and Z. Haiou, “Modeling of solar energy systems using artificial neural network: A comprehensive review,” *Solar Energy*, vol. 180, pp. 622–639, 2019. DOI: <http://dx.doi.org/10.1016/j.solener.2019.01.037>.
- [62] S. A. Kalogirou, “Artificial neural networks in renewable energy systems applications: a review,” *Renewable and Sustainable Energy Reviews*, vol. 5, no. 4, pp. 373–401, 2001. DOI: [http://dx.doi.org/10.1016/S1364-0321\(01\)00006-5](http://dx.doi.org/10.1016/S1364-0321(01)00006-5).
- [63] A. Qazi, H. Fayaz, A. Wadi, R. G. Raj, N. A. Rahim, and W. A. Khan, “The artificial neural network for solar radiation prediction and designing solar systems: A systematic literature review,” *Journal of Cleaner Production*, vol. 104, pp. 1–12, 2015. DOI: <http://dx.doi.org/10.1016/j.jclepro.2015.04.041>.
- [64] C. Voyant, G. Notton, S. Kalogirou, M. L. Nivet, C. Paoli, F. Motte, and A. Fouilloy, “Machine learning methods for solar radiation forecasting: A review,” *Renewable Energy*, vol. 105, pp. 569–582, 2017. DOI: <http://dx.doi.org/10.1016/j.renene.2016.12.095>.

- [65] S. A. Kalogirou, E. Mathioulakis, and V. Belessiotis, “Artificial neural networks for the performance prediction of large solar systems,” *Renewable Energy*, vol. 63, pp. 90–97, 2014. DOI: <http://dx.doi.org/10.1016/j.renene.2013.08.049>.
- [66] J. Hirvonen, H. ur Rehman, K. Deb, and K. Siren, “Neural network metamodelling in multi-objective optimization of a high latitude solar community,” *Solar Energy*, vol. 155, pp. 323–335, 2017. DOI: <http://dx.doi.org/10.1016/j.solener.2017.06.040>.
- [67] M. Arahal, M. Berenguel, and E. Camacho, “Nonlinear neural model-based predictive control of a solar plant,” pp. 985–990, 1997. DOI: <http://dx.doi.org/10.23919/ECC.1997.7082226>.
- [68] I. Muñoz, F. Cortés, A. Crespo, and M. Ibarra, “Development of a failure detection tool using machine learning techniques for a large aperture concentrating collector at an industrial application in chile,” vol. 2126, no. 1, p. 170008, 2019. DOI: <http://dx.doi.org/10.1063/1.5117678>.
- [69] A. A. Jiménez, C. Q. G. Muñoz, F. P. G. Marquez, and L. Zhang, “Artificial intelligence for concentrated solar plant maintenance management,” pp. 125–134, 2017. DOI: [http://dx.doi.org/10.1007/978-981-10-1837-4\\_11](http://dx.doi.org/10.1007/978-981-10-1837-4_11).



## **Anexo A**

### **Artículos en revistas internacionales**

*\*Los artículos a continuación expuestos contienen su bibliografía y material específicos, por lo tanto, las referencias de los artículo no corresponden a la sección de bibliografía principal sino a su sección particular.*

## **A.1. Optimal operating conditions analysis for a multi-effect distillation plant**

## Optimal operating conditions analysis of a multi-effect distillation plant

AQ2 Jose A. Carballo<sup>a,b</sup>, Javier Bonilla<sup>a,b</sup>, Lidia Roca<sup>a,b</sup>, Alberto de la Calle<sup>c</sup>, Patricia Palenzuela<sup>a,b</sup>, Manuel Berenguel<sup>b,d</sup>

<sup>a</sup>CIEMATPlataforma Solar de Almería, Ctra. de Senés s/n Tabernas, 04200 Almería, Spain, emails: jcarballo@psa.es (J.A. Carballo), jbonilla@psa.es (J. Bonilla) lidia.roca@psa.es (L. Roca), ppalenzuela@psa.es (P. Palenzuela)

<sup>b</sup>CIESOL Research Centre for Solar Energy, UAL-PSA, CIEMAT Joint Centre, Almería, Spain, emails: jcarballo@psa.es (J.A. Carballo), jbonilla@psa.es (J. Bonilla) lidia.roca@psa.es (L. Roca), ppalenzuela@psa.es (P. Palenzuela), beren@ual.es (M. Berenguel)

<sup>c</sup>CSIRO Energy, 10 Murra Dwyer Ct, Mayfield West, NSW 2304, Australia, email: acalle@psa.es (A. de la Calle)

<sup>d</sup>University of Almería, Ctra. Sacramento s/n, Almería 04120, Spain, email: beren@ual.es (M. Berenguel)

Received 22 June 2016; Accepted 16 September 2016

### ABSTRACT

A study which aims to determine the optimal operating conditions and the effects that the operational parameter variations produce on the experimental solar thermal desalination system at CIEMAT-Plataforma Solar de Almería (PSA) AQUASOL has been performed. A mathematical model of the experimental MED plant, previously developed, has been used to provide the information required for the analysis of the performance and improve the operation strategies in this plant. The mathematical model was implemented using the equation-based object-oriented modeling language Modelica and was validated using experimental data measured in the real facility. In this paper, a genetic optimization algorithm with three objectives and five decision variables has been considered and the results are shown and discussed.

**Keywords:** Optimal operation; Energy consumption; Multicriteria optimization; Desalination; Modelica

### 1. Introduction

Water has a very important role in society development. Recent history shows that unsustainable development and wrong policies can produce an immense pressure on water resources affecting their quality and availability. The main water consumption sources are industrial, human, agriculture and energy. Industrial water demand is expected to increase in all productive sectors [1]. Furthermore, it should be noted that the world's population is growing by about 80 million people per year and could reach 9.1 billion by 2050, with 2.4 billion people living in Sub-Saharan Africa, the region with the most heterogeneously distributed water resources [2]. Also, waste water from agriculture and fresh water required for energy pro-

duction, which are 15% and 70% of the total, respectively, can further exacerbate water scarcity in both sectors. With these predictions, United Nations expect that between 2 and 7 billion people will be facing water scarcity by the middle of the century [3].

Therefore, in the next decades, water problems are even expected in regions currently fresh water rich. Shortage of fresh water resources, salinization and contamination of the sources are some of the major problems to be tackled by humanity in the coming decades [4]. Considering that 50% of the population is living in coastal territories, water desalination could be very useful. For example, some countries of the Middle East make use of desalination of sea water as a vital source of fresh water.

Currently one of the main technologies used for

\*Corresponding author.

Presented at the EDS conference on Desalination for the Environment: Clean Water and Energy, Rome, Italy, 22–26 May 2016.

desalination is thermal distillation [5]. The advantages of thermal distillation processes are their ability to be driven by a low energy thermal source, their reliability, easier operation and maintenance, high purity fresh water and their capability to deal with harsh feed waters of high temperature and salinity or even with contaminated water. In thermal distillation, multi-stage flash (MSF), multi-effect distillation (MED) and mechanical or thermal vapor compression (MVC-TVC) can be considered the main techniques.

However, these techniques are energy inefficient as in any thermal distillation process the energy cost is 50% of the total fresh water cost. Thermal distillation processes demand two different forms of energy: thermal energy, which represents most of the energy consumed, and can come from different sources (fossil fuels, waste energy [6], solar energy [7], etc.), and electric power that is consumed for driving actuators and pumping systems (feeding, cooling, vacuum and removing system). Table 1 [8] summarizes the energy consumption of the three main thermal distillation techniques.

One way to reduce the energy inefficiency of both the existing and future plants is to study the influences of operational parameter, find the optimal operational conditions according to different criteria and develop efficient operational strategies, as shown by the several operational conditions studies [9].

There are operational conditions studies of the thermal distillation plants based on mathematical models and experimental data [10–17] that used the mathematical model to simulate the behavior of the plant and the experimental data to validate the results. These studies trying to find the best setting for the desalination process according to different criteria through optimization algorithms. In the case of the Plataforma Solar de Almería (PSA) MED plant specifically, there are mathematical models [18,19], that show a good agreement between the simulated and experimental results, and experimental studies of the optimal operational conditions of the PSA MED plant [20,21]. In the last one, an experimental study of out of its nominal working conditions concludes that influences of operational parameter are different for the criteria selected and show an irregular behavior over the range study. Although, there are mathematical models and experimental studies, there is no a study of the operational conditions based on the mathematical model and optimization algorithms for the PSA MED plant.

Table 1  
Thermal distillation energy consumption [8]

	MSF	MED	MVC
Electrical energy consumption (kWh/m <sup>3</sup> )	4–6	1.5–2.5	7–12
Thermal energy consumption (kJ/kg)	190–390	230–390	None
Total equivalent energy consumption (kWh/m <sup>3</sup> )	13.5–25.5	6.5–11	7–12

## 2. PSA MED plant and model

The studied plant in the present paper is a forward feed MED unit manufactured by ENTROPIE in 1987 consisting of 14 effects in a vertical arrangement with decreasing pressure from the 1st to the 14th effect. Originally, a low pressure boiler produced saturated steam at 70°C and 0.31 bar which was sent to the first effect, where the steam was condensed thus delivering thermal energy. Under the framework of AQUASOL project, whose main objective was the development of a hybrid solar-gas desalination system which met at the same time the requirements of low-cost, high efficiency and zero liquid discharge [20,22] the MED plant was modified. The current configuration allows for a 24-h plant operation and the system is flexible regarding the heat source in the first effect. Nowadays, at the AQUASOL facility a flat-plate collector solar field and a double-effect absorption heat pump (DEAHP) (which can be fed with a gas boiler or with a solar field composed by parabolic trough collectors, PTCs [23]), can provide the required heat. The DEAHP is coupled with the last effect of the MED plant recovering part of the wasted energy and can be connected to the MED plant directly or indirectly through the tanks [20]. In this indirect mode, the thermal energy can come from the DEAHP and the solar field at the same time.

In the PSA MED plant (see Fig. 1 [24]), each effect is composed by two heat exchangers, the first is called tube bundle evaporator or heater and it is employed to evaporate the feed water. The second one is called tube bundle cooled or preheater and it is employed to condensate the vapor by the feed water. Hot water flows inside the heater and delivers heat flow ( $q$ ) to the feed water that is sprayed over it, hot water flows from heater inlet ( $H_0$ ) to heater outlet ( $H_1$ ). The thermal energy released evaporates part of the feed water that comes from the preheaters of the effects

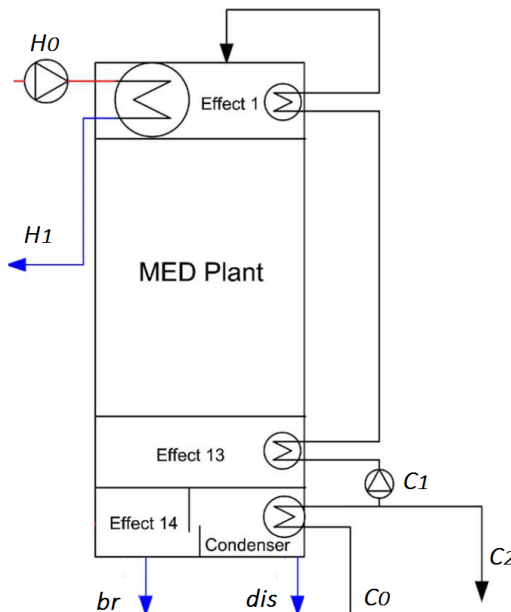


Fig. 1. MED plant unit scheme.

successively, ( $C_1$ ) and previously from the condenser inlet ( $C_0$ ). The vapor generated is partially condensed in the pre-heater, which is located next to the evaporator, and then the remaining vapor that has not been condensed is transported to the next heater in order to release its latent heat to the feed water which has not been evaporated (called brine) in the previous effect. This process is repeated successively in the next effects. Water condensed is collected in each effect and goes out of the MED unit through the distillate output ( $dis$ ), feed water that has not been evaporated falls by gravity from one effect to the following one, and finally leaves the plant through the brine output ( $br$ ). The pumping system is composed by four pumps (sea water, heater, vacuum, brine and distillate pump) and represent the main electric energy consumer ( $e$ ). Three hydro-ejectors connected to the 2nd effect, 7th effect and the condenser, do the vacuum to the MED plant and remove the non-condensable gases during the whole operation.

All these phenomena can be simulated by mathematical models that predict the behavior of the MED in different operating conditions, saving time, costs and preventing critical situations. A dynamic model developed by de la Calle et al. [19] is the most suitable to perform this study. This model predicts the steady-state and transient behavior of the PSA MED plant in the whole operating range using as inputs the natural inputs of the system, i.e., the inlet heater water flow rate and temperature, the inlet condenser seawater flow rate and temperature, the preheater seawater flow rate and the ambient temperature, and using as outputs of the system the natural outputs i.e., distilled and brine rate and performance parameters. It was developed with the non-proprietary object-oriented modeling language Modelica [25] which allows formulating the problems in an acausal way, being very suited for representing physical systems. The MED model is an index-1 differential algebraic equations (DAEs) system with 4,474 equations, of which 57 are continuous time states. In order to handle this system of equations, the model follows a modular and hierarchical arrangement of sub models where there are three levels of abstraction. The low level describes the main heat and mass transfer phenomena of the plant, the medium level describes each physical element such as effects and preheaters and the high level composes the complete model of the plant.

Even though the model has a low number of inputs, it predicts the heat and mass processes which happen inside the plant with a high level of detail. This model assumes that the fluids inside the MED plant are in thermodynamic equilibrium and only water vapor is considered inside the effect. This vapor is completely condensed at the tube bundles, and although heat losses to the environment are considered, the thermal capacity of the metal structure of the plant is neglected. The Nusselt film condensation theory is used to model the condensation of the vapor inside and outside the tube bundle. The evaporation of the steam from the seawater is calculated according to mass and energy balances where a Nusselt number correlation adjusted with real data of the plant, characterizes the heat transfer at the falling film evaporators. The pressure inside the effects is calculated with the ideal gases law. A simple model of the pipes with a single control volume calculates the sensible heat transfer inside the tubes of the preheaters.

Dymola 2015 [26] and DASSL [27] were the tool and the numerical solver selected for performing the simulations, respectively. The calibration and validation showed a good agreement between simulated results and experimental data. The average errors of some of the most relevant variables like the outlet temperatures were lower than the uncertainty range of the measurement instruments. In the case of the distillate mass flow rate, the value predicted resulted in absolute average error lower than 0.045 kg/s of for one day of simulation.

### 3. Optimization

The present work has employed the Optimization library included in Dymola [28]. The optimization problem in this library is formulated as follows:

$$\begin{aligned} \min_{p \in B} f(\text{diag}(d_1)^{-1} c_1(p)), \\ c_2(p) \leq d_2, \quad c_3(p) = d_3, \\ c = \begin{pmatrix} c_1 \\ c_2 \\ c_3 \end{pmatrix}, \quad d = \begin{pmatrix} d_1 \\ d_2 \\ d_3 \end{pmatrix} \\ f = \begin{cases} \max \text{ maximum criteria values,} \\ \| \cdot \|_1^2 \text{ sum of squared criteria value,} \\ \| \cdot \|_1 \text{ sum of absolute criteria values.} \end{cases} \end{aligned} \quad (1)$$

Here,  $p$  represents an editable parameter vector, in which the parameters are varied during the optimization process (tuner parameters) and belong to the decision space  $B$ .  $C_1$  represents the objectives vector of the optimization calculated by means of the objective function. Equality and inequality constrains vectors ( $C_2, C_3$ ), which enable some criteria restriction if needed, are optional.  $d_1$  vector serves as a reciprocal scaling factor of the criteria and they enable different weights for each criteria.  $d_2$  and  $d_3$  vectors contain the restrictions values. The goal is to minimize all these objectives ( $C_1$ ) with their respective weights ( $d_1$ ) subjected to the imposed optional constraints ( $d_2$  and  $d_3$ ).

These multi-criteria optimization formulation is transformed into a scalar optimization problem by means of the scalar objective function,  $f$ . This function can be configured in the library in three different ways, minimize the maximum, the sum of the square or the sum of the absolute values of the objectives.

Algorithms commonly used to solve this kind of energy system optimization problems are evolutionary programming, evolutionary strategies and genetic algorithm [11]. The latter, already implemented in the Optimization library, has been used to perform the optimizations.

In genetic algorithms, a population of individuals, which represents the potential solution space, is evaluated for each iteration. The performance of an individual is evaluated according to the scalar fittest function, also called scalar objective function ( $f$ ). The initial population evolves successively a number of specific generation to best regions in the search space selecting the fittest individuals

in the population and modifying them by recombination or mutation.

In order to provide information required for the analysis of the performance and operation strategies in the MED plant, it is necessary to find the optimal operational conditions according to different criteria, even more after all the modifications carried out in the MED plant. This study contributes to develop new designs and operational methodologies. There are some performance indices useful to find a trade-off between cost reduction and performance improvement, in other words decrease the energy consumption and the maximize the fresh water production. Performance ratio (PR), the gain output ratio (GOR) and the specific water cooling consumption (SFWC) are the most relevant performance indices used in thermal desalination plants related with energy consumption and fresh water production. GOR is the most extended PR and shows the ratio between the mass of the produced distilled water and the mass of steam delivered to the plant, but it is referred only for steam-fed plants. PR is defined as the ratio between the mass of distillate (in kg) and the thermal energy supplied to the process normalized to 2,326 kJ (1,000 Btu) that is the latent heat of vaporization of water at 73°C (see Table 2). Finally, SFWC is the ratio between distilled water flow rate and the feed water flow rate.

Another useful performance index is the specific energy consumption ( $\bar{E}$ ), which is the relation between the total inlet energy (thermal and electric) and distilled water flow rate. In particular, for MED plants with hot water as energy source, PR is the most representative performance index. PR along with fresh water or distilled rate production  $\dot{m}_{dis}$  and  $\bar{E}$  have been used as criteria in the present work integrating the criteria vector ( $C_i$ ) in the optimization problem. In multi-criteria optimization cases, the criteria have been

Table 2  
Symbols and abbreviations

	Description	Equation
$t$ , °C	Temperature	
$\dot{m}$ , kg/s	Mass flow rate	
$\dot{v}$ , m³/h	Volumetric flow rate	
$\dot{q}$ , kJ/s	Heat flow rate	
$\dot{e}$ , kJ/s	Electric flow rate	
$\Delta$ , %	Variation from nominal	
$\bar{E}$ , kJ/kg	Specific energy consumption	$(\dot{e} + \dot{q}) / \dot{m}_{dis}$
PR	Performance ratio	$(\dot{m}_{dis} \cdot 2326) / \dot{q}$
GOR	Gain output ratio	$\dot{m}_{dis} / \dot{m}_{steam}$
SFWC	Specific feed water consumption	$\dot{m}_{dis} / \dot{m}_{feedwater}$
$H_0$	Heater inlet	
$H_1$	Heater outlet	
$C_0$	Condenser inlet	
$C_1$	Condenser outlet	
$C_2$	Feed inlet	
$br$	Brine outlet	
$dis$	Distilled water outlet	

scaled using the maximum value of PR as demand values ( $d_1$  components), the maximum  $\dot{m}_{dis}$  and the minimum  $\bar{E}$  found previously. So that, in the optimization process there are no preferences, all the criteria have the same weight. There are no restrictions in the criteria space ( $d_2$ ,  $d_3$ ), only it has been considered each tuner parameter range as constraints. The objective scalar function  $f$  is selected to minimize the sum of the square of the objectives.

The PSA MED plant needs a thermal energy contribution in its first effect in the form of inlet hot water flow, defined by its flow rate ( $\dot{v}_{H0}$ ) and its temperature ( $t_{H0}$ ). Also a sea water flow, in the condenser, satisfies the condenser demands ( $\dot{v}_{C0}$ ,  $t_{C0}$ ), part of this water flow is used as feed water ( $\dot{v}_{C2}$ ) while the remaining part is returned to the sea-water pool. Note that the water temperature in  $C_2$  depends on the condenser outlet temperature so this temperature cannot be considered as a variable. Therefore, these variables ( $\dot{v}_{H0}$ ,  $\dot{v}_{C0}$ ,  $\dot{v}_{C2}$ ,  $t_{H0}$ ,  $t_{C0}$ ) form the tuner parameter vector ( $p$ ) in the optimization problem. Furthermore, the operational range of the tuner parameters form the decision space ( $B$ ). Table 3 shows the nominal, minimum and maximum values of the MED plant for each criteria and tuner parameter.

#### 4. Results

The decision space generated, considering minimum, maximum and some intermediate values of the tuner parameters, has been built and simulated with the model and the tool previously cited. The criteria space generated is showed in Fig. 2.

Grey points represent all the criteria results obtained simulating each tuner parameter combination of the decision space. Arrows represent the changes in the criteria space due to the variations of each tuner parameter and the end of the arrow shows the maximum value of the tuner parameter. Table 4 shows the values of the criteria for each maximum value of the tuner parameter.

As the simulated data in Table 4 shows, for nominal conditions and just considering one modification in a tuner parameter, distilled mass flow rate ( $\dot{m}_{dis}$ ) can be risen (16.4%) by increasing  $t_{H0}$  to the maximum, without significant

Table 3  
Criteria and tuner parameters, limits and nominal values [21]

		Nominal	Min	Max
Tuner	$t_{H0}$ (°C)	66.5	57	75
	$\dot{v}_{H0}$ (m³/h)	43.2	28	72
	$t_{C0}$ (°C)	20	0	35
	$\dot{v}_{C0}$ (m³/h)	24	8	28
	$\dot{v}_{C2}$ (m³/h)	8	4	12.5
	$\dot{m}_{dis}$ ( $\frac{kg}{s}$ )	0.7		
Criteria	PR	>9.5		
	$\bar{E}$ ( $\frac{kJ}{kg}$ )	>210		

variations in  $\bar{E}$ . Furthermore, when increasing  $\dot{v}_{C2}$  to its maximum value,  $\dot{m}_{dis}$  can reach an increment of 22.8% while reducing 1.2%  $\bar{E}$  from nominal conditions. Finally, reducing  $t_{C0}$  to its minimum value allows for an improvement of 19.7% in  $\dot{m}_{dis}$  and a reduction of 1.5% in  $\bar{E}$ .

Considering the optimization algorithm introduced in previous sections and according to the criteria, the results provided by the genetic algorithm in the optimization process are depicted in Fig. 3 and summarized in Table 5.

As the simulated and optimized data in Table 5 show,  $\text{Max } \dot{m}_{dis}$  point leads to an increase of the distillate mass flow rate in 79.1%, decrease in PR of 0.11 points and decrease in  $\bar{E}$  of 1.1% from nominal conditions.  $\text{Min } \bar{E}$  decreases  $\bar{E}$  a 3%, improves  $\dot{m}_{dis}$  36.4% and improves PR 1.5%. The main difference between  $\text{Max } \dot{m}_{dis}$  and  $\text{Min } \bar{E}$  points is that while  $\text{Max } \dot{m}_{dis}$  needs to increase  $\dot{v}_{H0}$  and  $v_{C0}$  to values close to its minimums,  $\text{Min } \bar{E}$  needs to reduce those turners or decisions variables to values lower than the nominal ones.  $\text{Max PR}$  improves  $\dot{m}_{dis}$  a 5.3%, PR 0.23 points and decreases  $\bar{E}$  2.8%.

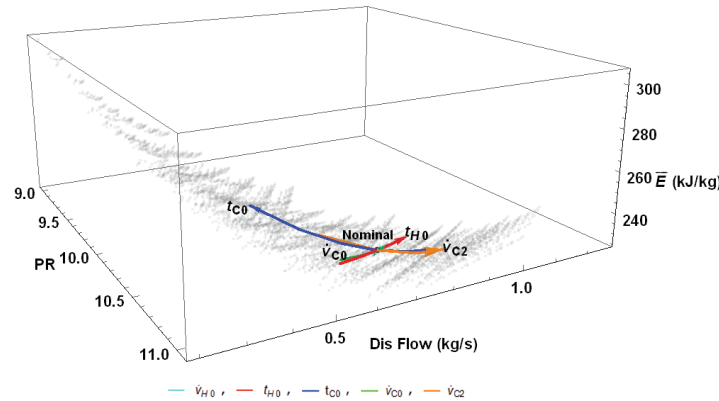


Fig. 2. Criteria space and variation relation of just one tuner parameters when considering nominal operating conditions.

Table 4  
Tuner parameter effects from nominal operating conditions

	$t_{H0}$	$\dot{v}_{H0}$	$t_{C0}$	$\dot{v}_{C0}$	$\dot{v}_{C2}$	$\dot{m}_{dis}$	$\Delta\dot{m}_{dis}$	PR	$\Delta\text{PR}$	$\dot{q}$	$\dot{e}$	$\bar{E}$	$\Delta E$
	$^{\circ}\text{C}$	$\frac{m^3}{h}$	$^{\circ}\text{C}$	$\frac{m^3}{h}$	$\frac{m^3}{h}$	$\text{kg}$	%		%	$\frac{kJ}{s}$	$\frac{kJ}{s}$	$\frac{kJ}{kg}$	%
Nominal	66.5	43.2	20	20	8	0.714	0	10.75	0	154.5	11.4	232.3	0
Max $t_{H0}$	75	43.2	20	20	8	0.831	16.4	10.67	-0.7	181.2	11.5	231.7	-0.3
Min $t_{C0}$	66.5	43.2	10	20	8	0.855	19.7	10.80	0.5	184.1	11.5	228.8	-1.5
Max $\dot{v}_{C0}$	66.5	43.2	20	28	8	0.735	2.9	10.75	0	159.1	12.2	233.0	0.3
Max $\dot{v}_{C2}$	66.5	43.2	20	20	12	0.877	22.8	10.84	1	188.2	13.1	229.5	-1.2

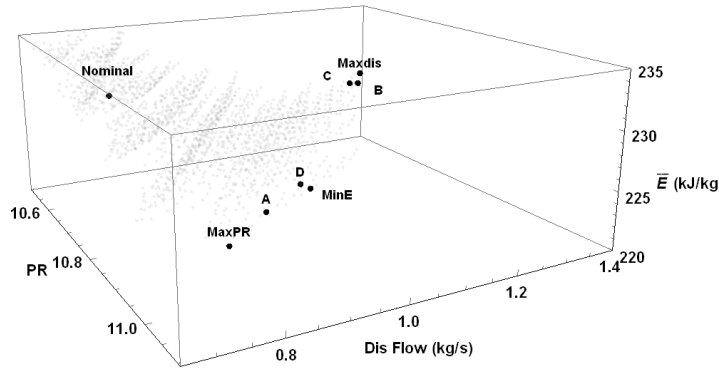


Fig. 3. Criteria space and optimized points.

Table 5  
Optimization

	$t_{H0}$	$\dot{v}_{H0}$	$t_{C0}$	$\dot{v}_{C0}$	$\dot{v}_{C2}$	$\dot{m}_{dis}$	$\dot{m}_{dis}$	PR	$\Delta PR$	$\dot{q}$	$\dot{e}$	$\bar{E}$	$\Delta \bar{E}$
	°C	$\frac{m^3}{h}$	°C	$\frac{m^3}{h}$	$\frac{m^3}{h}$	$\frac{kg}{s}$	%	%	%	$\frac{kJ}{s}$	$\frac{kJ}{s}$	$\frac{kJ}{kg}$	%
Nominal	66.5	43.2	20.0	20.0	8.0	0.714	0	10.75	0	154.5	11.4	232.3	0
$Max \dot{m}_{dis}$	75.0	66.1	10.2	27.1	12.5	1.279	79.1	10.64	-1.0	279.6	14.3	229.7	-1.1
$Min \bar{E}$	72.7	28.4	10.4	10.9	11.2	0.974	36.4	10.91	1.5	207.1	11.5	225.3	-3.0
Max PR	57.1	28.0	10.0	10.8	12.4	0.752	5.3	11.05	2.8	158.4	11.4	225.8	-2.8
$Min \bar{E}, Max PR(A)$	66.6	28.0	10.0	14.42	11.7	0.862	20.7	10.96	2.1	183.1	11.3	225.3	-2.9
$Min \bar{E}, Max \dot{m}_{dis}(B)$	74.6	63.0	10.0	23.94	12.4	1.255	75.7	10.67	-0.7	273.7	14.0	229.2	-1.3
$Max PR, Max \dot{m}_{dis}(C)$	74.4	70.3	11.9	25.84	12.3	1.228	72.0	10.68	-0.7	267.5	14.2	229.5	1.2
$Max PR, Max \dot{m}_{dis}$	74.0	28.8	10.6	10.6	12.5	0.968	26.2	10.89	1.3	206.8	11.4	225.3	-3.0
$Min \bar{E}(D)$													

## 5. Conclusions

Focusing on the PSA MED heater and operational parameters, simulation results show that  $\dot{v}_{H0}$  variations have a very small influence in the criteria result space. On the other hand, increments in  $t_{H0}$  mainly increase the fresh water production. Furthermore, increments in feed water flux  $\dot{v}_{C2}$ , lead to a decrease in  $\bar{E}$  and to an increase in the distillation production so that to an increase in PR. Very similar results are obtained when the temperature  $t_{C0}$  is reduced.

The fact that  $\dot{v}_{H0}$  variations have a very small influence in the criteria result space while increments in feed water flow  $\dot{v}_{C2}$  decreases  $\bar{E}$  and increases distillation production, in nominal conditions, suggests that the heater could be oversized or the feed flow could have been underestimated.

Seven operational parameter combinations due to different criteria and its performance has been studied and shown that, regarding the optimal criteria points,  $Max \dot{m}_{dis}$  is reached increasing  $t_{H0}$  and  $\dot{v}_{C2}$  to their maximum values, increasing  $\dot{v}_{C0}$  and  $\dot{v}_{H0}$  while decreasing  $t_{C0}$  to the minimum value.  $Min \bar{E}$  can be achieved decreasing to the minimum  $t_{C0}$  and decreasing  $\dot{v}_{C0}$  and  $\dot{v}_{H0}$ , the values of the remaining tuning parameters should be increased. Even in the  $Min \bar{E}$  point, the energy consumption continues being high.  $Max PR$  point is obtained decreasing all the tuning parameters to the minimum except  $\dot{v}_{C2}$ , which is increased. Therefore, in order to increase the operation performance of the plant according to the three selected criteria, it is necessary to decrease  $t_{C0}$  or/and increase  $\dot{v}_{C2}$ .

Although  $E$  and  $\dot{m}_{dis}$  have shown to be good optimization criteria to improve the process operation from the point of view mentioned previously,  $\bar{E}$  and  $\dot{m}_{dis}$  do not refer to the quality of the energy used or the quality of the process, only provide information in quantitative terms independently of the nature, temperature or the state in which the energy has been supplied or discharged into the environment, just some of the main thermal distillation advantages.

Although PR provides qualitative information when comparing distillation, it has been shown not to be a good optimization criterion by itself in order to improve the process operation. The effects of some operational parameters

are higher on distillate production and  $\bar{E}$  than in PR and it is not constant throughout the decision space, as already indicated in previous experimental studies [21]. Furthermore, PR only considers thermal energy without taking into account that the electric consumption in thermal distillation may be a 10% of the total energy consumption.

Optimization results show that the PSA MED plant can reach improved results according to the selected criteria, especially in  $Max \dot{m}_{dis}$  where the distillate production is increased while energy consumption is reduced.

Ongoing work includes the definition of appropriate optimization criteria which takes into account the energy quantity, as well as, the energy quality in order to increase the distillate production while preserving and reducing energy consumption. Another goal is to perform an experimental campaign in the PSA MED plant in order to validate the simulation results obtained from these optimizations.

## Acknowledgments

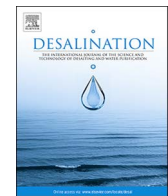
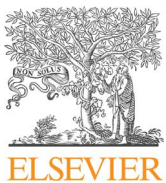
This work has been funded by the National R+D+i Plan Project DPI2014-56364-C2-1/2-R of the Spanish Ministry of Economy and Competitiveness and ERDF funds.

## References

- [1] UNESCO, The United Nations World Water Development Report 4: Managing Water Under Uncertainty and Risk, in World Water Assessment Programme, Vol. 1, 2012, p. 407.
- [2] United Nations Department of Economic and Social Affairs, Back to Our Common Future: Sustainable Development in the 21st Century (SD21) project, UNDESA, p. 39, 2012.
- [3] WWAP (United Nations World Water Assessment Programme), The United Nations World Water Development Report 2015: Water for a Sustainable World., United Nations Educational, Scientific and Cultural Organization, Paris, 2015.
- [4] F. Van Weert, J. Van der Gun, Saline and Brackish Groundwater at Shallow and Intermediate Depths: Genesis and World-Wide Occurrence, 2012 Congr. Can. Branch Int. Assoc. Hydrogeol., 2012, pp. 1–9.

- [5] C. Li, Y. Goswami, E. Stefanakos, Solar assisted sea water desalination: a review, *Renew. Sustain. Energy Rev.*, 19 (2013) 136–163.
- [6] P. Palenzuela, G. Zaragoza, D. C. Alarcón-Padilla, J. Blanco, Evaluation of cooling technologies of concentrated solar power plants and their combination with desalination in the mediterranean area, *Appl. Thermal Eng.*, 50 (2013) 1514–1521.
- [7] A. Gregorzewski, K. Genthner, E. Zarza, J. Leon, J. de Gunzbourg, G. Alfeld, J. Scharfe, Solar thermal desalination research project at the Plataforma Solar de Almeria, *Desalination*, 82 (1991) 145–152.
- [8] A. Al-Karaghouli, L.L. Kazmerski, Energy consumption and water production cost of conventional and renewable-energy-powered desalination processes, *Renew. Sustain. Energy Rev.*, 24 (2013) 343–356.
- [9] A. Ghobeity, A. Mitsos, Optimal design and operation of desalination systems: new challenges and recent advances, *Curr. Opin. Chem. Eng.*, 6 (2014) 61–68.
- [10] R. K. Kamali, A. Abbassi, S.A. Sadough Vanini, A simulation model and parametric study of MED-TVC process, *Desalination*, 235 (2009) 340–351.
- [11] I. Janghorban Esfahani, A. Ataei, K.V. Shetty, T. Oh, J.H. Park, C. Yoo, Modeling and genetic algorithm-based multi-objective optimization of the MED-TVC desalination system, *Desalination*, 292 (2012) 87–104.
- [12] E. Ali, Understanding the operation of industrial MSF plants. Part I: stability and steady-state analysis, *Desalination*, 143 (2002) 53–72.
- [13] F. Nematollahi, A. Rahimi, T.T. Gheinani, Experimental and theoretical energy and exergy analysis for a solar desalination system, *Desalination*, 317 (2013) 23–31.
- [14] H.S. Choi, T.J. Lee, Y.G. Kim, S.L. Song, Performance improvement of multiple-effect distiller with thermal vapor compression system by exergy analysis, *Desalination*, 182 (2005) 239–249.
- [15] C. Frantz, B. Seifert, Thermal analysis of a multi effect distillation plant powered by a solar tower plant, *Energy Procedia*, 69 (2015) 1928–1937.
- [16] T.H. Dahdah, A. Mitsos, Structural optimization of seawater desalination: II novel MED-MSF-TVC configurations, *Desalination*, 344 (2014) 219–227.
- [17] A.O.B. Amer, Development and optimization of ME-TVC desalination system, *Desalination*, 249 (2009) 1315–1331.
- [18] P. Palenzuela, A.S. Hassan, G. Zaragoza, D.C. Alarcon-Padilla, Steady state model for multi-effect distillation case study: Plataforma Solar de Almeria MED pilot plant, *Desalination*, 337 (2014) 31–42.
- [19] A. de la Calle, J. Bonilla, L. Roca, P. Palenzuela, Dynamic modeling and simulation of a solar-assisted multi-effect distillation plant, *Desalination*, 357 (2015) 65–76.
- [20] D.C. Alarcón-Padilla, J. Blanco-Gálvez, L. García-Rodríguez, W. Gernjak, S. Malato-Rodríguez, First experimental results of a new hybrid solar/gas multi-effect distillation system: the AQUASOL project, *Desalination*, 220 (2008) 619–625.
- [21] P. Fernández-Izquierdo, L. García-Rodríguez, D.C. Alarcón-Padilla, P. Palenzuela, I. Martín-Mateos, Experimental analysis of a multi-effect distillation unit operated out of nominal conditions, *Desalination*, 284 (2012) 233–237.
- [22] D.C. Alarcón-Padilla, L. García-Rodríguez, J. Blanco-Gálvez, Assessment of an absorption heat pump coupled to a multi-effect distillation unit within AQUASOL project, *Desalination*, 212 (2007) 303–310.
- [23] M. Ibarra, D.C. Alarcón-Padilla, J. Blanco-Gálvez, G. Zaragoza, P. Palenzuela, Performance of Small Parabolic Through Collector as Thermal Energy Supply to Steam Generation, Proc. SolarPACES Conference, 2012, p. 24997.
- [24] J. Blanco, D. Alarcón, E. Guillén, W. Gernjak, The AQUASOL system: solar collector field efficiency and solar-only mode performance, *J. Sol. Energy Eng.*, 133 (2011) 11009.
- [25] M. Association, Modelica ® – a unified object-oriented language for physical systems modeling language specification, *Interface*, 5 (2010) 250.
- [26] M. Otter, H. Elmquist, F.E. Cellier, Modeling of multibody systems with the object-oriented modeling language Dymola, *Nonlinear Dyn.*, 9 (1996) 91–112.
- [27] L.R. Petzold, A Description of Dassl: A Differential/Algebraic System Solver, Sand828637, January 1982, pp. 3–7.
- [28] A. Pfeiffer, Optimization Library for Interactive Multi-Criteria Optimization Tasks, Proc. 9th International Modelica Conference, 2012, pp. 669–680.

**A.2. Optimal operating conditions analysis for a multi-effect distillation plant according to energetic and exergetic criteria**



## Optimal operating conditions analysis for a multi-effect distillation plant according to energetic and exergetic criteria.

Jose A. Carballo<sup>a,c,\*</sup>, Javier Bonilla<sup>b,c</sup>, Lidia Roca<sup>b,c</sup>, Alberto De la Calle<sup>d</sup>, Patricia Palenzuela<sup>b,c</sup>, Diego C. Alarcón-Padilla<sup>b,c</sup>

<sup>a</sup> Universidad de Almería, Ctra. Sacramento, s/n, La Cañada, Almería 04120, Spain

<sup>b</sup> CIEMAT - Plataforma Solar de Almería, Ctra. de Senés s/n Tabernas, 04200 Almería, Spain

<sup>c</sup> CIESOL Research Centre for Solar Energy, UAL-PSA.CIEMAT Joint Centre, Almería, Spain

<sup>d</sup> CSIRO Energy, 10 Murray Dwyer Ct, Mayfield West, NSW 2304, Australia

### ARTICLE INFO

**Keywords:**

Optimization  
Multi-criteria  
Genetic algorithm  
Desalination  
Modelica

### ABSTRACT

In order to reduce the energy cost while improving the process operation, a study which aims to analyze the influence of the operational parameters variations and determine the optimal operating conditions of a pilot multi-effect desalination system (MED) at CIEMAT-Plataforma Solar de Almería (PSA) has been performed. An equation-based object-oriented mathematical model of the experimental MED plant, implemented using the modeling language Modelica and previously developed, calibrated and validated, has been adapted to carry out this study. Firstly, an energetic and exergetic analysis of the process under nominal conditions has been carried out, revealing the key sources of energy and exergy consumption. On the one hand, the thermal energy contained in the mass outflows are the main responsible source of the high energy consumption, on the other hand the entropy generation and the heat exchanged with the environment are the responsible of the exergy degradation. Secondly, a study on the influence of the operational parameters shows that the production of the real plant under nominal conditions is far from the maximum simulated values and some operational parameters have not a great influence in the process with respect to the rest. Finally, using a genetic optimization algorithm implemented in the modeling tool, a optimization process taking into account different energy and exergy performance criteria, sets optimal operational set points.

### 1. Introduction

The immense pressure on water resources due to unsustainable development and wrong policies have affected fresh water quality and its availability. In the next few decades, the shortage of fresh water resources will be some of the major problems to be tackled by humanity [1]. Seawater desalination represents an interesting solution for the problem of the water scarcity, even more if we consider that renewable energy sources have become a real alternative [2]. There are available different desalination technologies based on different principles, phase change thermal, membrane and alternative processes, all are operated by either conventional energy or renewable energy source [3].

Nowadays, reverse osmosis is covering the largest fraction of the new desalination world demand, although thermal distillation continues being one of the main technologies used in desalination [4], especially in energy-rich countries. Thermal distillation processes

present some benefits, for example they are able to be driven by a low energy thermal source, they are reliable, easy to operate and maintain and produce high purity fresh water. Furthermore, these processes are able to deal with harsh feed waters (high temperature, high salinity) or even with water pollution [5]. These thermal processes demand two different forms of energy: the main energy consumption is in the form of thermal energy and a smaller energy consumption is in the form of electric energy for driving actuators and pumping systems (feeding, cooling, vacuum, brine disposal and distillate extraction).

Among the thermal desalination technologies, multi-stage flash (MSF) and multi-effect distillation (MED) are the main ones monopolizing the largest part desalinated water world production by means of thermal processes. Table 1 summarizes the typical energy consumption of the MSF and MED processes. Thermal distillation technologies are considered energy inefficient, representing the energy cost the 50% of the total fresh water cost production. The high energy consumption has restricted its use to countries rich in fossil fuels or to

\* Corresponding author.

E-mail addresses: [jcarballo@psa.es](mailto:jcarballo@psa.es) (J.A. Carballo), [jbonilla@psa.es](mailto:jbonilla@psa.es) (J. Bonilla), [lidia.roca@psa.es](mailto:lidia.roca@psa.es) (L. Roca), [alberto.delacallealonso@csiro.au](mailto:alberto.delacallealonso@csiro.au) (A. De la Calle), [ppalenzuela@psa.es](mailto:ppalenzuela@psa.es) (P. Palenzuela), [diego.alarcon@psa.es](mailto:diego.alarcon@psa.es) (D.C. Alarcón-Padilla).

**Table 1**  
Thermal distillation energy consumption [12].

	MSF	MED
Electrical energy consumption (kWh/m <sup>3</sup> )	2.5–5	2–2.5
Thermal energy consumption (kJ/kg)	190–280	145–230
Total equivalent energy consumption (kWh/m <sup>3</sup> )	19.6–27.3	14.5–21.4

specific thermal solutions like dual purpose co-generation plants and solar desalination systems [6]. However, the fact that MED is less affected by water quality, feed salinity, and doesn't require intensive pretreatment, makes this technology a good option when working conditions are very hard.

In order to improve their performance, the trend in the last decades has been to couple the MED plants with heat pumps. Some works can be found in the literature at this respect, for example Al-Juwaihe et al. [7] analyzed four different types of single-effect evaporator desalination systems driven by heat pumps, thermal vapor compressor (TVC), mechanical vapor compressor (MVC), absorption, and adsorption. Garcia-Rodriguez et al. [8] and later Wang et al. [9] performed an analysis of an MED-double absorption heat pump.

Recently, new ways are being investigated to improve the process performance. On the one hand, forward osmosis [10] or nano filtration (NF) coupled to MED as a pretreatment [11], allows working at higher temperatures with higher efficiencies. This configuration eliminates the bivalent ions (soft scaling components), that limit the MED operation temperature at 70 °C, increasing in this way the operation temperature range. On the other hand, MED hybridizations with other thermodynamic cycles allows improving the efficiency, for example the hybrid MED adsorption cycle (AD) can operate below ambient conditions increasing even more the operation temperature range and the overall performance. Hybrid combinations between NF, RO and AD coupled with MED are proposed and show higher performance [11]. Finally, the use of solar energy (photovoltaic and thermal) for desalination processes is taking a significant role because it reduces energetic cost and environmental impact, specially for MED desalination processes due to its greater compatibility with solar energy and the electrical and thermal energy consumption.

The large difference between the theoretical minimum energy required for seawater desalination (4 kJ/kg [13] approximately) and the real requirements, not only for thermal distillation but for the rest of desalination technologies [14], leaves clear the importance to increase the knowledge regarding the potential improvements. The study of operational parameter influences and the optimal operational conditions according to different criteria are one of the ways to find the potential improvements that could allow developing efficient operational strategies. Nevertheless, the fact that different desalination techniques use diverse forms of energy, showing differences both in quantity and quality, makes more difficult to improve the knowledge and to optimize the process, or even the comparison between different facilities or technologies.

A lot of studies based on experimental data and mathematical models have been carried out in order to analyze and improve the performance of MED processes. For example, Fernandez-Izquierdo et al. [15] studied the energy performance of a multi-effect distillation unit operated out of nominal conditions and determined new operation points optimizing the performance ratio and the production. Ali and El-Fiki [16] developed a model to investigate the effect of the design parameters on the performance of an existing MED-TVC plant and of the operational parameter variations on the operating conditions. Kamali et al. [17,18] developed a model as an effective tool in order to perform parametric studies that assess the performance ratio and the optimum parameters of a MED-TVC plant, taking into account only the thermal energy consumption. Amer [19] developed a mathematical model to evaluate the thermal performance and to determine the

optimum operating and design conditions of a MED-TVC system. Janghorban et al. [20] modeled and optimized a MED-TVC plant based on thermal energy consumption criteria. Recently, Frantz and Seifert [21] performed a thermal analysis of a MED unit powered by a solar tower plant in order to optimize the thermal efficiency for a certain range of heating steam temperatures. Finally, Palenzuela et al. [22] characterized at steady state the influence of the variation in certain operational parameters over the thermal performance and the distillate production of the pilot MED plant used in the present work.

In these works, the most employed technique to find potential improvements and optimize the process is the analysis of the thermal energy balance, which is the most important factor in order to improve the performance of thermal driven desalination plants. But when the most evident energy savings have been achieved, find potential improvements and optimizing the process becomes a complex work where the traditional performance indices do not provide information about other types of energy used in the process or about the quality of the process. In these cases the exergy analysis could be a relevant tool since it helps to define potential improvements, to optimize the process, to find irreversibilities and with the problem of using different types and qualities of energy. Different works using this tool have been already presented. Choi et al. [23] presented an exergy analysis of a MED-TVC plant to identify the exergy losses due to irreversibilities. Sharqawy et al. [14] studied the effect of the system properties as well as the environment dead state on the exergy variation and performed an exergy analysis for a MED plant. Recently, Janghorban et al. [24] carried out an exergoeconomic analysis of a MED coupled to an absorption heat pump system to investigate the effect of key parameters on the energy performance of the system and to optimize it. Finally, Piacentino [25] developed an advanced thermodynamic and exergy costing study of a MED plant.

First, the present work contributes to the previous scientific production, studying and discussing the influence of the operational parameters variations over the traditional and exergetic performance indexes in a MED plant, also the present work shows the benefits of energetic and exergetic studies for advanced optimization tasks. Second, optimizations according to the traditional and exergetic performance as criteria have been performed using genetic optimization algorithms and a highly detailed dynamic mathematical model of a MED plant previously validated. Optimization based on exergetic performance indexes take advantage of the possibilities offered by a new exergetic approach proposed in this work that take into account both thermal and electrical consumption.

## 2. Materials and methods

### 2.1. AQUASOL system

The facility under consideration in this paper is a forward feed MED unit installed at Plataforma Solar de Almería (PSA). It was manufactured by ENTROPIE and consists in 14 effects in a vertical arrangement with decreasing pressure from the 1st to the 14th effect. This unit has been modified many times with different purposes, the largest under the framework of AQUASOL project [26]. The main objective of the project was the development of a hybrid solar-gas desalination system which met at the same time the requirements of low-cost, high efficiency and zero liquid discharge. The facility allows 24-hour plant operation and the system is flexible regarding the heat source.

In the MED plant (see Fig. 1), each effect is composed of two tube bundles, evaporator and preheater, being the thermal energy supplied to the MED plant through the first evaporator (*point 1* and *point 2*). Hot water flows inside this evaporator and delivers heat to the feed water being sprayed over the tube bundle, which is partially evaporated. The vapor generated in the evaporator is partially condensed over the tube bundle of the preheater, cooled by the feed water and the remaining vapor that has not been condensed is transported by natural convection

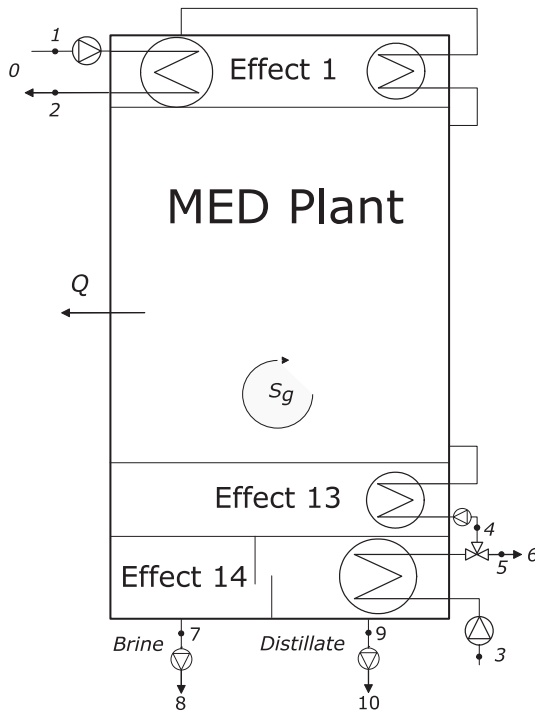


Fig. 1. MED plant scheme.

to the next evaporator in order to release its latent heat to the feed water that has not been evaporated (brine) in the previous effect. This process is repeated successively in the next effects. Finally, there is a bigger preheater located next to the 14th effect called condenser (*point 3*), where all the remaining vapor is condensed releasing the thermal energy to the cooling water that circulates inside. Distillate and brine are collected and leave the MED facility through the brine and distillate outputs (*point 7* and *point 9*). The pumping system, which is the main electric energy consumer, is composed of six pumps (vacuum, hot water, sea water, feed water, brine and distillate).

## 2.2. Model

The MED behaviour at different operating conditions can be simulated with mathematical models, saving time, costs and preventing critical situations. A dynamic model that predicts the steady-state and transient behaviour of the PSA MED plant was developed by de la Calle et al. [27] and it has been modified within this research work. It was developed with the non-proprietary object-oriented modeling language Modelica [28] which allows the acausal formulation of the problems, being very well suited for representing physical systems. Dymola 2015 [29,30] and DASSL [31] are the tool and the numerical solver selected for performing the simulations, respectively.

Due to the use of seawater as working fluid in the desalination process where the principal phenomenon is based on heat transfer, seawater thermophysical properties have a large importance in the model. In this work, IAPWS thermodynamic properties [32], considered in the model, have been completed and the formulation recommended in Sharqawy et al. [14] has been implemented to provide the seawater properties with the necessary accuracy in the operational range of the MED facility. It has also been required to include the pump quadratic models to predict their electric consumption and the mathematical formulation for the energetic and exergetic analysis that is shown below.

## 2.3. Energetic and exergetic analyses

As commented before, energetic and exergetic analysis is becoming a key factor in the performance improvement of many process like desalination [33]. Focusing in desalination, some recent works about exergy and desalination show the great potential of this analysis for improve the desalination processes [13,14,25,34], also show several considerations and assumptions that must be taken into account.

The mathematical formulation developed and employed in the analysis is shown in this section. Firstly, mass balance in a open system can be expressed by Eq. (1):

$$\dot{m} = \sum_i \dot{m}_i \quad (1)$$

where  $\dot{m}$  is the system mass variation and  $\dot{m}_i$  represents the input and output mass flows (positive and negative, respectively). Considering the mass balance, the first law of thermodynamics and a steady state system, the energy balance can be obtained according to Eq. (2):

$$\dot{U} = \sum_i (e_i \cdot \dot{m}_i) + \sum_i \dot{Q}_i - \sum_i \dot{W}_i \quad (2)$$

where  $\dot{U}$  is the overall system energy variation,  $e_i$  the specific internal energy of mass flows (internal, kinetics and potential), and  $\dot{Q}$  and  $\dot{W}$  the heat and work flows, respectively. In a similar way to the energy balance, the entropy balance can be formulated taking into account the second law of thermodynamics and the mass balance, quantifying in this way the entropy generation (irreversibility of the process):

$$\dot{S} = \sum_i (s_i \cdot \dot{m}_i) + \sum_i \frac{\dot{Q}_i}{T_i} + \dot{S}_g \quad (3)$$

where  $\dot{S}$  is the system entropy variation,  $\sum_i (s_i \cdot \dot{m}_i)$  represents the entropy of the mass flows,  $\sum_i \frac{\dot{Q}_i}{T_i}$  is the entropy due to the heat exchanged in the processes involved at certain temperature and  $\dot{S}_g$  represents the entropy generation.

If the exergy is defined as the maximum amount of work attainable when a system is brought to a equilibrium state from its initial state, the exergy balance can be expressed as a lineal combination of the energy and entropy balances at the temperature corresponding to the equilibrium state ( $T_0$ ). Equilibrium state is also called dead state that corresponds to subindex 0 in Fig. 1 (25 °C and 1 atm):

$$\dot{X} = \dot{U} - T_0 \cdot \dot{S}. \quad (4)$$

Replacing Eqs. (2) and (3) in Eq. (4) and reorganising the terms, the following equation is obtained:

$$\dot{X} = \sum_i (e_i - T_0 \cdot s_i) \cdot \dot{m}_i + \sum_i \left(1 - \frac{T_0}{T_i}\right) \dot{Q}_i - \sum_i \dot{W}_i - T_0 \cdot \dot{S}_g. \quad (5)$$

Note that in thermal distillation two facts must be considered about mass flows, the first of them is that the potential and kinetic terms of the internal energy of the mass flows can be neglected [35], the second one is that in a multi-component fluid such as seawater it must be taken into account the chemical potential [36]. Furthermore, considering that  $h = u + pv$ :

$$e = u + v^2 + gz + pv + \sum_i \mu_i \cdot n_i. \quad (6)$$

$$e = h + \sum_i \mu_i \cdot n_i. \quad (7)$$

where  $h$  represents the specific enthalpy,  $\mu_i$  and  $n_i$  the chemical potential and the mass fraction of each dissolution component, respectively. From Eqs. (5) and (7), the specific exergy of a mass flow ( $\dot{ex}$ ) according to the dead state, can be computed as follows:

$$\dot{x} = (e - (T_0 \cdot s)) - (e_0 - (T_0 \cdot s_0)). \quad (8)$$

$$\dot{x} = h - h_0 + \sum_i (\mu_i - \mu_{0,i}) \cdot n_i - T_0 \cdot (s - s_0). \quad (9)$$

Exergy balance in distillation Eq. (10) can be formulated using Eqs. (5), (9) and considering: the distillation plant as an open system of fixed volume (Fig. 1), the power consumed by the pumping system as a work delivered to the system to transport the fluids and finally the plant in steady state ( $\dot{U}$ ,  $\dot{S}$  and  $\dot{m}$  equal to 0).

$$\dot{X} = \sum_i \dot{x}_i \cdot \dot{m}_i + \sum_i \left(1 - \frac{T_0}{T_i}\right) \dot{Q}_i - \sum_i \dot{W}_i - T_0 \cdot \dot{S}_g \quad (10)$$

where  $\sum_i \dot{x}_i \cdot \dot{m}_i$  represents the exergy flows due to the input and output mass flows,  $\sum_i \left(1 - \frac{T_0}{T_i}\right) \dot{Q}_i$  denotes the sum of the maximum removable work in a heat flow and  $T_0 \cdot \dot{S}_g$  represents the total entropy generation.  $\dot{W}_i$  is computed by means of the pump quadratic models of each pump included in the general model. Finally,  $\dot{Q}_i$  and  $\dot{S}_g$  are computed according to the energy and entropy balances.

#### 2.4. Performance indexes

There are several performance indexes that characterize the thermal efficiency of a MED plant. In terms of thermal energy, the performance ratio (PR), specific water consumption or recovery ratio (SFWC) and specific thermal energy consumption ( $\bar{E}_{\text{Thermal}}$ ) are the main traditional performance indexes in thermal desalination [22]. PR can be defined as the ratio between the mass of distillate (kg) and the thermal energy supplied to the process, normalized to 2326 kJ (1000 Btu) that is the latent heat of vaporization of water at 73 °C,  $\bar{E}_{\text{Thermal}}$  is defined as the thermal energy consumption per fresh water production and SFWC is the ratio between distilled water flow rate and the feed water flow rate.

$$PR = \frac{\dot{m}_{\text{dis}} \cdot 2326}{(h_1 - h_2) \cdot \dot{m}_1}; \quad SFWC = \frac{\dot{m}_{\text{dis}}}{\dot{m}_{\text{feed}}} \quad (11)$$

$$\bar{E}_{\text{Thermal}} = \frac{(h_1 - h_2) \cdot \dot{m}_1}{\dot{m}_{\text{dis}}}. \quad (12)$$

On the other hand, considering the exergy balance, the specific exergy consumption ( $\bar{X}$ ) and the exergy efficiency ( $\eta_x$ ) are the main indexes. Unlike the previous ones, these indexes take into account the quantity as well as the quality of the thermal and electric energy employed. The first one is defined as the ratio between the exergy consumption and the fresh water production.

$$\bar{X} = \frac{x_{\text{con}}}{\dot{m}_{\text{dis}}} = \frac{(\dot{x}_1 - \dot{x}_2) \cdot \dot{m}_1 + (\dot{x}_3 \cdot \dot{m}_3) + (\dot{x}_5^{ch} \cdot \dot{m}_5) + \dot{W}_{\text{pump}}}{\dot{m}_{\text{dis}}} \quad (13)$$

The second one can be defined in two different ways: the outlet-inlet exergy fluxes ratio ( $\eta_{x1}$ ) and the ratio between the exergy employed to change the salinity of the products and the exergy consumption ( $\eta_{x2}$ ).

$$\eta_{x1} = \frac{\dot{x}_{out}}{\dot{x}_{in}} = 1 - \frac{\dot{S}_g}{(\dot{x}_1 \cdot \dot{m}_1) + (\dot{x}_3 \cdot \dot{m}_3) + \dot{W}_{\text{pump}}} \quad (14)$$

$$\eta_{x2} = \frac{-\dot{x}_{10}^{ch} \cdot \dot{m}_{10} - \dot{x}_8^{ch} \cdot \dot{m}_8}{(\dot{x}_1 - \dot{x}_2) \cdot \dot{m}_1 + (\dot{x}_3 \cdot \dot{m}_3) + (\dot{x}_5^{ch} \cdot \dot{m}_5) + \dot{W}_{\text{pump}}}. \quad (15)$$

In Eqs. (13), (14) and (15), subscripts are referred to those ones shown in Fig. 1 and *ch* superscript represents the chemical exergy (chemical potential) contribution in the exergy total flow in each point with respect to the dead state. Particularly, the sum of the chemical exergy of the distilled and brine flows ( $\dot{x}_{10}^{ch} \cdot \dot{m}_{10}$ ,  $\dot{x}_8^{ch} \cdot \dot{m}_8$ ) is the minimum work necessary to separate them from the feed water.

#### 2.5. Optimization

The main target of the optimization process is to find out new operating strategies that allow improving the performance of the MED

plant. For this purpose, it is necessary to find the optimal operational conditions according to different criteria and to identify the influences of the operational parameters variations over performance indexes.

In the present work, the optimization library included in Dymola [37] has been employed. This is a mathematical approach for multi-criteria optimization problems, which considers a set of optimal solutions (called *the Pareto optimal solutions*) and therefore is not possible to decrease one of the criteria without increasing another one. There are several heuristic algorithms that can be used to solve optimization problems, which are: evolutionary programming, evolutionary strategies and genetic algorithms [20]. The latter is the one used in the above mentioned optimization library, in which a scalar objective function transforms the multi-criteria problem into a scalar optimization problem.

For optimization purposes, the PSA MED unit can be considered as a black box which needs a thermal energy contribution in its first effect (*points 1–2* in Fig. 1) in the form of hot water, defined and controlled by its flow rate and its temperature. Also a seawater flow is provided to the condenser (*point 3*), part of this seawater is used as feed water for the MED plant (*point 4*) while the remaining part is returned to the seawater pool (*point 6*). Therefore, in the optimization process, mass flow rate and temperature in *point 1* and *point 3* and mass flow rate in *point 4* have been employed as optimization parameters. Notice that the water temperature in *point 4* cannot be considered as a optimization parameter because it depends on the condenser conditions, which depends on the conditions in *point 3*. The temperature in *point 3* (that is the seawater temperature) usually is not a manipulable parameter but in this experimental facility can be modified in a certain range. Table 2 shows the nominal values and operational ranges of the tuner parameters that compose the decision space.

The best combinations of the operational parameters of the MED PSA plant have been found considering different criteria: (max  $\dot{m}_{\text{dis}}$ , min  $\bar{E}_{\text{Thermal}}$ , max PR, min  $\bar{X}$ , max  $\eta_{x1}$ , max  $\eta_{x3}$ , min  $\bar{E}_{\text{Thermal}}$  and min  $\bar{X}$ , min  $\bar{E}_{\text{Thermal}}$  and max  $\dot{m}_{\text{dis}}$ , max  $\dot{m}_{\text{Dis}}$  and min  $\bar{X}$ ). The genetic algorithm was configured with an initial population of 200 individuals and the number of generations depends on the convergence speed of each optimization process according to the criteria defined.

### 3. Results and discussion

#### 3.1. Energetic and exergetic analyses

Table 3 and Fig. 2 show the energy and exergy content of each mass flow considered, obtained from the exergetic and energetic analysis. Energy and exergy flows corresponding to the points indicated in Fig. 1 have been determined in nominal conditions and computed according to the mass, energy and exergy balances included in the model described in the previous section.

Energetic analysis reveals that most inlet thermal energy leaves the system through *point 2*. Nevertheless, the *point 2* mass flow is completely used by the heat source in the PSA facility and it returns again to *point 1*, thus it does not represent a key energy consumption. Out of the rest of thermal energy, the largest part is wasted through *point 5* and the other part through the brine and distillate flows (*point 7* and *point 9*).

Regarding the exergetic analysis (see Fig. 2), as in the previous case, the largest part of exergy is wasted through *point 2*. As mentioned, it

**Table 2**  
Nominal values and operational ranges of the tuner parameters.

	$t_1$ (° C)	$\dot{m}_1$ (m <sup>3</sup> /h)	$t_3$ (° C)	$\dot{m}_3$ (m <sup>3</sup> /h)	$\dot{m}_4$ (m <sup>3</sup> /h)
Nominal	66.5	43.2	25	24	8
Min	57	28	5	8	4
Max	75	72	35	28	12.5

**Table 3**  
Analysis in nominal conditions.

Point	T	$n_n$	$\dot{m}$	$\dot{U}$	% $\dot{U}^*$	$\dot{X}^{ch}$	$\dot{X}^{th}$	$\dot{X}$	% $\dot{X}^*$
1	66.5	0	11.76	3274	85	0	131.2	131.2	92
2	63.7	0	-11.76	3135	81	0	114.7	114.7	80
3	25	0.0033	5.55	580	15	0	0	0	0
4	30.1	0.0033	2.22	280	7	-4.70	0.41	-4.28	3
5	30.1	0.0033	-3.33	421	11	-7.05	0.62	-6.43	4
6	25	0.0033	-3.33	0	0	0	0	0	0
7	30.1	0.0047	-1.57	197	5	-3.20	-0.11	-3.31	2
8	25	0.0047	-1.57	0	0	0.01	-0.16	-0.15	0
9	30.1	0	-0.65	82	2	-1.28	0.31	-0.96	1
10	25	0	-0.65	0	0	0.03	0.20	0.23	0
$W_{Pump}$	-	-	-	12	-	-	12	8	
$Q$	66.5	-	-	20	1	-	-	12.2	9
$S_g$	-	-	-	-	0	-	-	26.2	18

\* Based on the total inlet thermal energy and inlet exergy flow respectively.

would be not a key exergy consumption source since flow at point 2 is recirculated. The exergetic analysis reveals that the real main sources of exergy consumption are different to the main sources of energy consumption. In the case of the MED-PSA plant, entropy generation in dissipative processes and the exergy flux of the heat exchanged with the environment through the MED walls are the main sources of exergy consumption.

These differences between energy and exergy analysis reveal that the flows with a higher energy content present the lower quality, being the flows  $Q$  and  $S_g$  the main exergy consumption sources in nominal conditions (see Table 3).

### 3.2. MED optimization

The criteria space, shown in Fig. 3, has been obtained simulating 6000 different combinations of operational parameters distributed along the decision space (grey points). Arrows represent the variations in the criteria space caused by the increment of each operational parameter separately from the nominal conditions. Table 4 shows the optimized points obtained by the genetic optimization algorithm, according to the following criteria:  $\dot{m}_{dis}$ ,  $\bar{E}_{Thermal}$ ,  $\bar{X}$ ,  $\eta_{x1}$  and  $\eta_{x2}$ . Red dots represent the points that meet the Pareto optimal condition, and black dots represent the solution of optimization process. Criteria A, B and C correspond to the multi-criteria optimization processes solutions, where the inverse of its optimized value has been used as scaling factor for each criteria.

On the one hand, arrows in Fig. 3 show that variations in  $\dot{m}_l$  with respect the nominal conditions do not have a high influence in the criteria space represented. On the other hand, it can be seen that increments in  $\dot{m}_3$  cause an increase in  $\dot{m}_{dis}$ . This is due to the fact that the

higher the cooling flow rate through the condenser the lower the condensation temperature, which makes the temperature lift in the MED plant (temperature difference between the vapor temperature inside the first effect and the one inside the condenser) higher, assuming constant  $t_1$ . It causes a higher driving force for the evaporation process between the effects, producing more fresh water. Increments in  $\dot{m}_4$  reduce  $\bar{E}_{Thermal}$  and increase  $\dot{m}_{dis}$ . This facts suggest that the first effect evaporator could be oversized or the feed water flow underestimated.

Regarding the temperatures of the process, arrows in Fig. 3 show that a decrease in  $t_3$  leads to a high increase in  $\dot{m}_{dis}$  and in  $\bar{X}$ , as well as a reduction in  $\bar{E}_{Thermal}$  and in the heat exchanged with the environment. This is due to the increase in the temperature lift of the MED plant, assuming a fixed  $t_1$ . Notice that the minimum temperature in the condenser is limited by the minimum pressure achievable in the process (assuming saturation conditions). Finally, it can be seen that increments in  $t_1$  cause an increase in  $\dot{m}_{dis}$  and in  $\bar{E}_{Thermal}$ , due to the increase in  $t_7$ ,  $t_9$ ,  $t_5$  and temperature lift.

From the results shown in Table 4 and focusing on the optimum values of  $\dot{m}_{dis}$ , the maximum  $\dot{m}_{dis}$  can be found maximizing the parameters:  $t_1$ ,  $m_1$ ,  $\dot{m}_3$ ,  $\dot{m}_4$  and minimizing  $t_3$  obtaining an increase in  $\bar{E}_{Thermal}$  and  $\bar{X}$  of 1.4% and 29.8% respectively. Due to the fact that the quality of the energy supplied is higher (73 °C) and the difference between  $t_1$  and  $t_3$  is the highest. From the energy point of view,  $\bar{E}_{Thermal}$  ranges between 243 and 207 kJ/kg<sub>Dis</sub>, although most of the optimized points are in the range between 220 and 207 kJ/kg<sub>Dis</sub>. The optimum  $\bar{E}_{Thermal}$  (the minimum one) can be obtained by minimizing  $t_1$ ,  $t_3$  and  $\dot{m}_l$  (see the minimum values in Table 2), which decreases the energy wasted through points 7, 9 and 5.  $\bar{E}_{Thermal}$  as optimization criteria leads to low specific energy consumption and distilled production with a high exergy specific consumption, because it reduces the use of energy using

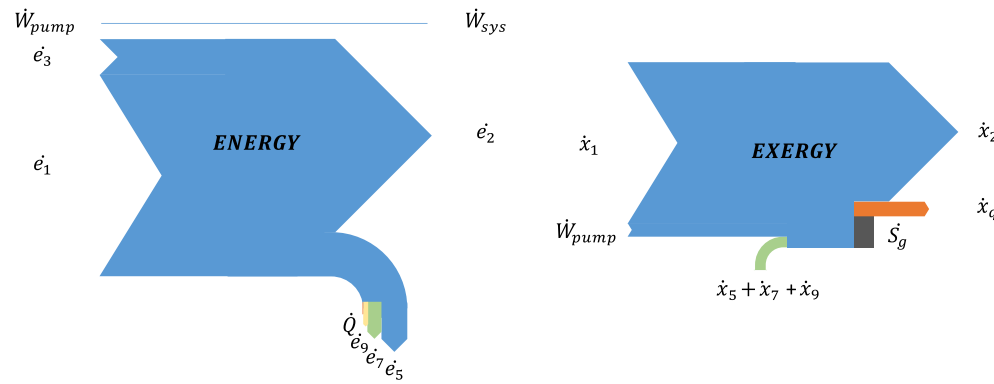


Fig. 2. Energy and exergy Sankey diagrams for the whole MED system in nominal conditions, see Table 3 for further information about subscripts.

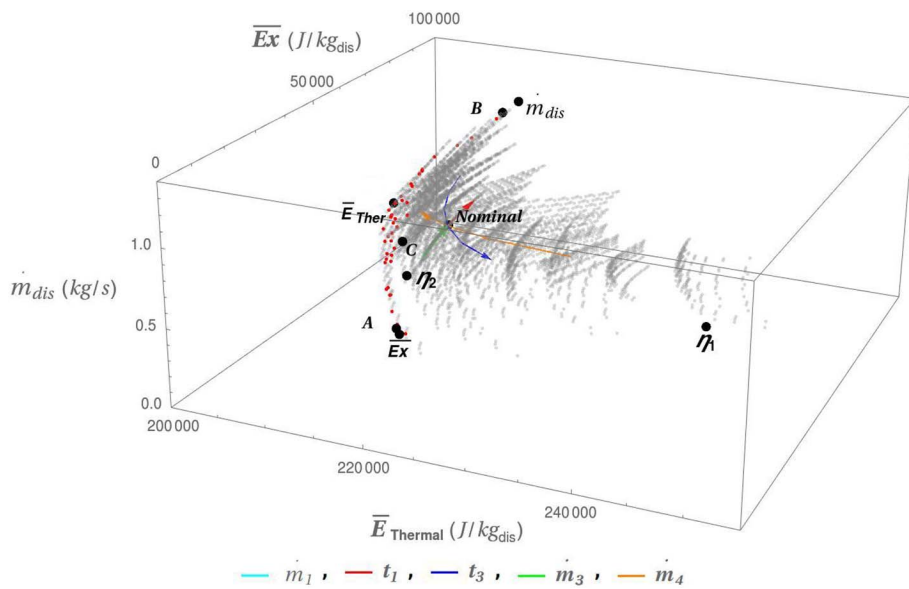


Fig. 3. Criteria space and optimized points according to different criteria.

Table 4  
Optimized points.

Criteria	$\dot{m}_{Dis}$	$E_{Thermal}$	$\bar{X}$	$\eta_{x1}$	$\eta_{x2}$
	(kg/s)	(kJ/kg <sub>Dis</sub> )	(kJ/kg <sub>Dis</sub> )		
Nominal	0.65	214	53.9	0.82	0.0011
$\dot{m}_{Dis}^{**}$	1.35	217	69.9	0.83	0.0010
$\bar{E}_{Thermal}^*$	0.68	207	57.7	0.66	0.0010
$\bar{X}^*$	0.40	218	19.9	0.69	0.0024
$\eta_{x1}^{**}$	0.33	243	49.4	0.97	0.0012
$\eta_{x2}^{**}$	0.60	216	31.3	0.82	0.0017
$A(\bar{E}_{Thermal}, \bar{X})$	0.42	217	20.9	0.70	0.0023
$B(\bar{E}_{Thermal}, \dot{m}_{Dis})$	1.29	216	67.5	0.80	0.0010
$C(\dot{m}_{Dis}, \bar{X})$	0.76	214	10.9	0.85	0.0015

\* Minimized criteria.

\*\* Maximized criteria.

higher quality energy.

From the exergy point of view, optimized points according to exergetic criteria achieve low exergy specific consumption and distilled production. Low quality energy reduces the distilled production. As shown in Table 4, the optimization based on the exergetic criteria leads to a reduction in the exergy consumption from 53.9 to 19.9 kJ/kg<sub>dis</sub>, operating at a low temperature in  $t_1$  (low energy quality) and at a low difference between  $t_1$  and  $t_3$  (see Table 5). The optimization based on the  $\eta_{x1}$  criteria leads to the minimum entropy generation and  $\dot{m}_{dis}$  and

high  $\bar{X}$ , operating the MED plant at the maximum  $t_1$ ,  $t_3$  and  $\dot{m}_1$ , also minimizing  $\dot{m}_3$  and  $\dot{m}_4$ . With this set point the MED plant distills less quantity of water using high quality energy. The optimization based on  $\eta_{x2}$  shows a reduction in  $\dot{m}_{dis}$  of 8% and 1% in  $\bar{X}$  with respect to the nominal conditions. This is achieved when the MED plant operates at high temperatures in the heat source supplied to the first effect and at low  $\dot{m}_1$  and temperature lift, using less energy but higher energy quality.

Finally, multi-criteria optimized points show intermediate compromises between optimized points. Changing the weight of each criteria in the optimization leads to a different optimum solution that moves along the Pareto optimal front.

#### 4. Conclusions

First, the energetic and exergetic analysis has shown to be a powerful tool to find new improved strategies. For example, nominal conditions of the MED unit explored in this work, are far from any optimized point considered in this work, as shown in Fig. 3. Energetic and exergetic analyses reveal that although the largest part of the thermal wasted energy leaves the system by point 5, most of the inlet exergy is degraded in entropy and other significant amount of it leaves the system by heat flow that the system exchanges with the environment. Some improvements include the optimization of the MED thermal insulation (from an exergetic point of view) and lower the temperature in  $t_3$  (from an energetic point of view).

Furthermore, the low influence of  $\dot{m}_3$  and  $\dot{m}_1$  suggest that the heat exchanger size in the first and the last effect are not optimized and  $\dot{m}_4$  is underestimated. As a matter of fact, the distillate production can be increased increasing the feed water flow rate ( $\dot{m}_4$ ). Regarding to the operational parameters related to the temperature, note that the lower  $\bar{E}_{Thermal}$  has been achieved using low values in  $t_1$ , and low differences between  $t_1$  and  $t_3$ , although it penalizes  $\dot{m}_{dis}$ . On the other hand, the maximum  $\dot{m}_{dis}$  has been achieved using the highest temperature in  $t_1$  and the highest difference between  $t_1$  and  $t_3$ .

Optimization based on  $\bar{E}_{Thermal}$  leads to reduce the specific thermal consumption with low temperature heat.  $\bar{X}$  as a optimization criteria leads to low quality energy demands and exergy consumption.  $\eta_{x1}$  leads to low entropy generation and  $\eta_{x2}$  leads to low specific exergy consumption according to the productive work. These proposed indexes can be useful to compare different plants and technologies, since they take all the energy supplies into account, their quality and the environmental conditions, in contrast to criteria based on energy analysis which only takes the thermal energy into account, special interest

Table 5  
Operational parameters optimized according to the criteria.

Criteria	$t_1$	$\dot{m}_1$	$t_3$	$\dot{m}_3$	$\dot{m}_4$
	(°C)	(m <sup>3</sup> /h)	(°C)	(m <sup>3</sup> /h)	(m <sup>3</sup> /h)
Nominal	66.5	43.2	25.0	24.0	8.0
$\dot{m}_{Dis}$	75	71.5	5.0	27.9	12.5
$\bar{E}_{Thermal}$	57.0	28.1	6.0	12.3	10.0
$\bar{X}$	57.4	31.7	35.0	16.4	12.5
$\eta_{x1}$	74.9	71.8	35.0	8.0	4.23
$\eta_{x2}$	73.2	31.6	34.4	14.4	10.8
A	58.1	32.4	34.8	16.4	12.5
B	73.4	59.1	5.7	25.5	12.5
C	75.0	49.5	34.2	18.4	12.5

deserves  $\eta_{x2}$  because it also considers the variations in water salinity.

## Nomenclature

$ch$	chemical potential
$con$	consumed
$dis$	distilled
$e$	internal energy
$E_{Thermal}$	specific thermal energy consumption
$feed$	feed flux
$h$	enthalpy
$\dot{m}$	mass variation
$\mu_n$	component chemical potential
$\eta$	performance
$n_n$	dissolution mass fraction
$PR$	performance ratio
$Pump$	pump system
$\dot{Q}$	heat flux
$q$	heat energy
$\dot{S}$	entropy variation
$s_n$	mass entropy
$SFWC$	specific flow water consumption
$S_g$	generated entropy
$T$	temperature
$\dot{U}$	system energy variation
$S_g$	generated entropy
$\dot{W}$	work flux
$x$	specific exergy
$\bar{X}$	specific exergy consumption
$\dot{X}$	exergy variation

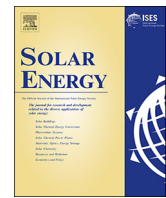
## Acknowledgements

This work has been funded by the National R + D + i Plan Project DPI2014-56364-C2-2-R of the Spanish Ministry of Economy and Competitiveness and ERDF funds.

## References

- [1] R. Connor, The United Nations World Water Development Report 2015: Water for a Sustainable World, vol. 1, UNESCO Publishing, 2015.
- [2] I.J. Esfahani, J. Rashidi, P. Ifaei, C. Yoo, Efficient thermal desalination technologies with renewable energy systems: a state-of-the-art review, Kor. J. Chem. Eng. 32 (4) (2016) 1–37, <http://dx.doi.org/10.1007/s11814-015-0296-3>.
- [3] M. Shatat, S.B. Riffat, Water desalination technologies utilizing conventional and renewable energy sources, Int. J. Low Carbon Technol. 9 (1) (2014) 1–19, <http://dx.doi.org/10.1093/ijlct/cts025>.
- [4] C. Li, Y. Goswami, E. Stefanakos, Solar assisted sea water desalination: a review, Renew. Sustain. Energy Rev. 19 (2013) 136–163, <http://dx.doi.org/10.1016/j.rser.2012.04.059>.
- [5] P. Palenzuela, A.S. Hassan, G. Zaragoza, D.C. Alarcón-Padilla, Steady state model for multi-effect distillation case study: plataforma solar de Almería MED pilot plant, Desalination. (1) 31–42, 10.1016/j.desal.2013.12.029.
- [6] P. Palenzuela, Evaluacion Del Acoplamiento De Plantas De Destilacion Multiefecto a Plantas Térmicas, CEMAT, Almería, 2013.
- [7] F. Al-Juwayhel, H. El-Dessouky, H. Ettonuey, Analysis of single-effect evaporator desalination systems combined with vapor compression heat pumps, Desalination 114 (3) (1997) 253–275, [http://dx.doi.org/10.1016/S0011-9164\(98\)00017-4](http://dx.doi.org/10.1016/S0011-9164(98)00017-4).
- [8] L. García-Rodríguez, C. Gómez-Camacho, Exergy analysis of the SOL-14 plant (Plataforma Solar de Almería, Spain), Desalination 137 (2001) 251–258, [http://dx.doi.org/10.1016/S0011-9164\(01\)00226-0](http://dx.doi.org/10.1016/S0011-9164(01)00226-0).
- [9] Y. Wang, N. Lior, Thermoeconomic analysis of a low-temperature multi-effect thermal desalination system coupled with an absorption heat pump, Energy 36 (6) (2011) 3878–3887, <http://dx.doi.org/10.1016/j.energy.2010.09.028>.
- [10] A. Altaee, A. Mabrouk, K. Bourouni, P. Palenzuela, Forward osmosis pretreatment of seawater to thermal desalination: high temperature FO-MSF/MED hybrid system, Desalination 339 (1) (2014) 18–25, <http://dx.doi.org/10.1016/j.desal.2014.02.006>.
- [11] M.W. Shahzad, M. Burhan, L. Ang, K.C. Ng, Energy-water-environment nexus underpinning future desalination sustainability, Desalination 413 (2017) 52–64, <http://dx.doi.org/10.1016/j.desal.2017.03.009>.
- [12] A. Al-Karaghoubi, L.L. Kazmerski, Energy consumption and water production cost of conventional and renewable-energy-powered desalination processes, Renew. Sustain. Energy Rev. 24 (2013) 343–356, <http://dx.doi.org/10.1016/j.rser.2012.12.064>.
- [13] G. Wall, M.E.I. Gong, On exergies, economics and desalination, Exergy Consultant (2013) 41.
- [14] M.H. Sharqawy, J.H. Lienhard V, S.M. Zubair, On exergy calculations of seawater with applications in desalination systems, Int. J. Therm. Sci. 50 (2) (2011) 187–196, <http://dx.doi.org/10.1016/j.ijthermalsci.2010.09.013>.
- [15] P. Fernández-Izquierdo, L. García-Rodríguez, D.C. Alarcón-Padilla, P. Palenzuela, I. Martín-Mateo, Experimental analysis of a multi-effect distillation unit operated out of nominal conditions, Desalination 284 (2012) 233–237, <http://dx.doi.org/10.1016/j.desal.2011.09.004>.
- [16] N.H. Aly, A.K. El-Fiqi, Thermal performance of seawater desalination systems, Desalination 158 (1–3) (2003) 127–142, [http://dx.doi.org/10.1016/S0011-9164\(03\)00443-0](http://dx.doi.org/10.1016/S0011-9164(03)00443-0).
- [17] R.K. Kamali, A. Abbassi, S.A. Sadough Vanini, M. Saffar Avval, Thermodynamic design and parametric study of MED-TVC, Desalination 222 (1–3) (2008) 596–604, <http://dx.doi.org/10.1016/j.desal.2007.01.120>.
- [18] R.K. Kamali, A. Abbassi, S.A. Sadough Vanini, A simulation model and parametric study of MED-TVC process, Desalination 235 (1–3) (2009) 340–351, <http://dx.doi.org/10.1016/j.desal.2008.01.019>.
- [19] A.O.B. Amer, Development and optimization of ME-TVC desalination system, Desalination 249 (3) (2009) 1315–1331, <http://dx.doi.org/10.1016/j.desal.2009.06.026>.
- [20] I. Janghorban Esfahani, A. Ataei, K.V. Shetty, T. Oh, J.H. Park, C. Yoo, Modeling and genetic algorithm-based multi-objective optimization of the MED-TVC desalination system, Desalination 292 (2012) 87–104, <http://dx.doi.org/10.1016/j.desal.2012.02.012>.
- [21] C. Frantz, B. Seifert, Thermal analysis of a multi effect distillation plant powered by a solar tower plant, Energy Procedia 69 (2015) 1928–1937, <http://dx.doi.org/10.1016/j.egypro.2015.03.190>.
- [22] P. Palenzuela, D.C. Alarcón-Padilla, G. Zaragoza, Experimental parametric analysis of a solar pilot-scale multi-effect distillation plant, Desalin. Water Treat. 57 (48–49) (2016) 23097–23109, <http://dx.doi.org/10.1080/19443994.2016.1180481>.
- [23] H.S. Choi, T.J. Lee, Y.G. Kim, S.L. Song, Performance improvement of multiple-effect distiller with thermal vapor compression system by exergy analysis, Desalination 182 (1–3) (2005) 239–249, <http://dx.doi.org/10.1016/j.desal.2005.03.018>.
- [24] I. Janghorban Esfahani, S. Lee, C. Yoo, Evaluation and optimization of a multi-effect evaporation-absorption heat pump desalination based conventional and advanced exergy and exergoeconomic analyses, Desalination 359 (2015) 92–107, <http://dx.doi.org/10.1016/j.desal.2014.12.030>.
- [25] A. Piacentino, Application of advanced thermodynamics, thermoeconomics and exergy costing to a multiple effect distillation plant: in-depth analysis of cost formation process, Desalination 371 (2015) 88–103, <http://dx.doi.org/10.1016/j.desal.2015.06.008>.
- [26] D.C. Alarcón-Padilla, L. García-Rodríguez, J. Blanco-Gálvez, Assessment of an absorption heat pump coupled to a multi-effect distillation unit within AQUASOL project, Desalination 212 (1–3) (2007) 303–310, <http://dx.doi.org/10.1016/j.desal.2006.10.015>.
- [27] A. de la Calle, J. Bonilla, L. Roca, P. Palenzuela, Dynamic modeling and simulation of a solar-assisted multi-effect distillation plant, Desalination 357 (2015) 65–76, <http://dx.doi.org/10.1016/j.desal.2014.11.008>.
- [28] P. Fritzson, Principles of Object-Oriented Modeling and Simulation with Modelica 3.3: A Cyber-Physical Approach, John Wiley & Sons, 2014.
- [29] S. Rajagopalan, V.V. Sastry, V. Ajjarapu, S.S. Venkata, Object-oriented measurement templates for power electronics education and research using DYMOLA (dynamic modeling laboratory), Annual Workshop on Computers in Power Electronics, (2000), pp. 166–171, <http://dx.doi.org/10.1109/CIEPE.2000.904710>.
- [30] D. Brück, H. Elmqvist, H. Olsson, S. Mattsson, Dymola for multi-engineering modeling and simulation, 2n'd, Int. Modelica Conf. 6 (2002) 0–8.
- [31] L.R. Petzold, A description of DASSL: a differential/algebraic system solver, Sci. Comput. (1983) 65–68.
- [32] IAPWS, Release on the IAPWS Industrial Formulation 1997 for the Thermodynamic Properties of Water and Steam, (Sep. 2007).
- [33] R. Gomri, Energy and exergy analyses of seawater desalination system integrated in a solar heat transformer, Desalination 249 (1) (2009) 188–196, <http://dx.doi.org/10.1016/j.desal.2009.01.021>.
- [34] K.R. Ranjan, S.C. Kaushik, Energy, exergy and thermo-economic analysis of solar distillation systems: a review, Renew. Sustain. Energy Rev. 27 (2013) 709–723, <http://dx.doi.org/10.1016/j.rser.2013.07.025>.
- [35] A. Valero, M.A. Lozano, Los Balances De Energía, Entroí, Exergía Y Energía Libre: Métodos Para El Diagnóstico De Instalaciones Industriales, no. (218), Ingeniería química, Alción, 1987.
- [36] K.S. Spiegler, Y.M. El-Sayed, The energetics of desalination processes, Desalination 134 (1–3) (2001) 109–128, [http://dx.doi.org/10.1016/S0011-9164\(01\)00121-7](http://dx.doi.org/10.1016/S0011-9164(01)00121-7).
- [37] A. Pfeiffer, Optimization Library for Interactive Multi-Criteria Optimization Tasks, Proc. 9th International Modelica Conference, Munich, Germany, 2012, pp. 669–680.

**A.3. New low-cost solar tracking system  
based on open source hardware for  
educational purposes**



## New low-cost solar tracking system based on open source hardware for educational purposes

Jose A. Carballo<sup>b,c,\*</sup>, Javier Bonilla<sup>a,b</sup>, Lidia Roca<sup>a,b</sup>, Manuel Berenguel<sup>b,c</sup>

<sup>a</sup> CIEMAT-Plataforma Solar de Almería, Ctra. de Senés s/n, Tabernas, 04200 Almería, Spain

<sup>b</sup> CIESOL Research Centre for Solar Energy, UAL-PSA.CIEMAT Joint Centre, Almería, Spain

<sup>c</sup> University of Almería, Ctra. Sacramento s/n, Almería 04120, Spain



### ARTICLE INFO

#### Keywords:

Solar energy  
Solar tracker  
Automatic control and computer sciences  
Computer vision  
Low cost  
Raspberry pi  
Educational tool  
Open source

### ABSTRACT

In this paper, due to the detected educational demands regarding automatic control and training in management of solar tracker systems, a small prototype based on low cost open source hardware and computer vision is built to test the control algorithms developed in Mathematica and Simulink. The new prototype has been developed with the aim of being a powerful tool for a wide range of applications regarding to the learning of automatic in solar energy. Finally, its educational application is discussed.

### 1. Introduction

Energy plays an essential role in the development of society, it has promoted great advances and has also generated inequalities and conflicts throughout history (Smil, 2010). In the last decades, due to industrial evolution and population growth, world's energy demand has been continuously increasing (Melorose et al., 2015).

Nowadays, different energy forms are consumed, electricity which is the most demanded is not a natural energy form and must be obtained from other energy sources. It is estimated that 77.9% of electricity is generated by traditional methods (fossil and nuclear) (Schou, 2000), which are heavily polluting the environment and contributing to the climate change and global warming (Kannan and Vakeesan, 2016). The continuous use of fossil energy sources may lead to climate change, which may in turn end up with heavy natural disasters (Schou, 2000).

Therefore it is crucial to go for ecofriendly energy sources, even more when the development carried out in different renewable energies sources (solar, wind, hydropower and geothermal) makes them viable sources of energy, even in places rich in fuel reserves. Recent studies (Scheer, 2013; Hohmeyer and Bohm, 2015; Jacobson et al., 2015) indicate that 100% of renewable electricity and energy in general supply can be achieved in the top industrialized countries, how the transition should be and its economic, environmental and social benefits. These studies include all renewable energy sources to provide energy and

propose an energy mix.

The transition to 100% of renewable supply demands a global agreement to focus the education on renewable energies (Broman, 1992). Although the need for this, education for suitable development at all levels is globally recognized (Kandpal and Broman, 2014), an extended review shows that the situation of the renewable energy educational practices is not satisfactory because it is not as developed as it should be (Ciriminna et al., 2016).

It is vital for the success of new renewable energy education programmes to use modern educational technology, accessible and low cost (Kandpal and Broman, 2014), which facilitates the integration with the emerging smart world (Liu et al., 2017). In the last decade, different educational paradigms had made use of flexible and modern educational technology (Jennings, 2009) like on-line educational programs, due to the urgent need for on-the-job training in renewable energies and to reach a wider audience. Educational tools based on videocast techniques (Torres-Ramírez et al., 2014) and virtual and/or remote labs have proven to be powerful tools with lot of benefits (Fabregas et al., 2011; Chao et al., 2015), great scientific impact (Heradio et al., 2016) and able to extend the access to science and engineering (Colwell et al., 2002).

Of all renewable energies, solar energy is the most abundant energy source (Panwar et al., 2011), it is inexhaustible and exceeds output efficiencies given by other energy sources, it does not have any negative

\* Corresponding author.

E-mail addresses: [jcarballo@psa.es](mailto:jcarballo@psa.es) (J.A. Carballo), [javier.bonilla@psa.es](mailto:javier.bonilla@psa.es) (J. Bonilla), [lidia.roca@psa.es](mailto:lidia.roca@psa.es) (L. Roca), [beren@ual.es](mailto:beren@ual.es) (M. Berenguel).

impact on the ecosystem and can help us to mitigate inequalities due to traditional energy sources.

The amount of scientific production (Sheikh et al., 2016) demonstrates that the solar energy is in demand, its use is growing and many researchers are undertaking investigations in order to increase efficiency and reduce cost (Kannan and Vakeesan, 2016). There are different technologies based on solar energy that improve the efficiency of the system by means of concentrating the solar flux with optical systems that demand a solar tracking system to control the system alignment with the Sun, becoming the solar tracking a key issue for the general system efficiency.

Despite the increasing interest and the educational demands in solar energy, there are few educational tools related to it. In solar photovoltaic technology some educational tools can be found, the most interesting ones being: photovoltaic solar cell remote trigger virtual lab (Freeman et al., 2012), e-training system for the renewable energy systems (Drigas et al., 2005), experimental determination of the current-voltage characteristic curve of a photovoltaic panel (Kandpal and Broman, 2014) and web based education resources for self-education in renewable energies (Bauer et al., 2013). Regarding to low and medium temperature solar systems, HTI e-learning laboratory (Michaelides et al., 2005), mobile remote lab system to monitor in situ thermal solar installations (Saez de Arregui et al., 2013) and an interactive tool to teach solar parabolic trough concepts (Silva et al., 2011) are available. It is necessary to increase the number of these resources and make them generally available.

With the aim of providing a powerful tool for solar educational purposes and specifically for solar tracking fields, reducing fixed costs associated with traditional labs and control system, a new solar tracking system based on computer vision (CV) implemented in low cost open source hardware has been developed and its main features are explained in the next sections. Also, the code has been published for free use ([GitLab](#), 2018).

## 2. Solar energy

### 2.1. Solar concentration technology

Renewable energies can be classified into categories such as wind power, solar energy, geothermal energy, ocean energy, hydro power, biomass and waste energy (Guney, 2016), although most of the energy sources on Earth are indirect solar energy kinds.

Solar energy technologies are those which employ directly the solar flux that reaches the solar system in three different ways: thermally (*heat engine or process heating*), photo chemically (*photosynthesis*) and photo physically (*photovoltaic*), to produce heat, chemical energy and electricity respectively in a collecting element (*receiver*). To increase the performance of the solar energy systems it is usual to previously concentrate the solar flux that reaches the solar system receiver to achieve higher peak temperatures and solar flux densities, improving thermodynamic efficiencies and reducing the heat loss area in relation to the receiver area (Khan and Arsalan, 2016).

This task is carried on by *solar concentrator systems*, that usually use mirrors (parabolic trough, heliostat, dish, or linear Fresnel) or lenses to

concentrate and reflect the solar flux on the receiver, see Fig. 1. Two main types of solar concentration technologies can be found: concentrated solar thermal power (*CSP*) and concentrated photovoltaic (*CPV*). In *CSP* the concentrated solar flux heats water or any other kind of heat transfer fluid flowing through the receiver. Usually *CSP* facilities produce high temperature heat, that can be used directly in a process (process heat) or to produce steam to spin turbines and generate electricity. On the other hand, *CPV* uses the concentrated solar radiation onto small photovoltaic cells that are made by specialized semiconductor materials. In these systems, each cell transforms the concentrated solar flux into electricity directly with a power-generating efficiency of more than 30%. Recently, the research advances have achieved the combination of the two technologies, *CPV* with *CSP*, which is called *concentrated photovoltaic thermal (CPVT)*. Studies show the very high potential of the *CPVT* technology due their unique features (Sharaf and Orhan, 2015a,b).

### 2.2. Solar tracking

As commented before, solar energy technologies take advantage of the solar flux to produce another type of energy, therefore knowing the availability and the nature of the source of energy is a key issue. The Earth is in a constant rotation, so the relative position of the Sun in the sky continuously changes but can be defined by means of *solar position algorithms* or optically, with enough precision. Most of the solar concentrators demand a mechanism that controls the systems alignment with the Sun (*solar tracker*), being this a key issue for the general system efficiency.

Solar trackers can be classified regarding the number and position of rotation axes. Systems with one rotation axis are employed with solar concentration systems like parabolic troughs or linear Fresnel, called linear concentrator systems. Horizontal, vertical and tilted-axis systems can be found as subcategories. On the other hand, systems with two rotation axes, called point-focus systems, are employed with heliostats and dish modules. Azimuth-elevation, target aligned and polar trackers can be found as subcategories depending on the rotation axes position.

Solar trackers can also be classified regarding to the control type as passive and active solar trackers. Passive solar trackers are composed by a couple of actuators working against each other, which are based on thermal expansion. Due to the different solar radiation conditions, these trackers orient the system in the direction where the radiation over both actuators is the same (Mousazadeh et al., 2009). Active trackers can be classified in microprocessor and electro-optical sensor based, PC controlled date and time based, auxiliary bi-facial solar cell based and a combination of these three systems (Mousazadeh et al., 2009). Sun trackers can guide the system with continuous or discrete movement depending on the rotation system and the controller. Most Sun tracker systems are developed for a specific solar technology.

Regarding control for active solar trackers, both closed-loop and open-loop controllers can be found. Closed-loop controllers of solar trackers are based on feedback transferred from sensors which measure environmental variables. On the other hand, an open-loop controller, estimates its inputs using only the current state and a computer algorithm, to determine if its inputs have achieved the desired goal without

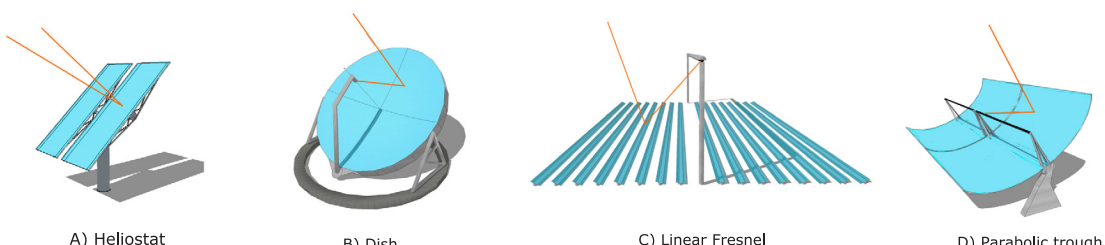


Fig. 1. Solar concentrator systems.

using feedback. This one is simpler than the closed-loop controller but it cannot correct any disturbances in the system (Lee et al., 2009).

Some errors linked to the geometry of the system and the movement are known as, *aiming offset* and *Sun tracking offset*, respectively. The first one is related to constant aberrations such as pedestal tilt errors, bad reference of the sensors, the second one is related to the type of movement, controller and tracker resolution in general.

With respect to active control solar trackers, computes controlled based on date and time computes the solar position according to solar equations that need time and location as inputs. The accuracy of this system is very conditioned by constant aberrations. On the other hand, bi-facial solar cell and electro-optical sensor systems are time and location independent, although most solar trackers based on these sensors are only able to obtain the relative solar position and control solar systems when the system optical axis is aligned with the Sun vector (Dish modules or PV trackers). For example, El Kadmiri et al. (2015) developed a solar tracker based on omnidirectional computer vision able to extract accurate information about the Sun position and Ruelas et al. (2017) developed a system based on a video processing sensor able to determine the Sun position. An exception is the tracking system based on CV capable of recognizing the Sun and the target to generate the feedback for a closed-loop control (Pfahl et al., 2017), although no implementation is known. The accuracy of these systems is mostly influenced by the controller and sensor resolution.

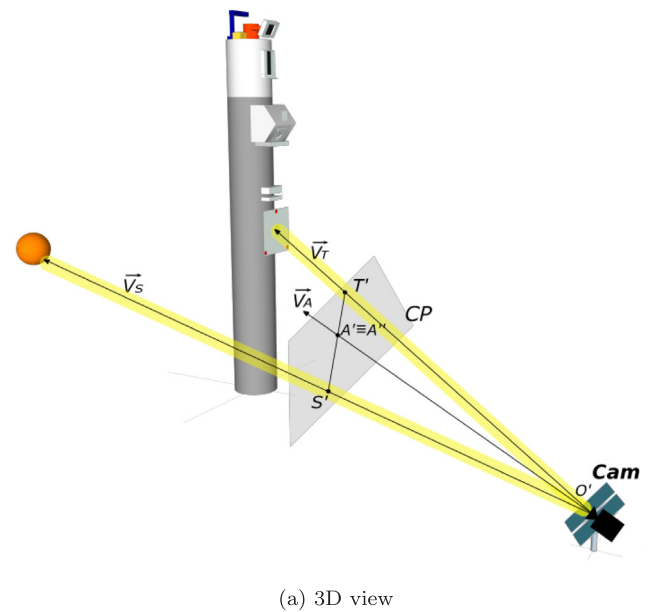
In the literature there are reviews about solar tracking systems (Mousazadeh et al., 2009; Lee et al., 2009; Prinsloo and Dobson, 2015), one and two axes tracking systems with open-loop, closed-loop, control based on continuous movements, maximum beam, electro-optical sensors, bi-facial cells, solar equations or a hybrid. In spite of this great variety, there are no indications about the existence of any solar tracking system able to be adapted to any solar technology, location and time independent. In this work a new solar trackers is proposed, with the main objective of developing a unique educational tool to understand solar tracking problems regardless of solar technology. The proposed system is able to detect the position of the Sun and the receiver, also it is time and location independent.

### 3. Computer vision solar tracking system proposal

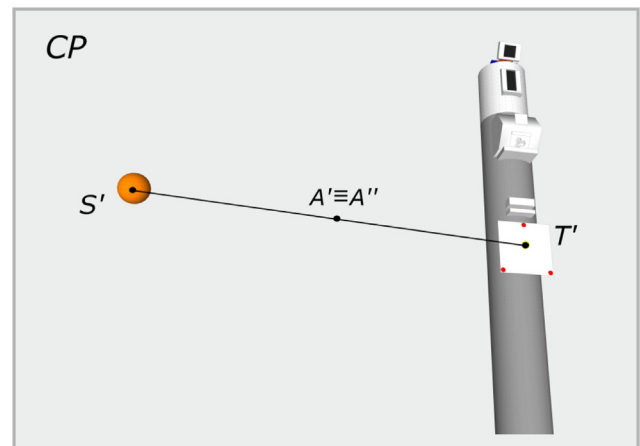
#### 3.1. Control based on computer vision

The new solar tracking system proposed uses a new concept for tracking systems based on CV, able to reduce costs, adaptable to any solar technology and implemented in open source hardware platform. CV is a well known technique used in CSP, for example in the measurement of the solar flux distribution (Ballestrín and Monterreal, 2004), the surface characterization by photogrammetry of solar concentrator systems (Fernández-Reche and Valenzuela, 2012; Blázquez et al., 2015) or automatic heliostat positioning for offset correction (Berenguel et al., 2004). As mentioned before, Sun tracking systems control the solar system alignment with the Sun and the receiver. Based on this objective, the key concept of this approach is the recognition of the optical axis of the solar concentrator system by a camera arranged in the concentrator rotation point/axis whose optical axis is aligned with the concentrator axis. Sun and target relative positions are identified through an analysis of the image, where certain patterns are looked for. The input of the automatic controller is computed in this way.

For example, in central receiver tower plants (see Fig. 2), that are one of the most complex solar tracking system, the optical axis of the heliostat ( $\vec{V}_A$ ) should be the bisector of the angle composed by the solar vector ( $\vec{V}_S$ ) and the target vector ( $\vec{V}_T$ ), being the target the point where the concentrated solar radiation has to aim at. These three vectors intersect the plane  $CP$  perpendicular to  $\vec{V}_A$  in  $A'$ ,  $S'$  and  $T'$ . This fact allows us to simplify a problem in 3 dimensions to 2 dimensions.



(a) 3D view



(b) Camera 2D view

Fig. 2. CSP tower system scheme in tracking.

An heliostat is correctly aligned (Fig. 2), with the Sun and the receiver (target), when the three points form a straight line in which  $A'$  is in the middle of the segment  $\overline{AS'}(A'')$ , otherwise the heliostat is not correctly aligned (Fig. 3). The representation of  $CP$ , which may have some imperfections such as optical deformations, can be obtained with a fish eye camera whose optical axis is aligned with the optical axis of the heliostat ( $\vec{V}_A$ ) and located in the heliostat rotation center ( $O'$ ). The center of the image corresponds to  $A'$ , and using image processing techniques  $S'$  and  $T'$  can be detected in this image, thus obtaining in this way the control set point. This approach can be employed for any solar technology like CCP, CPVT, tower, linear Fresnel or dish systems (Carballo et al., 2018).

In order to facilitate the detection of the target, the position of this has been marked by three red LED lights (Fig. 2). Therefore, in this proposal  $S'$  and  $T'$  are detected looking for the centroid of the largest region with the brightest pixels (Sun) and the centroid of the three brightest red pixels regions (target) in the image acquired respectively. The image color representation takes a relevant role in the detection of  $S'$  and  $T'$ , although the combination of Red-Green-Blue (RGB) is usually used, it is not suitable for this application because color levels are affected by the bright level. On the other hand, HSL color representation defines a color model in terms of saturation (the amount of chroma), its

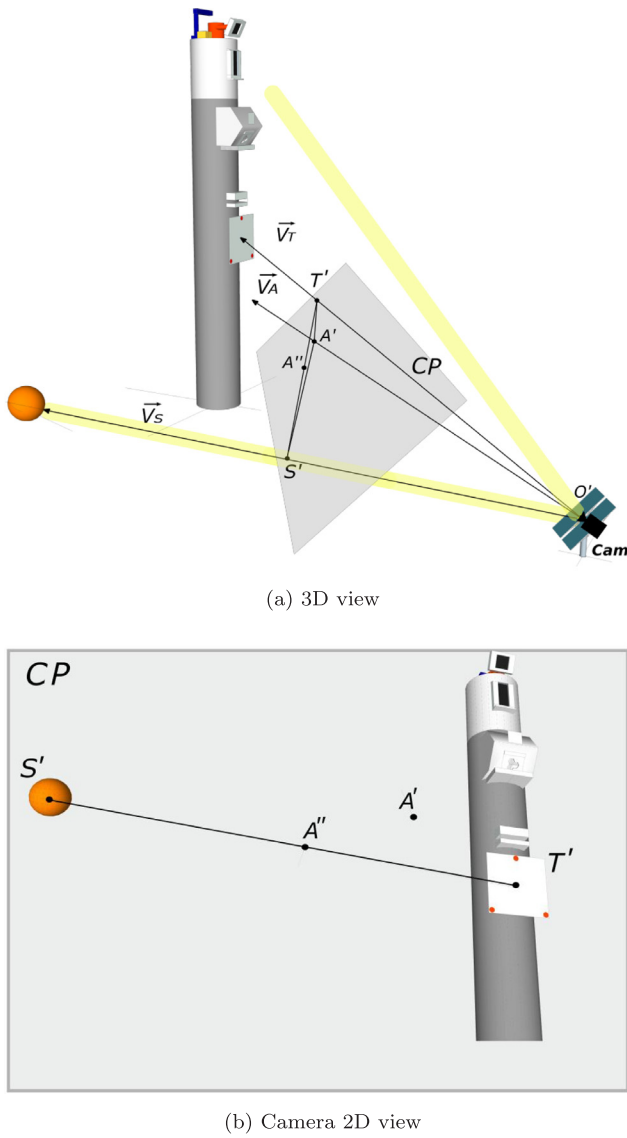


**Fig. 3.** CSP tower system scheme out of tracking.

constituent components HUE (the angle on the color wheel) and lightness (how bright the color is). In this color representation, brightness can be separated to make colors more independent of the light intensity and thus improving the recognition of the objects (Lee et al., 2013). For this reason, the HSL color system is employed.

As can be observed in the algorithm flowchart (see Fig. 4), the image is taken and processed every 0.1 s, if  $S'$  and  $T'$  have been found, the set point is computed and compared to the point  $A'$  (the center of the image with aiming corrections), thus obtaining the offset, otherwise the offset is set to zero. If the selected control is manual, the user can introduce an offset value, which will be an input to PI controller (Moliner and Tanda, 2016).

### 3.2. Matlab-simulink implementation

The control algorithm has been implemented in *Matlab-Simulink* add-on for *Raspberry Pi* (MATLAB, 2017). *Matlab-Simulink* is a commonly used tool in the science and education field. The main scheme (see Fig. 5) is composed by three blocks: parameters configuration (green), image processing and point detection (red), movement control (blue). In the first block, parameters that will be employed in the following tasks, such as hue and light levels ( $L, L_1, H, S$ ), controller dead

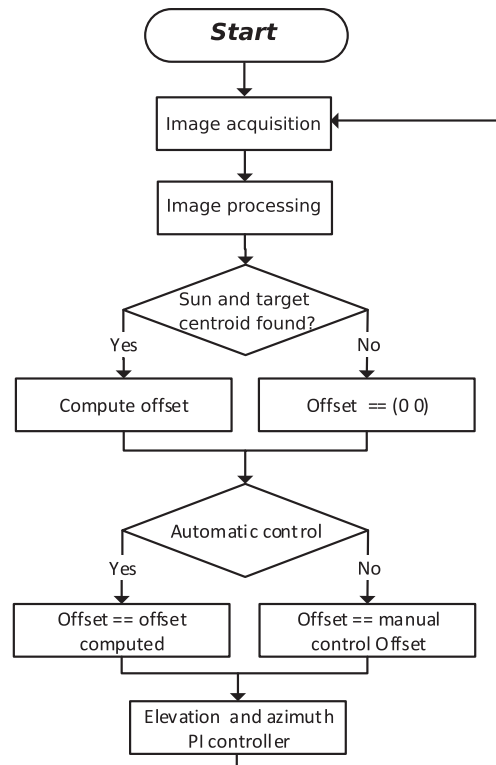


**Fig. 4.** Flowchart.

zone (signal error band where the output is zero  $X_{offsetT}, Y_{offsetT}$ ) or aiming point error correction ( $X_{offsetA}, Y_{offsetA}$ ) are defined manually, also image acquisition is performed, control type is selected and manual offset is configured. Image acquisition is carried out and immediately it is segmented obtaining two binary matrices in which the regions in the picture, that meet the conditions set by the parameter configuration, are represented as 1 in the binary matrix.

In the second block, two blob analysis blocks are employed to calculate statistics for regions in the binary images, providing the coordinates of the regions that meet the criteria of brightness and color. *Sun Selection* and *Target Selection* blocks select the coordinates of the largest region with brightest pixels and the centroid of the brightest red pixels regions, obtaining in this way the Sun and target pixel position coordinates ( $S'$  and  $T'$ ) respectively. The output of the block called *AimingPoint* is compared with  $A'$ , computed as the center of the image and adjusted by  $X_{offsetA}$  and  $Y_{offsetA}$ , obtaining the input signal to the controller in pixels, called *Offset*. In the last main block, responsible for the azimuth and elevation movements, whose outputs values represent the percentage of the pulse period that the tracker motor is on and the direction of rotation, in both controllers, the lower and upper saturation limit outputs have been established in -1 and 1 respectively. Also, an external reset has been included that resets the integrator when the offset is null or the control is set in manual mode. Then, a dynamic dead zone has been implemented according to industrial systems, thanks to which if the controller output is lower than 1% it will have no effect.

### 3.3. Mathematica implementation

With the same philosophy that *Matlab-Simulink* implementation, the control system has been implemented in *Mathematica* (2017), which is a commonly used tool in the science and education field. The implementation is based on the same previous functions and scheme, but in this case a very easy to use graphical user interface (*GUI*) has been also developed (see Fig. 6).

The *GUI* allows us to modify all the parameters described above,

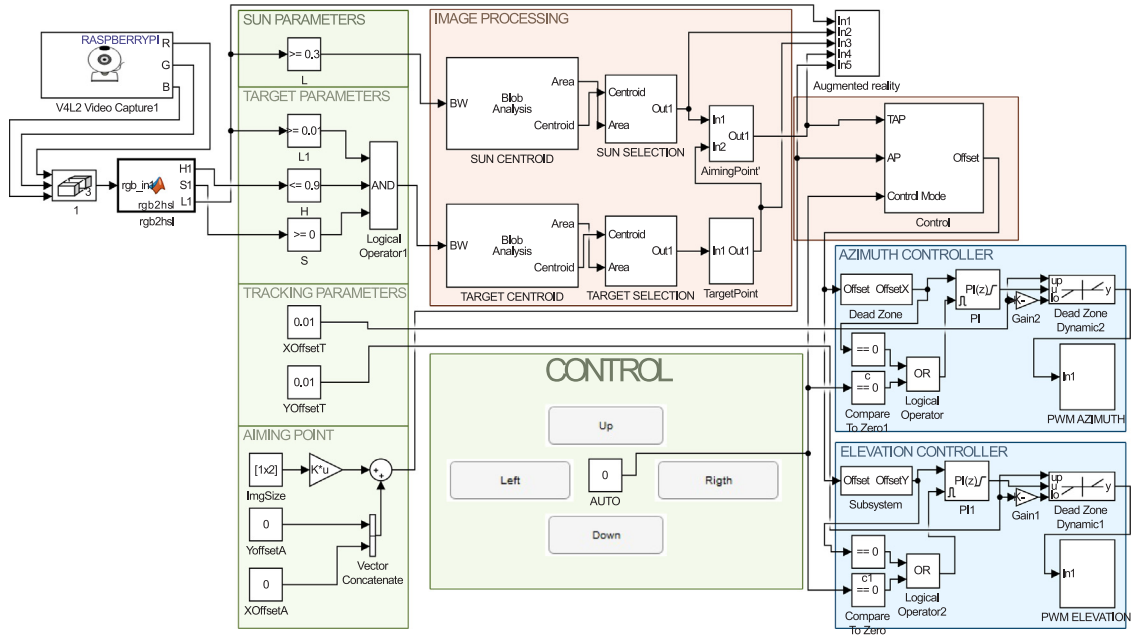


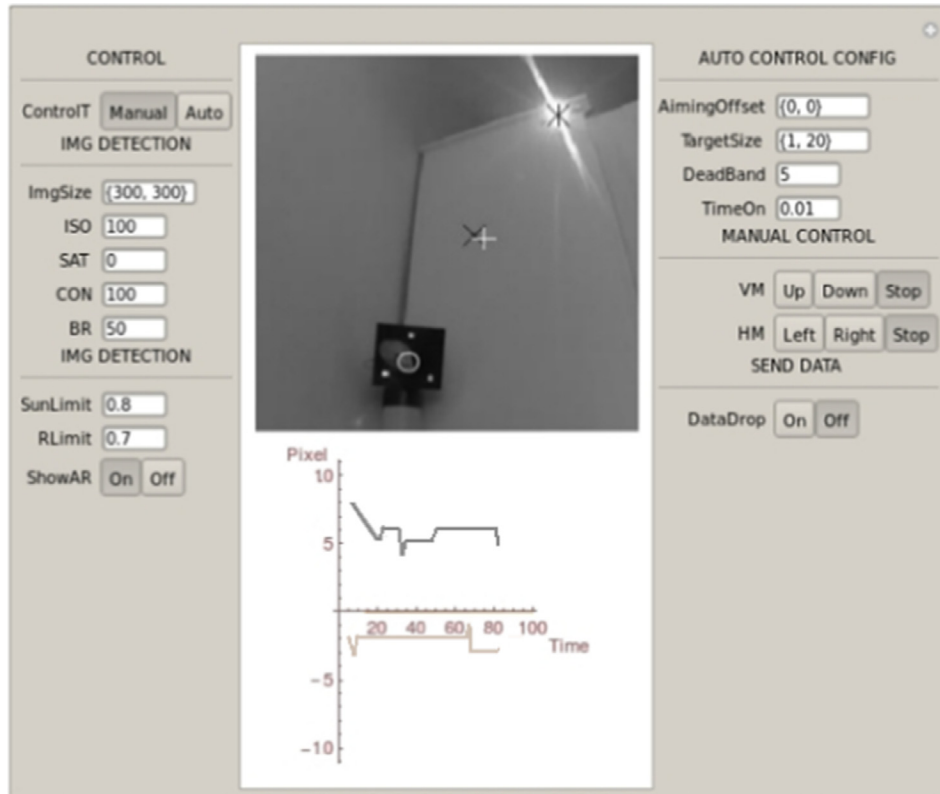
Fig. 5. Simulink scheme.

also it allows to send all the data to *Wolfram Data Drop*. This is a open service that makes it easy to accumulate data of any kind, from anywhere setting it up for immediate computation, visualization, analysis, querying, or other operations. This functionality further enhances the virtual laboratory character of the proposed system. The *GUI* shows an augmented reality image with  $S'$ ,  $T'$  and  $A'$  represented as black star, white circumference and black  $x$  respectively. Also the ideal aiming point as white cross and a graph with the errors measured in pixels and the simulation time, are represented. This implementation allows us to

access the hardware remotely through an Internet connection.

### 3.4. Hardware and prototype

The prototype (see Fig. 7), is assembled with a *Raspberry Pi 3*, a *Pi Cam*, a PWM electronic control and a relay module, all of them open source low cost hardware. *Pi Cam* is a CMOS camera with 5 Megapixels, pixel size  $1.4 \times 1.4$  micrometers, aperture  $2.35f$  and  $160^\circ$  field of view thanks to the wide-angle lens. Azimuth and elevation movements are

Fig. 6. Mathematica control *GUI* running on *Raspberry Pi 3*.

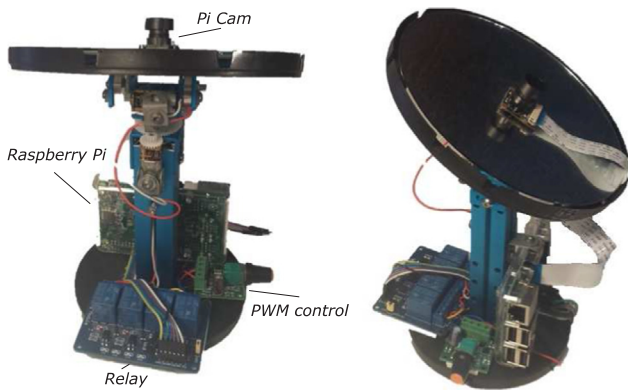


Fig. 7. Prototype.

carried out by two direct current (*DC*) motors that are provided with a reduction box.

In the wiring diagram, showed in Fig. 8, two electric diagrams can be differentiated, the relay module is the physical link although both are electrically separated. The *Raspberry Pi 3* is connected to the *Pi Cam* by the *CSI* port and to the input control relay module by a *GPIO* (general purpose input/output) port. On the other hand, the electronic *PWM* control feeds the power input of the relay board that connect or disconnect the motors in one direction or another. The relay module is composed by four relays that have been connected forming two *H* bridges. This configuration allows feeding the control and the motor systems with different sources, preventing problems in the quality of the supply and making it more flexible regarding the motor that the system can employ.

A large number of commercial and proprietary hardware implementations of tracking systems are available (*SolarTrack*, *SunTrack*, *Siemens SPA*, *Beckhoff TwinCAT*, *Lab-VIEW Solar*, *ABB Solar Tracker*, *SolTrk...*) and some open hardware implementations can also be found (*Solar Tracking with Arduino*, *Solar Tracking with Telescope or Satellite Tracking Hardware...*), but the proposed design is new since it is a low-cost open source hardware platform able to implement *CV* and to control any solar tracking system.

The control algorithm has been implemented in the *Raspberry Pi* hardware platform (Upton and Halfacree, 2014; University, 2016).

*Raspberry Pi* platform is an open source hardware whose main objective is providing low-cost, high-performance computers. This platform connects physical and virtual lab portals, which makes it an ideal choice for control education purposes (Sobota et al., 2013) and can solve several problems that remote labs present (Prada et al., 2015).

The *Raspberry Pi 3* used to develop the present work, is a fully featured credit-card sized computer, low cost, which allows running applications. The device contains a 1.2 GHz 64-bit quad-core ARMv8 CPU, onboard memory 1 GB RAM, Full HDMI port, Ethernet port, WiFi, Bluetooth Low Energy, wireless lan, 40 pin *GPIO*, *DSI* and *CSI* ports. It is considered a universal programmable control unit with Internet connectivity, data storage and enough memory and computational power.

WiFi connectivity helps connecting the system directly to an internal or external communication network making the integration in virtual labs portals easier, furthermore reducing the wiring costs (Romero et al., 2002) and can be a useful tool to study and develop autonomous heliostats (Pfahl et al., 2013; García et al., 2004) or wireless sensor network. Note that among all hardware features, one of the most powerful tool for control is the *GPIO* port, which is a physical interface. The input pins can be programmed and the input can come from a sensor or a signal, in the same way that output pins can be programmed as signal to other devices or just as a switch.

The cost of whole prototype hardware is less than \$90 (*Raspberry Pi 3 with pi cam* \$70, other small hardware less than \$20). The remaining costs are less than \$50 so total cost of the prototype is less than \$140. Compared with industrial hardware, the prototype hardware cost is lower while being fully functional and adding more capabilities. For example, nowadays in solar industry the cost of the electronic devices responsible of the control and solar tracking (processors, encoders, limit switches, etc.), as well as any other relatively low fixed costs per heliostat for other components (junction boxes, connectors, etc.), remain constant at \$1000–3000 although the solar system size changes (Blackmon, 2013; Kolb et al., 2007). Note that the optimum heliostat surface varies according to the manufacturers is higher than 20 and lower than 150 m<sup>2</sup>, although most studies estimate a cost optimum in the range of 50 m<sup>2</sup> (Pfahl et al., 2017; Coventry et al., 2016).

For example, particularly for the ATS (Advanced Thermal Systems Inc) 150 m<sup>2</sup> heliostat, drive motors and limit switches cost is 1.78 \$/m<sup>2</sup>, hardware control 1.90 \$/m<sup>2</sup>, wiring 7.40 \$/m<sup>2</sup>, for a total of \$"1640. From this point of view, the system proposed allows reducing, in the

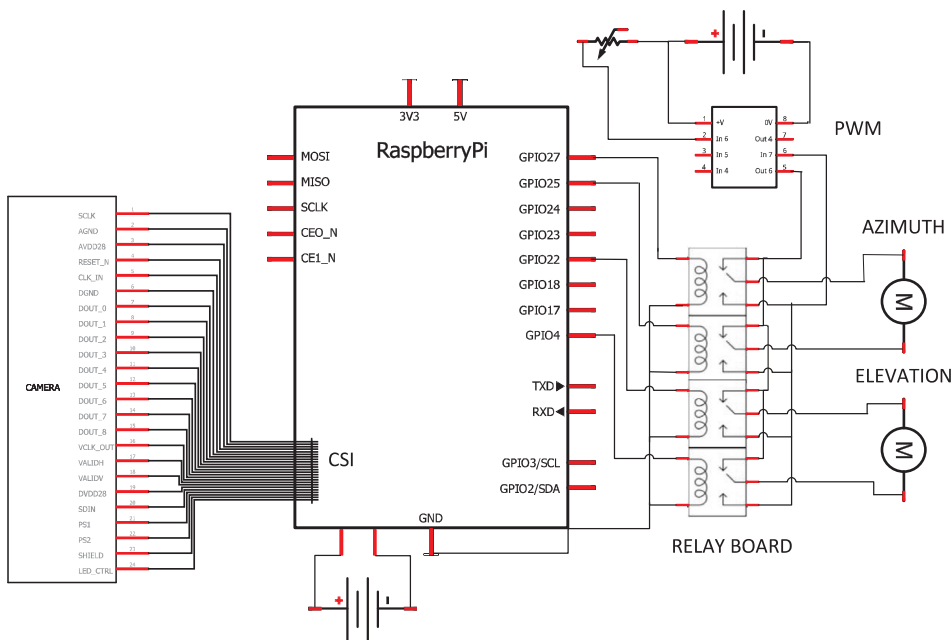


Fig. 8. Electric scheme.

first instance, the fixed cost of the hardware control from \$"290 to less than \$"75, furthermore reducing costs removing limit switches, GPS or encoders that are not required and makes the system more flexible and easier to use, to manufacture and to install. The fixed cost reduction is even more important for smaller heliostats, because in these cases fixed costs represent higher percentages of the total cost of the system.

Furthermore the use of low cost hardware enables low cost replacement, also the popularity of the hardware platform offers a lot of hardware extensions, generally low cost, which may improve the prototype. From an industrial point of view, fixed cost reduction promotes direct savings and also enables the reduction of the optimal heliostat area. This last fact also causes an additional cost reduction regarding to the structure cost and its dependence on imposed loads (Blackmon, 2013). Note that this brief cost reduction analysis is based on the proposed hardware, which is not an industrial hardware and its response to this specific use is unknown.

For all this, the low cost solution proposed is presented as a good alternative for labs with educational and scientific purposes whose main problems are usually the space and the funds for their establishment, assistance to maintenance and operation (Kandpal and Broman, 2014).

#### 4. Operating examples

The current configuration allows connecting the prototype via WiFi or LAN to a communication network through which the algorithm can be uploaded to the device and the information exchanged. At low level, users can act on the motors and move the solar concentrator in manual mode through the laptop. At medium level, users can modify parameters related with CV, working with image processing techniques. Also, automatic control allows working with PI controller parameters that can be modified to test new controllers and to understand the dynamic characteristics of the system. Advanced level users can completely modify the algorithm introducing new approaches to control, new image processing techniques and new outputs.

The control problem for this example is to keep the heliostat aligned despite the movement of the Sun and other disturbances with the smaller number of movements and as accurate as possible. Also, a small threshold offset, where no action is taken (dead zone), must be defined to avoid the constant movement of the heliostat due to small errors without relevance. For that, according to the offset signal measured in pixels, a control signal for the PWM block, that controls the active time of the motor in each sample time, should be generated. Furthermore, main issues in solar tracking control systems like dead zone, aiming offset and manual control have been considered. The PI controller parameters have been manually tuned with the aim of generating different answers in elevation and azimuth, to show the prototype capabilities.

In an initial instant, the prototype captures and processes the AR

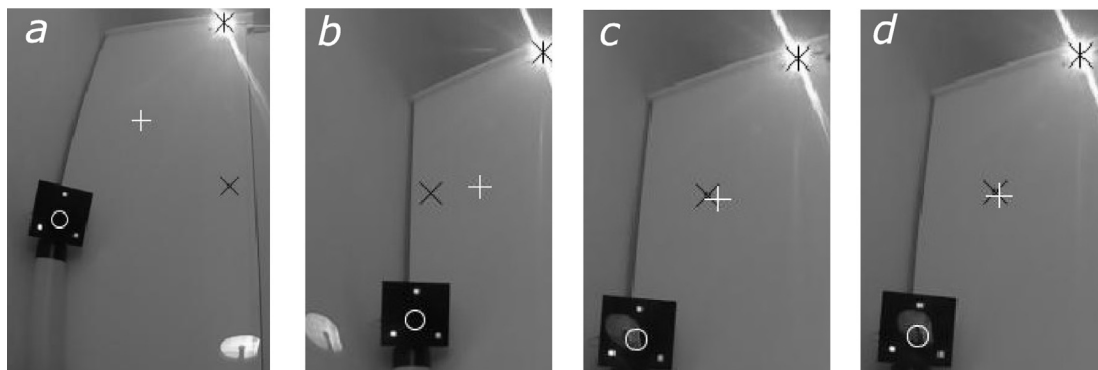


**Fig. 9.** Augmented reality image sequence. Simulated Sun center (black star), target (white circle), Midpoint between the simulated Sun and the target (white cross), heliostat aiming point (black cross).

image shown in Fig. 9a, where the midpoint (white cross) between the simulated Sun (black star) and the target (black square) is far from the heliostat aiming point (black cross) therefore concentrated solar radiation is reflected outside the area delimited by the three red dots in the target (white in the image), whose center is represented by a white circle. Then, the azimuth and elevation controllers act over the system and after a couple of oscillations in azimuth, the control system manage to focus the concentrated radiation over the target center, see Fig. 9d, so the mid point and heliostat aiming point positions match each other.

Also, this example is represented in Fig. 10, the initial instant elevation and azimuth offset, represented as a percentage of the total offset, are not zero so the controller generates two different control signals due to the different PI parameters employed and the different offset signal. The two PI is in a decoupled scheme, although this design could be modified. As shown in figure Fig. 10, the elevation controller is faster and generates fewer oscillations than the azimuth controller. The value of the controller output is equivalent to the pulse width in the sample time, controlling in this way the speed of movement. Note that the dead zone effect over the system introduces a systematic error in steady state, reduces the number of movements and makes the system more stable when the offset signal is low. In this example the  $XOffsetT$  and  $YOffsetT$  have been configured as 1%, which is approximately one pixel.

Regarding accuracy, notice that the resolution of the *Pi Cam* and the distance between the cam and the receiver (slant range,  $|\vec{V}_t|$ ) determines the minimum uncertainty of the system. Angular ( $\theta$ ) and linear ( $\varepsilon$ ) uncertainty measured in a plane perpendicular to the vector formed by the *Pi Cam* and the target point, see Fig. 11, can be expressed as follows:

$$\tan\left(\frac{\theta}{2}\right) = \frac{P/2}{f}. \quad (1)$$

$$\varepsilon = 2\left(\tan\left(\frac{\theta}{2}\right) \cdot SR\right). \quad (2)$$

In Eq. (1),  $P$  represents the pixel size and  $f$  the *Pi Cam* focal aperture, for the operating example the slant range was 1 m, so the angular and lineal uncertainties of the system determining  $S'$  was 0.6 mrad and 0.6 mm respectively.  $T'$  is computed as the centroid of three points, therefore the angular and lineal uncertainty of  $T'$  is 1.8 mrad and 1.8 mm respectively. Finally,  $A'$  is computed according to the difference between the pixel coordinates of  $T'$  and  $S'$ , so the uncertainty associated with  $A'$  in this conditions is 2 mrad and 2 mm.

These values are more than enough for the proposed use, although simply replacing the camera for other with a higher  $f$  or lower  $P$  (higher resolution) should reduce these values. For example, a camera with the same  $f$ , the same sensor size and higher resolution has a smaller  $P$ , this fact means that  $\theta$  is reduced. Therefore, the same camera with twice the

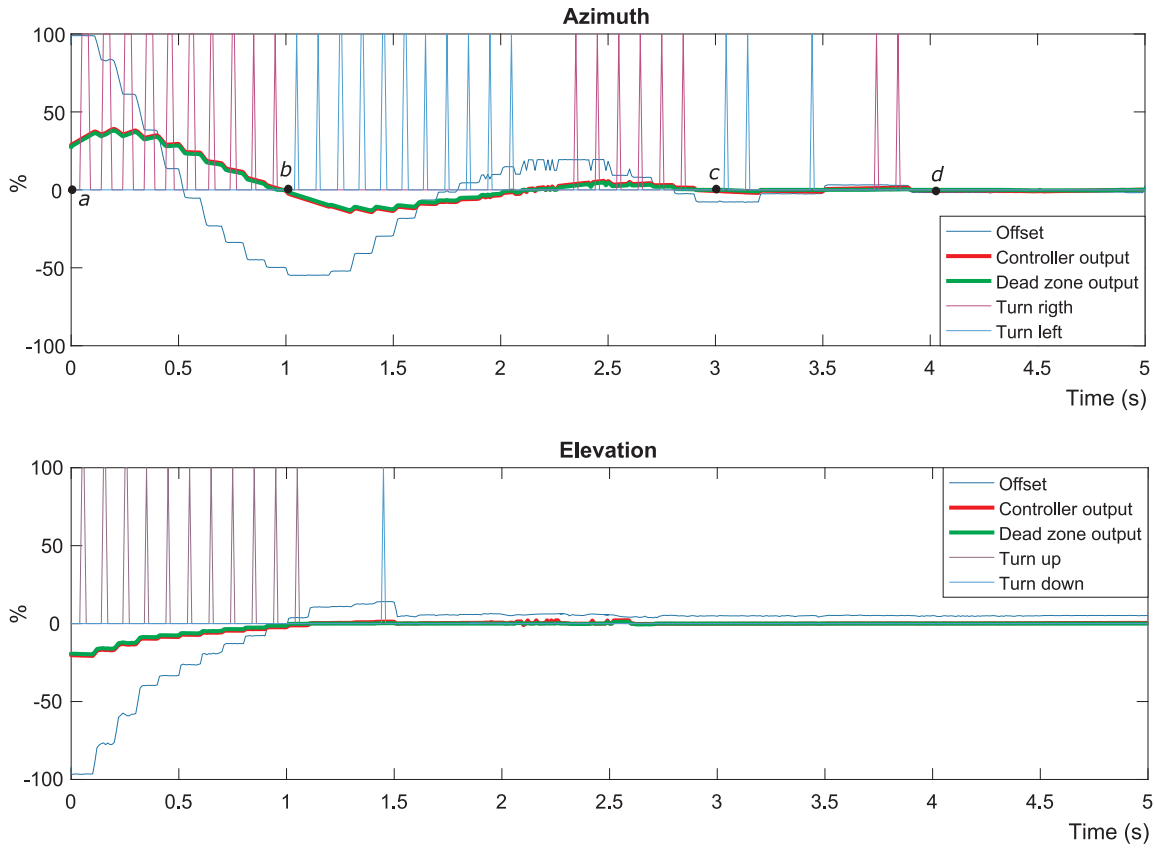


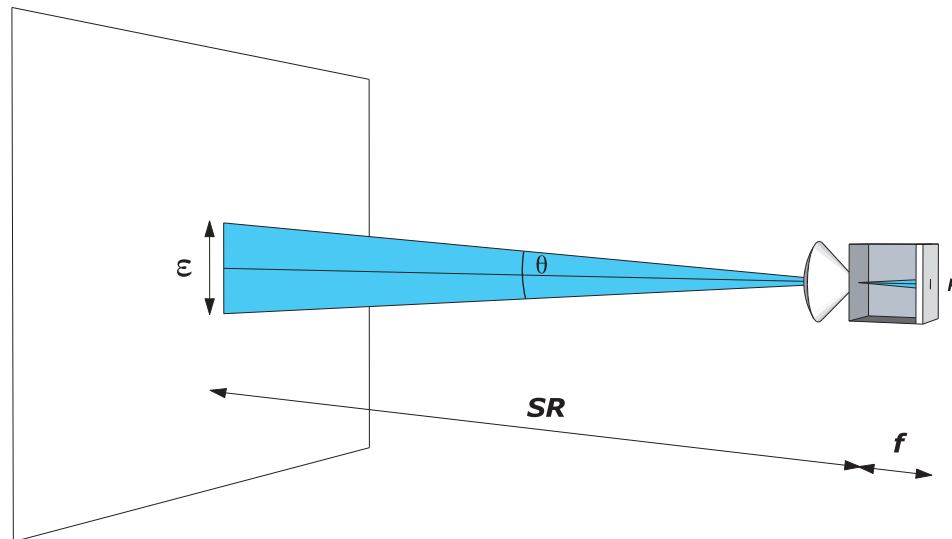
Fig. 10. Controller outputs and inputs.

resolution shows an  $S'$  angular uncertainty of 0.3 mrad and the uncertainty associated with  $A'$  less than 1 mrad. Another relevant error source is introduced by the CV algorithm, which is influenced by changes in lighting conditions and the environment. For that, the *Pi Cam* has been equipped with an auto image correction system that reduces the effects of changes in lighting conditions but this may be not enough since the camera is exposed to very bright spotlights. For this reason, *HSL* color system, that reduces the relation between the image and the lighting conditions, has been used. It could be further reduced by employing filters that reduce the amount of light reaching the sensor or selecting the wavelength. This last solution also provides environmental protection. Therefore, the final accuracy of the entire system is

conditioned by different factors such as camera resolution, fish eye lens, control algorithm errors, CV algorithm set-up and lighting conditions, accordingly the final accuracy must be determined by studying the influence of each of these factors.

##### 5. Educational interest

The prototype helps to understand the fundamentals of solar concentration systems and it can offer to the user the ability to work in other competences that can be related to solar concentrating systems. The system has been proposed taking into account the great potential and versatility that provides an educational tool based on new micro

Fig. 11. Uncertainty.  $\text{Pi cam}$  focal aperture ( $f$ ), pixel size ( $P$ ), slant range (SR), angular uncertainty( $\theta$ ), linear ( $\epsilon$ ) uncertainty.

controllers (Barrett, 2013; Blum, 2013).

From the automatic, the prototype helps knowing the different elements that form an automatic control system, designing a control system based on *CV* controllers and studying the effect of the disturbances. Furthermore, the new approach based on *CV*, that is independent of the hardware employed, can be interesting for students and researchers to study advanced control of solar plants (Camacho et al., 2012). The control algorithm can be modified to test new controllers, can be completely modified with another control philosophy or language and implemented in the hardware.

The prototype allows us to work with *CV* and image processing techniques, as well as allows studying cameras operation. From the point of view of the electric and electronic skills, a lot of electronic components make up the prototype, all of them are open source hardware and low cost, furthermore data sheets of the components are available. The prototype can be modified and the whole hardware and their connections replaced at a low cost.

Regarding to the programming competences, on the one hand although *Simulink* is not free software, it is a very common tool used for educational purposes. On the other hand *Wolfram Mathematica for Raspberry* is free software and also is commonly used for educational purposes. Furthermore, free or open source software and programming environments are available for *The Raspberry Pi* platform such as *BlueJ*, *Greenfoot* (Kölling, 2016) or *VirtualLabBuilder Modelica* (Martin-Villalba et al., 2013), also solar energy libraries like (Bonilla et al., 2017; Cabrerizo and Santos, 2017), for implementation of virtual-labs with elaborated user interfaces, and languages like *Python*, where the control algorithm can be developed, most of them with educational interest. The use of free or open source software is remarked because it is fast gaining popularity and acceptability. Furthermore open source software is considered the future of e-learning (Pankaja, 2013).

Finally, the *Raspberry* platform offers great possibilities of connectivity to work in *NICT* competences. For example, it is a very suitable hardware for implementing remote labs for automatic control purposes (Bermúdez-Ortega et al., 2015). In Bermúdez-Ortega et al. (2015), the authors introduced this new laboratory in some control subjects in the Universidad Complutense of Madrid. Furthermore, virtual and remote laboratories enable distance learning, improving lab accessibility to handicapped people and increasing safety for dangerous experimentation, these environments are welcome by students and provide a useful tool for the challenges of future education (Guzman et al., 2010; Erdem et al., 2016). In spite of large number of scientific production (Heradio et al., 2016) and some platforms for virtual and remote labs, virtual and remote labs about solar engineering are not available, making the proposed system more attractive.

## 6. Results

A better education focused on renewable energies is demanded and growing, so providing tools for educational use that can be employed to build better professional competences in solar energy are necessary since there are not enough educational resources with this approach. For this reason, a system for learning solar energy and solar tracking principles in addition to other related competences has been proposed with the main goal of to be a useful tool with a wide range of applications.

Depending on the approach, a lot of competences and knowledges can be worked from the point of view of solar energy like control, electronic concepts, *CV*, *NICTs*, programming or communication technologies. The present configuration is based on an approach that allows us to work mainly with concepts of concentrating solar energy, solar tracking control and *CV* at different levels.

Furthermore, the great connectivity offered by the open source hardware platform and the ability to implement virtual and remote labs environments or employ different open sources software and languages, allow us working in these types of environments making it an even

better tool that improves the learning process, especially for control science. CCD filters could improve the performance of the *Pi Cam* as well as extend its useful life and protect it from environmental conditions.

The low cost solution proposed is presented as a good alternative for labs with educational and scientific purposes whose main problems are usually their large requirements of space and funds for their establishment, assistance to maintenance and operation.

At present, the prototype has been presented during the *European ResearcherS' Night (Marie Skłodowska-Curie Actions)*, as a way to promote education on solar energy systems.

Future works will include the development of an interdisciplinary course using project-based learning methodology within the framework of the Solar Energy Master degree at the University of Almería. Successful examples of this methodology can be found. By using the prototype as a benchmark, students will develop basic competences on solar energy and solar tracking principles, and complementary ones, such as mechatronics, modeling and automatic control, electronics, computer vision and ICTs.

Ongoing works will include improving the control algorithms and the image processing techniques which detect the relevant points to reduce the uncertainty and introduce image error corrections. Other future works are the implementation of a model and control system in a remote and virtual laboratory platform so the community can use it, develop a closed loop control based on solar equations-*CV*, increase the reduction box ratio to achieve slower speeds and improve the information shown in the AR image. Also, an analysis will be carried out on the impact of the tool in the educational results in the course mentioned before (see Table 1).

## Acknowledgements

The research work leading to this article received ERDF funds from the Spanish government within the framework of the SOLTERMIN project (Ref. ENE2017-83973-R) of the Ministerio de Economía, Industria y Competitividad (Spanish Ministry of Economy, Industry and Competitiveness)

**Table 1**  
Acronyms and nomenclature.

A'	Aiming point	O	Rotation point
AR	Augmented Reality	P	Pixel size
ATS	Advanced Thermal Systems	PI controller	Proportional-Integrative controller
CMOS	Comp. Metal Oxide Semiconductor	PV	Photovoltaic
CP	Camera Plane	PWM	Pulse-Width Modulation
CPU	Central Processing Unit	RAM	Random Access Memory
CPV	Concentrated Photovoltaic	RGB	Red, Green and Blue
CPVT	Concentrated Photovoltaic-Thermal	S	Target saturation level
CSI	Camera Serial Interface	S	Solar point
CSP	Concentrated Solar Power	SR	Slant Range
CV	Computer Vision	T	Target point
DC	Direct Current	$\vec{V}_A$	Aiming vector
DSI	Display Serial Interface	$\vec{V}_S$	Solar vector
f	Focal length	$\vec{V}_T$	Target vector
GPIO	General Purpose Input/Output	Xoffset	Control input signal in X
GPS	Global Positioning System	XoffsetA	Aiming point offset in X
GUI	Graphical User Interface	XoffsetT	Tracking offset in X
H	Target saturation level	Yoffset	Control input signal in Y
HSL	HUE, Saturation Lightness	YoffsetA	Aiming point offset in Y
L	Solar lightness level	YoffsetT	Tracking offset in Y
L1	Target lightness level	$\epsilon$	Lineal uncertainty
LAN	Local area network	$\theta$	Angular uncertainty
NICT	New Information Communication Techs	"\$"	dollars

## References

- Ballestrín, J., Monterreal, R., 2004. Hybrid heat flux measurement system for solar central receiver evaluation. *Energy* 29 (5–6), 915–924. [https://doi.org/10.1016/S0360-5442\(03\)00196-8](https://doi.org/10.1016/S0360-5442(03)00196-8).
- Barrett, S.F., 2013. Arduino microcontroller processing for everyone!. *Synthesis Lect. Digit. Circ. Syst.* 8 (4), 1–513.
- Bauer, P., Rojko, A., Ionel, R., 2013. Distance learning module for solar electricity with programing of mppt. In: 2013 15th European Conference on Power Electronics and Applications (EPE). IEEE, pp. 1–8. <https://doi.org/10.1109/EPE.2013.6634716>.
- Berenguel, M., Rubio, F.R., Valverde, A., Lara, P.J., Arahal, M.R., Camacho, E.F., López, M., 2004. An artificial vision-based control system for automatic heliostat positioning offset correction in a central receiver solar power plant. *Sol. Energy* 76 (5), 563–575. <https://doi.org/10.1016/j.solener.2003.12.006>.
- Bermúdez-Ortega, J., Besada-Portas, E., López-Orozco, J.A., Bonache-Seco, J.A., De La Cruz, J.M., 2015. Remote web-based control laboratory for mobile devices based on EJSs, raspberry Pi and Node.js. *IFAC-PapersOnLine* 48 (29), 158–163. <https://doi.org/10.1016/j.ifacol.2015.11.230>.
- Blackmon, J.B., 2013. Parametric determination of heliostat minimum cost per unit area. *Sol. Energy* 97, 342–349. <https://doi.org/10.1016/j.solener.2013.08.032>.
- Blázquez, R., Carballo, J., Cadiz, P., Frasquet, M., Silva, M., Fontela, P., Ballesteros, J.C., 2015. Optical test of the DS1 prototype concentrating surface. *Energy Procedia* 69, 41–49. <https://doi.org/10.1016/j.egypro.2015.03.006>.
- Blum, J., 2013. Exploring arduino: Tools and Techniques for Engineering Wizardry. John Wiley & Sons.
- Bonilla, J., Roca, L., de la Calle, A., Dormido, S., 2017. Dynamic model of a molten salt-gas heat recovery system for a hybrid renewable solar thermal power plant. *Revista Iberoamericana de Automática e Informática Industrial RIAI* 14 (1), 70–81. <https://doi.org/10.1016/j.riai.2016.11.003>.
- Broman, L., 1992. Solar energy education: an important part of worldwide solar energy activities. In: Proc. 2nd World Renewable Energy Congress. Pergamon Press.
- Cabrerizo, J.A.R., Santos, M., 2017. Paratrough v1. 0: Librería en modelica para simulación de plantas termosolares. *Revista Iberoamericana de Automática e Informática Industrial RIAI* 14 (4), 412–423. <https://doi.org/10.1016/j.riai.2017.06.005>.
- Camacho, E.F., Berenguel, M., Rubio, F.R., Martínez, D., 2012. Control issues in solar systems. In: *Control of Solar Energy Systems*. Springer, pp. 25–47.
- Carballo, J.A., Bonilla, J., Fernandez, J., Garcia, G., 2018. Sistema de captacion solar mediante tecnicas de vision artificial ES P2018300773.
- Chao, K.M., James, A.E., Nanos, A.G., Chen, J.H., Stan, S.D., Muntean, I., Figliolini, G., Rea, P., Bouzgarrou, C.B., Vitliemov, P., Cooper, J., Van Capelle, J., 2015. Cloud E-learning for Mechatronics: CLEM. *Fut. Gen. Comput. Syst.* 48, 46–59. <https://doi.org/10.1016/j.future.2014.10.033>.
- Ciriminna, R., Meneguzzo, F., Pecoraino, M., Pagliaro, M., 2016. Rethinking solar energy education on the dawn of the solar economy. *Renew. Sustain. Energy Rev.* 63, 13–18. <https://doi.org/10.1016/j.rser.2016.05.008>.
- Colwell, C., Scanlon, E., Cooper, M., 2002. Using remote laboratories to extend access to science and engineering. *Comput. Educ.* 38 (1–3), 65–76. [https://doi.org/10.1016/S0360-1315\(01\)00077-X](https://doi.org/10.1016/S0360-1315(01)00077-X).
- Coventry, J., Campbell, J., Xue, Y.P., Hall, C., Kim, J.-S., Pye, J., Burgess, G., 2016. Heliostat cost down scoping study, final report. ANU Document Reference: STG-3261 Rev 01, ASTRL, Australia (5).
- Drigas, A.S., Vrettaros, J., Koukianakis, L.G., Glentzes, J.G., Paraskevi, A., 2005. A virtual lab and e-learning system for renewable energy sources. *Analysis* 2005, 149–153.
- ElKadmiri, Z., El Kadmiri, O., Masmoudi, L., Bargach, M.N., 2015. A novel solar tracker based on omnidirectional computer vision. *J. Sol. Energy* 2015, 1–6. <https://doi.org/10.1155/2015/149852>.
- Erdem, M.B., Kiraz, A., Eski, H., Çiftçi, Ö., Kubat, C., 2016. A conceptual framework for cloud-based integration of virtual laboratories as a multi-agent system approach. *Comput. Indus. Eng.* 102, 452–457. <https://doi.org/10.1016/j.cie.2016.04.011>.
- Fabregas, E., Farias, G., Dormido-Canto, S., Dormido, S., Esquembre, F., 2011. Developing a remote laboratory for engineering education. *Comput. Educ.* 57 (2), 1686–1697. <https://doi.org/10.1016/j.compedu.2011.02.015>.
- Fernández-Reche, J., Valenzuela, L., 2012. Geometrical assessment of solar concentrators using close-range photogrammetry. *Energy Procedia* 30, 84–90. <https://doi.org/10.1016/j.egypro.2012.11.011>.
- Freeman, J., Nagarajan, A., Parangan, M., Kumar, D., Diwakar, S., Achuthan, K., 2012. Remote triggered photovoltaic solar cell lab: effective implementation strategies for virtual labs. In: Proceedings - 2012 IEEE International Conference on Technology Enhanced Education, Amritapuri, India. doi:<https://doi.org/10.1109/ICTEE.2012.6208653>.
- García, G., Egea, A., Romero, M., 2004. Performance evaluation of the first solar tower operating with autonomous heliostats: PCHA project. In: Proceedings of the 12th SolarPACES International, Zurich, Switzerland.
- GitLab, Cv solar tracking repository (September 2018). <[https://gitlab.com/ciemat-psa/cv\\_solar\\_tracking.git](https://gitlab.com/ciemat-psa/cv_solar_tracking.git)>.
- Guney, M.S., 2016. Solar power and application methods. *Renew. Sustain. Energy Rev.* 57, 776–785. <https://doi.org/10.1016/j.rser.2015.12.055>.
- Guzman, J.L., Domínguez, M., Berenguel, M., Fuentes, J.J., Rodríguez, F., Reguera, P., 2010. Entornos de experimentación para la enseñanza de conceptos Básicos de modelado y control. *Revista Iberoamericana de Automática e Informática Industrial* 7 (1), 10–22. <https://doi.org/10.4995/RIAI.2010.01.01>.
- Heradio, R., de la Torre, L., Dormido, S., 2016. Virtual and remote labs in control education: a survey. *Annu. Rev. Control* 42 (August), 1–10. <https://doi.org/10.1016/j.arcontrol.2016.08.001>.
- Heradio, R., de la Torre, L., Galan, D., Cabrerizo, F.J., Herrera-Viedma, E., Dormido, S., 2016. Virtual and remote labs in education: a bibliometric analysis. *Comput. Educ.* 98, 14–38.
- Hohmeyer, O.H., Bohm, S., 2015. Trends toward 100% renewable electricity supply in Germany and Europe: a paradigm shift in energy policies. *Wiley Interdiscip. Rev.: Energy Environ.* 4 (1), 74–97. <https://doi.org/10.1002/wene.128>.
- Jacobson, M.Z., Delucchi, M.A., Bazouin, G., Bauer, Z.A., Heavey, C.C., Fisher, E., Morris, S.B., Piekutowski, D.J., Vencill, T.A., Yeskoo, T.W., 2015. 100% clean and renewable wind, water, and sunlight (wws) all-sector energy roadmaps for the 50 united states. *Energy Environ. Sci.* 8 (7), 2093–2117.
- Jennings, P., 2009. New directions in renewable energy education. *Renewable Energy* 34 (2), 435–439. <https://doi.org/10.1016/j.renene.2008.05.005>.
- Kandpal, T.C., Broman, L., 2014. Renewable energy education: a global status review. *Renew. Sustain. Energy Rev.* 34, 300–324. <https://doi.org/10.1016/j.rser.2014.02.039>.
- Kannan, N., Vakeesan, D., 2016. Solar energy for future world: a review. *Renew. Sustain. Energy Rev.* 62, 1092–1105. <https://doi.org/10.1016/j.rser.2016.05.022>.
- Khan, J., Arsalan, M.H., 2016. Solar power technologies for sustainable electricity generation – a review. *Renew. Sustain. Energy Rev.* 55, 414–425. <https://doi.org/10.1016/j.rser.2015.10.135>.
- Kolb, G.J., Jones, S.A., Donnelly, M.W., Gorman, D., Thomas, R., Davenport, R., Lumia, R., 2007. Heliostat cost reduction study. *ASME Energy Sustainability Conference SAND2007-3* (June), 1–158. <https://doi.org/10.2172/912923>.
- Kölling, M., 2016. Educational programming on the raspberry Pi. *Electronics* 5 (3), 33. <https://doi.org/10.3390/electronics5030033>.
- Lee, C.-Y., Chou, P.-C., Chiang, C.-M., Lin, C.-F., 2009. Sun tracking systems: a review. *Sensors* 9 (5), 3875–3890. <https://doi.org/10.3390/s90503875>.
- Lee, C.D., Huang, H.C., Yeh, H.Y., 2013. The development of sun-tracking system using image processing. *Sensors (Switzerland)* 13 (5), 5448–5459. <https://doi.org/10.3390/s130505448>.
- Liu, H., Ning, H., Mu, Q., Zheng, Y., Zeng, J., Yang, L.T., Huang, R., Ma, J., 2017. A review of the smart world. *Fut. Gen. Comput. Syst.* <https://doi.org/10.1016/j.future.2017.09.010>.
- Martin-Villalba, C., Urquia, A., Dormido, S., 2013. Development of an industrial boiler virtual-lab for control education using Modelica. *Comput. Appl. Eng. Educ.* 21 (1), 36–45. <https://doi.org/10.1002/cae.20449>.
- Wolfram Mathematica, <<https://www.wolfram.com>> (Noviembre 2017).
- MATLAB, <<https://es.mathworks.com/hardware-support/raspberry-pi-simulink.html>> (Noviembre 2017).
- Meloroso, J., Perroy, R., Careas, S., 2015. World population prospects. *United Nations* 1 (6042), 587–592. <https://doi.org/10.1017/CBO9781107415324.004..<arXiv:1011.1669v3>>.
- Michaelides, I., Eleftheriou, P., Economides, K., 2005. Solar energy e-learning laboratory - Remote experimentation over the Internet. In: Rev 2005: 2nd International Conference on Remote Engineering and Virtual Instrumentation, pp. 1–10.
- Moliner, R., Tanda, R., 2016. Herramienta para la sintonía robusta de controladores pi/pid de dos grados de libertad. *Revista Iberoamericana de Automática e Informática Industrial RIAI* 13 (1), 112–123. <https://doi.org/10.1016/j.riai.2015.05.003>.
- Mousazadeh, H., Keyhani, A., Javadi, A., Mobli, H., Abrinia, K., Sharifi, A., 2009. A review of principle and sun-tracking methods for maximizing solar systems output. *Renew. Sustain. Energy Rev.* 13 (8), 1800–1818. <https://doi.org/10.1016/j.rser.2009.01.022>.
- Pankaja, N., 2013. Proprietary software versus open source software for education. *Am. J. Eng. Res.* 2 (7), 124–130 2320-0936.
- Panwar, N.L., Kaushik, S.C., Kothari, S., 2011. Role of renewable energy sources in environmental protection: a review. *Renew. Sustain. Energy Rev.* 15 (3), 1513–1524. <https://doi.org/10.1016/j.rser.2010.11.037>.
- Pfahl, A., Randt, M., Holze, C., Unterschütz, S., 2013. Autonomous light-weight heliostat with rim drives. *Sol. Energy* 92, 230–240. <https://doi.org/10.1016/j.solener.2013.03.005>.
- Pfahl, A., Coventry, J., Röger, M., Wolfertstetter, F., Vásquez-Arango, J.F., Gross, F., Arjomandi, M., Schwarzbözl, P., Geiger, M., Liedke, P., 2017. Progress in heliostat development. *Sol. Energy* 152, 3–37. <https://doi.org/10.1016/j.solener.2017.03.029>.
- Prada, M.A., Fuertes, J.J., Alonso, S., García, S., Domínguez, M., 2015. Challenges and solutions in remote laboratories. Application to a remote laboratory of an electro-pneumatic classification cell. *Comput. Educ.* 85, 180–190. <https://doi.org/10.1016/j.compedu.2015.03.004>.
- Prinsloo, G., Dobson, R., 2015. Solar Tracking: High precision solar position algorithms, programs, software and source-code for computing the solar vector, solar coordinates & sun angles in Microprocessor, PLC, Arduino, PIC and PC-based sun tracking devices or dynamic sun following hardware. doi:<https://doi.org/10.13140/RG.2.1.4265.6329/1>.
- Romero, M., Egea, A., Gázquez, J.A., García, G., 2002. Implementing wireless communication into heliostat fields. In: Proceedings of the 11th SolarPACES International Symposium on Concentrated Solar Power and Chemical Energy Technologies, Oaxaca, Mexico, pp. 567–574.
- Ruelas, A., Velázquez, N., Villa-Angulo, C., Acuña, A., Rosales, P., Suastegui, J., 2017. A solar position sensor based on image vision. *Sensors* 17 (12), 1742. <https://doi.org/10.3390/s17081742>.
- Saez de Arregui, G., Plano, M., Lerro, F., Petrocelli, L., Marchisio, S., Concar, S., Scotta, V., 2013. A mobile remote lab system to monitor in situ thermal solar installations. *IJIM, Int. J. Interact. Mob. Technol.* 7 (1), 31–34. <https://doi.org/10.3991/ijim.v7i1.2292>.
- Scheer, H., 2013. The Solar Economy: Renewable Energy for a Sustainable Global Future. Routledge.

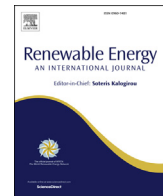
- Schou, P., 2000. Polluting non-renewable resources and growth. *Environ. Resource Econ.* 16 (2), 211–227.
- Sharaf, O.Z., Orhan, M.F., 2015a. Concentrated photovoltaic thermal (CPVT) solar collector systems: Part I—Fundamentals, design considerations and current technologies. *Renew. Sustain. Energy Rev.* 50, 1500–1565. <https://doi.org/10.1016/j.rser.2015.05.036>.
- Sharaf, O.Z., Orhann, M.F., 2015b. Concentrated photovoltaic thermal (CPVT) solar collector systems: Part II – Implemented systems, performance assessment, and future directions. *Renew. Sustain. Energy Rev.* 50, 1566–1633. <https://doi.org/10.1016/j.rser.2014.07.215>.
- Sheikh, N.J., Kocaoglu, D.F., Lutzenhiser, L., 2016. Social and political impacts of renewable energy: literature review. *Technol. Forecast. Soc. Change* 108, 102–110. <https://doi.org/10.1016/j.techfore.2016.04.022>.
- Silva, R., Pasamontes, M., Guzmán, J.L., Pérez, M., Berenguel, M., 2011. Interactive tool to teach solar parabolic trough concepts. In: Proceedings of the ISES Solar World Congress 2011 (September), pp. 1–12. doi:<https://doi.org/10.18086/swc.2011.06.11>.
- Smil, V., 2010. *Energy Transitions: History, Requirements, Prospects*. ABC-CLIO.
- Sobota, J., Pisł, R., Balda, P., Schlegel, M., 2013. Raspberry pi and arduino boards in control education. *IFAC Proc. Vol. (IFAC-PapersOnline)* 10 (PART 1), 7–12. <https://doi.org/10.3182/20130828-3-UK-2039.00024>.
- Torres-Ramírez, M., García-Domingo, B., Aguilera, J., De La Casa, J., 2014. Video-sharing educational tool applied to the teaching in renewable energy subjects. *Comput. Educ.* 73, 160–177. <https://doi.org/10.1016/j.compedu.2013.12.014>.
- Cambridge University, <<https://www.raspberrypi.org/>> (Noviembre 24 2016).
- Upton, E., Halfacree, G., 2014. *Raspberry Pi User Guide*. John Wiley and Sons.

**A.4. New approach for solar tracking systems based on computer vision, low cost hardware and deep learning**



Contents lists available at ScienceDirect

## Renewable Energy

journal homepage: [www.elsevier.com/locate/renene](http://www.elsevier.com/locate/renene)

## New approach for solar tracking systems based on computer vision, low cost hardware and deep learning

Jose A. Carballo <sup>b, c, \*</sup>, Javier Bonilla <sup>a, b</sup>, Manuel Berenguel <sup>b, c</sup>, Jesús Fernández-Reche <sup>a</sup>, Ginés García <sup>a</sup>

<sup>a</sup> CIEMAT- Plataforma Solar de Almería, Ctra. de Senés s/n Tabernas, 04200 Almería, Spain

<sup>b</sup> CIESOL-Research Centre for Solar Energy, UAL-PSA.CIEMAT Joint Centre, Almería, Spain

<sup>c</sup> University of Almería, Ctra. Sacramento s/n, Almería 04120, Spain



### ARTICLE INFO

#### Article history:

Received 12 May 2018

Received in revised form

22 August 2018

Accepted 29 August 2018

Available online 1 September 2018

#### Keywords:

Solar energy

Sun tracking

Computer vision

Deep learning

Convolutional neural networks

### ABSTRACT

In this work, a new approach for Sun tracking systems is presented. Due to the current system limitations regarding costs and operational problems, a new approach based on low cost, computer vision open hardware and deep learning has been developed. The preliminary tests carried out successfully in Plataforma solar de Almería (PSA), reveal the great potential and show the new approach as a good alternative to traditional systems. The proposed approach can provide key variables for the Sun tracking system control like cloud movements prediction, block and shadow detection, atmospheric attenuation or measures of concentrated solar radiation, which can improve the control strategies of the system and therefore the system performance.

© 2018 Elsevier Ltd. All rights reserved.

## 1. Introduction

Industrial evolution and population growth, have motivated the continuous increase of the world energy demand. The perspectives indicate that, world population will continue to increase, specially for non Organisation for Economic Co-operation and Development (*OECD*) countries demanding more energy for residential uses [1]. Furthermore, energy consumption due to the industrial sector, which continues to account the largest share of the energy consumption, is also expected to increase. For all that, it is predicted that World energy consumption will rise 28% between 2015 and 2040 [2].

In the past, the demand has been covered by traditional energy sources such as fossil and nuclear fuels which heavily pollute the ecosystem. The consequences are being revealed now [3]. For that, it is necessary to change the current energetic model to mitigate the environmental issues and reply to new demands in a clean and

sustainable way. Recent studies indicate that 100% of renewable electricity and energy in general supply can be achieved in the top industrialized countries. These studies show how the transition should be [4,5], its problems and its economic, environmental and social benefits [6].

These studies suggest that all kind of renewable energies sources should be employed, creating a sustainable and reliable energy mix. Note that the development carried out in different renewable energies sources (solar, wind, hydropower and geothermal) makes them viable sources of energy, even in places rich in fuel reserves. The contribution in the world energetic model of the renewables energies is the fastest growing [2].

Although several renewable technologies are already competitive, researchers are undertaking investigations in order to increase efficiency and reduce cost [4], as shown by the amount of scientific production related to it [7].

Among all renewable technologies, those that take direct advantage of solar radiation flux have lot of potential and they generated many different subcategories. Most of them improve the efficiency concentrating the solar flux by optical systems or exposing the receiver so it captures as much solar radiation as possible.

\* Corresponding author. CIESOL-Research Centre for Solar Energy, UAL-PSA.CIEMAT Joint Centre, Almería, Spain.

E-mail addresses: [jcarballo@psa.es](mailto:jcarballo@psa.es) (J.A. Carballo), [javier.bonilla@psa.es](mailto:javier.bonilla@psa.es) (J. Bonilla), [beren@ual.es](mailto:beren@ual.es) (M. Berenguel), [jesus.fernandez@psa.es](mailto:jesus.fernandez@psa.es) (J. Fernández-Reche), [gines.garcia@psa.es](mailto:gines.garcia@psa.es) (G. García).

### 1.1. Sun tracking

Solar energy technologies convert the solar radiation into other type of energy, therefore estimating the availability and the nature of the source of energy is a key issue. The most important characteristic of the solar radiation is that the relative position of the Sun in the sky is constantly changing generating daily and annual cycles due to the Earth rotation around its axis and revolution around the Sun. This fact causes that the systems do not receive all the radiation in an optimal way for a fixed position. For that, the solar energy collectors in energy generation systems demand a solar tracking system (STS) to control the alignment with the Sun to increase the received solar radiation. Furthermore, the STS is responsible for managing the basic tasks that guarantee the correct daily operation. Among these tasks the most relevant are: to compute the tracking setpoint, communications management, diagnosis of faults or errors, to control drive mechanism and the decision making in emergency situations.

In the literature there are some recent reviews about STSs that show the growing interest in these systems. For instance, Lee et all [8]. presented a review of the major algorithms for sun tracking systems developed over the past 20 years and concluded confirming the great applicability of sun tracking system for a diverse range of high-performance solar-based applications. Prinsloo and Dobson [9] carried out an extensive review about computer-based sun tracking devices, high-precision solar position algorithms, software for computing the solar vector, solar coordinates and sun angles, showing the potential and rapid growth in recent years. Later, Mousazadeh et all [10]. performed an extensive review and discussed pros and cons of each system. Recently, Nsengiyumva et all [11]. classified the current STSs and stated that closing the control loop in STSs could significantly improve the overall system performance.

Nowadays, STSs can be classified according to the definition method of the solar relative position in the sky. There are two main methods, solar position algorithms or optical methods/algorithms. Furthermore, STSs can be classified regarding the number and position of rotation axes in one or two rotation axes mainly. For one rotation axis, horizontal, vertical and tilted-axis systems can be found as subcategories. Azimuth-elevation and polar trackers can be found as subcategories for two rotation axes trackers.

Sun trackers can guide the system with continuous or discrete movement depending on the rotation system and the controller. Regarding to the control of movements, STSs can also be classified as passive and active controllers. Passive solar trackers usually are composed by a couple of actuators working against each other. Passive trackers are based on thermal expansion and using the different solar radiation conditions orient the system in the direction where the radiation over both actuators is the same [10]. Active trackers can be classified in microprocessor and electro-optical sensor based, computer controller date and time based, auxiliary bifacial solar cell based and a combination of these three systems [10]. Also, active solar trackers can be classified in closed-loop and open-loop controllers. Closed-loop controllers are based on feedback transferred from sensors which identify parameters induced by the environment. On the other hand, an open-loop controller, estimates its inputs using only the current state, without using feedback to determine if its inputs have achieved the desired goal, so this one is simpler than the closed-loop controller but it cannot correct any errors and may not counteract for disturbances in the system [8]. Finally, it can be found centralized or distributed STS controllers in large plants dedicated to the production of energy. Note that most of STSs are developed for a specific solar technology or purpose [12].

Among all the errors that can affect a solar energy collector [13],

aiming errors, tracking offset and optical errors are those directly related to the STS. The first one is related to constant aberrations such as, pedestal tilt due to displacement of the center of gravity, bad reference or structure deformations due to wind loads. Also, the effect of the refraction of solar radiation in the atmosphere can be classified as an aiming error because it can modify the apparent position of the Sun due to the conditions of the atmosphere [14]. The tracking offset is related to the STS abilities in general (movement, controller and tracker resolution). The last of the three is related to optical quality and it can be found astigmatic aberration as the most connected with the STS. Although astigmatic aberration is not caused by STS directly, correct control strategies of STSs can help to reduce its effects (spillage and decrease concentration factor).

With respect to active control solar trackers, computer controlled based on date and time, that are the most employed, gets the solar position according to solar equations that need time, date and location as inputs. The accuracy of this system is very conditioned by constant aberrations. On the other hand, bifacial solar cell and electro-optical sensor systems are time and location independent although they are only able to obtain the relative solar position and control solar systems when the system optical axis should be aligned with the Sun vector, for example parabolic dishes or photovoltaic (PV) two axes trackers. El Kadmiri et al. [15] developed a solar tracker based on omnidirectional computer vision able to extract accurate information about the Sun position and Ruelas et al. [16] developed a system based on a video processing sensor able to determine the Sun position using low cost devices. The accuracy of these systems is mostly influenced by the controller and sensor resolution. All of them demand a specific individual configuration during the first start-up of the system.

The new approach for STSs proposed in this work is based on the use of computer vision techniques to carry out the Sun tracking task, furthermore the proposed system enables computing some key variables related to this. Particularly, the new approach makes use of computer vision techniques related to object detection with region proposal techniques based on deep learning by means of convolutional neural networks (CNN). In this work the implementation of the approach in a real system is analyzed and discussed.

The authors of the present work have patented the Sun tracking approach based on computer vision presented [17]. Furthermore, they also presented a small prototype aims at educational purposes [18].

## 2. Solar tracking system based on computer vision

As commented before, STSs are employed to align in a optimum way the solar collector with the Sun. Thus, for a correct Sun tracking, STSs need to know the relative Sun position in the sky, the receiver position and the collector aiming point. Each of these three points together with the point on the origin collector surface closest to the rotation axis ( $O'$ ), form respectively the solar vector ( $\vec{V}_S$ ), the reflected or target vector ( $\vec{V}_T$ ) and the aiming vector ( $\vec{V}_A$ ). On the one hand, these three vectors are usually computed by solar equations, which is a functional method but has several limitations such as time and location dependence, on the other hand, electro optical sensors are only able to obtain  $\vec{V}_S$ , limiting the range of application of the system. In this work the new approach, that tries to eliminate these limitations, has been implemented in a central tower system (Fig. 1), which can require the most complex STSs.

For that the picture taken by a camera, placed in  $O'$  and whose optical axis is arranged parallel to the optical axis of the heliostat, enables detecting  $S'$ ,  $A'$  and  $T'$ , which represent the intersection

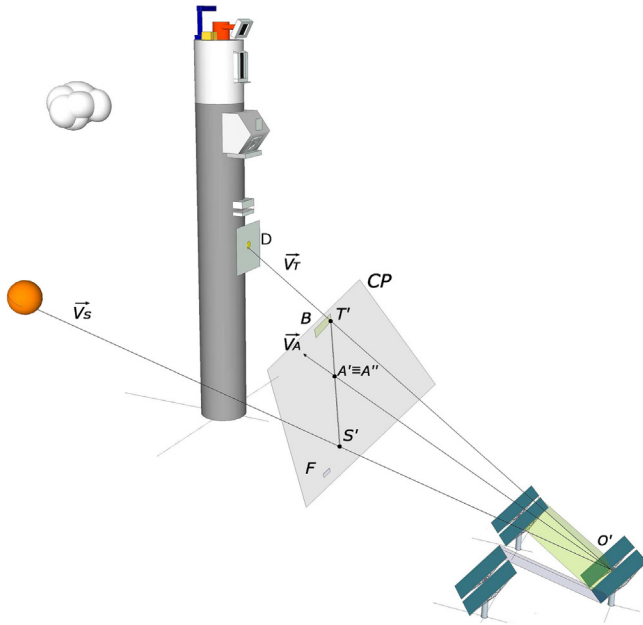


**Fig. 1.** Central tower system.

between the camera plane (*CP*) and  $\vec{V}_S$ ,  $\vec{V}_A$  and  $\vec{V}_T$  respectively. With this arrangement, for a correct heliostat alignment, the vector  $\vec{V}_A$  should intersect the middle point ( $A'$ ) of the segment formed by  $S'$  and  $T'$  in the *CP*. The differences between  $A'$  and  $A''$  are known as *tracking error* and it is employed as the main input for the control system. Note that considering some simplifications, this approach can be applied to any kind of solar collector system like parabolic trough collectors *PTC* (Fig. 2), parabolic dish or *STS* PV applications. For example, in the *PTC* systems (Fig. 2), the Sun tracking problem is reduced to one dimension, so only one of the *CP* and key vectors dimension are required. Also, for parabolic dishes or two axis PV trackers, the  $\vec{V}_A$  and  $\vec{V}_T$  are usually the same.

Furthermore, this approach enables detecting several key variables related to the control of *STSs* that currently are not considered or computed separately due to the difficulty for obtaining them. For example, Sun shadow (*F*) projected over the collector or concentrated solar flux blocked (*B*) by other heliostats or objects can be detected by analyzing the image.

Also, clouds detection enables predicting cloud movements,

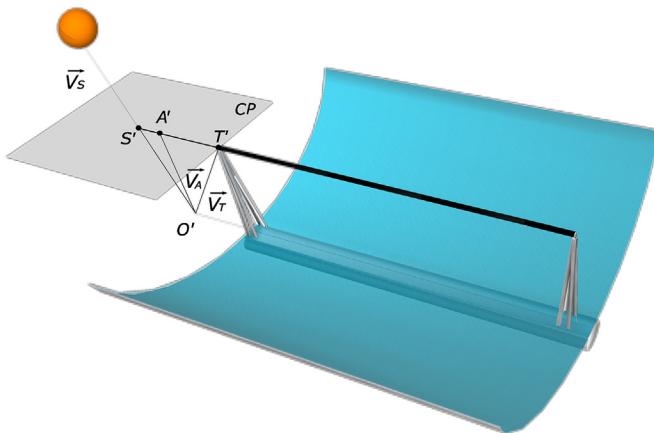


**Fig. 2.** PTC system.

helping in this way to mitigate the effects produced by these transients.

Another key variable is the concentrated solar flux distribution (*D*) or the total solar flux that reaches the receiver, previous works [19,20] make use of digital images to measure these variables. Also, recently a method for atmospheric extinction measurement based on digital images [21] has been presented. Atmospheric extinction of solar radiation flux reflected by the collectors is an important cause of energy loss in large solar tower plants. Therefore, the implementation of these methods based on digital images together with the new approach for *STS* based on computer vision, enables obtaining these key variables and develop new control strategies. Finally, the joint use of this new approach and traditional *STS* control techniques can lead to a closed loop control system.

In *STSs* based on computer vision, different camera settings and parameters (see Fig. 3) should be taken into account since they strongly affect the outcome. The required geometrical parameter, Field Of View (*FOV* in *mrad*), is determined by the *STS* application requirements related to the geometrical layout. For example, tower systems demand a *FOV* wider than PV trackers due to the angle between  $\vec{V}_S$  and  $\vec{V}_T$  is larger. Other relevant geometrical parameters are focal length (*f*, measured in *mm*) and sensor size, both related to the *FOV*. Camera resolution  $H \times W$  (image height and width in pixels) together with sensor size determine the pixel height and width in *mm* ( $p_W$  and  $p_H$ ), which usually have the same value (*p*).

The uncertainty of the aiming point angle (*U*) for *STSs* based on computer vision can be estimated as the pixel projection size in *mrad* over *CP* in  $A'$ . It can be computed from *p* and *f*, see Eq. (1). The minimum camera resolution can be therefore determined from a particular uncertainty.

$$U = \arctan\left(\frac{p}{f}\right). \quad (1)$$

## 2.1. Convolutional neural networks

The new approach is based on computer vision, specifically in deep Convolutional Neuronal Networks (*CNNs*) for objects localization and detection due to the large number of advantages that it presents, although any other technique based on computer vision could be used.

Models based on neuronal networks work like regular models, take an input (image), and generate an output (object positions). Neural networks models transform the input through a series of hidden stages (layers), composed by a set of neurons (small and simple processing unit). Each neuron is connected to many others neurons creating a massively parallel processing model. Neurons have learnable parameters (weights and biases), that modify the individual output.

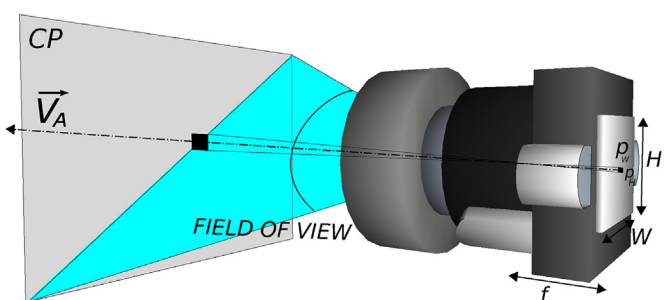


**Fig. 3.** Camera plane, field of view and accuracy.

Weights and biases and other general configuration parameters (such as the learning rate, number of epochs, etc.) must be adjusted in a iterative process called learning or training. The training is an optimization problem, where some parameters are set to minimize a loss function on a training dataset. The loss function expresses the discrepancy between the ground truth and the neural network prediction.

The goal of machine learning is not only to minimize the difference between predictions and the training dataset, but to generalize to be applicable to unseen samples. For that reason, there is commonly an independent dataset used for validation.

A deep neural network is a network with hidden layers between the input and output layers. A CNN is a particular class of deep neural network commonly applied to image and video recognition. Convolution networks are inspired by biological processes where the connectivity pattern between neurons resembles the organization of the visual cortex. Among the hidden layers of a CNN, there are convolutional layers. A convolutional layer applies a convolution operation to the input, which emulates the response to visual stimuli, and passes the result to the next layer. Convolutional layers have a fixed number of weights determined by the choice of filter size and number of filters, but independent of the input size. This improves performance and reduces memory footprint compared to fully connected layers. During training, a CNN learns the filters, which in traditional imaging processing are manually programmed.

Typical object detection networks such as Region-CNN (*R-CNN*) and *Fast R-CNN* use a region proposal algorithm to select the different regions of interest (*ROIs*) on a picture before running the CNN to classify the regions. The difference between them is how *ROIs* are selected to process and how these regions are classified. This work considers a new approach known as *Faster R-CNN* [22], in which a CNN is employed in the region proposal mechanism (Region Proposal Network *RPN*) and a detector based on *Fast R-CNN* classifies the *ROI*. *RPN* and *Fast R-CNN* can be merged into a unified network by sharing the common set of convolutional layers. This merger causes a problem in networks trainings, because two independent network trainings must be applied to each network, thus each training modifies in different ways the common convolutional layers. To solve this problem, a new training scheme is applied, it is implemented in the Computer Vision System Toolbox in Matlab [23,24], which alternates between the region proposal and the object detection, producing a unified network with convolutional features that are shared between both tasks.

A pretrained network called *Alexnet* has been employed in the present work as a starting point to learn the new task because transferring learning is much faster and easier than constructing and training a new network, furthermore the pretrained networks have already learned a rich set of features. *Alexnet* is a CNN composed by 25 layers and trained on a subset of the ImageNet database for ImageNet Large-Scale Visual Recognition Challenge (ILSVRC) [25].

In this work, *Alexnet* has been retrained with a large training image set (see Fig. 4) of CESA central tower system located in Plataforma Solar de Almería, which was taken for this purpose with the open hardware employed for the implementation. Also, the images have been analyzed and the *ROI* labeled according to the new four object classes (heliostat, target, Sun and cloud).

Fig. 5 shows one of the image analyzed by the new trained neuronal net, in which the results have been superimposed. In this figure, the red, blue, white and black marked *ROIs* indicate the regions that have been classified according to the new classes (Sun, cloud, heliostat and target respectively). Each *ROI* has a title with the class name and the score between 0 and 1, larger score values indicate higher confidence in the detection.

Notice that other image processing techniques can be employed

for this purpose. For example, Sun center is defined in this work by the segmentation of the Sun *ROI*. In computer vision techniques like segmentation, the image color representation takes a relevant role. The most usual color representation *RGB* is not suitable because *RGB* representation is affected by the bright level. Another color representation called *HSL* defines a color in terms of saturation (the amount of chroma), its constituent components hue (the angle on the color wheel) and lightness (how bright the color is). In *HSL*, brightness can be separated to make the colors less influential to the light intensity impact improving the discrimination of the object [26]. For this reason, the *HSL* representation is employed in this proposal to determine the position of the Sun's center in the Sun *ROI*.

## 2.2. Low cost hardware

Nowadays in solar industry, the collector fixed costs are one of the factors which determine the optimum collector size. For central tower systems the optimum heliostat surface size is 150 m<sup>2</sup>. The cost of the control electronic devices employed in STSs like processors, encoders, limit switches, junction boxes, connectors, wiring, remain constant at \$ 1000 – 3000, although the collector size changes [27,28].

The proposed approach in this work can simplify the system and reduce the number of components. Furthermore, in the implementation of the approach a low cost hardware platform called *Raspberry Pi* [29] has been employed. This reduces the fixed cost associate to the STS control hardware from \$ 290 to less than \$ 75 approximately, removing costs in electronic devices such as limit switches, GPS or encoders that are not needed. Communication wire costs can be removed due to the great connectivity offered by this type of platforms, in this case Wifi and bluetooth. Also, the new hardware can be powered with a small pv cell and a battery. For all that, this new approach can make STSs more flexible, autonomous [30], easy to use, cheap to manufacture and install, which leads to new cost reductions. Furthermore, cost reduction in fixed control costs results in direct savings and also enables the reduction of the optimal heliostat area with additional cost reductions in the cost per unit area due to the dependence on imposed loads [28]. Finally, this hardware facilitates the implementation of the Internet Of Thing (*IOT*) concept in solar energy and by extension, the integration of this type of technologies in the new energy distribution paradigm called smart grids [31].

The hardware employed (Fig. 6) was a *Raspberry Pi 3* together with a *Raspicam*. *Raspberry Pi 3* is a low cost credit-card-sized computer that compared with industrial hardware is cheaper while being fully functional and adding more capabilities. It can be found a large number of platforms like *Raspberry Pi* in the market that can be used for implementing this approach, most of them enable low cost replacements. The popularity of these hardware platform offers a lot of hardware extensions, generally low cost, which may improve the STS. The software employed in this work has been *Computer Vision System Toolbox* [22,24] and *MATLAB Support Package for Raspberry Pi Hardware*, although the great adaptability of the hardware enabling using other software packages.

## 3. Test

In order to test the new approach described above, the hardware was fixed to one of the heliostat of the CESA tower central system at PSA (Fig. 6) and two new image sets were taken while the heliostat remained under the control of the traditional control system. The heliostat selected (Fig. 7) is located in the eastern end of the CESA field, so it is one of the most distant from the white target. The



**Fig. 4.** Training image examples.

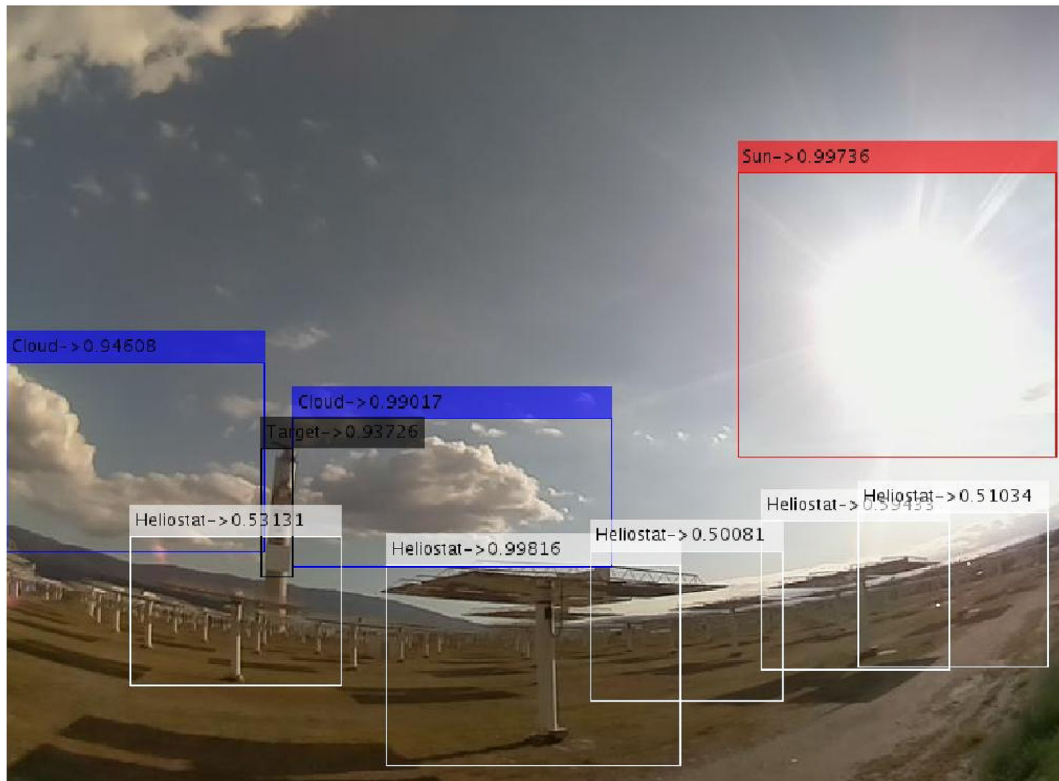


**Fig. 5.** Image analyzed example.

heliostat solar tracking uncertainty with the traditional Supervisory Control And Data Acquisition (SCADA) is 1.2 mrad for each axis.

Also with the configuration of the camera employed during the test (camera resolution 800x600 px, wide angle FOV lens 150°,

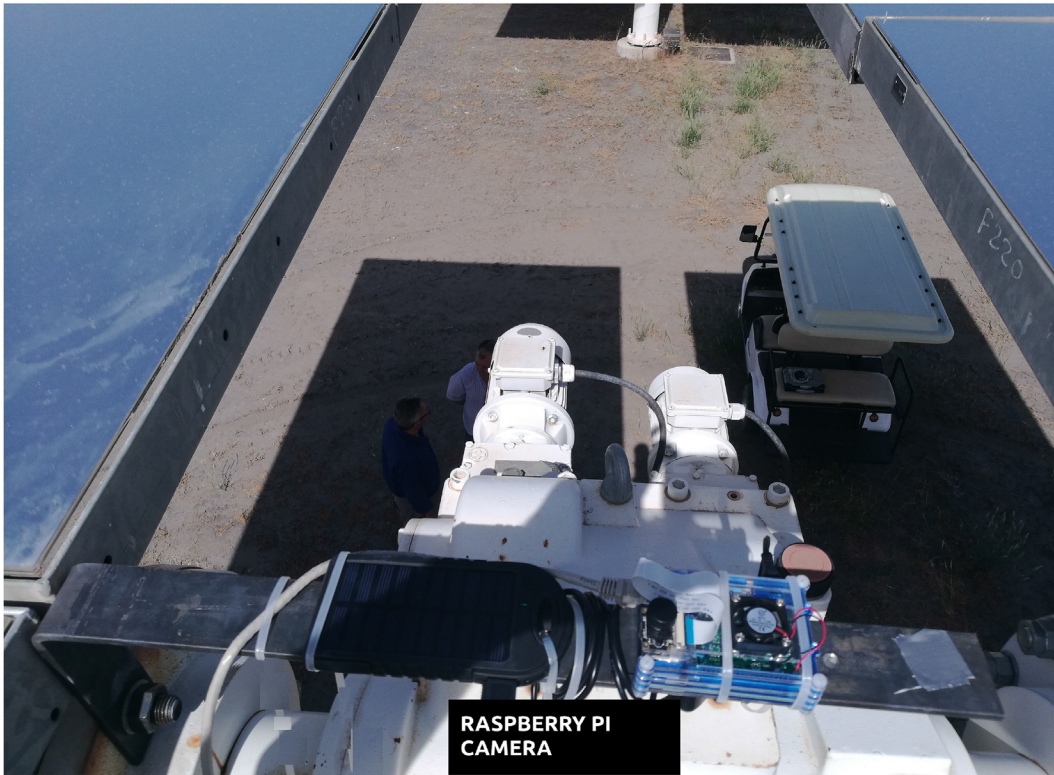


Fig. 6. Hardware assembly.



Fig. 7. Cesa scheme.

camera sensor size 3.76x2.74 mm,  $f$  2.35 mm [29]), the solar tracking uncertainty of the new approach based on CNN according to Eq. (1) is 2 mrad. Note that with this configuration, a camera resolution of 1600x1200 px, would reduce the uncertainty below 1 mrad.

The first image set was taken while the heliostat pointed directly at the Sun in tracking mode, with this configuration the mean differences between  $\overrightarrow{V_a}$  and  $\overrightarrow{V_s}$  during the test can be considered

as the constant aiming error and can be corrected in the following analyses. Fig. 8 shows one of these pictures analyzed and the differences in pixels between  $\overrightarrow{V_s}$  (red cross) and  $\overrightarrow{V_a}$  (blue star).

The second image set was taken in tracking mode where the white target is the aiming objective. Fig. 9.a shows the initial instant, where the white target is being focused by an heliostat and the modified heliostat (heliostat with new hardware) is also sent to focus at the white target. In Fig. 9.b, the concentrated solar

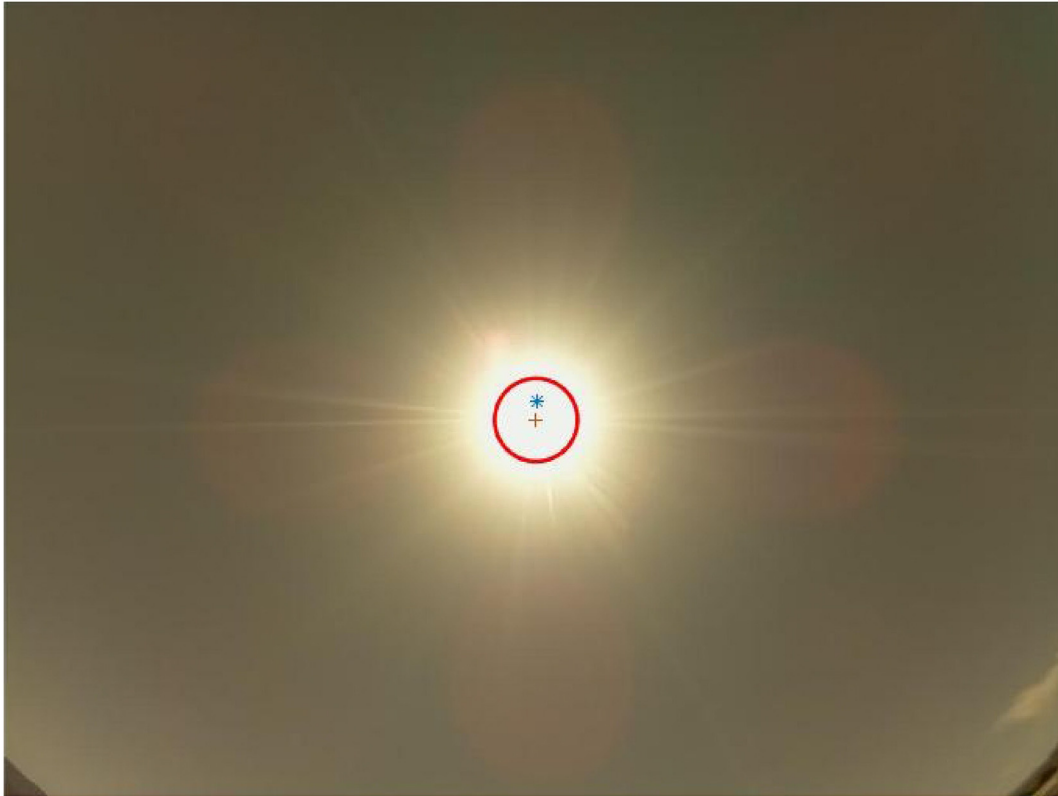


**Fig. 8.** Aiming error.

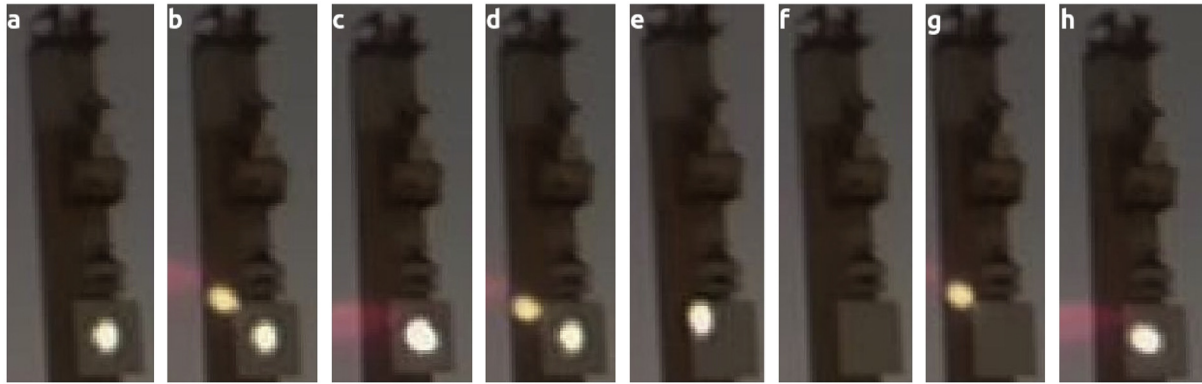


**Fig. 9.** Test captions.

distribution due to the modified heliostat is in transition through the upper corner to the center of the white target. Next, the concentrated solar distribution of each overlaps in the center of the white target (Fig. 9c). After that, the first heliostat was sent out of the white target (Fig. 9d), remaining the modified heliostat. The last pictures in Fig. 9 show how the modified heliostat was sent out and then sent back to the white target center. The data computed by the traditional STS of the modified heliostat was in turn stored for further analysis with the main goal to compare with the Convolutional Neural Networks object detector results.

#### 4. Results

The previous image sets were analyzed with an algorithm developed for this purpose. The algorithm analyzes the images one

by one by means of the Convolutional Neural Networks object detector to find all the classes to develop the Sun tracking task properly, as well as to find key parameters such as clouds or shadows and blocks originated by other heliostats. Results due to the analysis of the last image set are shown in Fig. 10. Blue and red lines represent the tracking error obtained through the analysis of the Convolutional Neural Networks object detector and data stored in the SCADA of the modified heliostat. The grey line represents the difference between both signals (CNN-SCADA Error).

It can be noted that the tracking error measured by the two methods (CNN object detector and traditional SCADA) behave in the same way for both axes, the widest differences (15 mrad) are seen in large transitions when the heliostat enters or leaves the tracking mode. Therefore, although they are important, these differences are not the most relevant for the heliostat performance. In these

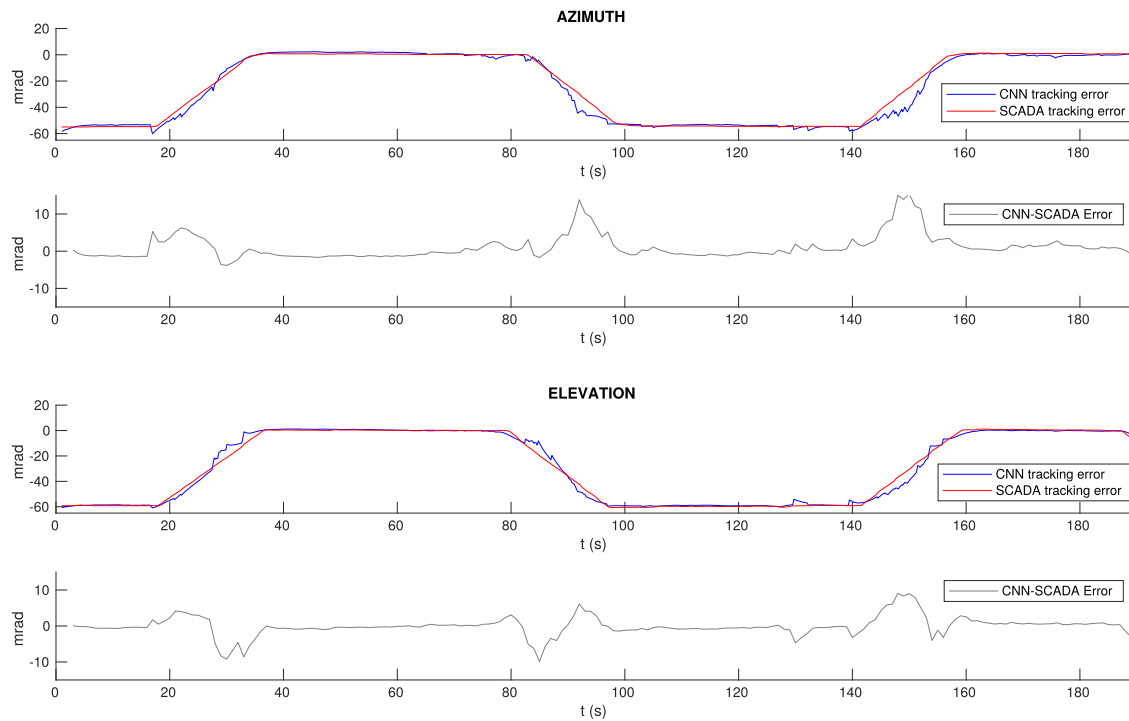


**Fig. 10.** Tacking signals and error evolution.

periods, the CNN-SCADA error patterns suggest that they could be caused by the deformation of the structure during large movements, when the heliostat rotates at the highest speed. Note that the STS based on CNN is less affected by structural deformations due to its position is directly determined by the concentrator optical axis, and not from the rotation axes.

The differences kept below 3 mrad for steady-state and narrow movements, besides at 130 s and 140 s time instants, when the error increased up to 4 mrad due to an inaccurate Sun detection caused by an incorrect camera set up.

The tracking error is measured by Convolutional Neural Networks object detector and traditional STS SCADA in pixel and mrad respectively, but in Fig. 10 both are shown in the same unit. Pixel and mrad are related by the camera sensor resolution, FOV and the geometry of the system (slant range and relative position), although the objective of the new approach is to perform the control directly with the error measured in pixel to avoid the individual configuration of the STS in a large system.

Nevertheless, the method proposed in this paper provides similar error values to the traditional method, with an error within the acceptable range for most applications. Better Convolutional Neural Networks object detector training and higher resolution cameras would significantly reduce this difference with the traditional system. The use of camera filters and fine-tuning of the camera setting may improve the performance to a higher level of precision.

Furthermore, it can be noted that the operation of other systems that jointly use certain parts of the system (white target), does not disturb the normal operation of the STS proposed.

## 5. Conclusions

According to the results obtained in the tests, it can be concluded that the new approach proposed for STSs is valid, fully functional and shows a wide margin for improvement. The new

approach is independent of solar technology, system size, location and time. It is not affected by *aiming errors* like pedestal tilt, wind loads or apparent Sun position. Furthermore, the proposed approach provides advantages such as the ability of cloud, block and shadow detection, atmospheric attenuation or concentrated solar radiation measurement, which can improve the control strategies of the system and therefore the system performance. The new approach combined with traditional control techniques makes possible closed-loop control schemes.

In addition, provide the system with a versatile and cheap microprocessor, enables to reduce costs related to the STS and other aspects such as communication or first start up and gives greater autonomy and flexibility.

Future work includes testing these methods and algorithms and performing extensive training of the neural network in order to further improve the obtained results while reduce the computational cost. Another important task is the autonomous control of an heliostat using the new presented tracking method.

## Acknowledgments

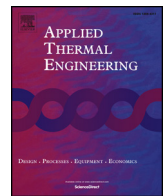
This work has been funded by the National R + D + i Plan Project DPI2014-56364-C2-2-R of the Spanish Ministry of Economy, Industry and Competitiveness and ERDF funds.

## References

- [1] P.D. United Nations, Department of Economic and Social Affairs, World Population Prospects the 2017 Revision Key Findings and Advance Tables, World Population Prospects the 2017, 2017, pp. 1–46, <https://doi.org/10.1017/CBO9781107415324.004>.
- [2] EIA, International Energy Outlook 2017 Overview, 2017 (2017), U.S. Energy Information Administration IEO, 2017, p. 143. arXiv:EIA-0484(2013), [www.eia.gov/forecasts/ieo/pdf/0484\(2016\).pdf](http://www.eia.gov/forecasts/ieo/pdf/0484(2016).pdf).
- [3] N. Kannan, D. Vakeesan, Solar energy for future world: - a review, Renew. Sustain. Energy Rev. 62 (2016) 1092–1105, <https://doi.org/10.1016/j.rser.2016.05.022>.
- [4] O.H. Hohmeyer, S. Bohm, Trends toward 100% renewable electricity supply in

- Germany and Europe: a paradigm shift in energy policies, Wiley Interdiscip. Rev. Energy Environ. 4 (1) (2015) 74–97, <https://doi.org/10.1002/wene.128>.
- [5] M.Z. Jacobson, M.A. Delucchi, G. Bazouin, Z.A. Bauer, C.C. Heavey, E. Fisher, S.B. Morris, D.J. Piekutowski, T.A. Vencill, T.W. Yeskoo, 100% clean and renewable wind, water, and sunlight (wws) all-sector energy roadmaps for the 50 United States, Energy Environ. Sci. 8 (7) (2015) 2093–2117.
- [6] H. Scheer, The Solar Economy: Renewable Energy for a Sustainable Global Future, Routledge, 2013.
- [7] N.J. Sheikh, D.F. Kocaoglu, L. Lutzenhiser, Social and political impacts of renewable energy: literature review, Technol. Forecast. Soc. Change 108 (2016) 102–110, <https://doi.org/10.1016/j.techfore.2016.04.022>.
- [8] C.-Y. Lee, P.-C. Chou, C.-M. Chiang, C.-F. Lin, Sun tracking systems: a review, Sensors 9 (5) (2009) 3875–3890, <https://doi.org/10.3390/s90503875>.
- [9] G. Prinsloo, R. Dobson, Solar Tracking, 2015, <https://doi.org/10.13140/RG.2.1.4265.6329/1>.
- [10] H. Mousazadeh, A. Keyhani, A. Javadi, H. Mobli, K. Abrinia, A. Sharifi, A review of principle and sun-tracking methods for maximizing solar systems output, Renew. Sustain. Energy Rev. 13 (8) (2009) 1800–1818, <https://doi.org/10.1016/j.rser.2009.01.022>.
- [11] W. Nsengiyumva, S.G. Chen, L. Hu, X. Chen, Recent advancements and challenges in solar tracking systems (STS): a review, Renew. Sustain. Energy Rev. 81 (August 2017) (2018) 250–279, <https://doi.org/10.1016/j.rser.2017.06.085>.
- [12] E.F. Camacho, M. Berenguel, F.R. Rubio, D. Martínez, Control issues in solar systems, in: Control of Solar Energy Systems, Springer, 2012, pp. 25–47.
- [13] M. Chiesi, E. Franchi Scarselli, R. Guerrieri, Run-time detection and correction of heliostat tracking errors, Renew. Energy 105 (2017) 702–711, <https://doi.org/10.1016/j.renene.2016.12.093>.
- [14] A. Jenkins, The Sun's position in the sky, Eur. J. Phys. 34 (3) (2013) 633–652, <https://doi.org/10.1088/0143-0807/34/3/633>, arXiv:1208.1043.
- [15] Z. El Kadmiri, O. El Kadmiri, L. Masmoudi, M.N. Bargach, A novel solar tracker based on omnidirectional computer vision, J. Solar Energy 2015 (2015) 1–6, <https://doi.org/10.1155/2015/149852>.
- [16] A. Ruelas, N. Velázquez, L. González, C. Villa-Angulo, O. García, Design, implementation and evaluation of a solar tracking system based on a video processing sensor, Int. J. Adv. Res. Comput. Sci. Software Eng. 3 (10).
- [17] J.A. Carballo, J. Bonilla, J. Fernandez, G. Garcia, Sistema de captacion solar mediante tecnicas de vision artificial ES P2018300773, 2018.
- [18] J. A. Carballo, J. Bonilla, L. Roca, M. Berenguel, New Low-cost Solar Tracking System Based on Open Source Hardware for Educational Purposes. Under review.
- [19] J. Ballestrín, R. Monterreal, Hybrid heat flux measurement system for solar central receiver evaluation, Energy 29 (5–6) (2004) 915–924, [https://doi.org/10.1016/S0360-5442\(03\)00196-8](https://doi.org/10.1016/S0360-5442(03)00196-8).
- [20] C.K. Ho, S.S. Khalsa, A photographic flux mapping method for concentrating solar collectors and receivers, J. Sol. Energy Eng. 134 (4) (2012), 041004, <https://doi.org/10.1115/1.4006892>.
- [21] J. Ballestrín, R. Monterreal, M.E. Carra, J. Fernandez-Reche, J. Barbero, A. Marzo, Measurement of solar extinction in tower plants with digital cameras, in: AIP Conference Proceedings 1734, 2016, <https://doi.org/10.1063/1.4949212>.
- [22] S. Ren, K. He, R. Girshick, J. Sun, Faster R-CNN: towards real-time object detection with region proposal networks, IEEE Trans. Pattern Anal. Mach. Intell. 39 (6) (2017) 1137–1149, <https://doi.org/10.1109/TPAMI.2016.2577031>, arXiv:1506.01497.
- [23] MATLAB Version (R2017b), The Mathworks, Inc., Natick, Massachusetts, 2017.
- [24] The MathWorks Inc., Computer Vision System Toolbox, (Mathworks), 2013. <http://www.mathworks.com/products/computer-vision/>.
- [25] O. Russakovsky, J. Deng, H. Su, J. Krause, S. Satheesh, S. Ma, Z. Huang, A. Karpathy, A. Khosla, M. Bernstein, A.C. Berg, L. Fei-Fei, ImageNet large scale visual recognition Challenge, Int. J. Comput. Vis. 115 (3) (2015) 211–252, <https://doi.org/10.1007/s11263-015-0816-y>, arXiv:1409.0575.
- [26] C.D. Lee, H.C. Huang, H.Y. Yeh, The development of sun-tracking system using image processing, Sensors 13 (5) (2013) 5448–5459, <https://doi.org/10.3390/s130505448>.
- [27] G.J. Kolb, S. a. Jones, M.W. Donnelly, D. Gorman, R. Thomas, R. Davenport, R. Lumia, Heliostat cost reduction study, in: ASME Energy Sustainability Conference SAND2007-3 (June), 2007, pp. 1–158, <https://doi.org/10.2172/912923>.
- [28] J.B. Blackmon, Parametric determination of heliostat minimum cost per unit area, Sol. Energy 97 (2013) 342–349, <https://doi.org/10.1016/j.solener.2013.08.032>.
- [29] Raspberry Pi, Raspberry Pi, 2013.
- [30] G. García, A. Egea, M. Romero, J.A. Gázquez, The stand-alone heliostat first operation results, in: Proceedings of the 10th SolarPACES International Symposium on Solar Thermal Concentrating Technologies, 2000, pp. 165–170.
- [31] R. Real-Calvo, A. Moreno-Munoz, V. Pallares-Lopez, M.J. Gonzalez-Redondo, I.M. Moreno-Garcia, E.J. Palacios-Garcia, Sistema Electrónico Inteligente para el Control de la Interconexión entre Equipamiento de Generación Distribuida y la Red Eléctrica, Revista Iberoamericana de Automática e Informática Industrial RIAI 14 (1) (2017) 56–69, <https://doi.org/10.1016/j.riai.2016.11.002>.

## A.5. Parabolic trough collector field dynamic model: Validation, energetic and exergetic analyses



## Research Paper

## Parabolic trough collector field dynamic model: Validation, energetic and exergetic analyses

Jose A. Carballo<sup>a,c,\*</sup>, Javier Bonilla<sup>b,c</sup>, Manuel Berenguel<sup>a</sup>, Patricia Palenzuela<sup>b,c</sup><sup>a</sup> Universidad de Almería, Ctra. Sacramento, s/n, La Cañada, 04120 Almería, Spain<sup>b</sup> CIEMAT-Plataforma Solar de Almería, Ctra. de Senés s/n Tabernas, 04200 Almería, Spain<sup>c</sup> CIESOL Research Centre for Solar Energy, UAL-PSA.CIEMAT Joint Centre, Almería, Spain

## HIGHLIGHTS

- Dynamic, highly customizable PTC field model.
- The key sources of energy and exergy consumption have been revealed.
- Model implemented in the equation-based object-oriented modeling language Modelica.
- A simulation tool, open source and freely available, to reproduce the results.

## ARTICLE INFO

## Keywords:

Solar thermal  
Modelica  
Process heat  
Transient behavior  
Parabolic trough

## ABSTRACT

Nowadays, a large part of the scientific community efforts, dedicated to Concentrated Solar Power (CSP) technologies, are focused on improving the efficiency and reducing the costs. This work presents a flexible, highly customizable, dynamic model that simulates the transient thermal behavior of a solar field in order to use it for optimization, performance evaluation and control tasks purposes. The model is based on the detailed physical principles described in a previously paper which has been extended with an exergetic approach, recommendation made by the author of the previous paper in order to improve the model. The model has been developed using the ThermoCycle library and implemented in the equation-based object-oriented modeling language Modelica. An experimental campaign has been carried out in a real facility in order to calibrate and validate the model. Energetic and exergetic analysis are also presented in this work.

## 1. Introduction

Significant developments in solar technologies are expected in the next few decades [1], making solar energy even more attractive. These advances will be focused on: improving the efficiency of solar collectors (particularly for small capacity systems), carrying out efficient operation and control strategies and development of suitable methods for the integration of the solar energy with the current electricity grid and district heating [2].

Focusing on thermal CSP systems, there are mainly four technologies: parabolic dish, linear Fresnel, central tower and Parabolic Trough Collectors (PTCs). This last technology allows concentrating the direct solar irradiance over a linear focus where an absorber tube cooled by a Heat Transfer Fluid (HTF) collects the thermal energy, transforming the solar radiation into thermal energy. PTC technology has experienced a great success at commercial level [3–5]. Although the potential of this

technology for process heat, it has been mainly used for electric power generation. The application field of PTCs for process heat include all processes which demand heat up to 400 °C [6]. Some industrial applications include air heating, desalination, refrigeration, chemistry and pumping. The temperature demanded by the majority of industrial processes is lower than 250 °C [7] where small aperture PTCs are suitable [8], as the installation used in the present work.

The PTC models state of the art reveals that there is still room to improve PTC thermal models [9]. Two examples are the combination of new thermodynamic models with the purpose of evaluating essential parameters of PTCs and the discard of important parameters to reduce the simulation time and computational efforts.

Recent works in the modeling of PTCs [10–16], are implemented in one of the main computational softwares used for the implementation of this type of systems: Engineering Equation Solver, Computational Fluid Dynamic tools and Modelica [17] tools. Among all, there are

\* Corresponding author.

E-mail addresses: [jcarballo@psa.es](mailto:jcarballo@psa.es) (J.A. Carballo), [jbonilla@psa.es](mailto:jbonilla@psa.es) (J. Bonilla), [beren@ual.es](mailto:beren@ual.es) (M. Berenguel), [ppalenzuela@psa.es](mailto:ppalenzuela@psa.es) (P. Palenzuela).

Nomenclature	
0	ambient
1	heat transfer fluid
2	inner wall of the absorber tube
3	outer wall of the absorber tube
4	inner wall of the glass cover
5	outer wall of the glass cover
6	convection to ambient
7	radiation to ambient
A	area
abs	absorbed
°C	Celsius degrees
cond	conduction
conv	convection
CSP	concentrated solar power technologies
CPVT	concentrated hybrid photovoltaic-thermal
CV	control volume
des	destroyed
DNI	direct normal irradiance
Ex	exergy
exp	experimental
FMI	functional mock-up interface
hc	inertia
HTF	heat transfer fluid
I	irradiance
in	inlet
loss	losses
MED	multi effect distillation
out	outlet
PTC	parabolic trough collector
Q	heat
rad	radiated
ref	reference
RMSE	root mean square error
sim	simulated
sol	solar
T	temperature
t	time
WS	wind speed
η	performance
ψ	Petela's index

available dynamic models implemented in Modelica [11,15,16]. The first of them is based on the one dimensional physical model proposed by Forristal [18], which has been adapted for transient simulations using the Modelica standard library. Simulation results presented a good agreement with experimental data. In [15], a PTC Modelica model is coupled to a solar industrial process heat model implemented in TRNSYS and ray-tracing model developed in SolTrace.

Finally, the model presented in [16] is a implementation of the Forristall steady-state thermal model [18] and proposes a dynamic 1D radial energy balance between the HTF and the atmosphere for each Control Volume (CV) in which the absorber tube is discretized. The model relies on physics-based equations and heat transfer mechanisms: conduction, convection, radiation, absorption and material thermal capacity, being the incident solar irradiance on the receiver area, optical and thermal losses effects also considered.

Despite the amount of works cited, they do not incorporate an approach from the point of view of the exergy analysis (or second law analysis), which has proven to be a powerful tool that can help to find inefficiencies and improve the performance in power generation systems [19]. Recently, it has proposed mathematical approaches for the exergy analysis of PTC [9,20] based on their own mathematical models. An exergetic approach in transient models could improve the operation and control strategies for plants, as well as can improve the system performance through the analysis of the nominal operating conditions.

As previously commented, the advances in PTC should be focused on the efficiency of solar collectors, operation and control strategies and in the development of suitable methods for integration with the current electricity grid and district heating [2]. The present work focuses on improving and validating the steady-state and dynamic response of a versatile PTC model [21] based on the well-known *Forristal* approach [18]. In addition, an energetic and exergetic analysis of a small PTC field has been carried out using this model. Furthermore, the work proposes a new methodology to analyze the performance from the exergetic point of view and makes available a free simulation tool based on the highly configurable model with which to analyze other issues or facilities.

The paper is organized as follows: firstly, a brief description of the solar facility used in this paper is included in Section 2. Secondly, Section 3 is devoted to the development of the PTC model. The energetic and exergetic analyses are performed in Section 4. Then Section 5 summarizes the experiments carried out in a real installation to get data for model calibration and validation purposes (Section 6). The



Fig. 1. Nep field.

paper ends with some concluding remarks (Section 7).

## 2. Solar facility description

The PTC field considered in this paper is erected in *Plataforma Solar de Almería* and integrated in the *Aquasol* system (Fig. 1). The PTC field is composed by small PTC PolyTrough 1200 units, manufactured and supplied by NEP Solar Pty Ltd [22]. The PTCs are disposed in 4 parallel rows, each one composed by two collectors in series. The PTC features are shown in Table 1. The HTF used in this field is Therminol 55 thermal oil [23]. *Aquasol* PTC field is equipped with automatic valves, pump, air cooler and a large sensor network. The field is monitored and controlled by a control and data acquisition system (Fig. 2). Due to the experimental nature of the installation, numerous operational parameters can be precisely controlled HTF flow, pressure or temperature.

## 3. The PTC model

The mathematical model of the NEP solar field has been developed using *Modelica* [17] as the modelling language and it has been implemented in *Dymola* 2017 [24]. Modelica is a powerful object oriented language for complex physic systems modeling that allows a flexible model declaration, and an efficient and easy maintainable code. The simulations were carried out in a laptop equipped with a i5 dual core processor and 8 Gb of RAM. The numerical solver used was DASSL [25] with relative and absolute tolerances of  $10^{-4}$ .

As commented before, the proposed model is based on the *Forristal* model [18], which focuses on the energy balance in a CV between the HTF and the atmosphere taking into account the concentrated solar flux

**Table 1**  
Nep field technical data [22,10].

Collector surface	Absorber
Aperture Area (m <sup>2</sup> )	28.8
Aperture (m)	1.2
Focal (m)	0.65
Rim angle (°)	50
Reflectivity (%)	>89
Support Material	Galvanised steel Aluminum
Cover	Field
Length (m)	2
Diameter (mm)	45
Thickness (mm)	3
Vacuum	No
Glass transm. (%)	89
Material	Borosilicate glass
Aperture Area (m <sup>2</sup> )	28.8
Aperture (m)	1.2
Focal (m)	0.65
Rim angle (°)	50
Reflectivity (%)	>89
Support Material	Galvanised steel Aluminum
Cover	Field
Length (m)	2
Diameter (mm)	45
Thickness (mm)	3
Vacuum	No
Glass transm. (%)	89
Material	Borosilicate glass
Length (m)	12
Diameter (mm)	28
Thickness (mm)	1.5
Selective coating	Black chrome
Absorptance (%)	93
Material	AISI 304 L

incident on the receiver area, the optical and thermal losses. The main heat transfer mechanism inside the receiver are considered (Fig. 3), as well as some assumptions instead of volumetric solar absorption, incompressible fluid and non uniformity due to discretization [18,16].

The transient effects are included in the modeling by means of differential equations in time, since they have a great impact on the results. Incorporating fully dynamic behavior in the modeling of physical components usually requires to model the corresponding control system in a reasonable level of detail. The present approach reveals a deep insight into the process and can be used in optimization tasks [16]. It is highly customizable and can be used to model any kind of PTC solar field. Also the model has been included in the open-source

ThermoCycle [26,21] Modelica library, and it is suitable for the modeling of small thermo-hydraulic systems.

This approach has been completed with an exergetic development which allows: performing analyses based on the exergy balance in transient and steady state, identifying some performance limitations and recognizing components that allows an improvement of the model.

#### 4. Energetic and exergetic analyses

The exergy balance in a CV is described by Eq. (1).

$$\frac{dEx}{dt} = \dot{Ex}_{sol} - \dot{Ex}_{htf} - \dot{Ex}_{loss} - \dot{Ex}_{hc} - \dot{Ex}_{des}, \quad (1)$$

where  $\dot{Ex}_{sol}$  represents the exergy contained in the solar irradiance concentrated by the collector ( $I_c$ ) and intercepted by the CV absorption surfaces ( $A_{cv}$ ). This exergy flow could be expressed according to Eq. (2), in where Petela's index  $\psi$  [27] represents the maximum useful work from solar radiation for a surface at a certain temperature ( $T_n$ ) and the sun surface temperature ( $T_{sol}$ ).  $\psi$  was redefined and modified by Parrot which introduces the effect of the sun cone angle ( $\delta$ ) [28].

$$\dot{Ex}_{sol} = I_c A_{cv} \psi \quad (2)$$

$$\psi = 1 - \frac{4}{3} \frac{T_n}{T_{sol}} (1 - \cos\delta)^{\frac{1}{4}} + \frac{1}{3} \left( \frac{T_n}{T_{sol}} \right)^4 \quad (3)$$

$\dot{Ex}_{htf}$  in Eq. (1) represents the HTF exergy differences between the input and output flows for a CV.

$$\dot{Ex}_{htf} = \dot{m}(ex_{out} - ex_{in}) \quad (4)$$

Exergy contained in any heat flux ( $\dot{Q}$ ) at a certain temperature ( $T_n$ ) with respect to the dead state at ambient temperature ( $T_0$ ) can be computed by Eq. (5). Therefore exergetic losses ( $\dot{Ex}_{loss}$ ) in Eq. (1) are computed as the exergy contained in the heat losses flux like in any

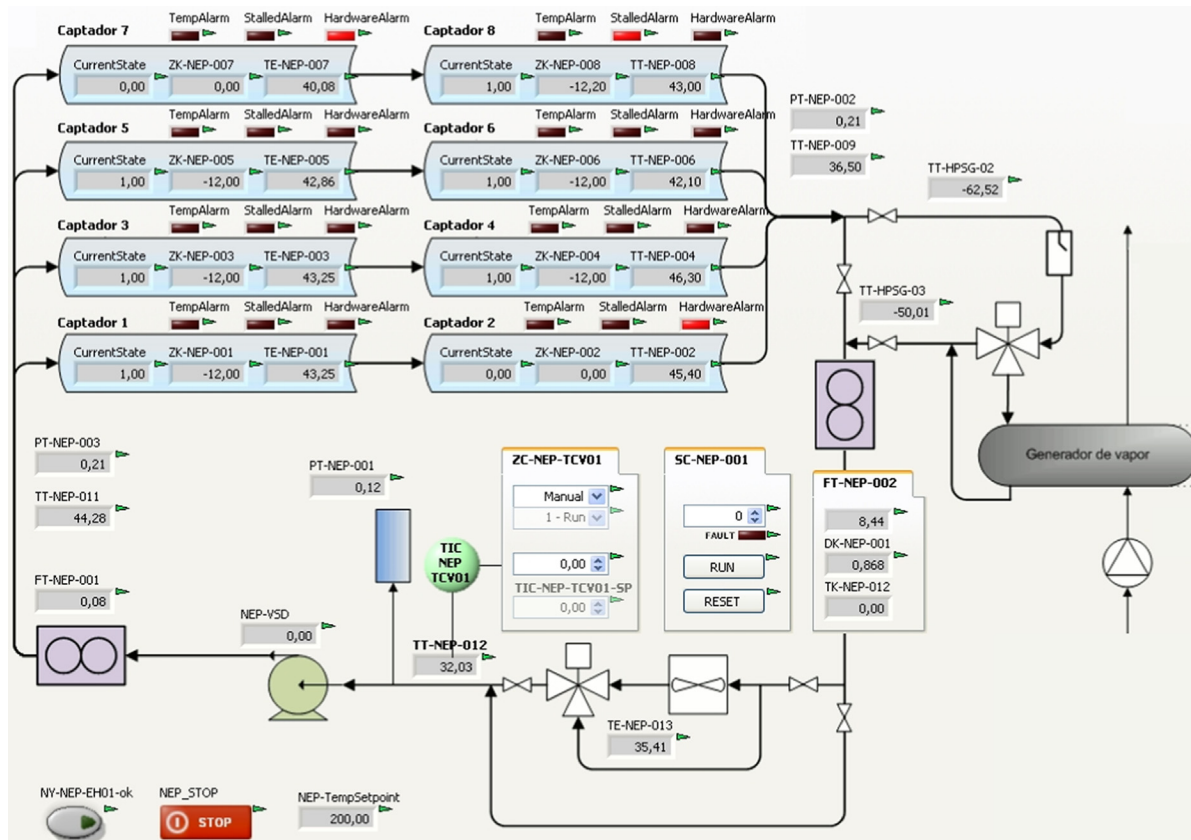


Fig. 2. NEP SCADA system.

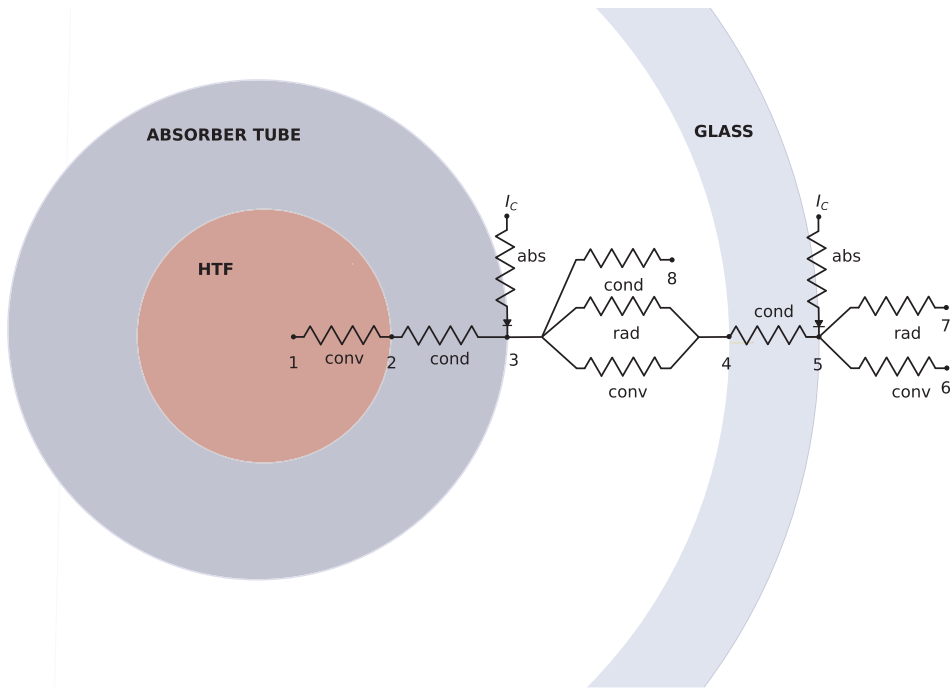


Fig. 3. Thermal model.

other exergy flux.

$$\dot{Ex}_{loss} = \left(1 - \frac{T_0}{T_n}\right)\dot{Q} \quad (5)$$

Similarly, exergy destroyed ( $\dot{Ex}_{des}$ ) in all the heat transfer processes considered (absorption, conduction, radiation and convection) can be obtained as the difference between the exergy contained in the thermal energy flux at a certain temperature, before ( $T_b$ ) and after ( $T_a$ ) the transfer process (Eq. (6)).

$$\dot{Ex}_{des} = \left(1 - \frac{T_b}{T_a}\right)\dot{Q} \quad (6)$$

For the transient state and transformations related to the conduction mechanism, the thermal inertia due to the heat capacity of the materials must be considered. Therefore the exergy balance (Eq. (1)) shows an exergy inertia term ( $\dot{Ex}_{hc}$ ). This term is computed as the difference between the sum of the exergy flows and exergy destroyed in this heat transfer processes.

The evaluation of the performance is carried out by the calculation of the total thermal performance ( $\eta_{th}^{total}$ ) and the absorber thermal performance ( $\eta_{th}^{abs}$ ). The total performance ( $\eta_{th}^{total}$ ) is defined as the ratio between the thermal energy increment in the HTF and the solar radiation on the PTC aperture area (Eq. (7)). The absorber thermal performance is defined as the relationship between the thermal energy increment in the HTF and the concentrated solar radiation absorbed in the receiver tube surface (Eq. (10)), taking into account the effects of the thermal inertia associated with the heat capacity.

into account.

$$\eta_{th}^{total} = \frac{\dot{Q}_{htf}}{\dot{I}\cos\theta A_{ref} + \dot{Q}^{hc}} \quad (7)$$

In where  $\dot{I}\cos\theta A_{ref}$  represent the product of the direct normal irradiance, the incident angle cosine and the aperture area of the collector or reference area respectively.

$$\eta_{th}^{abs} = \frac{\dot{Q}_{htf}}{\dot{Q}_{sol3}^{abs} + \dot{Q}_{32}^{hc}} \quad (8)$$

In Eq. (7) and thereafter, subindices correspond to thermal energy or exergy flows between points in Fig. 3.

The total exergy performance ( $\eta_{ex}^{total}$ ) can be defined (Eq. (9)) as the ratio between the exergetic increment in the HTF flux and the exergetic content in the solar radiation that reaches the collector aperture. Similarly the absorber exergy performance ( $\eta_{ex}^{abs}$ ) is defined as the relationship between the exergetic increment in the HTF and the exergy solar radiation absorbed in the receiver tube surface (Eq. (10)), taking into account the effects of the thermal inertia.

$$\eta_{ex}^{total} = \frac{\dot{Ex}_{htf}}{\dot{I}\cos\theta A_{ref}\psi + \dot{Ex}^{hc}} \quad (9)$$

$$\eta_{ex}^{abs} = \frac{\dot{Ex}_{htf}}{\dot{Ex}_{sol3}^{abs} + \dot{Ex}_{32}^{hc}} \quad (10)$$

These exergy performance ratios not take into account directly the

**Table 2**  
Ranges of operation during the test.

	Sensor	Symbol	Unit	Uncertainty	Min	Max	Nominal
Inlet temperature	TT-NEP-011	$T_{in}$	°C	± 0.4	–	–	200
Outlet temperature	TT-NEP-009	$T_{out}$	°C	± 0.4	–	230	230
Amb. temperature	TT-DES-030	$T_0$	°C	± 0.4	-10	–	30
Inlet flow	FT-NEP-001	$\dot{q}_1$	m³/h	± 0.01	4	12	8
DNI	RE-SF-001	$DNI$	W/m²	± 1	–	–	900
Wind sp.	NEP-WS	$WS$	m/s	± 0.1	–	–	2

exergy lost and destroyed, which can be helpful to determine thermal inefficiencies and operational strategies, specially for transient states. A third exergy performance that takes these effects into account is proposed in the present study (Eq. (11)).

$$\eta'_{ex} = 1 - \frac{\dot{Ex}_{des} + \dot{Ex}_{loss}}{\dot{Ex}_{sol3}^{abs} + \dot{Ex}_{32}^{hc}} \quad (11)$$

## 5. Experimental campaign

Mathematical models must be validated to estimate the quality of the predictions, by comparing such predictions with data obtained from test campaigns. In this section, the test campaign carried out in *NEP* solar field to validate the dynamic model in steady and transient states, is described.

The six main responsible variables for the changes in the thermal behavior of the *PTC* field are: Direct Normal Irradiance (*DNI*), ambient temperature ( $T_0$ ), wind speed (*WS*), inlet and outlet temperature and *HTF* flow rate in the *PTC* field ( $T_{in}$ ,  $T_{out}$  and  $\dot{q}_1$ ), see Table 2 and Fig. 2. The three last are manipulable variables in the *PTC* plant and are closely related to *HTF* outlet temperature ( $T_{out}$ ). *DNI*, ambient temperature, and wind speed are disturbances that can not be controlled. The most meaningful outputs are *HTF* field outlet temperature and flow rate. All these variables are the most relevant variables from the control, optimization and process operation point of view.

Heat flux and exergy flux are the main magnitudes used to analyze the performance in the present work. Considering the uncertainty of the measured variables and the last significant number of the thermodynamic properties provided by the *HTF* manufacturer [23] as uncertainty values, the uncertainty associated with heat flux and exergy flux values for the *HTF* is 10% in nominal conditions.

Three test blocks under different set points were designed to determine the agreement between the experimental and simulation results. The operational parameter was fixed until a steady state was reached after modifying the set points.

The first block is composed by three tests carried out on 22nd, 23rd and 28th June and were focused on the *PTC* solar field thermal behavior changes due to the *HTF* inlet flow rate  $\dot{q}_1$ . In this test block,  $\dot{q}_1$  was modified throughout the whole range in increments of 1 m<sup>3</sup>/h, setting  $T_{out}$  at 230 °C and modifying  $T_{in}$ . Finally, the  $\dot{q}_1$  was modified from its nominal value to the maximum and then it was set to its minimum value.

The aim of the second test block, carried on from 29th June to 11th July, is to study the response due to  $T_{in}$  changes.  $T_{in}$  was changed in steps of 10 °C for all the operation range for 4, 8 and 12 m<sup>3</sup>/h of *HTF* inlet flow.

Finally, the third test block main goal was to study the system under large *DNI* variations, for example for transients caused by clouds. The solar field was operated on 29th July under nominal conditions and *PTCs* were taken out of focus for 1, 5, 10, 15 and 20 min to simulate variations in the *DNI*. During this test campaign, the *PTC* was cleaned and the reflectivity was measured every two days. Note that the operational ranges tested in the three test blocks cover most of the operation points of the *PTC* field.

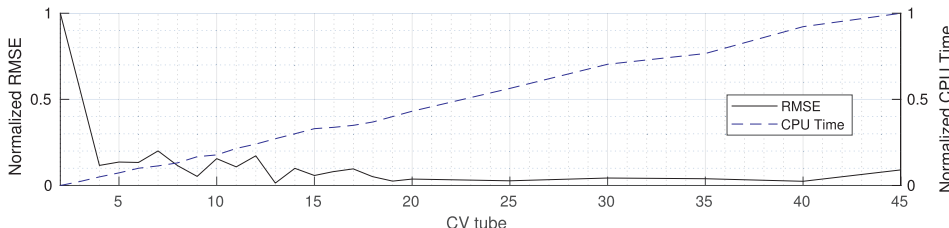


**Fig. 4.** RMSE and CPU Time with respect to CV per tube.

## 6. Results

The level of discretization of the model is studied in Section 6.1. The main results obtained from the model validation process and from energetic and exergetic analyses under nominal and transient conditions are described in Section 6.2 and Section 6.3 respectively. Additionally, a software simulator of the *NEP* solar field, freely available, reproduces all the results considered in this work is presented in (Section 6.4).

### 6.1. Level of discretization

The model sets finite CVs of the absorber tube. The number of CVs per tube ( $n$ ) with respect to the tube length is called spatial resolution and represents a compromise between the model accuracy and the computing effort. In previous studies, the spatial resolutions varies from 0.5 m to 150 m [11], for control, performance and optimization tasks with different *PTC* models. In the present work, the relation between the model accuracy, the computing effort and CV has been studied carrying out several simulations, modifying  $n$  and paying attention to the simulation time required by the computer (*CPU time*) and error variation. The error has been measured by means of the Root Mean Square Error (RMSE, Eq. (12)) between  $T_{out}$  measured and computed ( $T_{out}^{exp}$ ,  $T_{out}^{sim}$ ) during a certain simulation period of time ( $t_{sim}$ ). The results of this study are shown in Fig. 4, where the normalized *CPU time* and normalized RMSE with respect to  $n$  are represented.

$$RMSE = \sqrt{\frac{\sum (T_{out}^{exp} - T_{out}^{sim})^2}{t_{sim}}} \quad (12)$$

According to Fig. 4, the *CPU time* increases linearly with respect to  $n$  in the studied range. On the other hand, discretization levels higher than 20 CVs do not reduce the RMSE significantly, so the  $n$  value should be selected between 2 and 20 for daily simulations of the model depending on the computational time requirements, 10–60 s. Note that the transient model behavior is the most affected by the CV variations. Therefore, in order to have the most accurate results in transitory states, the number of CVs per tube has been set to 20.

In order to reduce the computer effort and improve the results, the measured signals were filtered trying to reduce the noise and smooth the rapid variations in the input data. To that end, a low-pass filter with a cutoff frequency of 10<sup>-2</sup> Hz was used.

### 6.2. Model validation

Model validation was carried out taking into account the experimental campaign described in Section 5 and the five most important variables as inputs (*DNI*,  $T_0$ ,  $T_{in}$ , *WS* and  $\dot{q}_1$ ), which can be easily measured. As  $T_{out}$  has been considered the most important signal for control, optimization tasks and performance analysis, it has been used to compare with experimental data.

Figs. 5–7 show the results of the three validation test blocks, where  $\dot{q}_{1exp}$  represents the inlet *HTF* flow rate,  $T_{in}^{exp}$  represents the experimental inlet temperature,  $T_{out}^{exp}$  and  $T_{out}^{sim}$  represent the experimental and simulated outlet temperatures, respectively. In Fig. 7, *Focus* shows the collector state according to the solar tracking and on focus state. Also, the other three main variables (*DNI*,  $T_0$  and *WS*) are shown in Fig. 8 for the

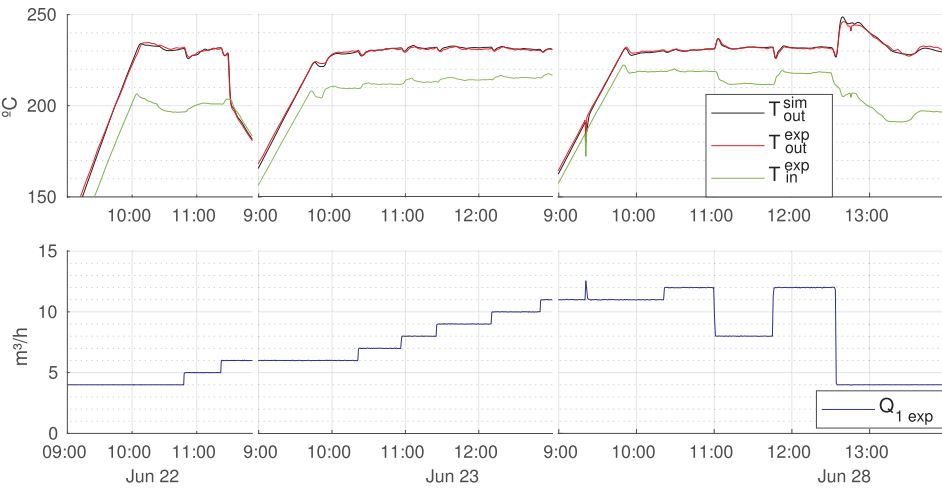


**Fig. 5.** First test block, changes in the HTF inlet flow rate.

three test blocks.

Fig. 5 shows that simulated outlet temperatures ( $T_{out}^{sim}$ ) are very close to experimental ones ( $T_{out}^{exp}$ ) in the whole range tested, even when the  $\dot{Q}_1$  value changes quickly from the highest to the lowest value.

Results reveal that the model maintains its accuracy even with sudden changes in  $T_{in}^{exp}$  regardless of  $\dot{Q}_1$  value (see Fig. 6).

Results of the third test block (Fig. 7) show how the model behaves against changes in the irradiance. When the solar field is defocused, the model slightly overestimate the outlet temperature, which seems to indicate that the thermal losses are underestimated when the *DNI* is low.

Max RMSE and max absolute error obtained in the previous simulations are 1.5 °C and 4.5 °C respectively. A small loss of precision is appreciated when the maximum limit of  $T_{out}$  is reached, although it should be taken into account that in the days in which these tests were carried out, the speed and wind conditions were high and changing.

### 6.3. Thermal and exergetic analyses

In order to analyze the dynamic thermal and exergetic behavior of the PTC solar field, the validated model was simulated considering a *DNI* transient. All the inputs were kept constant except *DNI*, which was varied as follows: from a steady state ( $t_1$ ) at 900 W/m<sup>2</sup> to 0 W/m<sup>2</sup> quickly; after 500 s, it was increased to 300 W/m<sup>2</sup> during 500 s, and after that the system reached a steady state at  $t_2$ . Then, in the instant 1200 s, the *DNI* value was increased until  $t_3$  was reached, when the *DNI* achieved its initial value of 900 W/m<sup>2</sup>.

Simulation results are shown in Fig. 9 and Table 3, according to the

main thermal energy and exergy flows considered in Fig. 3. On the one hand, Fig. 9 shows the evolution of the performance index and the main energetic and exergetic flows. To improve the comprehensibility of the figure, the values have been normalized according to the max values of thermal and exergetic flows respectively ( $Q_{sol}$ ,  $Ex_{sol}$ ), which represent the energy and exergy available in the collector aperture. On the other hand, Table 3 shows energetic and exergetic flows values for each simulation instants previously highlighted ( $t_1$ ,  $t_2$  and  $t_3$ ).

The evaluation of the variables according to heat flows (first graph in Fig. 9) shows how the total thermal inertia of the system ( $\dot{Q}^{hc}$ ) dampens the heat flux exchanged with the HTF flux when the solar heat flux absorbed in the receiver surface ( $\dot{Q}_{sol3}^{abs}$ ) changes. For example, at 200 s, the  $\dot{Q}_{sol3}^{abs}$  decreases with a different speed than  $\dot{Q}_{hf}$  by the action of the  $\dot{Q}^{hc}$ . The opposite effect can be observed at 700 and 1200 s, when the  $\dot{Q}_{sol3}^{abs}$  increases and the  $\dot{Q}_{hf}$  increment is damped by the  $\dot{Q}^{hc}$  effect.

Second graph in Fig. 9 shows the main exergy flows evolution. Note that the exergetic inertia ( $\dot{Ex}^{hc}$ ) dampens the exergetic contribution to HTF ( $\dot{Ex}_{hf}$ ) when the exergy absorbed in the tube surface ( $\dot{Q}_{sol3}^{abs}$ ) changes, in the same way that as in the previous case. The exergy destroyed in these cases increases faster than the  $\dot{Q}_{sol3}^{abs}$  variation. This fact can be explained by Eq. (6) and the increase in temperature difference between the absorber surface and the HTF when  $\dot{Q}_{sol3}^{abs}$  changes.

Both facts extracted from energetic and exergetic analyses are caused by thermal inertia of materials. These effects will be more noticeable in systems with larger collector rows.

Comparing the first two graphics in Fig. 9, it can be noted that the thermal inertia dampens the HTF contributions, but while thermal

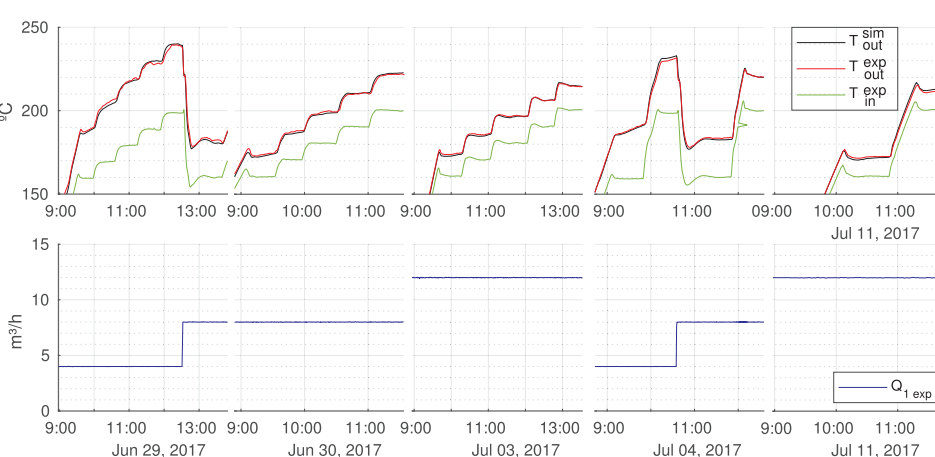


**Fig. 6.** Second test block, changes in the inlet temperature  $T_{on}$ .



Fig. 7. Third test block, changes in the DNI.

analysis reveals that the main thermal inefficiency is caused by thermal losses, the exergetic analysis reveals that the main exergetic inefficiency is caused by the exergy destruction, specially when the  $\dot{Q}_{sol3}^{abs}$  changes quickly.

The third graph in Fig. 9 shows the evolution of the performance indexes previously defined. Regarding the thermal performance indexes, the behavior of both resulted similar. It was observed that the higher the  $\dot{Q}_{sol3}^{abs}$  the better performance, being the variations in  $\dot{Q}_{sol3}^{abs}$  appreciate immediately. In the case of  $\eta_{th}^{abs}$ , it resulted less sensitive to the thermal inertia due to the low impact of  $\dot{Q}_{hc3}$  in such index because of its low value. The exergetic performance indexes  $\eta_{ex}^{abs}$  and  $\eta_{ex}^{total}$ , showed the same behavior with different values.

These four performance indexes behave similarly throughout the simulation, showing some differences in transient periods. All these performance indexes are highly influenced by the behavior of the solar energy absorption in tube surface (point 3 in Fig. 3). Among all performance indexes,  $\eta_{th}^1$  is the only one that showed a different behavior, which indicates that the largest inefficiencies occur during transients periods, when the system is heating up.

The losses and the destruction of exergy are reduced as the radiation is highest and a steady state is reached, (see Fig. 9).

From the results shown in Table 3, it can be extract that the largest flux in  $\dot{Ex}_{sol3}^{abs}$  (once the steady state is reached) reduces the inefficiencies from the exergetic point of view, which leads to achieve the highest transfer rate from the tube surface to the HTF.

On one hand, the thermal analysis revealed that the lower  $Q_{sol}$  available increases the percentage of thermal losses. The largest sources

of thermal losses are those produced by the optical performance, another remarkable losses source are the losses by convection with the environment ( $\dot{Q}_{56}^{conv}$ ) although they are smaller than ones previously mentioned. Note that the convection and radiation losses ( $\dot{Q}_{56}^{conv}$  and  $\dot{Q}_{57}^{rad}$ ) remain almost constant despite the DNI changes.

On the one hand, the exergy analysis showed that the main exergy inefficiency source is the exergy loss due to optical performance. Another relevant exergy loss source is the exergy destroyed in the absorber tube surface ( $\dot{Ex}_{sol}^{abs}$ ). Another relevant exergy loss source is the exergy destroyed in the absorber tube surface, the 50 % of the exergy that reach the tube surface is destroyed in any case, which is due to the low quality (temperature) of the thermal energy at which the solar radiation is transformed in the absorption process. The convection losses with the environment ( $\dot{Ex}_{56}^{conv}$ ) represent a notable source of exergetic losses despite of a lesser extent than the previous ones.

Comparing the thermal energy and exergy available in the collector aperture ( $Q_{sol}$  and  $\dot{Ex}_{sol}$ ) with the thermal energy and exergy transferred to the HTF, it can be noted that the larger  $Q_{sol}$  and  $\dot{Ex}_{sol}$ , the more energy is transferred efficiently, being the inefficiencies therefore minimized.

#### 6.4. NEP field software simulator

With the aim of providing a simulation tool to reproduce the results presented in this work, a simulator of the NEP solar field model has been built. This application can be also useful for studying the system dynamics and to evaluate the influence of the model parameters. This simulator is open source and is freely available at <https://ciemat-psa>.

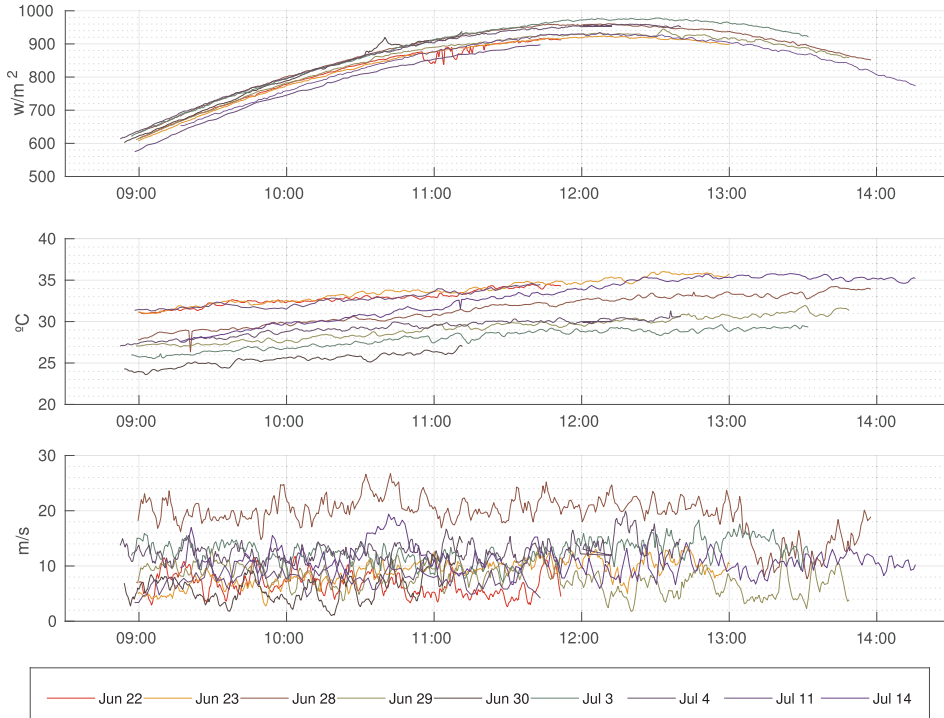


Fig. 8. DNI, ambient temperature and wind speed.

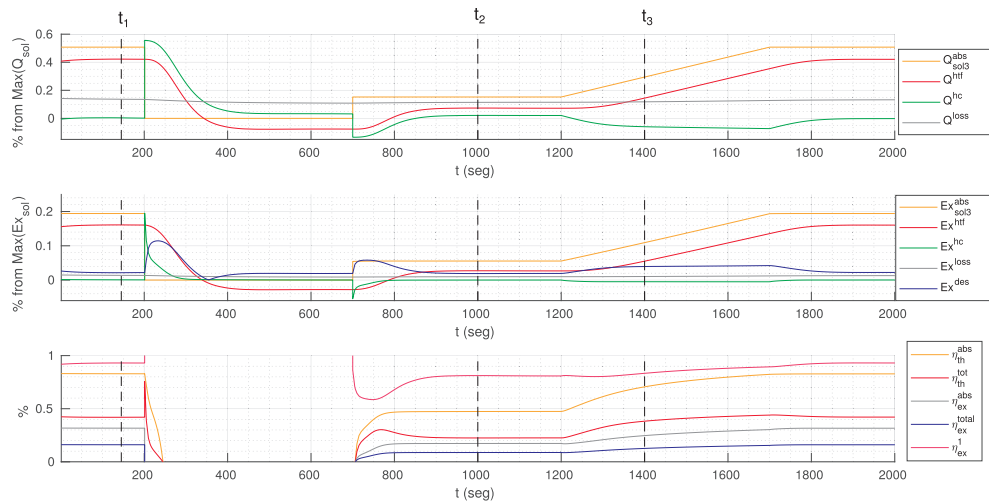


Fig. 9. Thermal and exergetic performance analysis.

[gitlab.io/surf-simulator/projects/NEP](https://gitlab.io/surf-simulator/projects/NEP). Currently, there are binary versions for Linux and Windows platforms.

Fig. 10 shows some screenshots of this simulator. The application includes the Modelica model exported following the Functional Mock-up Interface (FMI) standard, input files, experimental results, diagrams and documentation about the model and experiments.

In the *experiments* menu, any of the operating days, previously discussed in Section 6.2 can be selected. Model parameters are shown in a tree structure on the top left side, where the user can change their default values. Simulation controls are shown on the bottom left side. When the simulation is finished, a particular time instant can be selected by manipulating the simulation bar. Inputs and simulation results are shown on the right top side. Several tabs organize this information in plots. For instance, simulated and experimental outlet temperatures (see Fig. 10a), power and losses (see Fig. 10b), absorber CV temperatures (see Fig. 10c). On the bottom right side, there are three tabs, the *authors* tab provides information about the authors, the *resources* tab can include documents, pictures and external links and the *model & experiment* tab provides additional information. There is a thumbnail in this tab. A diagram of the process is displayed in another window when the thumbnail is clicked. This diagram can graphically

describe the process and displays information about a particular point in time of the simulation, i.e. inlet flow rate and temperatures (see NEP solar field diagram Fig. 10d).

Plots have contextual menus which allow the user to change their appearance and configuration. Additionally, results can be exported as data or graphs to files or the clipboard.

## 7. Conclusions

In this work, a methodology to perform exergetic analyses in PTC fields. This methodology has been implemented in an open-source dynamic model. It can be applied in steady state and transient simulations. Additionally, the PTC field dynamic model has been calibrated and validated with experimental data. The model accurately predicts the outlet fluid temperature (Max RMSE 1.5 °C). A small loss of accuracy is appreciated when estimating the outlet fluid temperate at its highest limit value, which is caused by an underestimation of thermal losses. It must be noticed that during the experimental campaign the wind speed was highly variable.

The spatial resolution employed for this validation was set at 20 CV per absorber tube with a simulation time cost of 60 s per simulation

Table 3

Energetic and exergetic analysis results ( $W$ ).

	$\dot{Q}$			$\dot{E}x$			$\dot{E}x_{des}$		
	$t_1$	$t_2$	$t_3$	$t_1$	$t_2$	$t_3$	$t_1$	$t_2$	$t_3$
$htf$	87534	15206	29946	33236	5599	11381	–	–	–
$21^{hc}$	243	250	–11338	0	0	–7720	36	170	3860
$21^{conv}$	87306	14953	38715	33200	5430	15240	–	–	–
$32^{hc}$	15	–3	–2568	43	0	944	97	3	23
$32^{cond}$	87291	14956	41284	33254	5433	16207	–	–	–
$sol3^{abs}$	105245	31574	61042	40108	11466	22561	64702	19976	38228
$34^{rad}$	4108	3491	3711	1568	1268	1372	2743	2576	2695
$34^{conv}$	13861	13123	13479	5286	4766	4982	1371	1287	1347
$45^{cond}$	17969	16614	17190	2698	2132	2272	–	–	–
$45^{hc}$	504	4096	1573	99	4	–64	212	180	190
$sol5^{abs}$	9787	2936	5677	245	62	124	2192	669	1289
$56^{conv}$	21746	18155	18775	2178	1543	1646	–	–	–
$57^{rad}$	6515	5491	5664	652	467	496	–	–	–
$loss$	120589	51344	84990	102084	31787	59710	–	–	–
$sol$	207360	62208	127270	206501	61950	119770	–	–	–
$hc$	762	4343	–12334	142	4	1008	–	–	–
$des$	–	–	–	–	–	–	71394	24900	47672

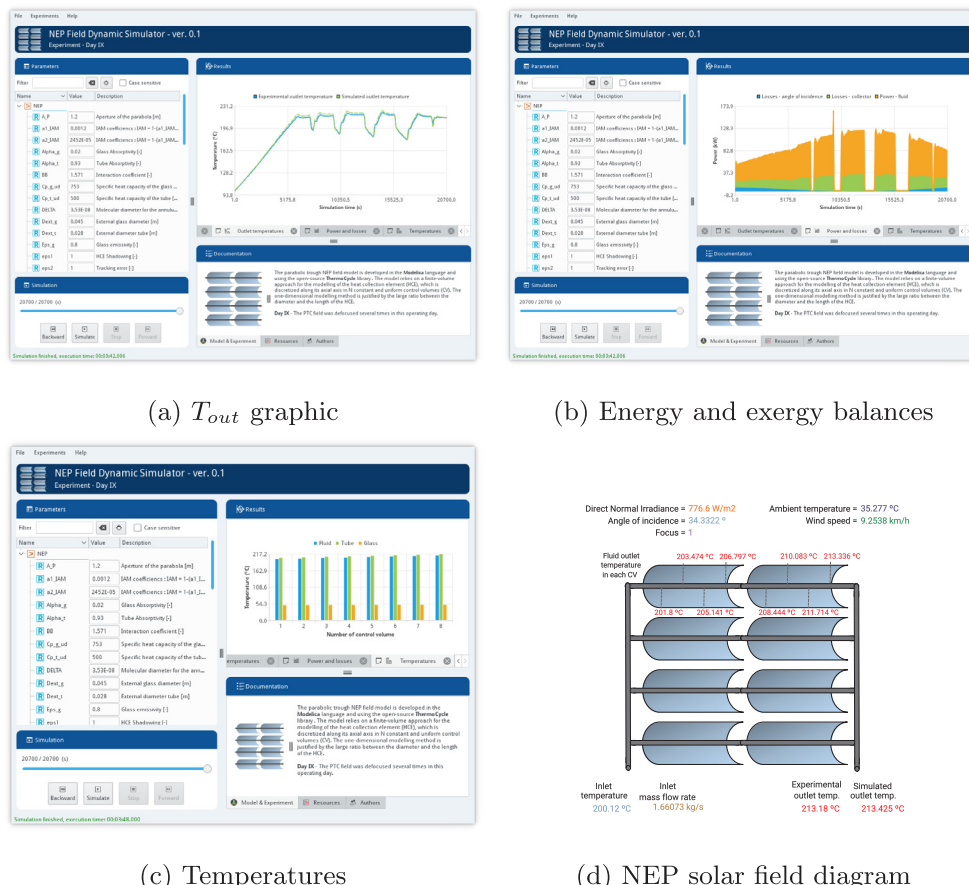


Fig. 10. NEP solar field simulation tool.

day. Nevertheless, the simulation time can be reduced significantly (to less than 10 s) by reducing the spatial resolution and therefore a slight increase in the error of the model.

The energetic and exergetic analyses showed that the highest *DNI* levels improve the thermal and exergetic performance indexes. On the contrary, fast changes in *DNI* values cause a reduction in performance. Thermal performance indexes showed highest values than exergy performance indexes except  $\eta_{ex}^1$ , despite the fact that they showed a very similar behavior during the simulation. The thermal analysis revealed that the largest losses occur in the *DNI* reflection and concentration, while the exergetic analysis pointed out that the exergy destruction in the absorber tube surface due to the low absorber tube surface temperature is another important source of inefficiencies.

## Acknowledgements

This work has been funded by the National R + D + i Plan DPI2014-56364-C2-2-R Spanish Ministry of Economy, Industry and Competitiveness funds.

## References

- [1] M.S. Guney, Solar power and application methods, Renew. Sustain. Energy Rev. 57 (2016) 776–785, <https://doi.org/10.1016/j.rser.2015.12.055>.
- [2] A. Modi, F. Bühlér, J.G. Andreasen, F. Haglind, A review of solar energy based heat and power generation systems, Renew. Sustain. Energy Rev. 67 (2017) 1047–1064, <https://doi.org/10.1016/j.rser.2016.09.075>.
- [3] A. Fernández-García, E. Zarza, L. Valenzuela, M. Pérez, Parabolic-trough solar collectors and their applications, Renew. Sustain. Energy Rev. 14 (7) (2010) 1695–1721, <https://doi.org/10.1016/j.rser.2010.03.012>.
- [4] H.L. Zhang, J. Baeyens, J. Degrève, G. Cacères, Concentrated solar power plants: review and design methodology, Renew. Sustain. Energy Rev. 22 (2013) 466–481, <https://doi.org/10.1016/j.rser.2013.01.032>.
- [5] V.K. Jebasingh, G.M. Herbert, A review of solar parabolic trough collector, Renew. Sustain. Energy Rev. 54 (2016) 1085–1091, <https://doi.org/10.1016/j.rser.2015.10.043>.
- [6] R. Silva, M. Berenguel, M. Pérez, A. Fernández-García, Thermo-economic design optimization of parabolic trough solar plants for industrial process heat applications with memetic algorithms, Appl. Energy 113 (2014) 603–614, <https://doi.org/10.1016/j.apenergy.2013.08.017>.
- [7] P. Horta, I. IhG, Process heat collectors: state of the art and available medium temperature collectors, SolarPaces Annex IV: IEA SHC Task 49.
- [8] R. Silva, M. Pérez, M. Berenguel, L. Valenzuela, E. Zarza, Uncertainty and global sensitivity analysis in the design of parabolic-trough direct steam generation plants for process heat applications, Appl. Energy 121 (2014) 233–244, <https://doi.org/10.1016/j.apenergy.2014.01.095>.
- [9] L. Salgado Conrado, A. Rodríguez-Pulido, G. Calderón, Thermal performance of parabolic trough solar collectors, Renew. Sustain. Energy Rev. 67 (2017) 1345–1359, <https://doi.org/10.1016/j.rser.2016.09.071>.
- [10] S.A. Kalogirou, A detailed thermal model of a parabolic trough collector receiver, Energy 48 (1) (2012) 298–306, <https://doi.org/10.1016/j.energy.2012.06.023>.
- [11] F. Zaversky, R. Medina, J. García-Barberena, M. Sánchez, D. Astrain, Object-oriented modeling for the transient performance simulation of parabolic trough collectors using molten salt as heat transfer fluid, Sol. Energy 95 (2013) 192–215, <https://doi.org/10.1016/j.solener.2013.05.015>.
- [12] I.H. Yilmaz, M.S. Söylemez, Thermo-mathematical modeling of parabolic trough collector, Energy Convers. Manage. 88 (2014) 768–784, <https://doi.org/10.1016/j.enconman.2014.09.031>.
- [13] F.A. Al-Sulaiman, M.I. Zubair, M. Atif, P. Gandhidasan, S.A. Al-Dini, M.A. Antar, Humidification dehumidification desalination system using parabolic trough solar air collector, Appl. Therm. Eng. 75 (2015) 809–816, <https://doi.org/10.1016/j.apithermeng.2014.10.072>.
- [14] E.M. Mokheimer, Y.N. Dabwan, M.A. Habib, S.A. Said, F.A. Al-Sulaiman, Techno-economic performance analysis of parabolic trough collector in Dhahran, Saudi Arabia, Energy Convers. Manage. 86 (2014) 622–633, <https://doi.org/10.1016/j.enconman.2014.06.023>.
- [15] R. Silva, M. Pérez, A. Fernández-García, Modeling and co-simulation of a parabolic trough solar plant for industrial process heat, Appl. Energy 106 (2013) 287–300, <https://doi.org/10.1016/j.apenergy.2013.01.069>.
- [16] A. Desideri, R. Dickes, J. Bonilla, L. Valenzuela, S. Quoilin, V. Lemort, Steady-state and dynamic validation of a parabolic trough collector model using the thermocycle modelica library, Sol. Energy 174 (2018) 866–877, <https://doi.org/10.1016/j.solener.2018.08.026>.

- [17] P. Fritzson, Principles of Object-Oriented Modeling and Simulation with Modelica 3.3: A Cyber-Physical Approach, John Wiley & Sons, 2014.
- [18] F. Russell, 27–Heat transfer analysis and modeling of a parabolic trough solar receiver implemented in engineering equation solver, Natl. Renew. Energy Lab. (2003) 164 NREL/TP-550-34169.
- [19] C. Xu, Z. Wang, X. Li, F. Sun, Energy and exergy analysis of solar power tower plants, Appl. Therm. Eng. 31 (17–18) (2011) 3904–3913, <https://doi.org/10.1016/j.applthermaleng.2011.07.038>.
- [20] R.V. Padilla, A. Fontalvo, G. Demirkaya, A. Martinez, A.G. Quiroga, Exergy analysis of parabolic trough solar receiver, Appl. Therm. Eng. 67 (1–2) (2014) 579–586, <https://doi.org/10.1016/j.applthermaleng.2014.03.053>.
- [21] A. Desideri, A. Hernandez, S. Gusev, M. van den Broek, V. Lemort, S. Quoilin, Steady-state and dynamic validation of a small-scale waste heat recovery system using the ThermoCycle Modelica library, Energy 115 (2016) 684–696, <https://doi.org/10.1016/j.energy.2016.09.004>.
- [22] Nep Solar, <<http://www.nep-solar.com/products/polytrough-1200/>>, 2017.
- [23] Therminol 55, <[http://blueoceanoil.com/wp-content/uploads/2015/04/therminol\\_55.pdf](http://blueoceanoil.com/wp-content/uploads/2015/04/therminol_55.pdf)>, 2017.
- [24] Dassault Systemes Dymola, <https://www.3ds.com/es/productos-y-servicios/catia/productos/dymola/>, 2017.
- [25] L.R. Petzold, A description of DASSL: a Differential/Algebraic System Solver, *Scient. Comput.* (1983) 65–68.
- [26] S. Quoilin, A. Desideri, J. Wronski, I. Bell, V. Lemort, Thermocycle: a modelica library for the simulation of thermodynamic systems, Proceedings of the 10th International Modelica Conference; Lund; Sweden, Linköping University Electronic Press; Linköpings universitet (2014) 683–692, <https://doi.org/10.3384/ecp14096683>.
- [27] R. Petela, Exergy of heat radiation, *J. Heat Transf.* 86 (2) (1964) 187, <https://doi.org/10.1115/1.3687092>.
- [28] R. Petela, Exergy of undiluted thermal radiation, *Sol. Energy* 74 (6) (2003) 468–469, [https://doi.org/10.1016/S0038-092X\(03\)00226-3](https://doi.org/10.1016/S0038-092X(03)00226-3).

## A.6. Machine learning for solar trackers

# Machine Learning for Solar Trackers

Jose A. Carballo<sup>2, 3, b)</sup>, Javier Bonilla<sup>1, 3, a)</sup>, Manuel Berenguel<sup>2, 3, c)</sup>, Jesús Fernández-Reche,<sup>1, d)</sup> Ginés García<sup>1, e)</sup>

<sup>1</sup>*CIEMAT - Plataforma Solar de Almería, Ctra. de Senés s/n, 04200 Almería, Spain*

<sup>2</sup>*University of Almería, Ctra. Sacramento s/n, 04120 Almería, Spain,*

<sup>3</sup>*CIESOL, Solar Energy Research Center, Joint Institute University of Almería - CIEMAT, Almería, Spain*

a) Corresponding author: [javier.bonilla@psa.es](mailto:javier.bonilla@psa.es)  
b) [jcarballo@psa.es](mailto:jcarballo@psa.es) c) [beren@ual.es](mailto:beren@ual.es) d) [jesus.fernandez@psa.es](mailto:jesus.fernandez@psa.es) e) [gines.garcia@psa.es](mailto:gines.garcia@psa.es)

**Abstract.** A new approach for solar tracking, based on deep learning techniques, is being studied and tested using Tensorflow, an open source machine learning framework. Tensorflow makes the implementation more flexible and increases the development capabilities. Tensorflow facilitates the neural network implementation on several kinds of devices (embedded and mobile devices, mini computers, etc.). Furthermore, Tensorflow supports different types of neural networks which can be tuned and retrained for particular purposes. The presented results are promising, since the retrained networks correctly identify the Sun and the target, with this information the system can be controlled to properly track the Sun's apparent trajectory without further information.

## INTRODUCTION

In CSP technologies, the Sun Tracking Subsystem (STS) is one of the keystones to improve the performance of the whole system and reduce costs. Numerous researchers are attempting to change the future of STSs as revealed by the high number of publications related to this topic, especially in recent years [1-4]. Nowadays, several types of STSs can be found in the literature. They are commonly specific to the type of solar technology they were developed for and present some limitations regarding to the cost, operation or error correction.

With the main goal of mitigating the present limitations of current STSs, a new control approach of STSs based on computer vision can be carried out by detecting the Sun and the tower target area by means of a camera place at 0' and whose optical axis is arranged parallel to the optical axis of the collector ( $V_A$ ). Once the elements have been identified, it is computed the midpoint ( $A'$ ) between  $S'$  and  $T'$  of the solar ( $V_s$ ) and target ( $V_t$ ) vectors intersections with the plane of an image (PC) taken by a camera aligned with the optical axis of the concentrator ( $V_A$ ) which also intersect PC in  $A''$ . The differences between  $A'$  and  $A''$  is called tracking error and it is employed as input for the STS controller. This approach can be used in any solar technology regardless of the type of solar tracker, as shown in "FIGURE 1".

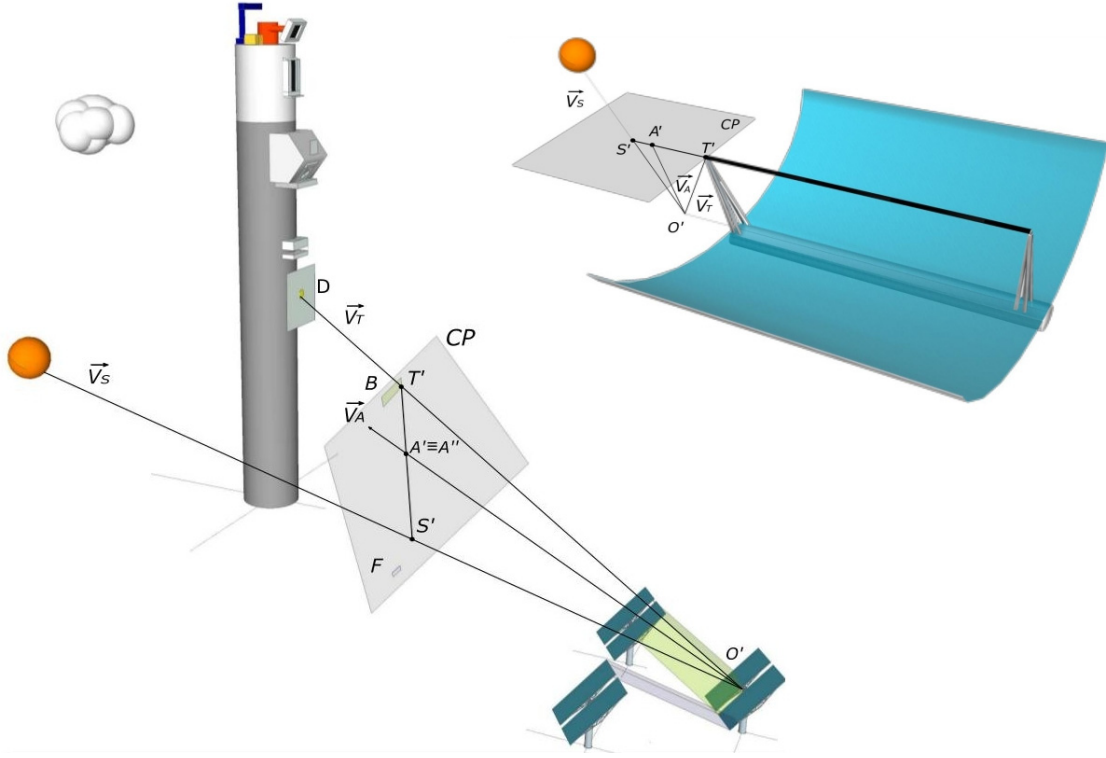


**FIGURE 1.** Central Receiver System (CRS) and Parabolic Trough-Collector (PTC) solar tracking

A small mockup heliostat, whose STS was based on traditional computer vision techniques, was successfully tested at Plataforma Solar de Almería [5]. The computer vision approach was improved by using low-cost open hardware and machine learning techniques (deep learning) [6] implemented using proprietary tools (Matlab [7] and Mathematica [8]). This last approach was tested at Plataforma Solar de Almería (PSA) and revealed the great potential of smart STSs, also the authors of the present work have patented the new approach for Sun tracking systems [9]. Preliminary results match with the main conclusion of an extended review by Al-Rousan [2], which indicates that the use of smart STSs is the most promising development path for concentrated solar power and photovoltaic technologies.

With the main goal of making the computer vision implementation more flexible, the approach for STSs based on machine learning was implemented using an open source machine learning framework, Tensorflow [10] developed by Google. Tensorflow facilitates on-device machine learning implementation on mobile and low-end embedded devices. Tensorflow also adds more flexibility, since different kinds of neural network models can be designed, implemented and used. This work presents the preliminary results obtained with the latest approach.

## NEURAL NETWORK MODELS

There are several pretrained models available in Tensorflow [11]. A pretrained model is a good starting point for creating new neural network models, since such models already learned a rich set of general features that will be useful for new networks. This approach also reduces the time required for the training process.

Several pretrained models were considered in this work, see "**TABLE 1**". They were modified and tuned to suit our needs. That is to identify the Sun, target, heliostats and clouds. Guidelines on how to tune these models are given in [12].

**TABLE 1.** Neural network models

MODEL	DESCRIPTION	Reference
SSD MobileNet V1 optimized	Depth- wise separable convolutions to build light weight deep neural networks	[13]
SSD MobileNet V1 0.75 depth	Lighter SSD MobileNet V1	[13]
SSD MobileNet V1 quantized	Quantization scheme allows that detection can be carried out using integer-only arithmetic	[14]
SSDLite Mobilenet V2	New architecture, that improves the performance of models and benchmark marks	[15]
SSD Inception V2	Inception block replaces the extra layers in SSD Mobilenet V2	[16]
Mask RCNN Inception V2	Simple, flexible, and general framework for object instance segmentation	[17]

## TRAINING

A small heterogeneous training image set (350 images) of the CESA central tower system located at PSA was used. Four object classes (heliostat, target, Sun and cloud) were labeled in the image set. "**FIGURE 2**" shows some images of the training image set.



**FIGURE 2.** Some images from the training image set

Neural model training is a iterative process, among all the training strategies provided by Tensorflow, the RMSPropOptimizer has been employed in this study. It implements an adaptive version of Stochastic Gradient Descent called RMS Prop "Root Mean Squared Propagation. "**FIGURE 3**" shows the evolution of the neural model results, which was trained from 0 to 15000 iterations (epochs).

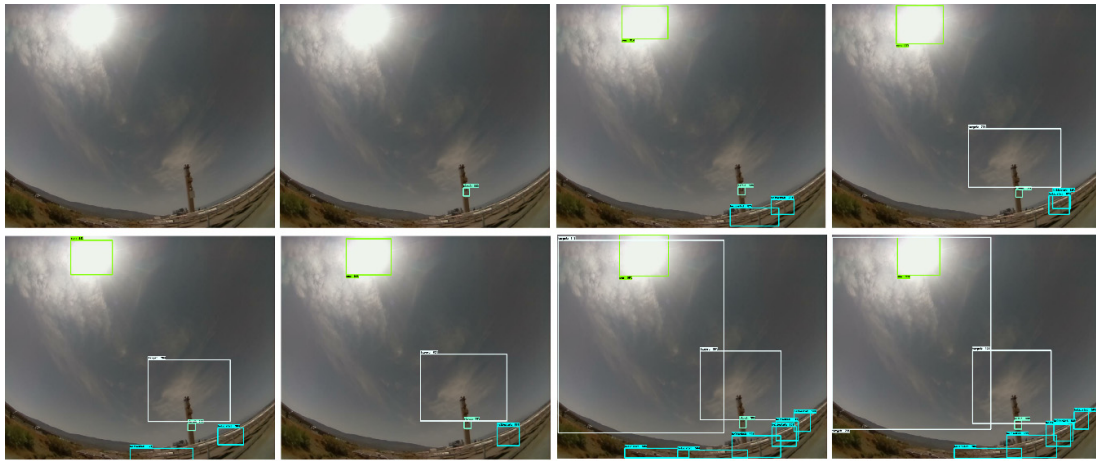


**FIGURE 3.** Result evolution with training

Neural network training is a computationally expensive process. In order to reduce the training time, the computing facilities of Extremadura Research Centre for Advanced Technologies (CETA-CIEMAT) were used. A Graphics Processing Unit (GPU) cluster with Compute Unified Device Architecture (CUDA) support was used for training the networks, see "**FIGURE 4**". The average training time was around 24 hours.

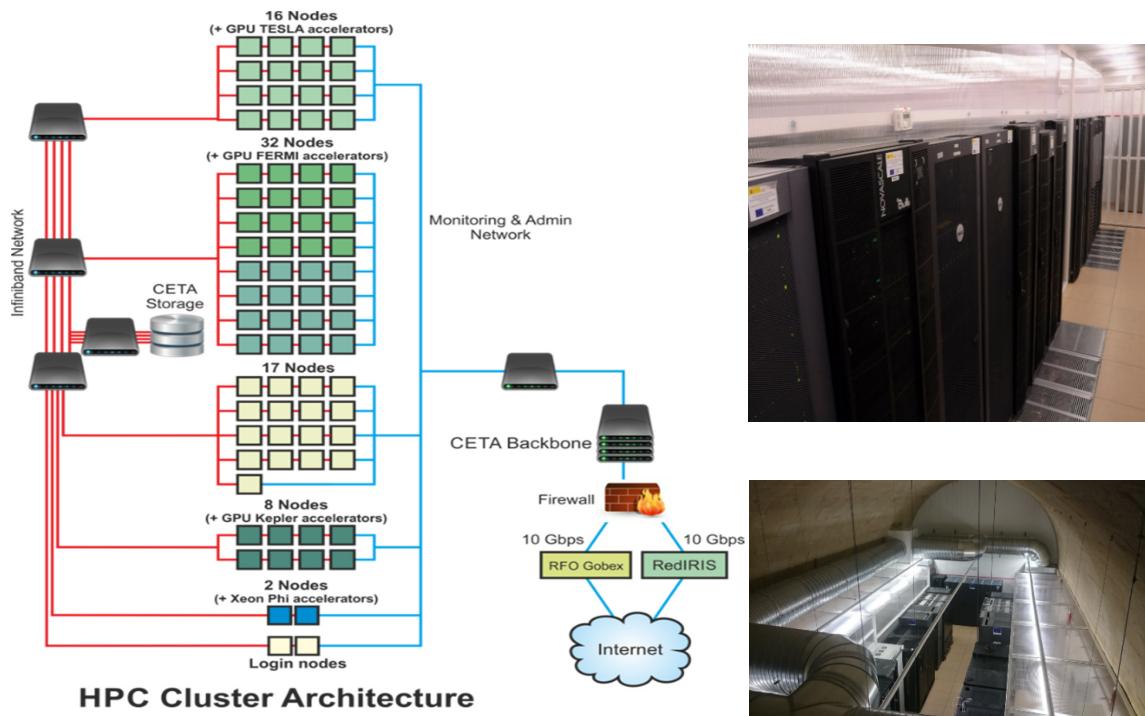


**FIGURE 4.** Computing facilities of Extremadura Research Centre for Advanced Technologies (CETA-CIEMAT)

## VALIDATION

Besides the training image set, there is an independent image set for validation (25 images). This set of images is used to validate the neural network results and provides information about the mean average precision (mAP) and inference time (speed of processing an image on CPU in this case). Mean average prediction is computed as the ratio of true object detections to the total number of objects that the classifier predicted, mAP is always calculated over a validation dataset. The predicted box is considered a true detection if a predicted box shares more than a percentage of its pixels with the ground-truth box (overlap criterion). In this work, the overlap criterion is defined as an Intersection-over-Union (IoU) greater than 0.5. Values of mAP close to 1.0 show high probability that whatever the classifier predicts as a positive detection is in fact a correct prediction. Inference time and mAP are common metrics to evaluate object detectors, for that reason they are shown for the evaluation of the neural networks shown in "**TABLE 2**". These metrics are provided by a Tensorflow tool called Tensorboard, which provides detailed information about the neural network learning process.

**TABLE 2.** Neural network validation metrics.

MODEL	Speed (ms)	Precision (mAP@0.5IoU)
SSD MobileNet V1 optimized	100	0.63
SSD MobileNet V1 0.75 depth	90	0.78
SSD MobileNet V1 quantized	110	0.79
SSDLite Mobilenet V2	400	0.35
SSD Inception V2	350	0.41
Mask R-CNN Inception V2	1100	0.55

"**TABLE 2**" reveals that "SSD MobileNet V1 0.75 depth" is the fastest neural model, whereas "SSD MobileNet V1 quantized" is the most accurate. "SSD MobileNet V1 optimized" also shows a good behavior. The rest of the models show similar results, although they are slightly slower or less precise. This fact reveals that better configuration of the model or training parameters may improve the results given by those networks.

It should be noted that "Mask R-CNN Inception V2" is not only an object detector, it is also a semantic segmentator, that is it provides object masks, not only bounding boxes. This could offer new capabilities to the smart STS approach, while achieving a good precision mark.

## IMPLEMENTATION

The previously introduced smart STS approach has been mainly implemented for two kinds of devices: low-end embedded and mobile devices, although it also works in common computers. Tensorflow is the machine learning framework.

- **Embedded devices:** A Raspberry Pi 3 model B+ and Pi camera was the hardware used. Software was implemented using the open source programming language Python. This is an open-source and low-cost implementation ideal to test and evaluate this approach in real facilities, since this kind of devices can control and communicate with the solar collectors.
- **Mobile devices:** An app for iOS and Android devices was also implemented. This app is multiplatform and can be also executed in common computers (Linux, macOS and Windows operating systems). The app is programmed in the V-Play engine [18], which facilitates the app deployment to several devices and operating systems. V-Play is a Standard Developer Kit (SDK) based on the Qt framework [19]. The programming languages used were C++ for the computer logic and QML for the Graphical User Interface (GUI). This app is intended to be used for easily demonstrating the concept and as an educational resource. It might be also used for other purposes that must be studied, for instance for on-site testing and calibration.

## EXAMPLES

"FIGURE 5" shows an augmented reality image taken from Raspberry Pi in the CESA solar field at PSA. The distance to the tower was more than 400 m. The objects detected are shown in colored boxes (Sun, target and heliostats). The numerical values represent the confidence levels of the detections, it is computed as the softmax probability (Neural Network output) of each of bounding boxes being on object.

As commented before, from the Sun ( $S_0$ ) and target ( $T_0$ ) box detections the black cross and gray circle positions can be computed. The black cross represents the solar collector aiming point ( $A'$ ), whereas the gray circle represents the correct Sun tracking point  $A''$ . The Sun tracking error can be computed as the distance between the black cross and the gray circle. This error is used to compute the control signal [6] and to properly aim the solar collector to follow the Sun's apparent trajectory.

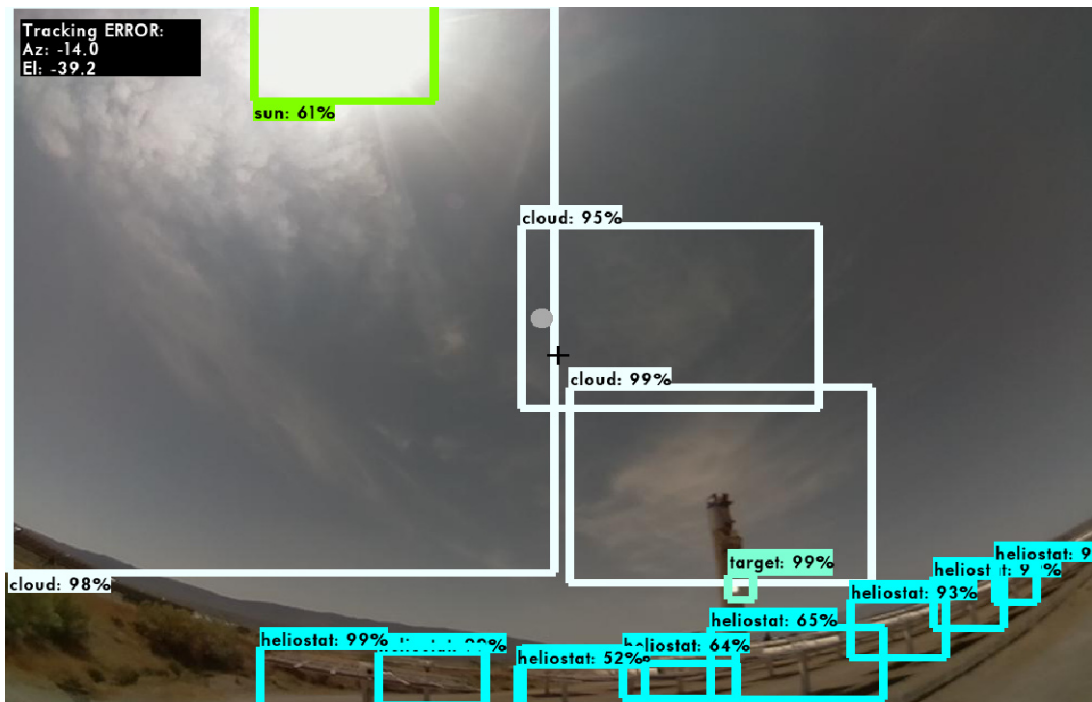
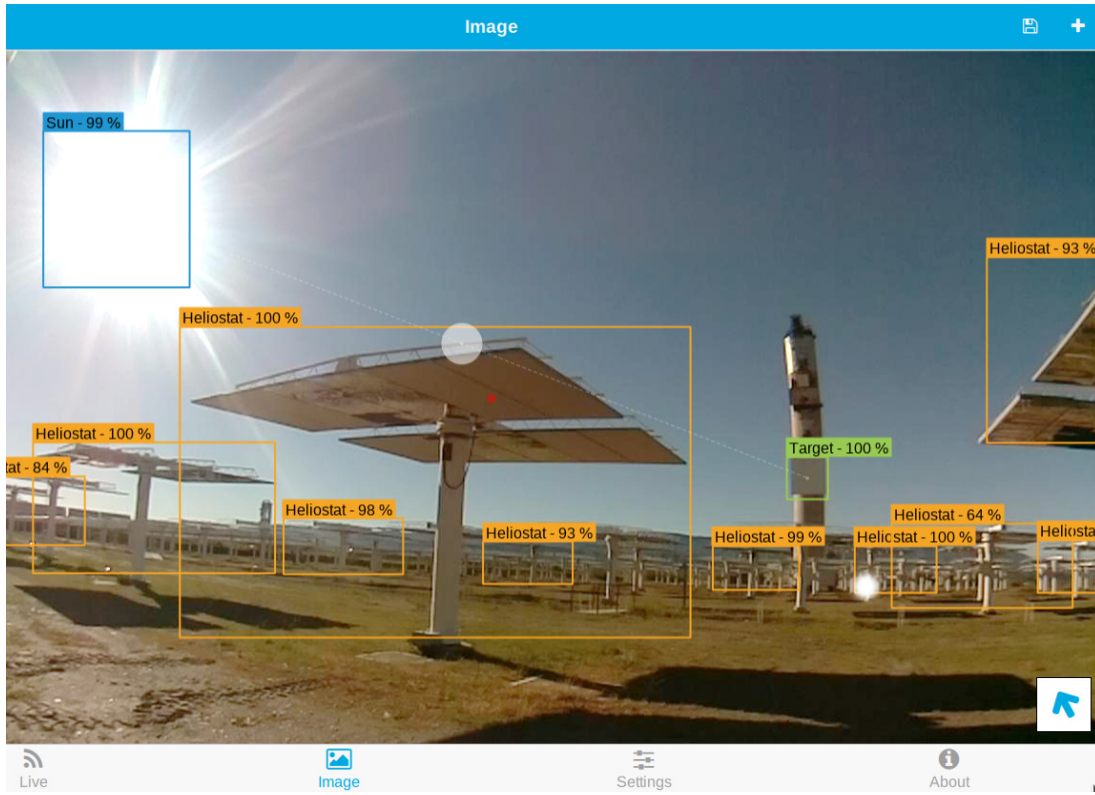


FIGURE 5. Augmented reality image taken and processed from Raspberry Pi at CESA solar field

"FIGURE 6" shows an augmented reality image taken from a mobile device in the CESA solar field at PSA. This app presents the same behavior than the developed software for embedded devices. Several objects were detected in colored boxes, the semi-transparent gray circle represents the correct Sun tracking point, its size matches the target size. The red dot represents the current heliostat aiming point (center of the screen), therefore the red dot must be placed inside the gray circle to reflect the Sun irradiance onto the target.



**FIGURE 6.** Augmented reality image processed on a mobile device at CESA solar field

## CONCLUSION AND FUTURE WORK

The new machine learning framework is faster and more accurate than the original implementation [6] according to results from "**TABLE 2**". The rapid growth of Tensorflow and the large number of contributions from the open community augurs a substantial improvement of the marks obtained in a short time.

"SSD MobileNet V1 optimized", "SSD MobileNet V1 quantized" and "SSD MobileNet V1 0.75 depth" show the best behavior in terms of speed and precision of all the evaluated models.

The new framework is open and more flexible, it allows implementing the smart STS approach in almost every kind of device. Embedded and mobile implementations have been carried out in this work.

The good results obtained in terms of speed and precision, make it possible to use this approach to design new control strategies based on artificial intelligence and computer vision that can take into account key factors for solar collector such as block, shadow and cloud detections.

Ongoing work includes training and validating the neural networks with larger image sets, evaluate new neural networks and further optimize the approach implementations.

Future work includes the autonomous control of a heliosstat using the embedded device implementation in order to estimate the control accuracy in terms of mrad, as well as determine the optimal image resolution for minimizing such error.

## ACKNOWLEDGMENTS

This work has been funded by the National R+D+i Plan DPI2014-56364-C2-2-R Spanish Ministry of Economy, Industry and Competitiveness funds. This work was also partially supported by the computing facilities of Extremadura Research Centre for Advanced Technologies (CETA-CIEMAT), funded by the European Regional Development Fund (ERDF). CETA-CIEMAT belongs to CIEMAT and the Government of Spain.

## REFERENCES

1. Hafez, A. Z., Yousef, A. M., & Harag, N. M. (2018). Solar tracking systems: Technologies and trackers drive types – A review. *Renewable and Sustainable Energy Reviews*, 91(November 2017), 754–782. <https://doi.org/10.1016/j.rser.2018.03.094>
2. AL-Rousan, N., Isa, N. A. M., & Desa, M. K. M. (2018). Advances in solar photovoltaic tracking systems: A review. *Renewable and Sustainable Energy Reviews*, 82(September), 2548–2569. <https://doi.org/10.1016/j.rser.2017.09.077>
3. Nsengiyumva, W., Chen, S. G., Hu, L., & Chen, X. (2018). Recent advancements and challenges in Solar Tracking Systems (STS): A review. *Renewable and Sustainable Energy Reviews*, 81(August 2017), 250–279. <https://doi.org/10.1016/j.rser.2017.06.085>
4. Camacho E.F., Berenguel M., Rubio F. R., Martínez D., Control issues in solar systems, in: Control of Solar Energy Systems, Springer, 2012, pp. 25–47.
5. Carballo, J. A., Bonilla, J., Roca, L., Berenguel, M. New low-cost solar tracking system based on open source hardware for educational purposes. Under Review.
6. Carballo, J. A., Bonilla, J., Berenguel, M., Fernández-Reche, J., García, G. New approach for solar tracking systems based on computer vision, low cost hardware and deep learning. Under Review.
7. The MathWorks Inc. (2018) MATLAB R2018a, <http://www.mathworks.es/products/matlab>
8. Wolfram (2018). Mathematica 11, <http://www.wolfram.com/mathematica>
9. J. A. Carballo, J. Bonilla, J. Fernandez, G. Garcia, (2018). Sistema de captación solar mediante técnicas de visión artificial ES P2018300773.
10. Abadi, M., Agarwal, A., Barham, P., Brevdo, E., Chen, Z., Citro, C., Zheng, X. (2016). *Tensorflow: Large-Scale Machine Learning on Heterogeneous Distributed Systems*. <https://doi.org/10.1038/nn.3331>
11. Google (2018). Tensorflow detection model zoo, [https://github.com/tensorflow/models/blob/master/research/object\\_detection/g3doc/detection\\_model\\_zoo.md](https://github.com/tensorflow/models/blob/master/research/object_detection/g3doc/detection_model_zoo.md)
12. Huang, J., Rathod, V., Sun, C., Zhu, M., Korattikara, A., Fathi, A., Murphy, K. (2017). Speed/accuracy trade-offs for modern convolutional object detectors. Proceedings - 30th IEEE Conference on Computer Vision and Pattern Recognition, CVPR 2017, 2017-January, 3296–3305. <https://doi.org/10.1109/CVPR.2017.351>
13. Howard, A. G., Zhu, M., Chen, B., Kalenichenko, D., Wang, W., Weyand, T. Adam, H. (2017). MobileNets: Efficient Convolutional Neural Networks for Mobile Vision Applications. <https://doi.org/arXiv:1704.04861>
14. Jacob, B., Kligras, S., Chen, B., Zhu, M., Tang, M., Howard, A. Kalenichenko, D. (2017). *Quantization and Training of Neural Networks for Efficient Integer-Arithmetic-Only Inference*. <https://doi.org/10.1109/CVPR.2018.00286>
15. Sandler, M., Howard, A., Zhu, M., Zhmoginov, A., & Chen, L.-C. (2018). *MobileNetV2: Inverted Residuals and Linear Bottlenecks*. <https://doi.org/10.1134/S0001434607010294>
16. Ning, C., Zhou, H., Song, Y., & Tang, J. (2017). Inception Single Shot MultiBox Detector for object detection. 2017 IEEE International Conference on Multimedia and Expo Workshops, ICMEW 2017, (July), 549–554. <https://doi.org/10.1109/ICMEW.2017.8026312>
17. He, K., Gkioxari, G., Dollar, P., & Girshick, R. (2017). Mask R-CNN. Proceedings of the IEEE International Conference on Computer Vision, 2017–Octob, 2980–2988. <https://doi.org/10.1109/ICCV.2017.322>
18. V-Play GmbH (2018). V-Play Engine, <http://www.v-play.net>
19. The Qt Company (2018). Qt – Cross-platfrom software development for embedded & desktop, <https://www.qt.io>

**A.7. Solar tower power mockup for the assessment of advanced control techniques**

# Solar tower power mockup for the assessment of advanced control techniques

Jose A. Carballo<sup>b,c</sup>, Javier Bonilla<sup>a,b,\*</sup>, Manuel Berenguel<sup>c,b</sup>, Jesús Fernández<sup>a</sup>, Ginés García<sup>a</sup>

<sup>a</sup>*CIEMAT - Plataforma Solar de Almería, Ctra. de Senés s/n, 04200 (Tabernas) Almería, Spain*

<sup>b</sup>*CIESOL Research Centre for Solar Energy, UAL-PSA.CIEMAT Joint Centre, Almería, Spain*

<sup>c</sup>*University of Almería, Ctra. Sacramento s/n, 04120 Almería, Spain*

## Abstract

This work presents a solar tower power mockup with the aim of acting as a test-bed facility for evaluating new advanced control techniques. The mockup comprises low-cost hardware, open-source software together with 3D-printed structures for the elements in the system: a heliostat and a tower. The tower includes an open-hardware Arduino board, a Photovoltaic (PV) panel and a Liquid Crystal Display (LCD) to measure and show the incident power. The heliostat includes a Raspberry Pi, a touchscreen display, and two servo motors. The main goal of this mockup is to serve as a first stage test-bed and demonstration facility for analyzing new developments with respect to advanced control techniques, for instance new heliostat tracking methods. This paper presents this mockup together with a new heliostat tracking method based on computer vision and deep learning that it is currently under development.

**Keywords:** Automatic control, concentrated solar power, solar power tower, computer vision, deep learning, object detection, 3D printing, test-bed mockup

## 1. Introduction

Environmental issues and concerns about sustainability are constantly encouraging research and investment in renewables. They are, by definition, the only way we can keep producing energy for a virtually infinite period of time. Solar energy is appealing due to its high potential; it is the most abundant energy source on Earth.

The two major solar energy technologies are solar PV and solar thermal. The most efficient way of storing heat in solar thermal energy makes it more appropriate for large-scale energy production. Optical concentration is used to achieve maximum conversion at little heat loss by reflecting and concentrating the solar flux onto a reduced-area receiver. This technology is known as Concentrating Solar Thermal (CST) technology. When CST is applied to electricity production is known as Concentrating Solar Power (CSP) or Solar Thermal Electricity (STE). Four CST technologies are presently available: Dish/Engine (DE) systems, Linear Fresnel (LF) systems, Parabolic Trough (PT) collectors and Solar Tower Power (STP) systems, also known as central receiver systems.

Solar power tower yields the highest efficiency and has the greatest scaling-up potential of all CSP technologies. The International Energy Agency market analysis and forecast from 2018 to 2023 on renewables predicts a CSP growth of 87% (4.3 GW). Furthermore, CSP Today Global Tracker [1] reveals that STP plants account for 70% of the total capacity of CSP projects under development. However, CSP still needs significant cost reduction to get a large share of the energy market.

Industry 4.0 is a digital revolution that has potential to disrupt the entire conventional approaches to manufacturing. It is expected to have an impact on key areas, including energy [2], and guide countries to a new era of modern manufacturing [3]. The strategic research agenda of the European technology platform on smart systems integration states that smart system-based devices play a key role for achieving higher energy efficiencies and an intelligent use of energy.

\*Corresponding author.

Email address: [javier.bonilla@psa.es](mailto:javier.bonilla@psa.es) (Javier Bonilla)

Nonetheless, CSP plants have not incorporated innovations included in other industrial sectors. Current CSP components incorporate a low degree of intelligence and autonomy. However, the emerging SMARTCSP concept [4] has the goal of replicating the Industry 4.0 approach in CSP.

With the aim of contributing to the development of smart and advanced STP control techniques, a test bench solar tower power mockup was developed. This test bench is suitable for testing and evaluating heliostat automatic control techniques at an early development stage.

To the knowledge of the authors, there are no references in the literature regarding STP mockups or 3D-printed components. However, there is a recent work related to 3D-printed PV solar cells [5] and an ongoing project concerning the assessment of 3D-printed fractal receivers for STP plants [6] at Sandia Labs. There are also works related to mechatronics systems for sun tracking, such as a two-axes sun tracking photovoltaic system driven by a robotic sensor [7] and an active sun tracker for solar streetlight [8] which combines two tracking strategies: a main photoelectric tracking mode with an auxiliary time-based tracking mode.

This paper is divided in five sections. This section (Section 1) is an introduction about the motivation and goals of this work. Section 2 briefly introduces solar tower power systems. Section 3 describes the design, hardware and software of the developed STP mockup. Section 4 presents an under development new heliostat automatic tracking control system based on computer vision and deep learning. Finally, the main conclusions, ongoing and future work tasks are detailed in Section 5.

## 2. Solar tower power

A STP plant is made up of a heliostat field, a receiver placed at the top of a tower and a Thermal Energy Storage (TES) system (see Fig. 1). There are mainly two TES configurations: thermocline and two-tank (hot & cold) storage configurations.

Each heliostat tracks the Sun's apparent trajectory to reflect and concentrate the incoming solar irradiance onto the receiver. Heliostat calibration is usually performed using a white Lambertian target placed in the tower.

The reflected solar flux is absorbed by the receiver and transformed into thermal energy by heating up a Heat Transfer Fluid (HTF). The hot HTF provides thermal energy to a power cycle to produce electricity.

Commonly, the heliostat field is oversized with respect to the thermal demand of the power cycle, hence part of the hot HTF thermal energy is stored in a TES system for later use. The TES system provides the needed thermal energy to produce electricity at night or under unfavorable meteorological conditions.

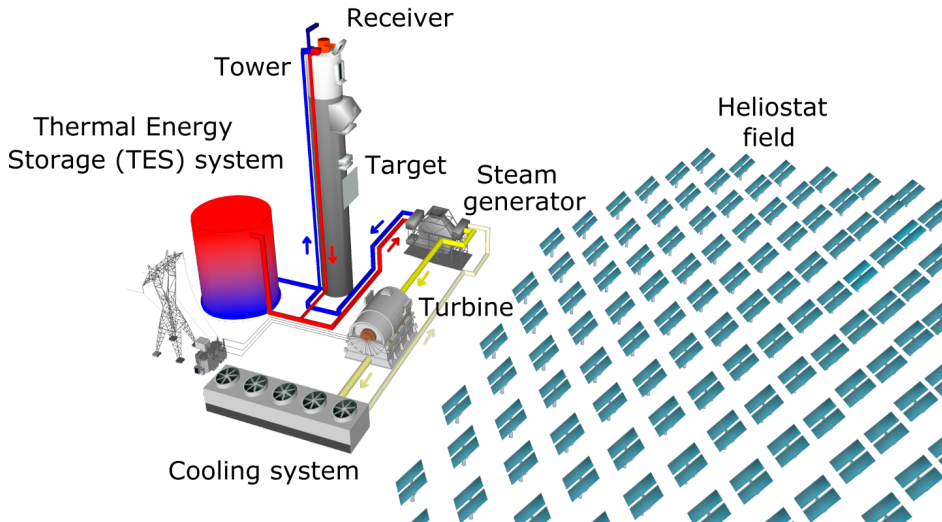


Figure 1: Solar tower power

50 **3. Solar tower power mockup**

The test bench solar tower power mockup comprises a tower and a heliostat, both elements are described in the following sections in terms of structure, hardware and software.

55 **3.1. Tower**

The mockup tower design (see Fig. 2a) is based on the tower of the real CESA-I STP plant located at CIEMAT - Plataforma Solar de Almería. CESA-I facility (see Fig. 2b) has a 330x250-m south-facing solar field of 300 39.6-<sup>m<sup>2</sup></sup> heliostats distributed in 16 rows. The 80-m-high concrete tower has a white Lambertian target and a volumetric receiver at the top of the tower. The SolAir 3000 receiver is a 3 MW<sub>th</sub> open volumetric air receiver with a modular ceramic absorber [9]. The TES system is a thermocline tank with filler materials.



(a) Mockup



(b) CESA-I STP plant

Figure 2: 3D-printed tower and real one

60 **Structure.** SketchUp [10] was the Computer-Aided Design (CAD) tool used for the design of the tower structure (see Fig. 3). The final design was built thanks to a 3D printer.

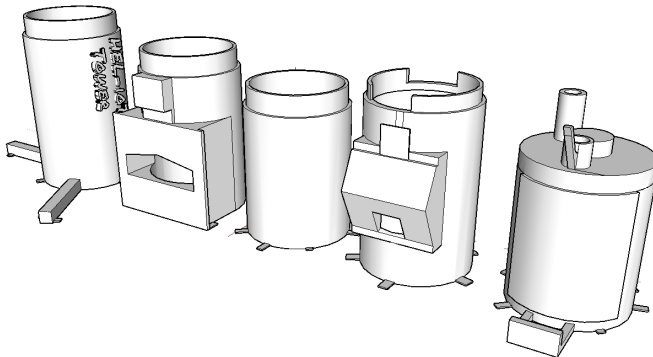


Figure 3: CESA-I tower design

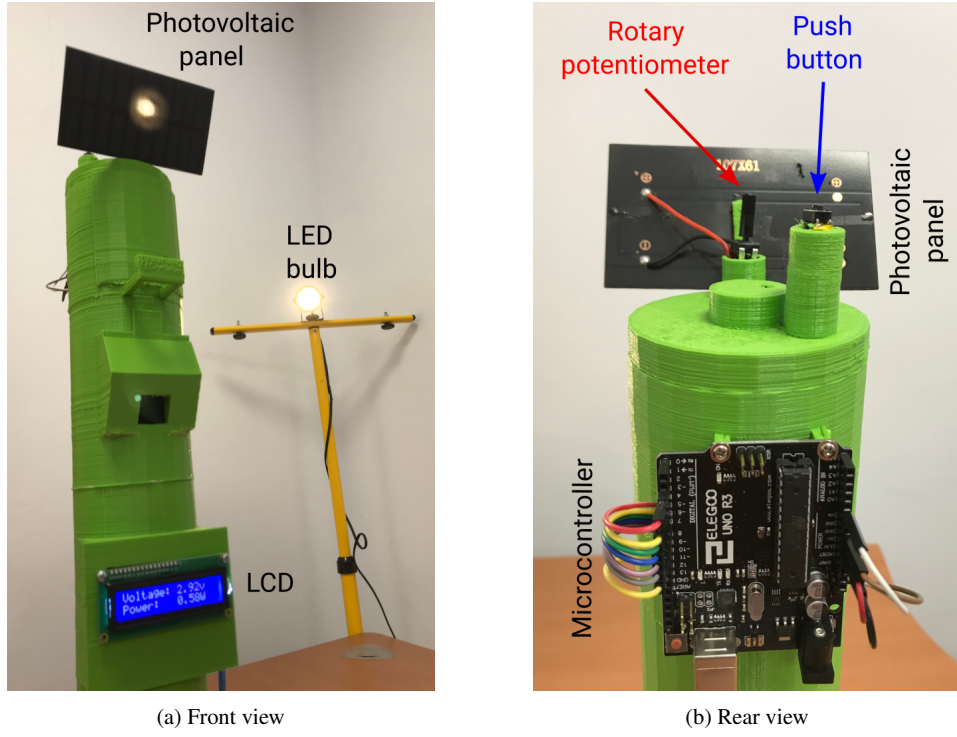


Figure 4: Tower mockup

*Hardware.* The tower is equipped with a PV panel, a LCD (see Fig. 4a for front view), a microcontroller (an open-hardware Arduino UNO R3 compatible development board), a push button and a rotary potentiometer (see Fig. 4b for rear view). The PV panel in the solar tower power mockup acts as the receiver in the real STP facility. The push button is used to select the information shown in the LCD, whereas the potentiometer controls the brightness of the LCD.

*Software.* The program loaded in the microcontroller measures the voltage in the PV panel and estimates the generated power. Arduino programming language [11] together with Arduino Integrated Development Environment (IDE) [12] were used to code and upload the program to the microcontroller.

### 3.2. Heliostat

A preliminary prototype was presented in [13]. However, this prototype required a significant amount of work for its assembly. The new design presented in this work is based on a 3D-printed structure which considerably reduces the time required for its construction and assembly.

*Structure.* The new heliostat design is based on a traditional pylon structure but further simplifying it to minimize the moving parts while still providing the necessary support to all the heliostat components. The heliostat structure is composed of parts that can be easily assembled (see Fig. 5a). The heliostat was also 3D printed based on a SketchUp design.

*Hardware.* The heliostat hardware comprises two servo motors (horizontal rotation and elevation), a Raspberry Pi 3 Model B+, Raspberry Pi V2 8-megapixel camera, a 7-inch touchscreen display and a status LED (see Fig. 5b). Raspberry Pi [14] is a low-cost low-power consumption computer with wireless: WiFi and Bluetooth, together with local: General Purpose Input/Output (GPIO) port (to control the servo motors) communication capabilities.

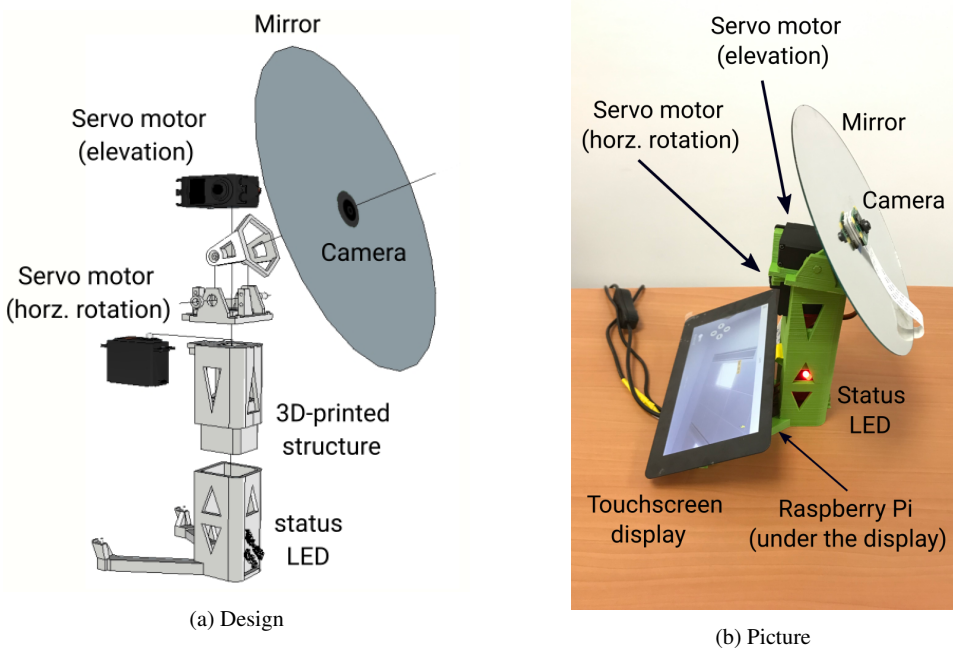


Figure 5: Heliostat mockup

*Software.* Raspbian [15] is Raspberry Pi operating system. This is an open-source Linux distribution tailored for Raspberry Pi with plenty of software for education and programming. It supports a wide range of programming languages together with open-source and proprietary software tools. The current software is implemented in C++. The open-source Qt toolkit [16] is used for interacting with the camera, the touchscreen, wireless communication capabilities (WiFi and Bluetooth), and for the design of the Graphical User Interface (GUI). The heliostat can be manually moved from arrow buttons in the touch screen or from paired Bluetooth devices. Manual or automatic control can be also selected in the touch screen. The C++ pigpio library [17] is used to interface with the Raspberry Pi GPIO port and control the servo motors by means of Pulse-Width Modulation (PWM). Any controller implemented in C++ can be easily integrated with the current software version. The software can be also adapted to support controllers implemented in other programming languages and tools, such as Python, MATLAB/Simulink, etc.

#### 4. Automatic heliostat tracking based on computer vision and deep learning

CSP technologies take advantage of the incoming solar flux to produce thermal energy and electricity. Therefore, knowing and tracking the exact position of the Sun in the sky is a key issue to properly control the power plant.

##### 4.1. Current industrial approach for automatic heliostat tracking

Presently, the most widely extended industrial solution is open-loop tracking based on Solar Position Algorithms (SPAs) using an error model that is periodically calibrated [18]. Calibration is usually performed using a white Lambertian target placed in the tower (see Fig. 1).

Manual or automatic techniques are used to calibrate each heliostat. The SPA + beam characterization system [19] was applied in Solar One and Solar Two STP plants [20, 21]. Gemasolar plant implemented an SPA + Computer Vision (CV) approach [22] similar to the one described in [23]. Sierra SunTower also considered an SPA + CV approach [24]. PS10 and PS20 STP plants also have targets mounted on their towers [25].

The main issue with the previous approaches is that they are open-loop solutions. This means that they cannot determine if their actions have achieved the desired result, because they operate without feedback. Additionally,

they demand expensive tracking equipment and a strict heliostat installation procedure where the desired accuracy is difficult to guarantee. In practice, they need an error model to account for misalignments that must be periodically calibrated. Calibration can take several weeks or months in extensive heliostat fields and is usually performed individually defocusing each heliostat, reducing the overall plant performance.

On the other hand, available closed-loop heliostat tracking approaches have been labeled as impractical, too complex or too expensive by the industry. Some recent closed-loop research approaches managed to reduce or remove the calibration time at the expense of increasing the complexity. In [26], infrared lights in the heliostat field and tower enable night calibration while reducing the calibration time from weeks to days. In [18], the calibration is performed by geolocation at the same time the STP plant is being operated. This approach requires to install wireless transmitting towers close to the STP plant. Heliostats must also be equipped with wireless-communication devices.

#### 4.2. New heliostat tracking approach

The new closed-loop heliostat tracking method is currently under development. It is based on computer vision and machine learning, where deep learning techniques are applied in this particular case. Deep-learning Artificial Neural Network (ANN) perform automatic feature extraction without manual intervention, unlike most conventional machine-learning algorithms.

Software includes an ANN able to detect the Sun and the receiver. The general idea is to calculate the heliostat aiming position from detections of the Sun and receiver in the camera video frames. This approach does neither require a strict heliostat installation procedure, expensive equipment nor calibration.

#### 4.3. Heliostat tracking principle

The general procedure to aim a heliostat is detailed as follows (see Fig. 6). This example considers the target as the element where the concentrated flux is reflected; the same applies for the receiver. The first step is to determine the heliostat-to-sun vector ( $V_S$ ), i.e. the vector from the heliostat surface mirror's center point ( $O'$ ) to Sun center's point. Then, the heliostat-to-target vector ( $V_T$ ) is determined, i.e. the vector from the heliostat surface mirror's center point ( $O'$ ) to target center's point. Finally, the heliostat normal vector ( $V_A$ ) is aimed at the bisector of the angle between the heliostat-to-sun ( $V_S$ ) and heliostat-to-target ( $V_T$ ) vectors.

The same previous procedure considering the approach presented in this work is now introduced. It is assumed that the camera is attached to the heliostat surface mirror's center point ( $O'$ ) and moves with it; other locations are also possible. The camera provides a plane view (CP) of the scene. The ANN detects the Sun's ( $S'$ ) and target's ( $T'$ ) center points. The middle point ( $A''$ ) between  $S'$  and  $T'$  is the desired heliostat aiming point. The current heliostat aiming point ( $A'$ ) is the center point in the plane view (CP). The heliostat is then moved to place the current aiming point ( $A'$ ) at the desired aiming point ( $A''$ ).

Figs. 6a and 6b show 3D and 2D camera views for an out-of-focus heliostat, whereas Figs. 6c and 6d show the same views but for a focused heliostat.

#### 4.4. Previous work and current implementation

Preliminary feasibility results were published in [27]. In this previous work, a Convolutional Neural Network (CNN) called AlexNet [28] was tuned and trained in MATLAB [29] using its CV toolbox [30] to detect the Sun, target, heliostats and clouds with a small subset of 300 images taken in the CESA-I STP facility, located at Plataforma Solar de Almería (PSA).

The new automatic heliostat tracking method presented in this work uses TensorFlow Lite [31, 32] as the machine learning framework. Tensorflow Lite, developed by Google, is open-source, lightweight and targets mobile and embedded devices. It enables on-device machine learning inference with low latency and small application size. It integrates seamlessly with C++ and Python.

A pre-trained ANN has been considered in this work: SSD MobileNet V1. MobileNets [33] are open-source CNN models for efficient on-device vision. Single Shot Multibox Detector (SSD) [34] is the object detector used by the ANN. This ANN was initially trained with a set of images from the Microsoft Common Objects in Context (COCO) dataset [35]. A pre-trained ANN was used since such ANN already learned a rich set of general features that are useful for new ANNs. This is known as transfer learning and it also reduces the time required for the training process.

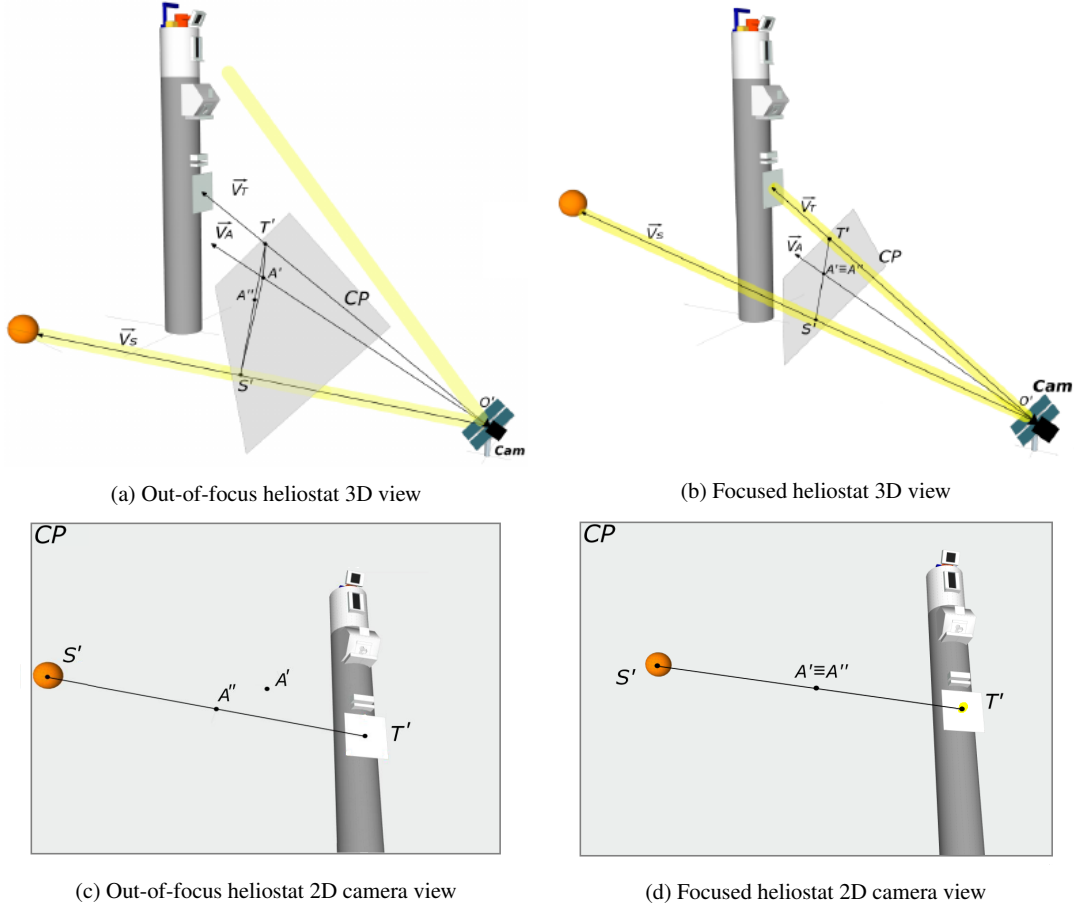


Figure 6: Heliostat tracking principle

SSD MobileNet V1 ANN was trained to detect objects that mimic the Sun (a LED bulb) and the target or receiver (a small-size PV panel) in STP plants. The ANN provides a confidence level and a bounding box per detected object.

The automatic control system calculates the current aiming point (the center pixel in the current video frame,  $A'$  in Figs. 6c and 6d and the on-focus aiming point ( $A''$ ), i.e. the middle point between the straight line from the center pixel of the Sun bounding box ( $S'$ ) and the center pixel of the target bounding box ( $T'$ )).

The next step is to align the current ( $x_c, y_c$ ) and on-focus ( $x_f, y_f$ ) aiming points. To do that, the controller must calculate the distance in pixel in both axes between both aiming points ( $x_d, y_d$ ) (Eqs. (1) and (2)). The top-left corner pixel on each video frame corresponds to (0, 0). These linear distances in pixels must be translated to angular distances to move the servo motors. The angle per pixel determines the angle increment or decrement to move the camera video frame one pixel in a particular axis, this value depends on the camera's horizontal and vertical angles of view and on the camera resolution. The angle per pixel on each axis ( $\beta_x, \beta_y$ ) is calculated by Eqs. (3) and (4), where  $\alpha_h$  and  $\alpha_v$  are the camera's horizontal and vertical angles of view (radians),  $w$  is the video frame width (pixels) and  $h$  is the video frame height (pixels).

$$x_d = x_c - x_f, \quad (1) \quad y_d = y_c - y_f. \quad (2) \quad \beta_x = \alpha_h/w, \quad (3) \quad \beta_y = \alpha_v/h, \quad (4)$$

$$\gamma_x = x_d \cdot \beta_x, \quad (5) \quad \gamma_y = y_d \cdot \beta_y, \quad (6)$$

These values depend on each particular camera (angle of view) and its configuration (resolution). They can be easily set and configured in the developed app. Finally, the angular distances ( $\gamma_x, \gamma_y$ ) are the product of the linear

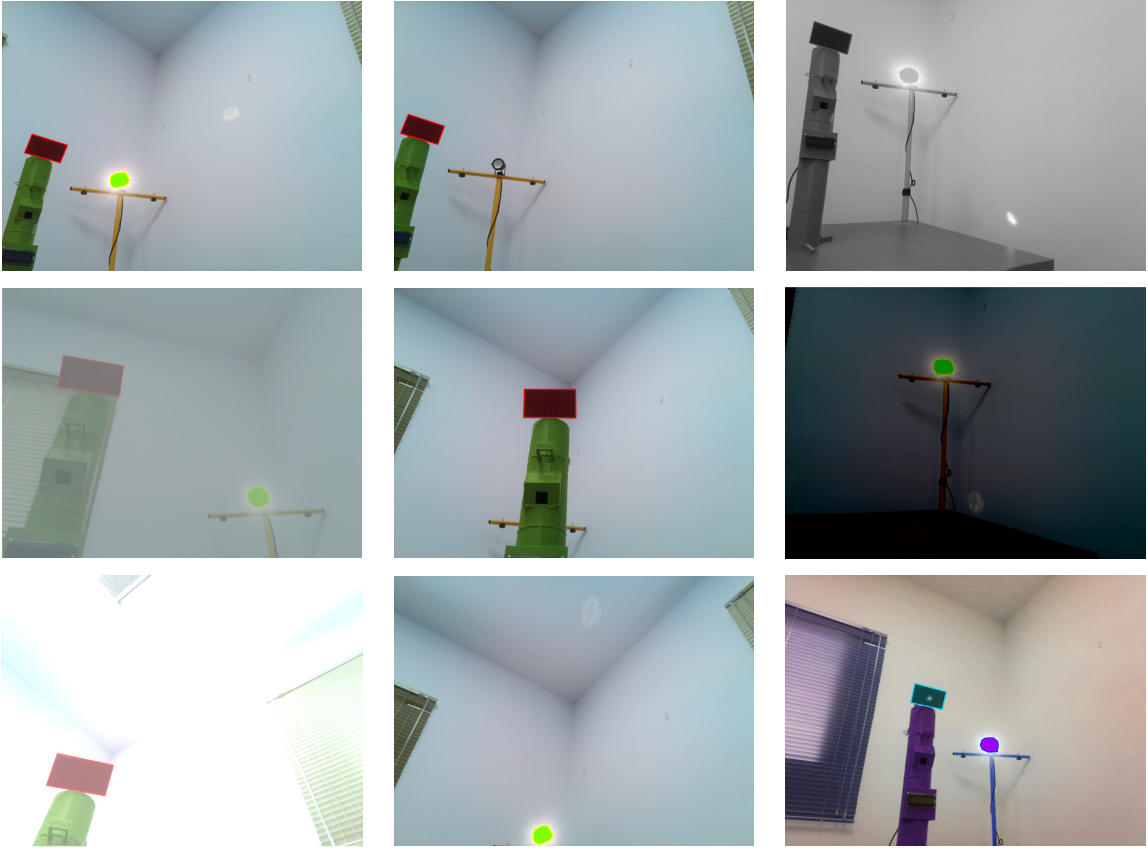


Figure 7: Some pictures of the ANN training image set

distances ( $x_d, y_d$ ) and the angles per pixels ( $\beta_x, \beta_y$ ) (see Eqs. (5) and (6)).

If the absolute value of  $\gamma_x$  or  $\gamma_y$  is lower than a certain threshold (1.8 mrad/px), it is assumed that the system is on focus. This threshold can be configured in the app. A deadband prevents the system to be continuously moving due to small errors, i.e. once the system is on focus the controller only acts when  $\gamma_x$  or  $\gamma_y$  is higher than another threshold (2 mrad/px) that can be also adjusted in the app.

The Raspberry Pi Camera V2 has  $\alpha_h = 62.2^\circ$  and  $\alpha_v = 48.8^\circ$ . It is configured for  $w = 1024$  px and  $h = 768$  px, therefore,  $\beta_x = 1.1$  mrad/px and  $\beta_y = 1.1$  mrad/px. The camera resolution can be increased to obtain a higher angular resolution. It supports up to 3280 x 2464 pixels for static images,  $\beta_x = 0.33$  mrad/px and  $\beta_y = 0.35$  mrad/px, and 1920 x 1080 for video,  $\beta_x = 0.57$  mrad/px and  $\beta_y = 0.79$  mrad/px. However, the controller accuracy is restricted due to the servo motors' resolution =  $0.1^\circ \approx 1.8$  mrad.

In a real STP plant, wide-angle lenses will be needed in order to keep tracking the Sun at sunrise and sunset. In the worst case scenario, summer solstice on the North Pole for maximum Sun azimuth displacement or on the Equator for maximum Sun elevation, a lens with  $\alpha_h = 160^\circ$ ,  $\alpha_v = 90^\circ$  and 3032 x 2008 resolution (6 Mpixel) would be enough to keep the error lower than 1 mrad ( $\beta_x = 0.92$  mrad/px and  $\beta_y = 0.78$  mrad/px).

The heliostat' servo motors have sensors that provide current angles in the  $[0^\circ, 180^\circ]$  interval. The controller queries the current position on each axis and adds the previously calculated angular distances ( $\gamma_x, \gamma_y$ ) to set the new angle on each servo motor. Angle values are set applying PWM.

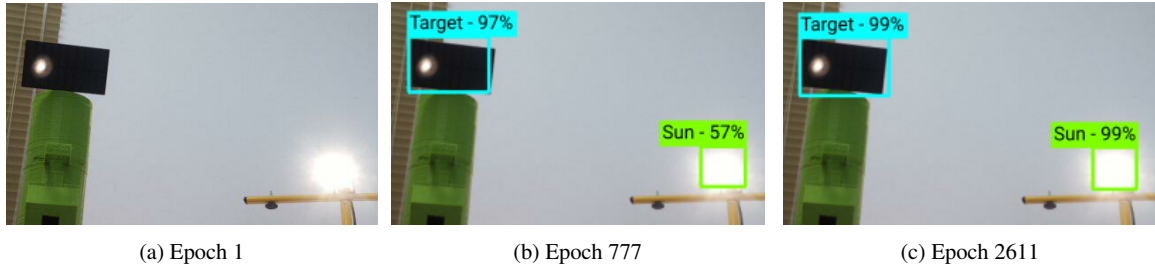


Figure 8: Training evolution in a picture of the validation set

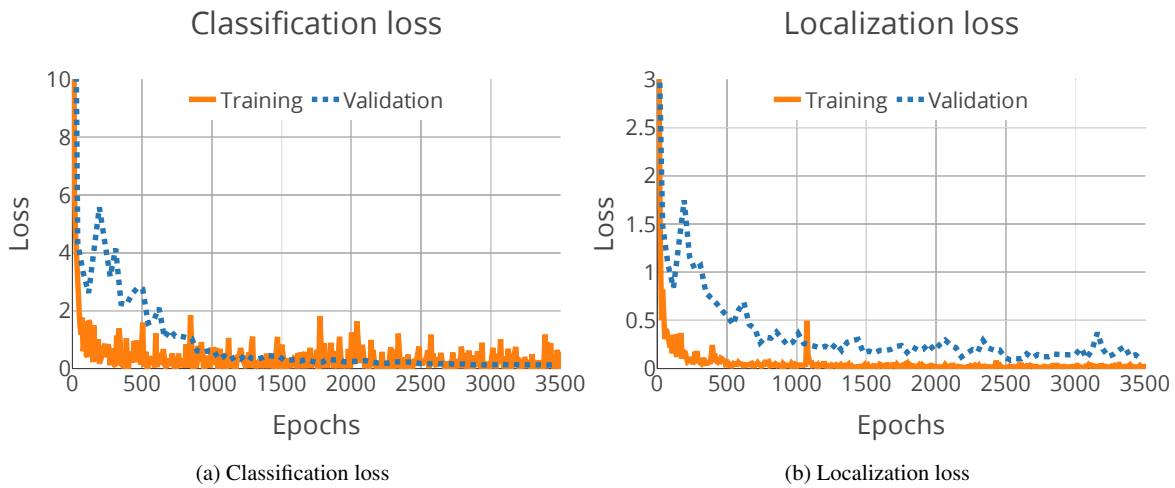


Figure 9: Training statistics

#### 185 4.5. Training and validation

ANN training is a computationally expensive process. In order to reduce the training time, a Graphics Processing Unit (GPU) cluster with Compute Unified Device Architecture (CUDA) support was used for the ANN training. This cluster belongs to the computing facilities of Extremadura Research Centre for Advanced Technologies (CETA-CIEMAT) [36].

190 Two image sets were defined in this work, one set was used for training, whereas the other set was used for validation. Fig. 7 shows some pictures of the training set, where the objects that must be detected (a PV panel and a turned-on LED bulb) are annotated with polygons. The ANN was trained to be robust and invariant with respect to object translation, viewpoint, size and illumination by using a diverse training set and applying data augmentation techniques. These techniques enlarged the training set because they make changes (random crop, image flips, brightness changes, hue changes, contrast changes, etc.) to the existing images in the training set.

195 The training process consists in adjusting the ANN parameters to properly predict objects and their bounding boxes in the training set. An epoch is defined as a single step in the training process. The ANN is trained with all the images in the training set on each step. The ANN was trained for 3,500 epochs. After each epoch, the validation set is evaluated in terms of classification (object detection accuracy) and location (bounding boxes accuracy of the correctly classified object) losses. Details, about how both metrics are calculated, are given in [34].

200 Fig. 8 shows the evolution of one of the images in the validation set. None of the objects was detected at epoch 1 (see Fig. 8a). However, objects were detected at epoch 777. Fig. 8b shows the detected object, together with their bounding boxes and confidence levels at this epoch. Fig. 8c shows that higher confidence levels and more accurate bounding boxes were predicted at epoch 2611.

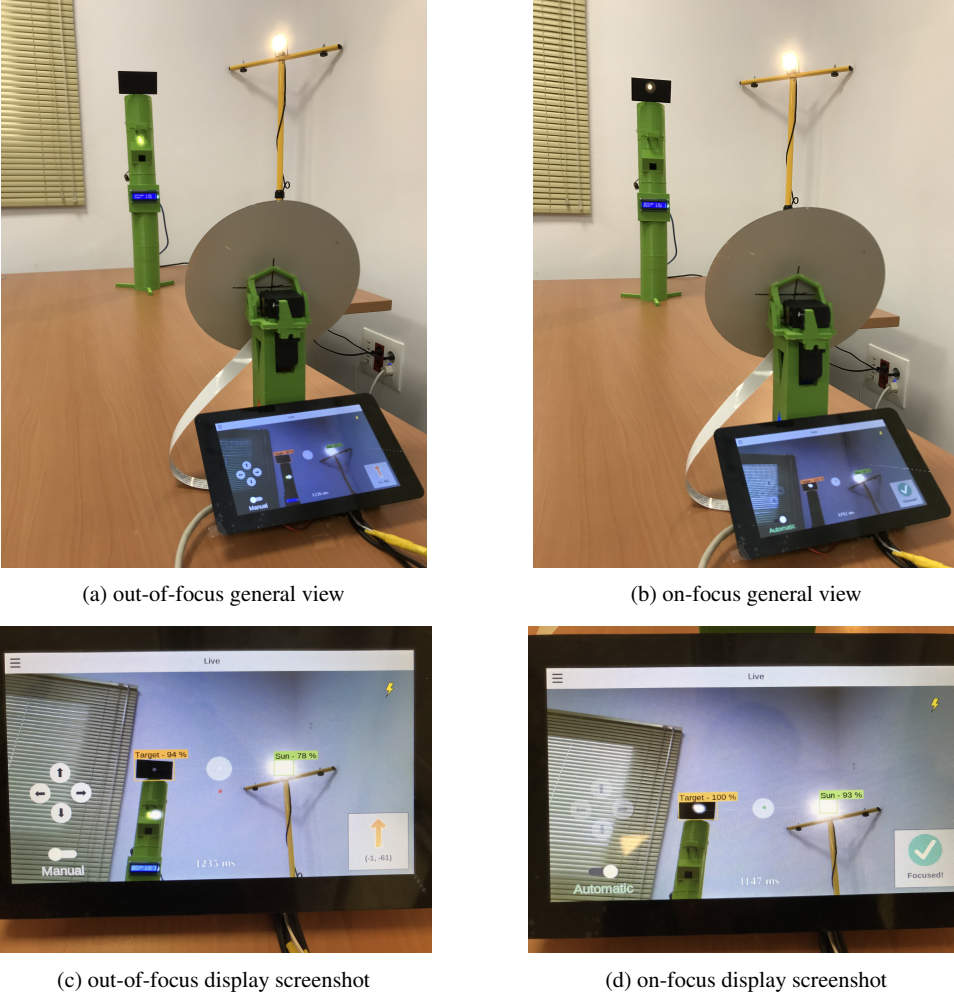


Figure 10: Working example

205 The evaluation of the validation set together with the training set also helps us to identify if the ANN is reducing the losses without overfitting the training set, i.e. the ANN is only valid for the training set and it does not predict properly the system that is being modeled. This situation happens when the validation losses increase, even though the training loss keep decreasing on each new epoch. In the treated case, both losses sets decreased during the whole training process. Figs. 9a and 9b show the normalized classification and localization losses [34] for the training (orange solid line) and validation (blue dashed line) sets during the whole training process (3,500 epochs).

210

#### 4.6. Working example

Fig. 10 shows the solar power tower mockup in two different scenarios. In both cases, the heliostat' camera captures a live video feed. Then, the ANN detects the objects of interest on each video frame, if objects are detected they are overlaid on each video frame and shown in the screen, together with the on-focus and current heliostat aiming points, as described in Fig. 6. The LCD shows the voltage across the PV panel and an estimation of the generated power.

215

In Figs. 10a and 10c, the heliostat is in manual mode. It is out of focus because the on-focus (big white circle) and current heliostat aiming point (red dot) are not aligned (see Fig. 10c) and therefore the bulb's light is reflected under

the PV panel (see Fig. 10a). In this mode, the user can perform manual tracking to align both aiming points by means  
220 of the buttons shown in the touchscreen display or by an attached Bluetooth device. The aiming error is also shown on the screen in pixels (see Fig. 10c, (-1,-61) in this case).

On the other hand, the heliostat is in automatic mode in Figs. 10b and 10d. In this case, the heliostat controller acts over the servo motors to continuously align the current and on-focus heliostat aiming points. The heliostat is indeed on focus because the bulb's light is reflected on the PV panel (see Fig. 10b). Notice that the current heliostat aiming  
225 point (green dot) is placed inside of the the on-focus heliostat aiming point (big white circle) in Fig. 10d.

## 5. Conclusions and ongoing work

To the knowledge of the authors, this is the first STP mockup for the assessment of advanced control techniques.  
230 The developed mechatronic system allows researchers to evaluate control techniques at early development stage, prior to the evaluation in a real STP facility. The system is designed to be easily built and assembled. It is based on low-cost low-consumption open-hardware components, open-source software and 3D-printed parts. It includes sensors (camera and motors' positions) and smart features (wireless communication and on-device machine learning) for the design of new Industry 4.0 heliostats. The mockup is a useful resource for education and demonstration purposes, since an ANN can be trained with objects that mimic the Sun and the receiver, such as a bulb and a PV panel as shown in this work. This is not possible with current industrial heliostat trackers since they are based on SPAs.

Ongoing work includes additional experiments for evaluating the mean error committed in the heliostat aiming  
235 by evaluating the Intersect over Union (IoU) values given by the ANN. IoU is an evaluation metric used to measure the accuracy of an object detector. It measures how much two regions overlap: the ground truth and the prediction. Currently, objects are detected using bounding boxes, this means that square or rectangular shapes are assumed. Traditional computer vision techniques or ANNs with segmentation support may decrease the localization loss. For  
240 instance, Mask R-CNN [37] could be applied for object instance segmentation. It is a CNNs that detects objects while simultaneously generate a high-quality segmentation mask at pixel level for each instance.

Future work will consider extensive training, validation and testing of the ANN to make it robust in real conditions (dust, partial clouds, etc.) and evaluate this new control technique in experimental campaigns at real STP plants.

## Acknowledgments

This work has been funded by the National R+D+i Plan Project ENE2017-83973-R (SOLTERMIN project) of the  
245 Spanish Ministry of Economy, Industry and Competitiveness and ERDF funds. This work was also partially supported by the computing facilities of Extremadura Research Centre for Advanced Technologies (CETA-CIEMAT), funded by the European Regional Development Fund (ERDF). CETA belongs to CIEMAT and the Government of Spain.

## References

- [1] New Energy Update, CSP Today Global Tracker (2019).  
URL <http://tracker.newenergyupdate.com/tracker/projects>
- [2] B. Schätz, M. Törngren, S. Bensalem, M. Cengarle, H. Pfeifer, J. McDermind, R. Passerone, A. Sangiovanni-Vincentelli, CyPhERS: Cyber-Physical European Roadmap & Strategy, Brussels (2015).
- [3] M. Kotýnková, Industry 4.0: Europe's (re)industrialization needs a Global Level, in: 16th International Scientific Conference on Globalization and its Socio-Economic Consequences, 2016, pp. 1014–1021.
- [4] C. Villasante, J. Mabe, I. Les, A. Peña, M. Sánchez, L. S., Smartcsp: The industry 4.0 approach for an effective csp cost reduction, in: 24th SolarPACES Annual Conference, Casablanca, Morocco, 2018.
- [5] K. Hwang, Y. S. Jung, Y. J. Heo, F. H. Scholes, S. E. Watkins, J. Subbiah, D. J. Jones, D. Y. Kim, D. Vak, Toward large scale roll-to-roll production of fully printed perovskite solar cells, Advanced Materials 27 (7) (2015) 1241–1247. doi:10.1002/adma.201404598.
- [6] K. Meub, Sandia labs news releases: New fractal-like concentrating solar power receivers are better at absorbing sunlight (2017).  
URL [https://share-ng.sandia.gov/news/resources/news\\_releases/fractal-solar/](https://share-ng.sandia.gov/news/resources/news_releases/fractal-solar/)
- [7] D. A. Flores-Hernández, S. Palomino-Resendiz, N. Lozada-Castillo, A. Luviano-Juárez, I. Chairez, Mechatronic design and implementation of a two axes sun tracking photovoltaic system driven by a robotic sensor, Mechatronics 47 (2017) 148–159. doi:<https://doi.org/10.1016/j.mechatronics.2017.09.014>.
- [8] P. Zhang, G. Zhou, Z. Zhu, W. Li, Z. Cai, Numerical study on the properties of an active sun tracker for solar streetlight, Mechatronics 23 (8) (2013) 1215–1222. doi:<https://doi.org/10.1016/j.mechatronics.2013.08.007>.

- [9] F. Téllez, M. Romero, P. Heller, A. Valverde, G. Dibowski, S. Ulmer, Thermal performance of solair 3000 kwth ceramic volumetric solar receiver, in: 12th SolarPACES Annual Conference, 2004.
- [10] Trimble, Sketchup - 3d design software (2019).  
URL <https://www.sketchup.com>
- [11] Arduino, Arduino Reference (2019).  
URL <https://www.arduino.cc/reference/en/>
- [12] Arduino, Arduino Software (IDE) (2019).  
URL <https://www.arduino.cc/en/main/software>
- [13] J. A. Carballo, J. Bonilla, L. Roca, M. Berenguel, New low-cost solar tracking system based on open source hardware for educational purposes, *Solar Energy* 174 (July) (2018) 826–836. doi:10.1016/j.solener.2018.09.064.
- [14] Raspberry Pi Foundation, Raspberry Pi - Teach, Learn, and Make with Raspberry Pi (2019).  
URL <https://www.raspberrypi.org/>
- [15] Raspberry Pi Foundation, Raspbian for Raspberry Pi (2019).  
URL <https://www.raspberrypi.org/downloads/raspbian/>
- [16] The Qt Company, Qt - Cross-platform software development for embedded & desktop (2019).  
URL <https://www.qt.io>
- [17] J. Abyz, The pigpio library (2019).  
URL <http://abyz.me.uk/rpi/pigpio/>
- [18] B. D. Swart, H. A. Engelbrecht, J. Treurnicht, A method for accurate measurement of heliostat mirror orientation, in: 4th Southern African Solar Energy Conference (SASEC), Stellenbosch, South Africa, 2016.
- [19] R. S. Baheti, P. F. Scott, Design of self-calibrating controllers for heliostats in a solar power plant, *IEEE Transactions on Automatic Control* AC-25 (6) (1980) 1091–1097.
- [20] McDonnell Douglas Astronautics Co., Solar One beam characterization system design description and requirements document, Tech. rep., Sandia National Laboratories, SAND-86-8179 (1986).
- [21] S. Jones, K. Stone, Analysis of strategies to improve heliostat tracking at Solar Two, Tech. rep., Sandia National Laboratories, SAND99-0092C (1999).
- [22] J. I. Burgaleta, A. Ternero, D. Vindel, I. Salbidegoitia, G. Azcarrraga, Gemasolar, key points for the operation of the plant, in: 18th SolarPACES Annual Conference, Marrakech, Morocco, 2012.
- [23] M. Berenguel, F. R. Rubio, A. Valverde, P. J. Lara, M. R. Arahal, E. F. Camacho, M. López, An artificial vision-based control system for automatic heliostat positioning offset correction in a central receiver solar power plant, *Solar Energy* 76 (5) (2004) 563–575. doi:10.1016/j.solener.2003.12.006.
- [24] S. Schell, Design and evaluation of esolar's heliostat fields, *Solar Energy* 85 (4) (2011) 614–619. doi:10.1016/j.solener.2010.01.008.
- [25] B. D. Swart, A method for accurate measurement of heliostat mirror orientation, Master thesis, Stellenbosch University (2017).  
URL <http://hdl.handle.net/10019.1/101038>
- [26] M. Burisch, M. Sánchez, X. Olano, A. Olarra, C. Villasante, D. Olasolo, R. Monterreal, R. Enrique, J. Fernández, Scalable HeliOstat calibRation sysTem (SHORT) – How to calibrate your whole heliostat field in a single night, in: 23rd SolarPACES Annual Conference, Chile, 2017.
- [27] J. A. Carballo, J. Bonilla, M. Berenguel, J. Fernández-Reche, G. García, New approach for solar tracking systems based on computer vision, low cost hardware and deep learning, *Renewable Energy* 133 (2019) 1158–1166. doi:10.1016/j.renene.2018.08.101.
- [28] A. Krizhevsky, I. Sutskever, G. E. Hinton, ImageNet classification with deep convolutional neural networks, in: F. Pereira, C. J. C. Burges, L. Bottou, K. Q. Weinberger (Eds.), Advances in Neural Information Processing Systems 25, Curran Associates, Inc., 2012, pp. 1097–1105.
- [29] The MathWorks Inc., MATLAB R2017b (2016).  
URL <http://www.mathworks.es/products/matlab/>
- [30] The MathWorks Inc., MATLAB - Computer Vision System Toolbox (2013).  
URL <http://www.mathworks.com/products/computer-vision/>
- [31] M. Abadi, A. Agarwal, P. Barham, E. Brevdo, Z. Chen, C. Citro, Corrado. G. S., A. Davis, J. Dean, M. Devin, S. Ghemawat, I. Goodfellow, A. Harp, G. Irving, M. Isard, Y. Jia, R. Jozefowicz, L. Kaiser, M. Kudlur, J. Levenberg, D. Mané, R. Monga, S. Moore, D. Murray, C. Olah, M. Schuster, J. Shlens, B. Steiner, I. Sutskever, K. Talwar, P. Tucker, V. Vanhoucke, V. Vasudevan, F. Viégas, O. Vinyals, P. Warden, M. Wattenberg, M. Wicke, Y. Yu, X. Zheng, TensorFlow: Large-scale machine learning on heterogeneous systems (2015).  
URL <https://www.tensorflow.org/>
- [32] Google AI, TensorFlow Lite - Deploy machine learning models on mobile and IoT devices (2019).  
URL <https://www.tensorflow.org/lite>
- [33] A. G. Howard, M. Zhu, B. Chen, D. Kalenichenko, W. Wang, T. Weyand, M. Andreetto, H. Adam, Mobilenets: Efficient convolutional neural networks for mobile vision applications, *CoRR* abs/1704.04861. arXiv:1704.04861.  
URL <http://arxiv.org/abs/1704.04861>
- [34] W. Liu, D. Anguelov, D. Erhan, C. Szegedy, S. E. Reed, C. Fu, A. C. Berg, SSD: single shot multibox detector, *CoRR* abs/1512.02325. arXiv:1512.02325.  
URL <http://arxiv.org/abs/1512.02325>
- [35] T. Lin, M. Maire, S. J. Belongie, L. D. Bourdev, R. B. Girshick, J. Hays, P. Perona, D. Ramanan, P. Dollár, C. L. Zitnick, Microsoft COCO: common objects in context, *CoRR* abs/1405.0312. arXiv:1405.0312.  
URL <http://arxiv.org/abs/1405.0312>
- [36] CETA-CIEMAT, Centro Extremeño de Tecnologías Avanzadas (2019).  
URL <https://www.ceta-ciemat.es/>
- [37] K. He, G. Gkioxari, P. Dollár, R. B. Girshick, Mask R-CNN, *CoRR* abs/1703.06870. arXiv:1703.06870.  
URL <http://arxiv.org/abs/1703.06870>

**A.8. Optimal Operation of solar thermal desalination systems coupled to double-effect absorption heat pumps**

# Optimal Operation of Solar Thermal Desalination Systems Coupled to Double-Effect Absorption Heat Pumps

Jose A. Carballo<sup>a,c</sup>, Javier Bonilla<sup>b,c</sup>, Lidia Roca<sup>b,c</sup>, Alberto de la Calle<sup>d</sup>, Patricia Palenzuela<sup>b</sup>, Diego C. Alarcón-Padilla<sup>b,c</sup>, Manuel Berenguel<sup>a,c</sup>

<sup>a</sup>*Universidad de Almería, Ctra. Sacramento, s/n, La Cañada, 04120 Almería, Spain.*

<sup>b</sup>*CIEMAT- Plataforma Solar de Almería, Ctra. de Senés s/n Tabernas, 04200, Spain.*

<sup>c</sup>*CIESOL Research Centre for Solar Energy, UAL-PSA.CIEMAT Joint Centre, Spain.*

<sup>d</sup>*CSIRO Energy, 10 Murray Dwyer Ct, Mayfield West, NSW 2304, Australia.*

---

## Abstract

A large part of the scientific community efforts are focused on improving the efficiency and reducing costs of desalination processes. This work presents a highly customizable dynamic model set for the design, control and optimization of solar thermal desalination systems. A methodology for the generation of system's optimal operation conditions according to several criteria based on genetic algorithms optimizations is also described.

The methodology has been tested in a solar-gas hybrid plant configuration modeled in this work considering the model set. Test results show that the methodology can find optimal operation according to one or several criteria, even in very adverse conditions.

**Keywords:** Multi-effect distillation, Heat pump, Parabolic trough collector, Multiobjective optimization, Modelica

---

*Email addresses:* jcarballo@psa.es (Jose A. Carballo), javier.bonilla@psa.es (Javier Bonilla), lidia.roca@psa.es (Lidia Roca), alberto.delacallealonso@csiro.au (Alberto de la Calle), patricia.palenzuela@psa.es (Patricia Palenzuela), diego.alarcon@psa.es (Diego C. Alarcón-Padilla), beren@ual.es (Manuel Berenguel)

## 1. Introduction and motivation

The traditional energy model and the world population growth are contributing to the fresh water scarcity and accelerating other problems arising from climate change. Humanity should adopt a more environmentally friendly energetic model and sustainable exploitation of natural resources to overcome these problems. Desalination techniques and solar energy are powerful technologies which can mitigate the energetic problems and fresh water scarcity since water-stressed regions are commonly arid regions with high levels of solar radiation.

Despite the efforts carried out in the last decades, there is still room for improvement in current desalination techniques, as shown by the large difference between the theoretical minimum required energy and the real requirements [1]. This room for improvement has driven the effort of the scientific community to work on new configurations to improve the process efficiency as shown by the latest works in this field [2, 3].

Among all desalination techniques, Multi-Effect Desalination (MED) is one of the main applied techniques at industrial level due to its ability to work in very hard conditions, since it is less affected by water quality or feed salinity than other technologies and it does not require water pretreatment [4]. However, MED technology is commonly replaced by other techniques because thermal distillation systems in general are considered energy-inefficient systems. This fact has limited its application to processes which can reuse waste thermal energy or to locations rich in fossil fuels where the energy cost is low. Furthermore, discontinuous energy supply is not suitable for MED technology, as well as for most desalination technologies, since it negatively impacts its reliability.

The coupling of MED with absorption heat pumps has been studied in the last decade [5, 6, 7] as an alternative to improve its thermal efficiency. The main drawback of this configuration is that its operation becomes more complex. Solar energy can provide thermal energy in a sustainable and cheap way [8, 9] for thermal desalination systems. However, the discontinuous nature of this energy

source is disadvantageous to operate the plant. Therefore, reducing the energetic production cost, developing new sustainable configurations based on renewable energy sources and optimal operation techniques can highly contribute to the development of thermal desalination processes.

As in many other research fields, the use of mathematical models enable to simulate the system behavior in different situations and configurations. This can save time, costs and avoid dangerous situations for people and resources. Due to the very complex thermal behavior of most of the subsystems that can be found in desalination systems powered by solar energy, dynamic modeling and simulation techniques are one of the most recommended options to develop studies about system design and operation strategies.

Previous works about thermal distillation include studies based on mathematical models and experimental data to find the optimal operating condition of MED systems according to different criteria [10]. Also, new criteria and performance indexes based on energy and exergy analyses have been proposed for a MED facility [11]. This study shows how exergy-based indexes can be useful to analyze and compare different systems and techniques, due to exergy-based indexes consider all energy demands, energy quality and environmental conditions. On the other hand, performance indexes based on thermal energy analyses only consider thermal energy.

There are also previous studies about the optimization of heat pumps coupled to MED for optimal operating conditions according to energetic and exergetic criteria, which aim to reduce energy consumption and increase the fresh water production of the whole system [7, 12]. Most of these studies set the optimal operation assuming a constant energy input, without taking into account that the heat energy source could be variable over time, as it happens with solar energy. In solar desalination systems, hybridization with other energy sources or large energy storage tanks enable to continuously operate the system in the optimal conditions, however both solutions could increase the cost of the fresh water, due to the initial investment. Note that hybridization can also harm the environment if fossil fuels are used. Therefore, in solar thermal

desalination aided by heat storage or hybridized with others energy sources, it is necessary to adjust the setpoint taking into account the available solar energy in order to minimize the energetic support, maximize the solar energy exploitation and extend the system operation. Therefore the main challenge of solar thermal desalination is to obtain fresh water by solar energy at a reasonable cost simplifying and optimizing the system operation.

This paper presents a set of dynamics models for thermal desalination to simulate the dynamic thermal behavior of different configurations and to optimize the system operation according to different criteria, for example maximizing the fresh water production. The structure of this paper is as follows. This section (Sec. 1) presents the introduction and motivation of this work. Then, Sec. 2 describes the system under study. Subsystem models are described (Sec. 3). Sec. 4 presents the evaluated plant configuration. After that, in Sec. 5, the optimal generator methodology is explained. The main results of this work are presented in Sec. 6. Finally, the main conclusions of this study are summarized in Sec. 7.

## 2. AQUASOL system

The research facility employed in this work has been extended and modified many times until reaching its current configuration (see Fig. 1). The most important modification was during the European Project *AQUASOL* that gives its name to the research facility. The *AQUASOL* project started in 2002 at Plataforma Solar de Almería (PSA) with the main goal of improving the solar thermal seawater desalination technology based on the MED process [13]. An existing MED system was coupled with a new Double-Effect Absorption Heat Pump (DEAHP) to improve the process efficiency [14], at the demonstration phase of the *AQUASOL* project. The systems was also completed with a smoke-tube gas boiler and a stationary compound parabolic concentrator solar collector field that was replaced later.

The present work considers the most relevant subsystems that are currently

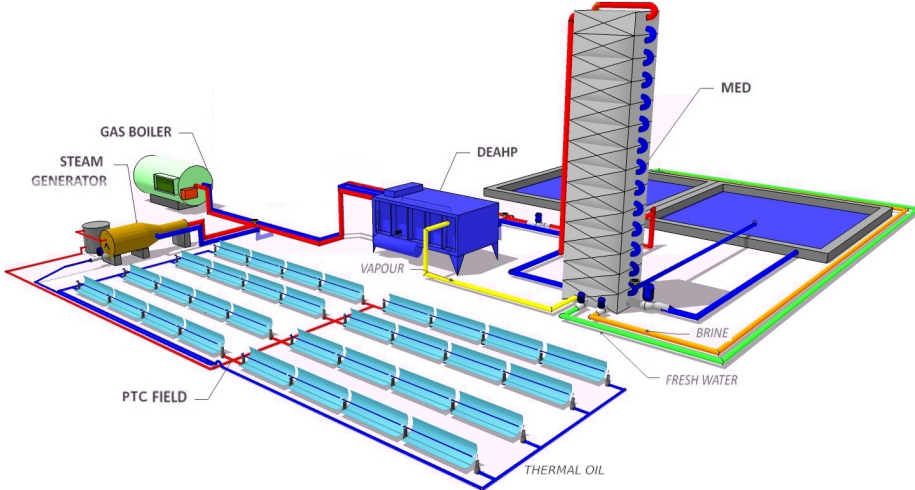


Figure 1: *AQUASOL* system

part of the *AQUASOL* facility (Fig. 2). Such subsystems are: a MED plant, a DEAHP, a small-aperture Parabolic Trough Collector (PTC) solar field, a steam generator and a generic gas boiler. The whole system is flexible since these components can be interconnected in different ways, enabling testing and evaluation of several configurations.

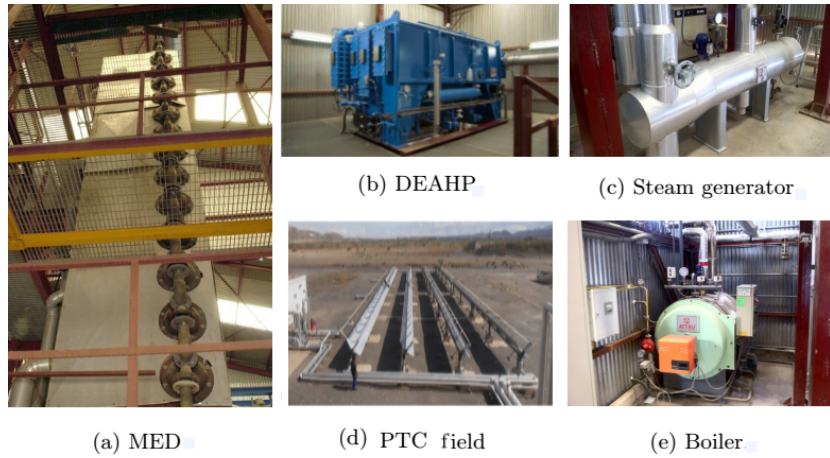


Figure 2: AQUASOL subsystems

**Multi-Effect Distillation plant.** The MED plant at the *AQUASOL* system dates from 1987, when a unit manufactured by *Entropie* was erected at PSA. The MED plant has been modified several times over the years, in 2005 the first effect was replaced by one with the ability to work with hot water instead of saturated steam. Nowadays, the MED plant is composed by 14 cells in a vertical arrangement, each cell is composed by a horizontal-tube bundle and a seawater pre-heater, where seawater evaporation is produced and part of this vapor is condensed, respectively. All the cells are identical besides the first and the last cells. The first cell effect has a special tube bundle configuration that is able to work with sensible heat from hot water [15] whereas the last cell pre-heater, called condenser, is much bigger than the other pre-heaters because it has to condense all the vapor generated in the last effect of the MED plant [16].

**Double-Effect Absorption Heat Pump.** Also in the framework of the *AQUASOL* project, a *DEAHP*, whose working fluid is  $LiBr/H_2O$ , was installed at PSA with the aim of making the desalination process based on MED more efficient from the thermal energy point of view. This system has exhibited a difficult operation due to its working limitations and complex behaviour, where the optimum operation conditions were hard to maintain while preventing the fluid crystallization [7]. Some previous works focused on settings optimal operating parameters that ensure *DEAHP* operation in steady state conditions [7, 12].

**Parabolic Trough Collector field.** The *AQUASOL* system includes a small aperture PTC field. It has 8 units of the PolyTrough 1200 PTCs [17] which are disposed in 4 parallel rows with 2 collectors in series per row. The PTC field uses *Therminol 55* [18] thermal oil as Heat Tranfer Fluid (HTF). This PTC field was designed to provide part of the thermal energy demanded by the absorption heat pump.

**Steam generator.** The *AQUASOL* system also includes a shell-and-tube steam generator where the HTF flows through the tubes, and the water is inside a pressure vessel where saturated steam is generated.

**Gas boiler.** The AQUASOL system has a commercial smoke-tube gas boiler. This boiler was designed to generate the steam demanded by the DEAHP.

### 3. AQUASOL subsystem modelling

*Modelica* [19] was the non-proprietary object-oriented modeling language used for the development of the dynamic model set. This language facilitates to formulate complex physical multi domain systems in an acausal way. The *Modelica* standard library [20] and the *Thermocycle* library [21] were used for modeling all the subsystems. *Dymola* [22] was the development tool used for the implementation and simulation tasks. Simulations carried out in this work used Direct Normal Irradiance (DNI) (Fig. 3), ambient temperature and wind speed open data from the Photovoltaic Geographical Information System (PVGIS) [23]. These hourly data are available online free of charge [24], in order to use them it have been interpolated. Simulations and optimization were performed considering the spring equinox day at PSA.

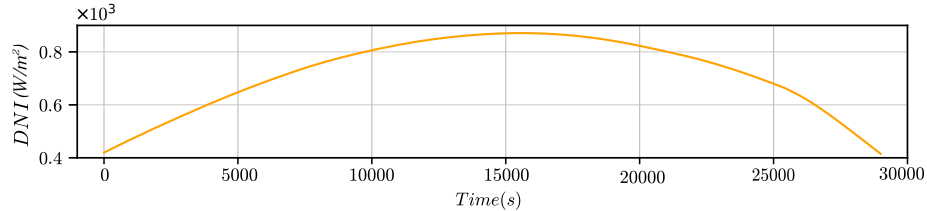


Figure 3: DNI data employed in the simulations.

#### 3.1. Multi-Effect Distillation model

A dynamic model of the PSA MED unit was designed according to the mathematical formulation of the physical principles which describe the main heat and mass transfer phenomena that take place in this system [16]. The model was calibrated and validated with experimental data. Recently, the model has been updated with the exergy formulation to develop new performance indexes based on exergy analyses. This new formulation was used to find optimal

operation [10, 11]. The model has been extended in the present work to support interconnection with other systems, the condenser was removed and the last MED cell was connected to an absorption heat pump.

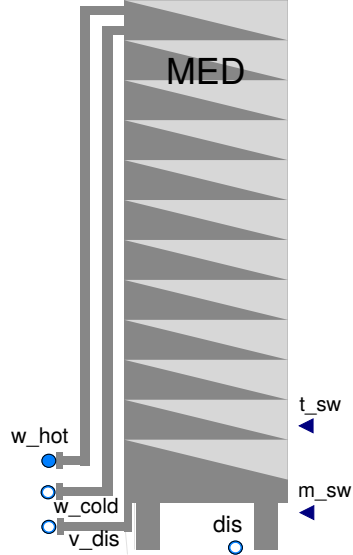


Figure 4: MED unit interface

Fig. 4 shows the highest layer of abstraction of the MED model where the connection with other models is performed through the input and output ports: inlet hot water to the MED heater ( $w_{hot}$ ), outlet cold water from the MED heater ( $w_{cold}$ ), outlet vapor from the last effect ( $v_{dis}$ ), outlet distillate ( $dis$ ), seawater mass flow rate ( $m_{sw}$ ) and temperature ( $t_{sw}$ ) input signals. Since *Modelica* support acausal modeling, ports can act as inputs or outputs (circular connectors in Fig. 4), also support input and outputs signal (triangle connector). *Modelica* support different kinds of connectors, for example fluid connectors transmit mass flow rate, pressure, enthalpy and mass fraction of a particular fluid, whereas heat connectors propagate information about heat flow rate and temperature. In Sec. Appendix A, Fig. A.15 shows the internal components of this model.

### 3.2. Double Effect Absorption Heat Pump model

A non-linear first-principles dynamic model of the DEAHP was developed to study the main thermochemical processes which drives the system [25]. This model was calibrated and validated with experimental data from experimental campaigns in the pilot plant at *PSA*.

To reduce the complexity of the model and facilitate the optimization process, the dynamic model has been linearized using the System Identification Toolbox<sup>TM</sup> provided by MATLAB<sup>®</sup>. Such linear equations have been implemented in *Modelica* (Sec. [Appendix A](#), Fig. [A.16](#)) and encapsulated in a higher layer of abstraction (see Fig. 5). Input and output ports of the DEAHP model are: inlet and outlet steam ( $s_{in}$  and  $s_{out}$ ), inlet and outlet water ( $w_{cold}$  and  $w_{hot}$ ), inlet vapor ( $v_{dis}$ ), outlet distillate ( $dis$ ), temperature difference between the *LiBr* solution inside the high-temperature generator and the water at the outlet of the low-temperature generator ( $D1$ ), temperature difference between the *LiBr* solution inside the low-temperature generator and the water at the outlet of condenser vessel ( $D2$ ), distillate vapor pressure ( $p_{dis}$ ) and hot water mass flow rate ( $m_{w\_hot}$ ).

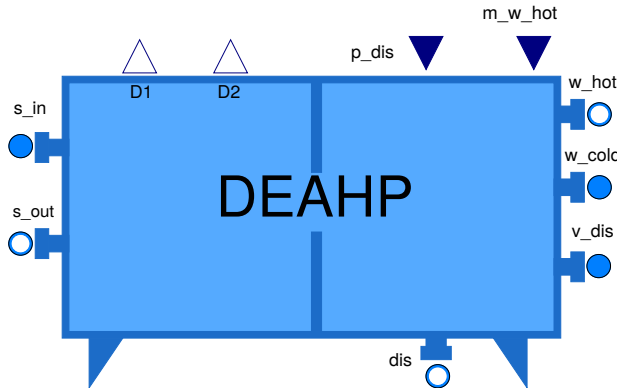


Figure 5: DEAHP Interface

The linear approximation was obtained by fitting a linear model to the simulated response of the non-linear model. For the simulation process, the inputs of the model were varied in their operating ranges: steam pressure inlet through

*s\_in* (*s\_p*) [6-11] bar, *p\_dis* [35-70] mbar, *m\_w\_hot* [9-12] kg/s and *t\_w\_cold* [56-60] °C. The main outputs of the model are the temperature at the outlet of the DEAHP (*t\_w\_hot*) and the condensate mass flow rate at the outlet of the high-temperature generator (*m\_s\_out*). It is important to mention that two additional outputs have been added to assure that the DEAHP operation is outside of the crystallization zone (*D1* and *D2*). Following the manufacturer recommendations, the operation of the DEAHP must assure that *D1* < 50 °C and *D2* < 45 °C.

The linear model of the system can be described as follows (Eq. 1),

$$H_i(s) = \sum_{j=1}^n H_{ij}(s) = \sum_{j=1}^n \frac{Y_i(s)}{U_j(s)} = \sum_{j=1}^n \frac{a_{2,j}s^2 + a_{1,j}s + a_{0,j}}{b_{2,j}s^2 + b_{1,j}s + b_{0,j}}, \quad (1)$$

where index *i* refers to the output of the system, *j* to the input, *n* is the number of inputs of the model and the values of the transfer function polynomial coefficients ( $a_{xj}$  and  $b_{xj}$ , for *x* in [0 – 2]), see Tab. 1.

Output (i)	Input(j)	$a_2$	$a_1$	$a_0$	$b_2$	$b_1$	$b_0$
$t\_w\_hot$ (1)	$s\_p$ (1)	-	$2.13 \cdot 10^{-2}$	$4.16 \cdot 10^{-6}$	1	$2.22 \cdot 10^{-2}$	$5.89 \cdot 10^{-6}$
	$p\_dis$ (2)	-	-	$6.46 \cdot 10^{-1}$	-	1	$8.5 \cdot 10^{-3}$
	$m\_w\_hot$ (3)	-	-	$-1.18 \cdot 10^{-1}$	-	1	$3.7 \cdot 10^{-2}$
	$t\_w\_cold$ (4)	-	-	$1.68 \cdot 10^{-2}$	-	1	$2.65 \cdot 10^{-2}$
$m\_s\_out$ (2)	$s\_p$ (1)	$4.69 \cdot 10^{-2}$	$1.01 \cdot 10^{-3}$	$7.14 \cdot 10^{-8}$	1	$2.22 \cdot 10^{-2}$	$5.87 \cdot 10^{-6}$
	$p\_dis$ (2)	-	$4.01 \cdot 10^{-3}$	$2.31 \cdot 10^{-5}$	1	$4.69 \cdot 10^{-2}$	$1.17 \cdot 10^4$
	$m\_w\_hot$ (3)	-	$1.4 \cdot 10^{-5}$	$1.52 \cdot 10^{-7}$	1	$2.03 \cdot 10^{-2}$	$2.23 \cdot 10^4$
	$t\_w\_cold$ (4)	-	-	$1.68 \cdot 10^{-2}$	-	1	$2.65 \cdot 10^{-2}$
$D1$ (3)	$s\_p$ (1)	-	-	$7.18 \cdot 10^{-3}$	-	1	$3.42 \cdot 10^{-3}$
	$p\_dis$ (2)	-	-	$3.23 \cdot 10^{-3}$	1	$1.21 \cdot 10^{-2}$	$2.51 \cdot 10^{-5}$
	$m\_w\_hot$ (3)	-	-	$2.872 \cdot 10^{-6}$	1	$1.77 \cdot 10^{-2}$	$8.56 \cdot 10^{-5}$
	$t\_w\_cold$ (4)	-	$-7.99 \cdot 10^{-5}$	$5.37 \cdot 10^{-7}$	1	$4.37 \cdot 10^{-3}$	$8.76 \cdot 10^{-6}$
$D2$ (4)	$s\_p$ (1)	-	$-2.72 \cdot 10^{-3}$	$1.43 \cdot 10^{-3}$	1	$4.97 \cdot 10^{-2}$	$6.93 \cdot 10^{-4}$
	$p\_dis$ (2)	-	-3.49	$-8.66 \cdot 10^{-3}$	1	$9.66 \cdot 10^{-2}$	$3.8 \cdot 10^{-4}$
	$m\_w\_hot$ (3)	-	$1.27 \cdot 10^{-2}$	$1.18 \cdot 10^{-4}$	1	$5.11 \cdot 10^{-2}$	$7.39 \cdot 10^{-4}$
	$t\_w\_cold$ (4)	-	$-1.52 \cdot 10^{-2}$	$-2.034 \cdot 10^{-4}$	1	$3.3 \cdot 10^{-2}$	$5.60 \cdot 10^{-4}$

Table 1: Polynomial coefficient values of the DEAHP lineal model

Fig. 6 shows the validation test of the linear model. The simulation results with the linear model (*linear*) are similar to the simulation results with the non-linear model (*non - linear*), where the maximum error is lower than 0.5 °C. Therefore, the first one can be employed to simulate the DEAHP thermal behavior without an important loss of accuracy.

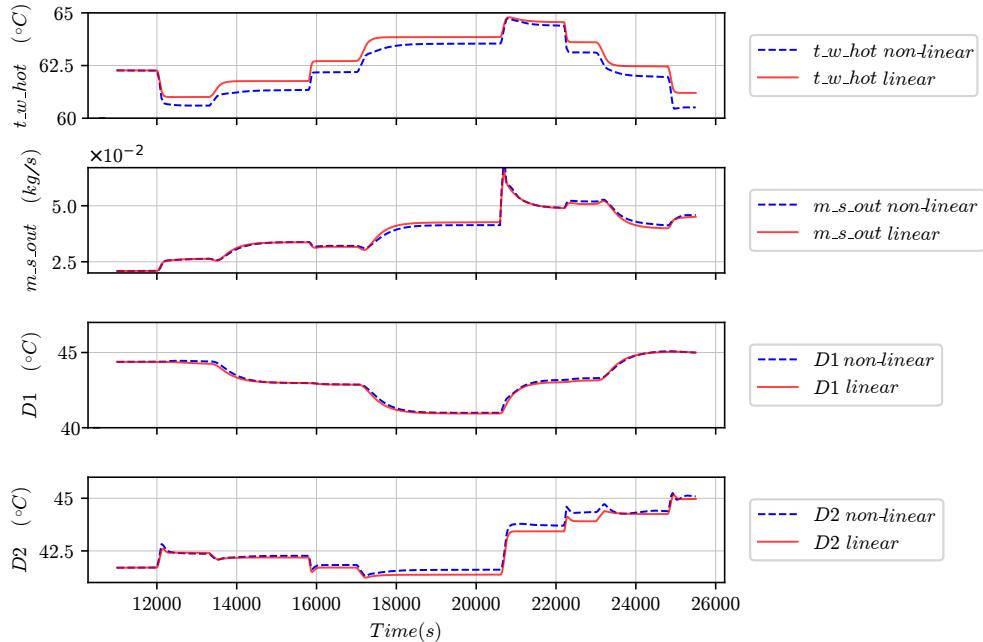


Figure 6: DEAHP linear model validation

### 3.3. Parabolic through collector model

A previous work about *AQUASOL* PTC solar field, presented a dynamic model developed using *Modelica* and the *ThermoCycle* library. This model was calibrated and validated with data from test campaigns carried out at *PSA*. This model is suitable for optimization, performance evaluation and control purposes [26].

Fig. 7 shows the highest abstraction layer and the internal components. This model requires environmental variables as inputs: wind speed ( $v_{wind}$ ), solar

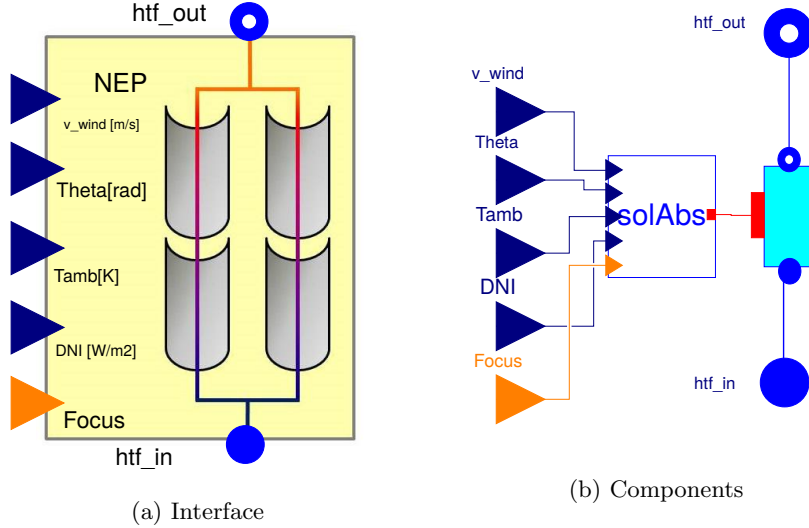


Figure 7: PTC field

incidence angle ( $\Theta$ ), ambient temperature ( $T_{amb}$ ), DNI and PTC on-focus status ( $Focus$ ). It also has two HTF input-output ports ( $htf\_out$  and  $htf\_in$ ).

### 3.4. Steam Generator model

The steam generator model was implemented using the Modelica Fluid library. The tube bundle exchanges energy from the hot HTF to the water inside the generator to generate saturated steam. This last physical process was implemented considering the dynamic model of a drum boiler [27]. The steam generator interface has five input and output ports (see Fig. 8): inlet and outlet HTF ( $htf\_in$  and  $htf\_out$ ), inlet water ( $s\_in$ ), outlet vapor ( $s\_out$ ) and the liquid water level inside the steam generator tank ( $w\_level$ ).

### 3.5. Gas Boiler model

There is not enough available design information about the commercial gas boiler at the *AQUASOL* system to properly model its dynamic behavior. Therefore, the gas boiler has been modeled as a simple thermal energy source that provides a specified amount of heat flow prescribed by an input signal ( $q\_boiler$ ),

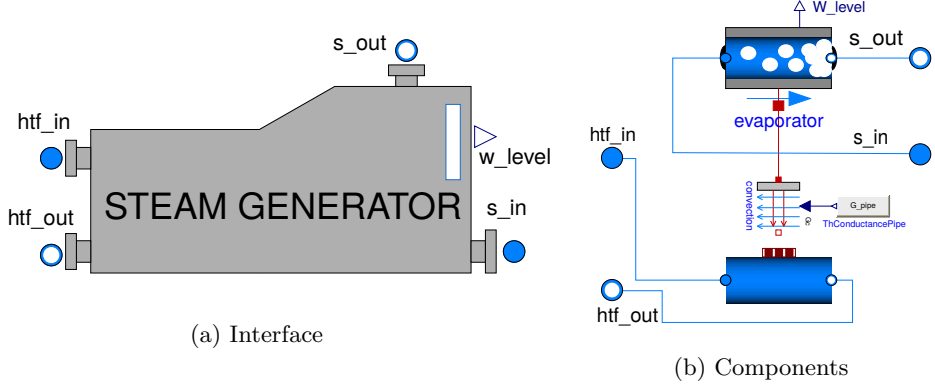


Figure 8: Steam generator

see Fig. 9. The HTF flows inside the boiler from  $htf\_in$  to  $htf\_out$  and acquires the prescribed heat flow increasing its temperature.

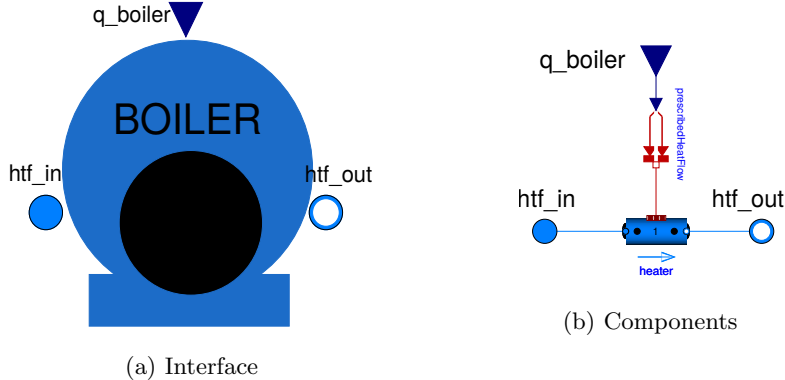


Figure 9: Gas boiler

#### 4. Hybrid solar-gas DEAHP-MED configuration

For the present work, a hybrid solar-gas configuration is proposed (see Fig. 10). In this configuration, the thermal energy demanded by the system is provided by the PTC field and the gas boiler connected in series. The HTF from the PTC field is heated up in the gas boiler and exchanges heat with the

water inside the steam generator which supplies steam to the DEAHP. The thermal energy from the last MED effect together with the thermal energy of the steam from the steam generator is employed to feed the MED first effect thermal energy demands. As commented before, some *AQUASOL* subsystems exhibit complex dynamics at startup, partial load operation and transitory states which make this configuration one of the most complex configurations to optimally operate.

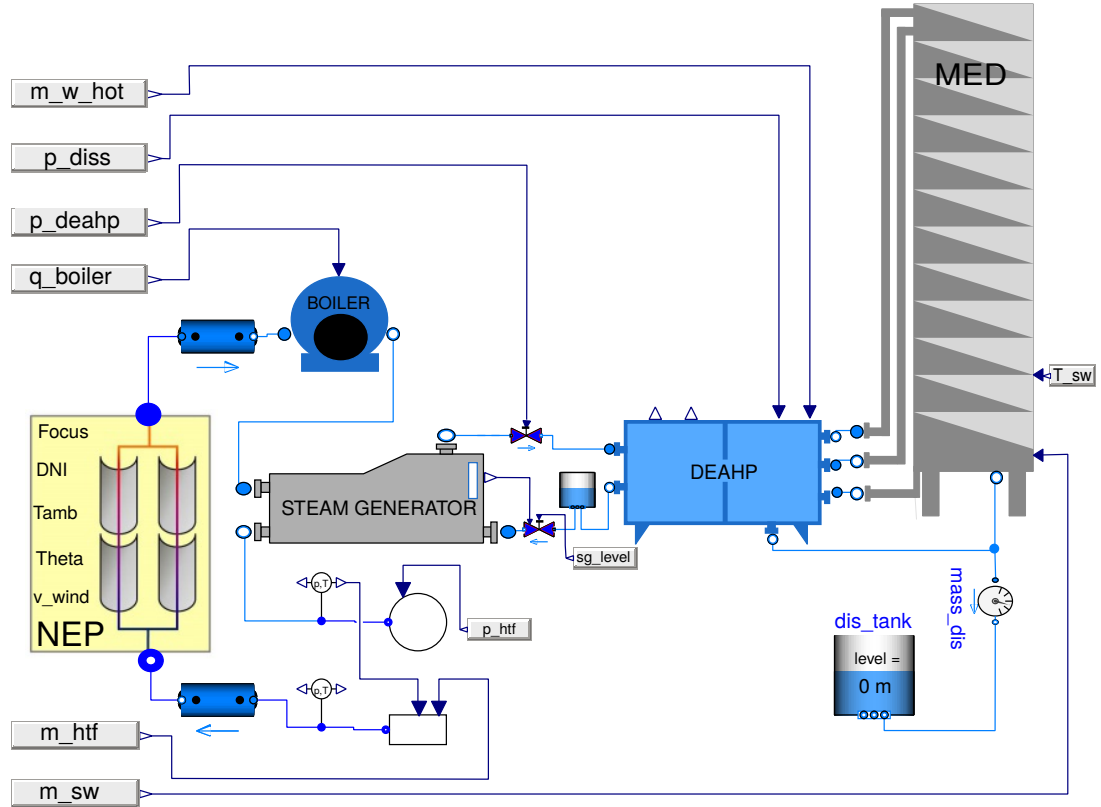


Figure 10: Hybrid gas-solar

The HTF mass flow rate in the PTC field ( $m_{htf}$ ), the distillate vapor pressure ( $p_{dis}$ ), steam pressure in the DEAHP ( $p_{deahp}$ ), thermal energy provided by the boiler ( $q_{boiler}$ ), the hot water mass flow rate in the MED heater

( $m_w_{hot}$ ) and seawater feed mass flow rate ( $m_{sw}$ ), have been selected as main manipulable variables signals.

Note that each subsystem was independently designed, therefore some of them will operate out of their nominal conditions when working together.

## 5. Optimal operation

As commented before, some subsystems require special operating conditions which impose limitations to the operation strategy. This is especially relevant in the initialization and operation at partial load. Furthermore, the overall system operation strategy must ensure that the whole system works in optimal global conditions, which can be different from the optimal operation conditions for each isolated subsystem. For this reason, it is necessary to create a top control layer that guarantees optimal operation of the entire system.

In this work, a flexible optimal manipulable variables generator method is proposed. It is based on a multiobjective optimization process that employs the model set previously described to simulate the thermal transient behavior of the *AQUASOL* system.

Within this optimization process, the first step is to study the system configuration and the manipulable variables which make up the operation conditions. The dependencies of the manipulable variables with other variables are also studied and described mathematically. Then the system configuration replicated using the model set is employed to evaluate the values of the manipulable variables that guarantees the optimal operation based on one or several criteria.

In this case the optimization is based on a genetic algorithm and the manipulable variables highly depends on the DNI and Operation time ( $t$ ), therefore every manipulable variable ( $m_{sw}$ ,  $m_w_{hot}$ ,  $p_{dis}$ ,  $m_{htf}$ ,  $p_{deahp}$  and  $q_{boiler}$ ) is computed considering the Taylor multivariable series order 2 centered on 0 (see Eq. 2). Taylor series, centered on 0 also called Maclaurin series, is employed for polynomial approximation of functions. According to Eq. 2, six parameters ( $u_{ai}$ ,  $u_{bi}$ ,  $u_{ci}$ ,  $u_{di}$ ,  $u_{ei}$  and  $u_{fi}$ ) together with the inlet DNI and  $t$  are demanded

to compute each manipulable variable ( $u_i$ ). Therefore, the manipulable variable values could change (trajectory) during the operation according to the DNI and  $t$  values. In addition to the relationship described in Eq. 2, other kinds of relationships can be also considered if required, such as exponential, logarithmic, etc. Additional variables could be also easily included, for instance ambient or seawater temperature.

$$u_i = u_{ai} + u_{bi} \cdot t + u_{ci} \cdot DNI + \frac{1}{2}(u_{di} \cdot t^2 + 2 \cdot u_{ei} \cdot DNI \cdot t + u_{fi} \cdot DNI^2) \quad (2)$$

The main goal of the optimization process is to provide the optimal value for the six parameters ( $u_{ai}$ ,  $u_{bi}$ ,  $u_{ci}$ ,  $u_{di}$ ,  $u_{ei}$  and  $u_{fi}$ ) of each  $u_i$ . The optimization tasks are carried out through the *Dymola* optimization library [28]. The optimization problem can be formulated as optimize (minimize or maximize) several objective functions  $f(u)$  (multi objective) that depend on a number of manipulable variable parameters ( $u_{a1}$ ,  $u_{b1}$ ,  $u_{c1} \dots u_{di}$ ,  $u_{ei}$  and  $u_{fi}$ ) subject to several constraints: upper and lower bounds for design variables ( $u_l$  and  $u_u$ ), equality constraints ( $g(u)$ ) and inequality constraints ( $h(u)$ ), see Eq. 3.

$$\begin{aligned} & \text{optimize} && f(u) \\ & \text{with respect to} && u \in B \\ & \text{subject to} && u_l \leq u \leq u_u, \\ & && g(u) = 0, \\ & && h(u) \leq 0, \end{aligned} \quad (3)$$

where,

$$\begin{aligned} f(u) &= \{f_1(u) \dots f_i(u)\}, \\ u &= \{u_{a1}, u_{b1}, u_{c1} \dots u_{di}, u_{ei}, u_{fi}\}, \\ u_l &= \{u_{l,1} \dots u_{l,k}\}, \\ u_u &= \{u_{u,1} \dots u_{u,k}\}, \\ g(u) &= \{g_1(u) \dots g_k(u)\}, \\ h(u) &= \{h_1(u) \dots h_n(u)\}. \end{aligned}$$

The optimizer applies evolutionary programming, in particular a genetic algorithm implemented within the *Dymola* optimization library [28]. The genetic algorithm modifies  $u$  vector values and simulate the system with the new configuration to find the optimum while satisfying the imposed restrictions.

Two different optimizations have been carried out, in the first one, the maximization of the distillate production ( $dis\_tank$ ) has been selected as the optimization criterion. The second one is a multi-objective optimization and considers two optimization criteria, maximize the distillate production and minimize the total boiler thermal energy contribution ( $Q\_boiler$ ). Note that optimizations do not consider the electricity consumption of the different pumps present in the plant, because currently this consumption is not monitored. As a restriction, it is considered that the system only works when the DNI is higher than 400 W/m<sup>2</sup>.

Tab. 2 shows the initial, nominal, minimum and maximum values of each manipulable variable employed for the optimizations. Initial values have been defined manually constant along the simulation. Nominal, minimum and maximum values have been set from individual subsystems technical requirements.

Manipulable Variable	Unit	Min	Max	Nominal	Initialization
$m_{sw}$	$kg/s$	0.5	2.5	2.2	0.6
$m_{w\_hot}$	$kg/s$	6	15	12	12
$p_{dis}$	$Pa$	$3.5 \cdot 10^3$	$5.1 \cdot 10^3$	$4.2 \cdot 10^3$	$4.5 \cdot 10^3$
$m_{htf}$	$kg/s$	1.1	3.3	2	1.3
$p_{deahp}$	$bar$	7.5	8.5	8	7.5
$q_{boiler}$	$kW$	0	250	—	80

Table 2: Restrictions, nominal and initial values of each manipulable variable.

## 6. Optimization results

### 6.1. Fresh water production maximization

The genetic algorithm optimization was limited to 1000 generations with 10 individuals per generation. During the optimization, the improvement of the results from the simulation number 1200 to 1700 was lower than 0.5%, therefore 1700 evaluations are assumed to be enough for the optimizer to converge to optimal solutions. More than 70 % of the simulations did not end satisfactorily, due to the operational system restrictions or due to problems in the initialization of the model. This fact shows how difficult it is to find the operation strategy for the proposed system that maintains the operating conditions in the allowed ranges while optimizing the plant operation.

Optimized results show a total thermal energy consumption from gas boiler ( $Q_{boiler}$ ) of 240 kWh for a total distillate production ( $dis\_tank$ ) of 7.1 m<sup>3</sup>, 20% more of distillate production and a total thermal energy consumption increment of 37% with respect to the initial conditions manually determined Tab. 2. The system was able to operate during the optimized time series, despite the adverse conditions of partial loads and transitory states. For example, the nominal fresh water production of the MED plant is 0.65 kg/s, far from the distillate production range obtained in this optimization (around 0.25 kg/s see, Fig. 11) for the solar-gas hybrid design proposed. Nevertheless, the generator keeps the system running despite the overall system limitations. Note that it is not possible to operate this configuration considering the subsystems nominal operation conditions due to the different individual nominal conditions.

All of the optimized manipulable values (see Tab. 3, Fig. 12 and Fig. 13) are within the values range (see Tab. 2), this means that the optimal values is within the decision space analyzed.

Fig. 12 and Fig. 13 show the evolution during the simulation of the optimized manipulable variables values. Note that  $q\_boiler$  is mainly inversely proportional to the DNI and experiments the largest variation respect to its initial value, in contrasts to  $m\_w\_hot$ ,  $p\_dis$  and  $p\_deahp$  that are directly proportional to

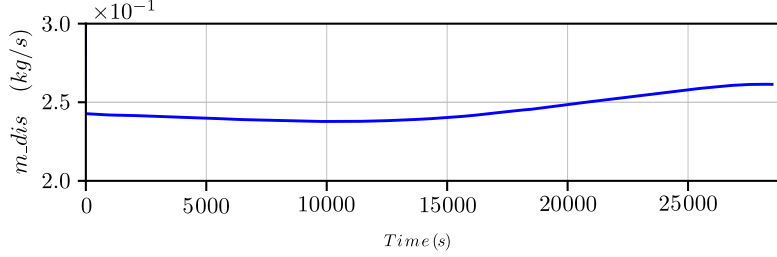


Figure 11: Total fresh water production mass flow (*total\_m\_dis*).

---


$$\begin{aligned}
m_{sw} &= 0.846 - 4.36 \cdot 10^{-6} \cdot t + 3.06 \cdot 10^{-4} \cdot DNI + \frac{1}{2}(2.57 \cdot 10^{-10} \cdot t^2 \\
&\quad + 2 \cdot 9.70 \cdot 10^{-9} \cdot DNI \cdot t - 8.72 \cdot 10^{-7} \cdot DNI^2) \\
m_{w\_hot\_b} &= 11.7 + 7.60 \cdot 10^{-6} \cdot t + 3.22 \cdot 10^{-5} \cdot DNI + \frac{1}{2}(8.77 \cdot 10^{-10} \cdot t^2 \\
&\quad + 2 \cdot 2.25 \cdot 10^{-9} \cdot DNI \cdot t - 2.96 \cdot 10^{-7} \cdot DNI^2) \\
p_{dis\_b} &= 4.57 \cdot 10^3 + 5.70 \cdot 10^{-4} \cdot t - 3.58 \cdot 10^{-2} \cdot DNI + \frac{1}{2}(8.77 \cdot 10^{-7} \cdot t^2 \\
&\quad + 2 \cdot 7.53 \cdot 10^{-6} \cdot DNI \cdot t + 7.83 \cdot 10^{-5} \cdot DNI^2) \\
m_{htf\_b} &= 1.63 + 9.75 \cdot 10^{-9} \cdot t - 5.86 \cdot 10^{-4} \cdot DNI + \frac{1}{2}(-3.54 \cdot 10^{-10} \cdot t^2 \\
&\quad + 2 \cdot 5.05 \cdot 10^{-8} \cdot DNI \cdot t + 1.26 \cdot 10^{-7} \cdot DNI^2) \\
q_{boiler} &= 9.88 \cdot 10^4 + 6.84 \cdot 10^{-5} \cdot t - 9.45 \cdot 10 \cdot DNI + \frac{1}{2}(-3.69 \cdot 10^{-7} \cdot t^2 \\
&\quad + 2 \cdot 2.35 \cdot 10^{-6} \cdot DNI \cdot t + 9.78 \cdot 10^{-8} \cdot DNI^2) \\
p_{deahp} &= 7.51 \cdot 10^5 + 5.40 \cdot 10^{-3} \cdot t + 2.69 \cdot 10^{-1} \cdot DNI + \frac{1}{2}(5.40 \cdot 10^{-7} \cdot t^2 \\
&\quad - 2 \cdot 9.30 \cdot 10^{-6} \cdot DNI \cdot t - 9.96 \cdot 10^{-5} \cdot DNI^2)
\end{aligned}$$


---

Table 3: Optimized functions to compute manipulable variables according to DNI and t.

the operation time (t) and their variations are not so significant, specially for  $p_{deahp}$  and  $m_{w\_hot}$ . Finally,  $m_{htf}$  and  $m_{sw}$  show a similar DNI and t dependent pattern.

In Fig. 11 shows the total fresh water mass flow (*total\_m\_dis*) evolution according to the optimal values. Initially, distillate or fresh water production starts with a slight decrease rate, after 10000 seconds the production increases until reaching a maximum close to the end of the simulation. This

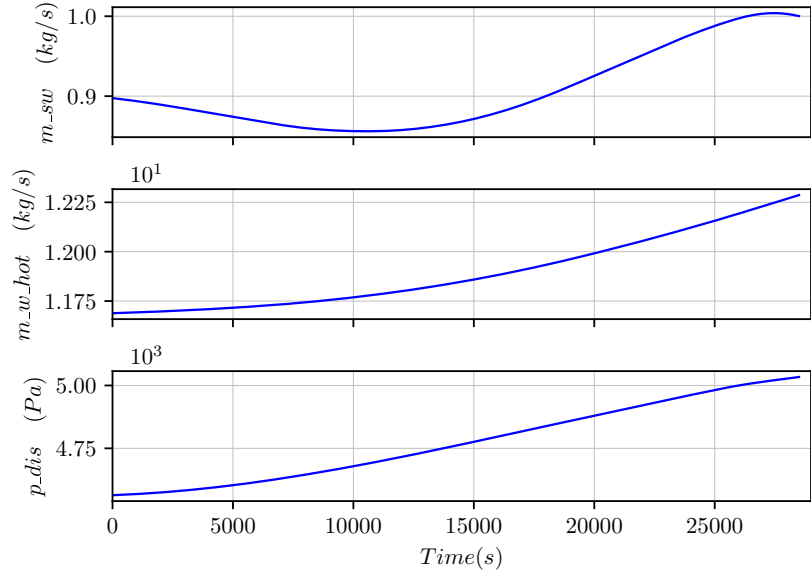


Figure 12: Optimized manipulable variables evolution during the simulation.

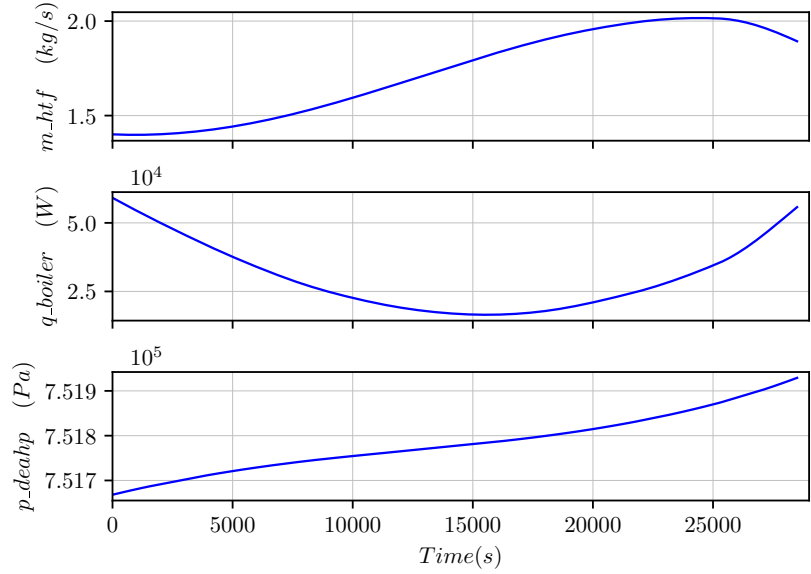


Figure 13: Optimized manipulable variables evolution during the simulation.

behavior is similar to the optimized values of  $m_{sw}$  and  $m_{htf}$  during the simulation (Fig. 12 and Fig. 13), therefore the fresh water or distillate production

is very related to these two manipulable variables.

### 6.2. Fresh water production maximization and thermal energy consumption minimization

The second optimization process tried to maximize the distillate production and minimize the thermal energy consumption from the boiler at the same time (multicriteria optimization). In this case, the genetic algorithm converged with less than 2000 simulations. An optimal solution in the Pareto front achieves a total distillate production (*dis\_tank*) of  $6.7 \text{ m}^3$ , consuming all the solar energy collected in the PTC field and  $193 \text{ kWh}$  of thermal energy from the boiler (*Q\_boiler*). This is a 14% increase of the distillate production and 10% increase of the thermal energy from gas boiler consumption with respect to the initial case.

The thermal energy consumption from the boiler represents the 80% of the consumption in the previous optimization, also *dis\_tank* is the 94%. Fig. 14 shows the criteria space and the Pareto optimal front (red line) computed by the genetic algorithm in the two optimization processes. Pareto optimal front and the previous results suggest that the thermal energy demand to increase the fresh water production grows exponentially. The multiobjective optimization provides a set of solutions that are a trade-off between thermal energy consumption and fresh water production. These optimizations can be used to select the optimal solution that guarantees the maximum of distillate production at minimum cost by setting weights to each criteria, for instance the cost of thermal energy and the price of fresh water.

## 7. Conclusions

A set of customizable dynamic models for solar thermal desalination systems have been presented. Such models were calibrated and validated against experimental data. The model set has proven to be a powerful and highly configurable tool for modeling, control and optimization tasks for solar energy desalination

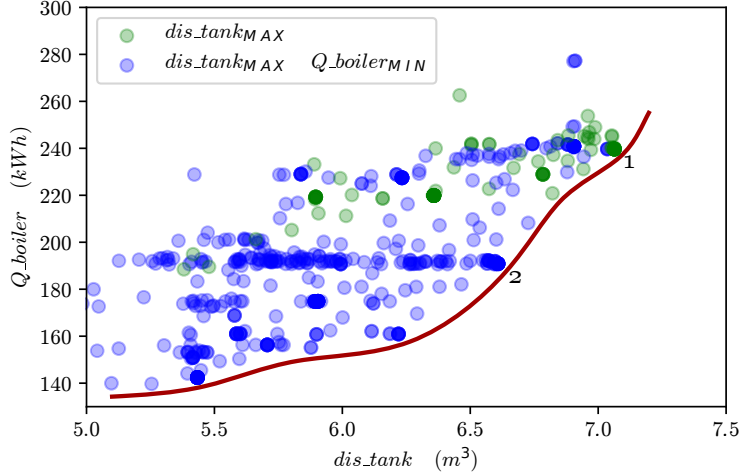


Figure 14: Optimization criteria space, Pareto front, maximum distillate point (1) and minimum thermal energy consumption from boiler together maximum distillate point (2).

systems, since it enables to replicate real systems or to design new configurations. Note that the model set simulates the system thermal behavior taking into account the operation limitations of the subsystems.

A method for the generation of system optimal operation conditions according to one or several criteria and modify it regarding one or several variables with different relations is described. The operation strategy of the system proposed was optimized using this method and attending to different criteria: maximize water production and/or minimize energy usage.

The method enabled to find an optimal manipulable variables values with respect to some criteria, even for configurations with complex operation schemes while keeping the system in operation despite the limitations imposed by the subsystems, the partial load operation or the transients states. The optimized trajectories to maximize the distillate production along the day increases the production and the optimized trajectories to minimize the thermal consumption and to maximize the production generate a optimum Pareto front.

Future work includes enriching the model set with additional models (tanks,

flat-plate solar collectors, etc.) and performing economic optimizations. Several additional factors can be included for more precise economic optimizations, such as investment costs, fixed costs and consumption of electric devices (pumps, valves, etc.). Also, optimizations will be carried out with more simulation days to generalize the optimal operating strategy along the year and different DNI profiles.

## **8. Acknowledgements**

This work has been funded by the National R+D+i Plan Project ENE2017-83973-R (SOLTERMIN project) and DPI2017-85007-R (CHROMAE project) of the Spanish Ministry of Economy, Industry and Competitiveness and ERDF funds.

## Nomenclature

---

$a$	Linear model parameter	$m\_w\_hot$	Hot water mass flow rate
$B$	Decision space	$n$	Number of inputs
$b$	Linear model parameter	$p\_dis$	Dist. vapor pressure
$c$	Criteria vector or matrix	$q\_boiler$	Boiler heat flux
$c_1$	Objective vector	$Q\_boiler$	Boiler thermal energy
$c_2$	Inequality parameters	$s\_in$	Inlet steam
$c_3$	Equality parameters	$s\_out$	Outlet steam
$d_1$	Scaling factor	$s\_p$	Steam pres.
$d_2$	Inequality functions	$t\_sw$	Salt water temp.
$d_3$	Equality functions	$t\_w\_cold$	Feed water temp.
$D1$	T <sup>a</sup> diff. high-temp. gen.	$t\_w\_hot$	Hot water temp.
$D2$	T <sup>a</sup> diff. low-temp. gen.	$T_{ambient}$	Ambient temp.
$dis$	Condensate dist. outlet	$Theta$	Solar incidence angle
$dis\_tank$	Distillate production	$total\_m\_dis$	Dist. production
$H$	Linear model	$u_{xi}$	Manipulable parameter
$htf\_in$	Inlet heat transfer fluid	$u_i$	Manipulable variable
$htf\_out$	Outlet heat transfer fluid	$u$	Manipulable variable vector
$i$	System outputs	$v\_dis$	Last-effect vapor mass flow rate
$j$	System inputs	$v\_wind$	Wind speed
$m\_htf$	HTF mass flow rate	$w\_cold$	Outlet cold water mass flow rate
$m\_s\_out$	Steam condensate flow	$w\_hot$	Inlet hot water mass flow rate
$m\_sw$	Salt water feed flow	$w\_level$	Liquid level

---

## Appendix A. Figures

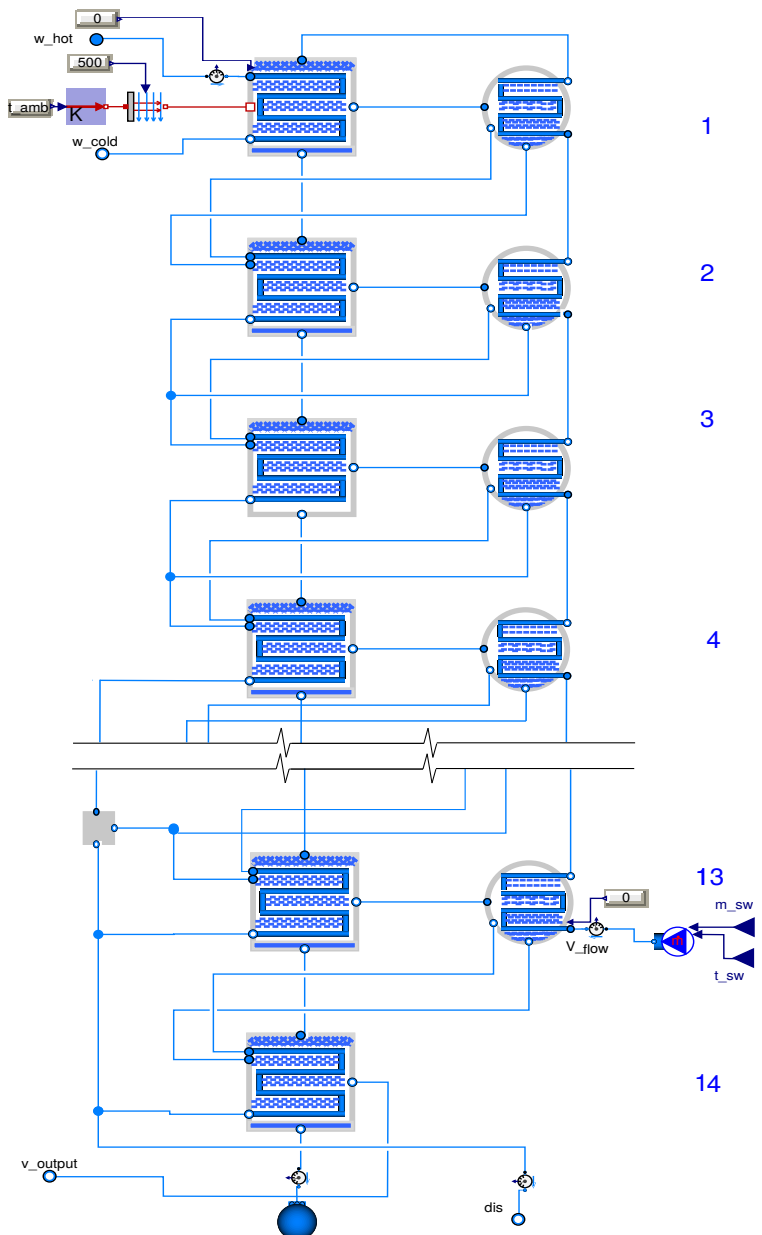


Figure A.15: MED plant components

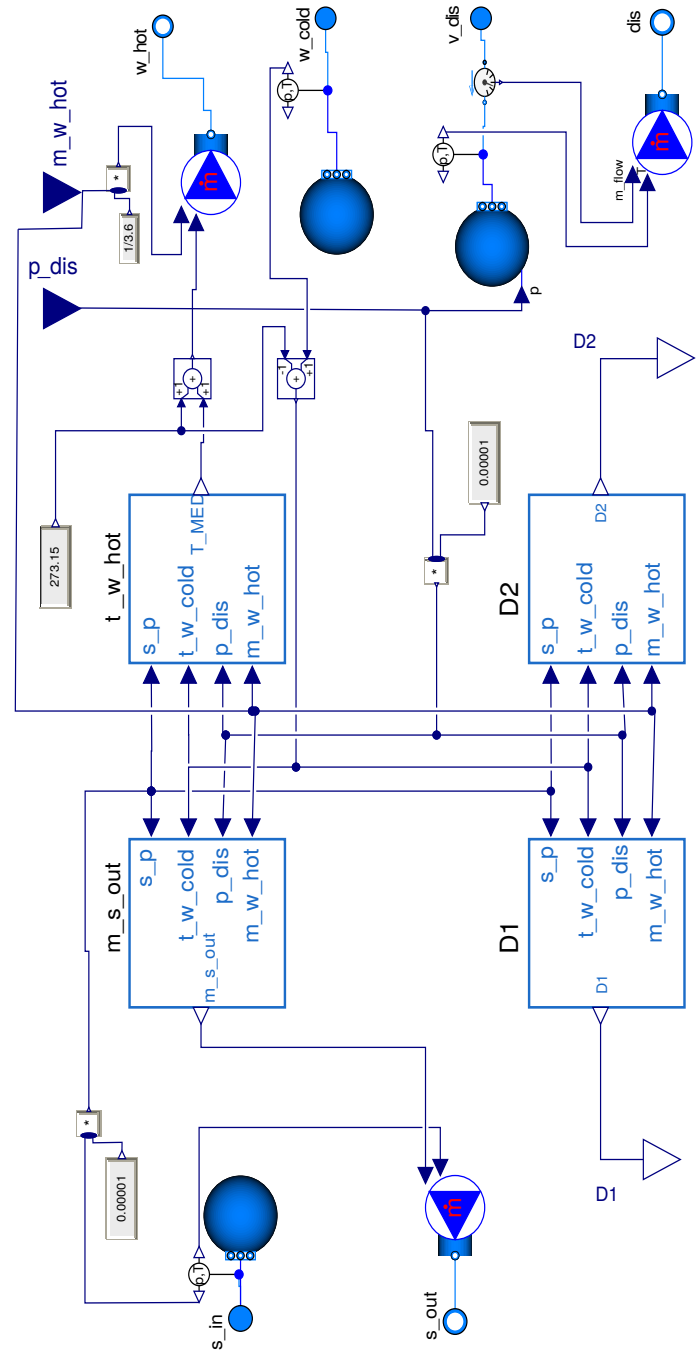


Figure A.16: DEAHP components

## References

- [1] M. H. Sharqawy, J. H. Lienhard V, S. M. Zubair, On exergy calculations of seawater with applications in desalination systems, International Journal of Thermal Sciences 50 (2) (2011) 187–196. [doi:10.1016/j.ijthermalsci.2010.09.013](https://doi.org/10.1016/j.ijthermalsci.2010.09.013).
- [2] M. Chandrashekara, A. Yadav, Water desalination system using solar heat: A review, Renewable and Sustainable Energy Reviews 67 (2017) 1308–1330. [doi:10.1016/j.rser.2016.08.058](https://doi.org/10.1016/j.rser.2016.08.058).
- [3] F. E. Ahmed, R. Hashaikeh, N. Hilal, Solar powered desalination technology, energy and future outlook, Desalination 453 (December 2018) (2019) 54–76. [doi:10.1016/j.desal.2018.12.002](https://doi.org/10.1016/j.desal.2018.12.002).
- [4] P. Palenzuela, A. S. Hassan, G. Zaragoza, D. C. Alarcón-Padilla, Steady state model for multi-effect distillation case study: Plataforma Solar de Almería MED pilot plant, Desalination 337 (1) (2014) 31–42. [doi:10.1016/j.desal.2013.12.029](https://doi.org/10.1016/j.desal.2013.12.029).
- [5] F. Al-Juwayhel, H. El-Dessouky, H. Ettonuey, Analysis of single-effect evaporator desalination systems combined with vapor compression heat pumps, Desalination 114 (3) (1997) 253–275. [doi:10.1016/S0011-9164\(98\)00017-4](https://doi.org/10.1016/S0011-9164(98)00017-4).
- [6] Y. Wang, N. Lior, Thermo-economic analysis of a low-temperature multi-effect thermal desalination system coupled with an absorption heat pump, Energy 36 (6) (2011) 3878–3887. [doi:10.1016/j.energy.2010.09.028](https://doi.org/10.1016/j.energy.2010.09.028).
- [7] P. Palenzuela, L. Roca, G. Zaragoza, D. C. Alarcón-Padilla, L. García-Rodríguez, A. de La Calle, Operational improvements to increase the efficiency of an absorption heat pump connected to a multi-effect distillation unit, Applied Thermal Engineering 63 (1) (2014) 84–96. [doi:10.1016/j.applthermaleng.2013.10.050](https://doi.org/10.1016/j.applthermaleng.2013.10.050).

- [8] P. Horta, Process heat collectors: State of the art and available medium temperature collectors, Solar Process Heat for Production and Advanced Applications. IEA SHC Task 49.
- [9] A. Modi, F. Bahler, J. G. Andreasen, F. Haglind, A review of solar energy based heat and power generation systems, *Renewable and Sustainable Energy Reviews* 67 (2017) 1047–1064. [doi:10.1016/j.rser.2016.09.075](https://doi.org/10.1016/j.rser.2016.09.075).
- [10] J. A. Carballo, J. Bonilla, L. Roca, P. Palenzuela, M. Berenguel, Optimal operating conditions analysis of a Multi-Effect Distillation, Desalination and Water Treatment 0703 (2017) 1–10. [doi:10.5004/dwt.2017.0703](https://doi.org/10.5004/dwt.2017.0703).
- [11] J. A. Carballo, J. Bonilla, L. Roca, A. de la Calle, P. Palenzuela, D. C. Alarcón-Padilla, Optimal operating conditions analysis for a multi-effect distillation plant according to energetic and exergetic criteria, *Desalination* 435 (2018) 70–76. [doi:10.1016/j.desal.2017.12.013](https://doi.org/10.1016/j.desal.2017.12.013).
- [12] J. A. Carballo, J. Bonilla, L. Roca, A. de la Calle, P. Palenzuela, Optimal operating conditions analysis for a double-effect absorption heat pump coupled to a multi effect distillation plant, in: Porceedings of the EuroMed 2017 Desalination for Clean Water and Energy: Cooperation around the World, p. 113. [doi:10.13140/RG.2.2.33029.04320](https://doi.org/10.13140/RG.2.2.33029.04320).
- [13] D. Alarcón, J. Blanco, S. Malato, M. I. Maldonado, P. Fernández, Design and setup of a hybrid solar seawater desalination system: The AQUASOL project, in: Proceedings of the ISES 2005 Solar World Congress, Orlando, FL, 2005.
- [14] E. Commission, Aquasol project (2019).  
URL <https://cordis.europa.eu/project/rcn/61224/factsheet/en>
- [15] A. de La Calle, J. Bonilla, L. Roca, P. Palenzuela, Dynamic modeling and performance of the first cell of a multi-effect distillation plant, *Applied Thermal Engineering* 70 (1) (2014) 410–420. [doi:10.1016/j.applthermaleng.2014.05.035](https://doi.org/10.1016/j.applthermaleng.2014.05.035).

- [16] A. de la Calle, J. Bonilla, L. Roca, P. Palenzuela, Dynamic modeling and simulation of a solar-assisted multi-effect distillation plant, *Desalination* 357 (2015) 65–76. [doi:10.1016/j.desal.2014.11.008](https://doi.org/10.1016/j.desal.2014.11.008).
- [17] NEP, *Polytrough 1200* (2019).  
URL <http://www.nep-solar.com/products/polytrough-1200/>
- [18] Solutia, *Therminol 55* (2019).  
URL [http://blueoceanoil.com/wp-content/uploads/2015/04/therminol\\_55.pdf](http://blueoceanoil.com/wp-content/uploads/2015/04/therminol_55.pdf)
- [19] T. M. Association, *Modelica* (2019).  
URL <https://www.modelica.org/>
- [20] T. M. Association, *Modelica standard library* (2019).  
URL <https://github.com/modelica/ModelicaStandardLibrary>
- [21] S. Quoilin, A. Desideri, J. Wronski, I. Bell, V. Lemort, Thermocycle: A modelica library for the simulation of thermodynamic systems, in: 10th International Modelica conference, Linköping University Electronic Press, 2014. [doi:10.3384/ecp14096683](https://doi.org/10.3384/ecp14096683).
- [22] D. Systemes, *Dymola* (2019).  
URL <https://www.3ds.com/products-services/catia/products/dymola/>
- [23] T. Huld, R. Müller, A. Gambardella, A new solar radiation database for estimating PV performance in Europe and Africa, *Solar Energy* 86 (6) (2012) 1803–1815. [doi:10.1016/j.solener.2012.03.006](https://doi.org/10.1016/j.solener.2012.03.006).
- [24] European Commission, *PVGIS data download* (2019).  
URL [http://re.jrc.ec.europa.eu/pvg\\_download/data\\_download.html](http://re.jrc.ec.europa.eu/pvg_download/data_download.html)
- [25] A. de la Calle, L. Roca, J. Bonilla, P. Palenzuela, Dynamic modeling and simulation of a double-effect absorption heat pump, *International Journal*

of Refrigeration 72 (2016) 171–191. [doi:10.1016/j.ijrefrig.2016.07.018](https://doi.org/10.1016/j.ijrefrig.2016.07.018).

- [26] J. A. Carballo, J. Bonilla, M. Berenguel, P. Palenzuela, Parabolic trough collector field dynamic model: Validation, energetic and exergetic analyses, Applied Thermal Engineering 148 (2019) 777–786. [doi:10.1016/j.aplthermaleng.2018.11.093](https://doi.org/10.1016/j.aplthermaleng.2018.11.093).
- [27] K. Åström, R. Bell, Drum boiler dynamics, Automatica 36 (3) (2000) 363–378. [doi:10.1016/S0005-1098\(99\)00171-5](https://doi.org/10.1016/S0005-1098(99)00171-5).
- [28] A. Pfeiffer, Optimization library for interactive multi-criteria optimization tasks, in: Proceedings of the Proc. 9th International Modelica Conference, Munich, Germany, 2012. [doi:10.3384/ecp12076669](https://doi.org/10.3384/ecp12076669).